

Kinesin-5 in plants – Characterisation of AtKRP125b suggests a new function beyond cell division

Dissertation with the aim of achieving a doctoral degree at the Faculty of Mathematics,
Informatics, and Natural Sciences

Department of Biology

Universität Hamburg

Submitted by

Tobias Strauß

November 2020 in Hamburg

This work was carried out in the Department of Molecular Plant Physiology at the Institute of Plant Science and Microbiology at Universität Hamburg under the supervision of Prof. Dr. Stefan Hoth and Prof. Dr. Wim Walter between October 2016 and November 2020 (interrupted by parental leave).

Head of examination commission: Prof. Dr. Sigrun Reumann

First reviewer: Prof. Dr. Stefan Hoth

Second reviewer: Prof. Dr. Wim Walter

Date of the oral defense: 5th February 2021

Table of Contents

Table of Contents	I
List of Abbreviations.....	V
Zusammenfassung.....	X
Abstract	XII
1 Introduction	1
1.1 Transport mechanisms in cells	1
1.2 The microtubule cytoskeleton.....	2
1.3 The mitotic spindle	4
1.4 Microtubule interacting motor proteins – Kinesins	8
1.5 The kinesin-5 family.....	13
1.6 Kinesin-5 in plants.....	17
1.7 <i>Arabidopsis thaliana</i> AtKRP125b.....	18
Aim of the Doctoral Thesis	22
2 Results and Discussion	23
2.1 Results of <i>in vitro</i> experiments.....	23
2.1.1 Expression and purification of AtKRP125b in <i>Escherichia coli</i>	23
2.1.2 Expression of AtKRP125b in <i>Pichia pastoris</i>	26
2.1.3 Expression and purification of AtKRP125b in insect cells	27
2.1.4 KIN5b moves along microtubules towards the plus-end at a low velocity.....	29
2.1.5 Single AtKRP125b molecules move in a processive manner.	30
2.1.6 AtKRP125b crosslinks microtubules and slides them apart.....	32
2.2 Results of <i>in vivo</i> experiments.....	36
2.2.1 <i>At2g36200/AtKRP125b</i> is not expressed in mitotic tissue.	36
2.2.2 T-DNA insertion lines of <i>AtKRP125b</i>	40

2.2.3	The knockout of <i>AtKRP125b</i> in <i>kin5b-1</i> did not result in distinct phenotypes. .	41
2.2.4	Generation of knockout mutants via CRISPR/Cas9	51
2.2.5	GFP-AtKRP125b is not exclusively localised inside the nucleus.....	53
2.3	General discussion	58
2.3.1	Functions of kinesin-5 in vesicle transport	58
2.3.2	Functions of kinesin-5 in microtubule organisation	61
3	Conclusion.....	64
4	Material and Methods	65
4.1	Organisms	65
4.1.1	Bacterial strains.....	65
4.1.2	Plant lines	66
4.2	Material	68
4.2.1	Vectors.....	68
4.2.2	Chemicals	69
4.2.3	Kits.....	69
4.2.4	Antibodies	70
4.2.5	Enzymes.....	70
4.2.6	DNA-Oligonucleotides	71
4.3	Molecular biological methods	72
4.3.1	Isolation of genomic DNA from <i>Arabidopsis thaliana</i>	72
4.3.2	DNA amplification by polymerase chain reaction (PCR)	72
4.3.3	Colony PCR	73
4.3.4	Agarose gel electrophoresis	74
4.3.5	Isolation of total RNA from <i>Arabidopsis thaliana</i>	74
4.3.6	Synthesis of cDNA.....	75
4.3.7	Reverse transcriptase-PCR (RT-PCR)	75

4.3.8	Restriction and ligation cloning.....	76
4.3.9	Overlap extension cloning (OEC).....	76
4.3.10	Gateway cloning.....	79
4.3.11	Preparation of chemically competent <i>Escherichia coli</i> cells	80
4.3.12	“Heat shock” transformation of chemically competent cells	81
4.3.13	Preparations of electrocompetent <i>Agrobacteria tumefaciens</i> cells.....	81
4.3.14	Transformation of electrocompetent cells	82
4.3.15	Generation of glycerol stocks.....	82
4.3.16	Plasmid extraction from bacteria.....	82
4.3.17	Sanger Sequencing	83
4.4	Plant handling.....	83
4.4.1	Growth conditions.....	83
4.4.2	Sterilisation, stratification and sowing of <i>Arabidopsis thaliana</i> seeds	84
4.4.3	Isolation and transformation of <i>Arabidopsis thaliana</i> leaf protoplasts.....	85
4.4.4	<i>Agrobacteria</i> -mediated transformation of <i>Arabidopsis thaliana</i>	86
4.4.5	<i>Agrobacteria</i> -mediated transformation of <i>Nicotiana benthamiana</i>	87
4.4.6	Confocal laser scanning microscopy	87
4.4.7	Selection of transformed plants.....	88
4.4.8	β -glucuronidase (GUS) staining.....	89
4.4.9	Evaluation of root size by coloured pixel counting	89
4.4.10	CRISPR/Cas9	90
4.5	Protein biochemical methods.....	96
4.5.1	Sodium dodecyl sulphate-polyacrylamide gel electrophoresis (SDS-PAGE).....	96
4.5.2	Coomassie staining.....	97
4.5.3	Western blot.....	97
4.5.4	Protein expression test	98

4.5.5	Protein expression in <i>Escherichia coli</i>	99
4.5.6	Protein expression in <i>Pichia pastoris</i>	99
4.5.7	Protein expression in insect cells	102
4.5.8	Cell lysis of bacteria, yeast and insect cells	103
4.5.9	Protein purification by affinity chromatography	103
4.5.10	Tubulin purification from porcine brain	104
4.5.11	Tubulin labelling	105
4.5.12	Preparation of microtubules	107
4.6	Methods for characterisation of kinesin motor proteins	109
4.6.1	Cleaning and silanisation of cover slips	109
4.6.2	Preparation of flow cell chambers	109
4.6.3	Gliding assay	110
4.6.4	Stepping assay	110
4.6.5	Sliding assay	111
4.6.6	Imaging of motility assays	111
4.7	Software and Databases	112
4.7.1	Tracking of filaments and single molecules and analysis of velocity	112
4.7.2	Software and databases used in this thesis	112
5	References	114
6	Supplement	137
	Acknowledgments	149
	Eidesstattliche Versicherung	151

List of Abbreviations

%	percent
°C	degree Celsius
μl	microliter
μm	micrometre
μM	micromolar
<i>A. thaliana</i>	<i>Arabidopsis thaliana</i>
<i>A. tumefaciens</i>	<i>Agrobacterium tumefaciens</i>
aa	amino acid
ABA	abscisic acid
ADP	adenosine diphosphate
AEBSF	4-(2-aminoethyl)benzenesulfonyl fluoride
APP	AMYLOID PRECURSOR PROTEIN
ARM	ARMADILLO
AtKRP125b	ARABIDOPSIS THALIANA KINESIN RELATED PROTEIN 125b
ATP	adenosine triphosphate
Aβ	amyloid beta peptide
BASS	bipolar assembly
BC12	BRITTLE CULM 12
BiFC	bimolecular fluorescence complementation
BimC	blocked in mitosis C
bp	base pair
BRB80	Britton-Robinson buffer with 80 μM PIPES
CARTS	carriers of the trans-Golgi network to the cell surface
Cas9	CRISPR associated protein 9
CC	coiled-coil
CDK	cyclin-dependent kinase
cDNA	complementary deoxyribonucleic acid

CHS1	CHILLING SENSITIVE 1
CLS	confocal laser scanning
Col-0	Columbia wild type
CRISPR	clustered regularly interspaced short palindromic repeats
Cys	cysteine
<i>D. carota</i>	<i>Daucus carota</i>
DLK	DUAL LOCATED KINSIN
DNA	deoxyribonucleic acid
DTT	dithiothreitol
<i>E. coli</i>	<i>Escherichia coli</i>
E1	Enzyme 1 (ubiquitin activating enzyme)
E2	Enzyme 2 (ubiquitin conjugating enzyme)
E3	Enzyme 3 (ubiquitin ligase)
EGTA	ethylene glycol-bis (β -aminoethyl ether)-N,N,N',N'-tetraacetic acid
et al.	et alii/and others
FIESTA	fluorescent image evaluation software for tracking & analysis
FIAsH	fluorescein arsenical hairpin binder
fmol	femtomole
FRA1	FRAGILE FIBER 1
FRA1	FRAGILE FIBER 1
GA	gliding assay
gDNA	genomic deoxyribonucleic acid
GDP	guanosine diphosphate
GFP	green fluorescent protein
GMPCPP	guanosine-5'-[(α,β)-methylene]triphosphate
GTP	guanosine triphosphate
GUS	β -glucuronidase
h	hour
HEPES	4-(2-hydroxyethyl)-1-piperazineethanesulfonic acid
His	histidine

HRP	HORSERADISH PEROXIDASE
HSP70	heat shock protein of 70 kDa
Hz	Hertz
kb	kilobase
kDa	kilodalton
KIF	kinesin family member
KLP	kinesin-like protein
KRP	kinesin-related protein
LDLR	LOW-DENSITY LIPOPROTEIN RECEPTOR
M	molar
MAP	microtubule-associated protein
MCAK	MITOTIC CENTROMERE-ASSOCIATED KINESIN
MDP25	MICROTUBULE-DESTABILIZING PROTEIN 25
MES	2-(N-morpholino)ethanesulfonic acid
min	minute
ml	millilitre
mM	millimolar
MSA	mitosis activation motif
MTOC	microtubule organising center
MVB	multi-vesicular bodies
<i>N. benthamiana</i>	<i>Nicotiana benthamiana</i>
Ncd	Drosophila melanogaster kinesin-14
NEM	N-ethylmaleimide
NLR	NOD-like receptors
nm	nanometre
nM	nanomolar
NMDA	N-methyl-D-aspartate
OD ₆₀₀	optical density at 600 nm wavelength
Os	<i>Oryza sativa</i>
<i>P. pastoris</i>	<i>Pichia pastoris</i>

PAGE	polyacrylamide gel electrophoresis
PAUF	PANCREATIC ADENOCARCINOMA UP-REGULATED FACTOR
PBS	phosphate buffered saline
PCR	polymerase chain reaction
PEG	polyethylene glycol
pH	potential of hydrogen
PIPES	piperazine-N,N'-bis(2-ethanesulfonic acid)
pN	piko-Newton
RAM	root apical meristem
RNA	ribonucleic acid
RT	room temperature
RT-PCR	reverse transcriptase polymerase chain reaction
s	second
SA	salicylic acid
SAM	shoot apical meristem
SAUL1	SENESCENCE-ASSOCIATED E3 UBIQUITIN LIGASE 1
SD	standard deviation
SDS	sodium-dodecyl-sulphate
SEC	size-exclusion chromatography
seg. WT	segregating wild type
siRNA	small interfering RNA
SLA	sliding assay
SOC3	SUPRESSOR OF CHILLING SENSITIVE 1, 3
S-phase	synthesis phase
STA	stepping assay
T-DNA	transfer-deoxyribonucleic acid
TGN	trans-Golgi network
TIRF	total internal reflection fluorescence
TKRP125	TOBACCO KINESIN RELATED POLYPEPTIDE OF 125 kDa
TPX2	targeting protein for Xklp2

TRIM8	TRIPARTITE MOTIF 8
UTR	untranslated region
V	volt
WT	wild type
x g	times gravity
X-Gluc	5-bromo-4-chloro-3-indolyl glucuronide
XKLP2	Xenopus kinesin-like protein 2
γ TuRC	γ -tubulin ring complex

Zusammenfassung

Die hochpräzise Organisation der Zellteilung erfordert komplexe Strukturen aus Mikrotubuli, die von mehreren mit Mikrotubuli interagierenden Motor-Proteinen gebildet und aufrechterhalten werden. Eine besondere Bedeutung bei diesen Prozessen haben Motor-Proteine der Kinesin-5 Familie, welche in fast jedem eukaryotischen Organismus vorkommen. Diese homotetrameren Proteine spielen eine wesentliche Rolle in der bipolaren Organisation der mitotischen Spindel. Sie sind in der Lage, Mikrotubuli zu vernetzen, und können antiparallel orientierte Mikrotubuli gegeneinander verschieben. Dadurch wird eine korrekte Trennung der Chromatiden während der Mitose gewährleistet. Neben Ihrer Funktion während der Zellteilung werden zusätzliche Funktionen diskutiert, zum Beispiel der Transport von Vesikeln aus dem trans-Golgi Netzwerk zur Zelloberfläche oder das Wachstum von Dendriten und Axonen. Eine neu entdeckte Interaktion zwischen AtKRP125b, einem von vier Kinesin-5 Proteinen in *Arabidopsis thaliana*, und der E3-Ubiquitin Ligase SAUL1, welche eine Rolle in der pflanzlichen Immunantwort spielt, eröffnet neue Perspektiven für weitere Funktionen von Kinesin-5 in Pflanzen.

In dieser Arbeit wurden die biophysikalischen und biochemischen Eigenschaften von AtKRP125b in verschiedenen *in-vitro* Experimenten charakterisiert. Das dafür benötigte rekombinante Protein konnte in der erforderlichen Menge und Qualität heterolog in Insektenzellen hergestellt werden. Die *in-vitro* Experimente zeigten, dass AtKRP125b in der Lage ist, sich prozessiv entlang von Mikrotubuli in Richtung deren Plus-Endes mit einer Geschwindigkeit von etwa 17 nm s^{-1} zu bewegen. Zudem ist AtKRP125b in der Lage, Mikrotubuli zu vernetzen und in einer bestimmten Orientierung gegeneinander zu verschieben.

Des Weiteren wurde die physiologische Funktion von AtKRP125b mit Hilfe einiger *in-vivo* Experimente untersucht. Die Analyse der Promotoraktivität von *AtKRP125b* in transgenen Promotor-GUS Pflanzen zeigte eine deutliche Aktivität im vaskulären Gewebe von Wurzeln, Blättern und Blüten. Interessanterweise konnte keine Promotoraktivität in mitotischen Geweben, wie zum Beispiel dem Wurzel- oder Blütenmeristem nachgewiesen werden. Um zu untersuchen, ob der Verlust von *AtKRP125b* in Geweben mit hoher Promotoraktivität einen abweichenden Phänotyp verursacht, wurde eine T-DNA Insertionsmutante etabliert und untersucht. Es konnten jedoch weder unter normalen Wachstumsbedingungen, noch bei abiotischem Stress konsistente Unterschiede zwischen der Mutante und dem segregierenden

Wildtyp festgestellt werden. Dies deutete darauf hin, dass das Ausschalten eines einzelnen Kinesin-5 Gens in *Arabidopsis thaliana* nicht ausreicht, um einen ausgeprägten Phänotyp zu verursachen. Die Erzeugung zusätzlicher *Knockout*-Mutanten wurde mittels der CRISPR/Cas9-Technologie angestrebt, es konnten jedoch keine weiteren Mutantenlinien generiert werden. Abschließend konnte die subzelluläre Lokalisation von AtKRP125b während der Interphase durch die konfokale Analyse von GFP-Fusionsproteinen bestimmt werden, welche vorwiegend im Zellkern und im Zytoplasma vorlag.

Die im Rahmen dieser Dissertation erzielten Ergebnisse weisen darauf hin, dass AtKRP125b in der Lage ist, die klassischen Funktionen eine Kinesin-5 hinsichtlich der Interaktion mit Mikrotubuli zu erfüllen. Das Fehlen von Promotoraktivität in meristematischem Gewebe, sowie die Lokalisation im Zytoplasma während der Interphase deuten jedoch auf zusätzliche, noch unbekannte Funktionen hin.

Abstract

The sophisticated organisation of cell division requires complex structures of microtubule arrays that are formed and maintained by several microtubule-interacting motor proteins. Among them, members of the kinesin-5 family are one of the most important microtubule-interacting motor proteins. Members of this highly conserved kinesin-5 family are found in almost every eukaryotic organism and play an essential role in the bipolar organisation of the mitotic spindle. These homotetrameric proteins can crosslink microtubules and slide anti-parallel microtubules apart, and thereby guarantee the precise and correct separation of chromatids. Apart from their function in cell division, an increasing number of publications point towards additional functions of kinesin-5s during other stages of cell development, for example the transport of vesicles from the trans-Golgi network to the cell surface or the growth of dendrites and axons. A newly found interaction between one of the four kinesin-5s in *Arabidopsis thaliana*, AtKRP125b and the E3 ubiquitin ligase SAUL1, which is involved in plant immunity, provides a new prospect for additional functions of kinesin-5s in plants.

In this thesis, the biophysical and biochemical motility properties of AtKRP125b were characterised in controlled *in vitro* motility assays, using a recombinant protein whose necessary quality could only be achieved when produced heterologously in insect cells. The motility assays revealed that AtKRP125b can move along microtubules towards their plus-end with a velocity of about 17 nm s^{-1} in a processive manner. It was further discovered that AtKRP125b can crosslink microtubules and slide them apart.

Additionally, the physiological function of AtKRP125b was investigated. Analysis of the *AtKRP125b* promoter activity, using promoter-GUS constructs, revealed a main activity in the vascular tissue of roots, leaves and flowers. Interestingly, no promoter activity could be detected in mitotic tissues, such as root- or floral meristems. To investigate whether the loss of AtKRP125b causes a distinct phenotype in tissues with high promoter activity, a T-DNA insertion mutant was examined. However, no consistent differences between the mutant and the wild type could be observed under normal growth conditions nor with applied abiotic stress, thus indicating that a single knockout of one kinesin-5 is not sufficient to cause a distinct phenotype in *A. thaliana*. The generation of additional knockout mutants with the CRISPR/Cas9 technology though did not yield new mutant lines. Finally, the subcellular localisation of AtKRP125b could be determined with GFP-fusion constructs predominantly within the nucleus and cytoplasm.

Taken together, these results may suggest that AtKRP125b is able to fulfil the canonical functions of a kinesin-5 regarding the interaction with microtubules. However, the absence of promoter activity in meristematic tissue and the localisation within the cytoplasm during interphase point to additional functions beyond its putative role in cell division.

1 Introduction

Life is motion. From a hunting cheetah to a gliding snail, every living being is in motion. Even sessile organisms are moving in their own way. The movement of a sunflower towards the sun for example takes a lot of time and is therefore hard to track with our eyes but it is still moving every day. With help of technical innovation, scientists could observe even the tiniest and slowest movements. If we look just close enough, in fact, we can see movement within a single cell.

1.1 Transport mechanisms in cells

Within each cell, numerous processes take place at the same time in different parts of the cell. Vesicles, filled with proteins and chemical compounds, have to be transported from the Golgi-network to the plasma membrane to be secreted into the extracellular environment ¹. Organelles, such as chloroplasts have to be moved and rearranged in response to changing environmental conditions ². These complex processes in cells require directed movement. Therefore, a cytoskeleton is needed, consisting of microtubules, microfilaments like actin and intermediate filaments like keratin. These filaments fulfil several important functions: They build and support the shape of cells; they shoulder many forms of cell movement, like the movement of cilia or flagella; and they build the very roadways, on which motor proteins carry out intracellular transportation.

All three types of the cytoskeleton polymers are built out of small, identical protein subunits that are joined together in thousands to form filaments eventually stretching from one side of the cell to the other. The advantage of these small subunits is that filaments can constantly gain or lose them, resulting in a dynamic and adaptable cytoskeleton. In the last years, it became more apparent that many procedures in the cell require more than one type of cytoskeleton polymer to function ³, for example, the nuclear transport in *Physcomitrella patens* or general tip cell growth in many organisms and cell types ³⁻⁶. Except for intermediate filaments, cytoskeleton polymers possess a polarity with a plus- and minus-end, which makes them the ideal roadway for directed movement. This movement is mostly carried out by motor proteins that can interact with the respective cytoskeleton polymer and move along these by consuming ATP. With regard to actin filaments, this motor protein is called myosin. Kinesin and dynein are the motor proteins that interact with microtubules ⁷.

1.2 The microtubule cytoskeleton

Microtubules are the largest cytoskeleton polymers. They are composed of α - and β -tubulin, two small, globular proteins that form heterodimers. Each of these subunits can bind GTP. While GTP binding to α -tubulin is trapped between α - and β -tubulin and cannot be hydrolysed, GTP binding to β -tubulin is exposed and can be hydrolysed over time. These heterodimers polymerise head-to-tail into longitudinally organised protofilaments, resulting in polarity within the protofilament with an α -tubulin at the minus-end and a β -tubulin at the plus-end. These protofilaments assemble to a hollow tube, most often comprised of thirteen protofilaments. When the protofilaments form a microtubule, a seam can be noticed between the first and thirteenth protofilament, caused by a slight staggering in the orientation of adjacent tubulin dimers. The result is a cylindrical microtubule with a diameter of 25 nm and a length that can vary dynamically and reach up to 50 μm (**Figure 1**)^{8,9}.

Microtubules can either shrink or grow and thereby change their length over time. These changes only occur at the ends of the microtubule. The lateral bonds between the protofilaments make microtubules very stable. Under *in vitro* conditions, tubulin can polymerise spontaneously if sufficient tubulin and GTP are available. First, a few α - and β -tubulin dimers form nuclei that can bind additional dimers or fall apart again. Only some of these nuclei reach a sufficient size to become stable and add new dimers more frequently than old ones disassociate. As long as enough free tubulin dimers are present in the solution the growth of the microtubule can be quite rapid. During this elongation phase, tubulin dimers are added to both ends of the microtubule. As soon as the tubulin concentration falls below a critical level, the rapid elongation stops and a steady-state is reached. In this steady-state, the microtubule continuously switches between growth and shrinkage. This dynamic instability at the plus-end describes the abrupt transitions from fast-shrinking events, called catastrophe, and growing events, called rescue¹⁰. During this steady-state, the minus-end hardly grows any more. It is either stable or starts to depolymerise slowly¹¹. The reason for these catastrophe shrinking events of the plus-end is the hydrolysis of GTP in the β -tubulin subunit at the plus-end of the microtubule. A protofilament containing GTP is most stable in a straight position, enhancing the formation of lateral bonds between each neighbouring protofilament. However, protofilaments containing GDP are most stable in a slightly curved position, which hinders the formation of lateral bonds. The tip of the microtubule begins to fray like a cord and single tubulin dimers start to dissipate from the frayed tip^{12,13}. A shrinking microtubule

does not have to dissolve completely. A so-called “rescue” event can stop the shrinking and opens the opportunity for new growth. Along the lattice of a microtubule, islands of GTP-rich β -tubulin are present (**Figure 1**). At these GTP-rich islands, the shrinkage stops because the microtubule tip is not frayed anymore due to the presence of GTP-containing β -tubulin ^{14,15}.

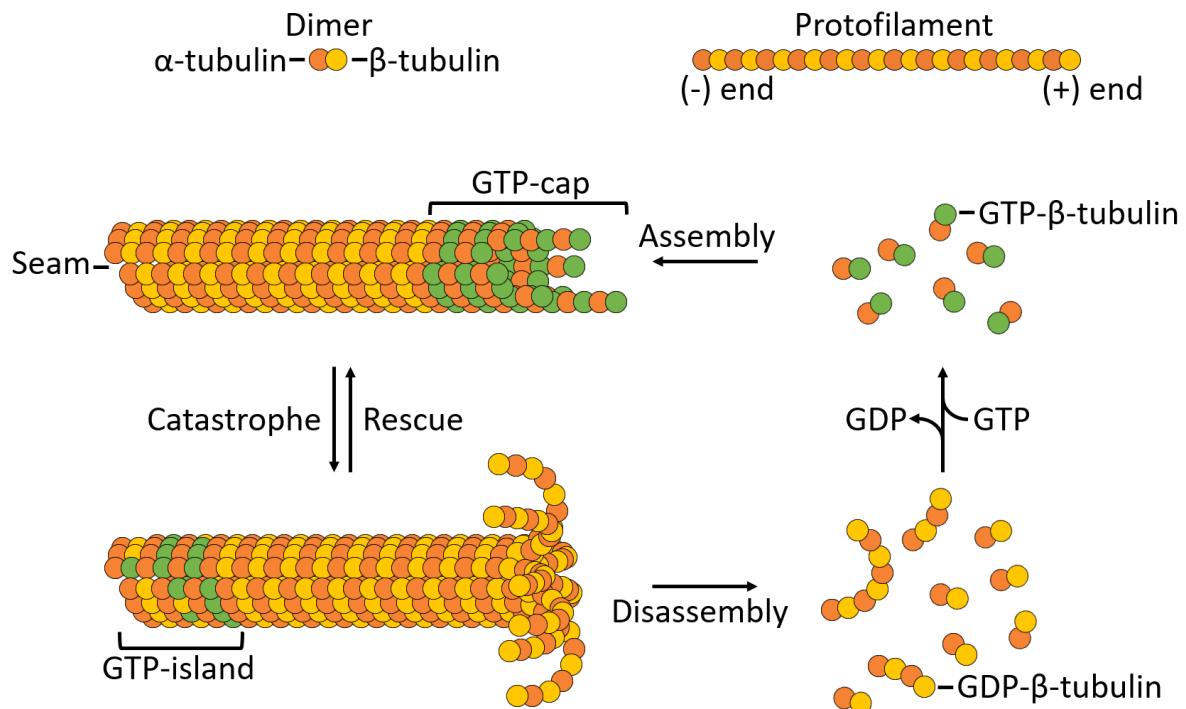


Figure 1: Structure and dynamics of microtubules.

Microtubules consist of α - and β -tubulin heterodimer subunits. Both kinds of tubulin can interact with GTP. While the GTP in α -tubulin is stabilised, the GTP in β -tubulin can be hydrolysed over time. These subunits can form polar, linear protofilaments, with a plus- and minus-end. Thirteen of these protofilaments form a cylindrical, hollow microtubule with a diameter of 25 nm.

Microtubules are dynamic structures, switching between assembly and disassembly. While the microtubule is growing the plus-end is stabilised by GTP in the β -tubulin. GDP- β -tubulin is slightly curved, compared to GTP- β -tubulin, resulting in a frayed tip if the GTP gets hydrolysed. This often results in a fast-shrinking process, called catastrophe. This catastrophe can be rescued by GTP-islands along the microtubule shaft, restoring the growth of the microtubule. Modified from Lodish et al. 2008 and Cassimeris et al. 2011.

Though it has been observed, the formation of spontaneous nuclei is often too unreliable for the formation of specific microtubule arrays in living organisms ¹⁶. Therefore, a microtubule-organising center (MTOC), composed of γ -tubulin and stabilising proteins evolved. These form a γ -tubulin ring complex (γ TuRC) that promotes the polymerisation of α - and β -tubulin dimers. In most cases, this complex remains attached to the minus-end and stabilises it. However, it is also possible that microtubules are released from the MTOC and transported to other regions of the cell ¹⁷. The most prominent MTOCs are the centrosomes of animal cells. In plants, however, such an organelle is missing. Most microtubules in plants start forming at a γ TuRC, just as in animals. These γ TuRCs are forming at the nuclear surface, as well as next to existing microtubules ¹⁸⁻²¹.

Though microtubules form in a self-assembly process without the need of other proteins, microtubule-associated proteins (MAPs) can enhance the dynamic of microtubules or stabilise them^{22,23}. MAPs can accelerate the polymerisation of tubulin-dimers at the ends of the microtubule or enhance the rate at which catastrophes occur, resulting in a shrinkage of the microtubule. Kinesin-13 for example facilitates the microtubule depolymerisation by promoting curved protofilaments at the microtubule tip and thereby inhibiting the formation of lateral bonds²⁴. These changes in the dynamic cannot only be caused by MAPs but also by small chemical compounds. These chemicals often have an enormous impact on mitosis by altering the mitotic spindle. They are often used in cancer treatment and plant breeding^{25,26}. Taxol, for example, an alkaloid from the Pacific yew tree (*Taxus brevifolia*) can stabilise microtubules and prevent their depolymerisation²⁷. On the contrary, compounds like colchicine, a steroid derived from autumn crocus (*Colchicum autumnale*) or the man-made chemical oryzalin cause depolymerisation and therefore disruption of microtubules^{28,29}. Interestingly, oryzalin inhibits microtubule polymerisation only in some plants at very low concentrations, while it requires 1000 times higher concentrations in other plants and most animals, showing the small but sometimes significant differences between tubulin from different organisms³⁰⁻³³.

1.3 The mitotic spindle

Mitosis, which is the correct duplication and accurate segregation of genetic material from one cell to two daughter cells is one of the most critical processes in life. The loss or gain of a chromosome often leads to severe complications or is even lethal. A special form of microtubule arrangement is needed to equally separate the chromosomes that were duplicated during S-phase (synthesis phase). This microtubule array is called the mitotic spindle or spindle apparatus. Its organisation and maintenance require a vast number of MAPs and even more proteins that regulate these MAPs so they act at a precise time point.

The appearance of the mitotic spindle changes greatly during the different mitotic phases. The first dramatic event is the breakdown of interphase microtubules. Instead of connecting and stabilising the cell, microtubules form asters, starting at the duplicated centrosomes. During this prophase, not only microtubules change their appearance, chromosomes start to condense into sister chromatids. These sister chromatids are linked together by cohesins at the centromeric region. The next phase, the prometaphase, begins with the breakdown of the

nuclear envelope. As the sister chromatids are now free in the cytoplasm, microtubules start to “search and capture” these chromatids³⁴. During mitosis, microtubules display different dynamics than during interphase. They are much shorter and much more dynamic than interphase microtubules. After a catastrophe event, they depolymerise almost completely before they are rescued again³⁵. Recent studies show that these microtubule dynamics are modulated by cytosolic calcium concentrations³⁶. Microtubules start emerging from the spindle poles towards the midzone and either, by chance, bind to the kinetochore of a chromatid or depolymerise. Each sister-chromatid has its own kinetochore complex and gets eventually attached to the plus-end of a microtubule. When all kinetochores have been “found” by a microtubule, the sister chromatids are aligned in equal distances to each spindle pole along the metaphase plate. This alignment of chromosomes to the metaphase plate is called congression. Once all sister chromatids are positioned in the metaphase plate, metaphase is reached. Anaphase is induced by the activation of a complex that promotes the destruction of cohesins, resulting in the separation of sister chromatids. Once they are separated, each sister chromatid is pulled towards the pole, from which the microtubule connected to its kinetochore has emerged. During anaphase, these poles themselves move further away from each other towards the cell membrane. In the following telophase the nuclear envelope is formed around the now divided sister chromatids and a contractile ring, made of actin, is formed in animal cells. The final stage of mitosis is the cytokinesis in which the separation of both daughter cells is completed and interphase microtubules are restored (**Figure 2**)^{25,26,37,38}.

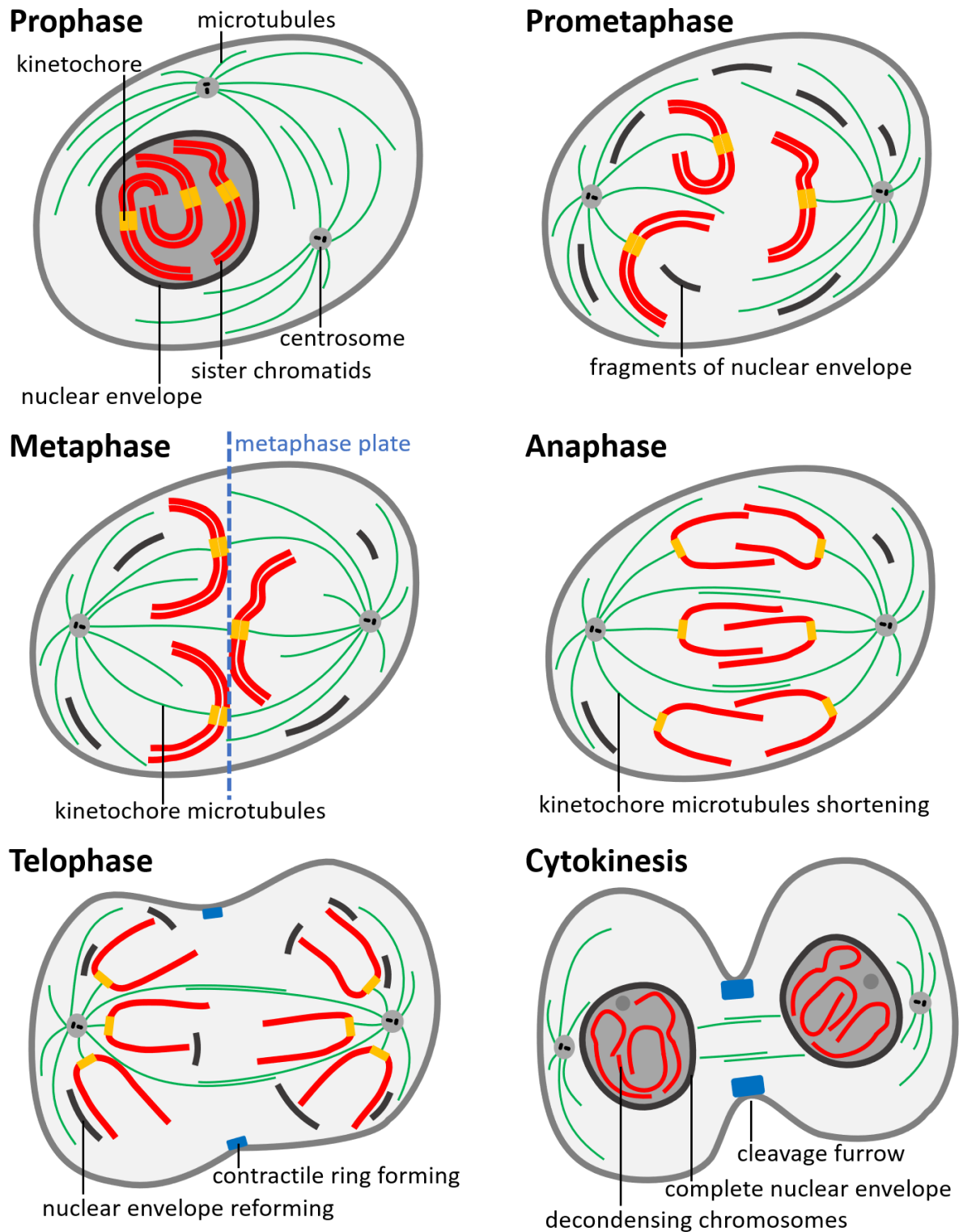


Figure 2: Schematic stages of mitosis in a vertebrate cell

Prophase: Chromosomes have doubled and are condensed into sister chromatids; microtubules start emerging from centrosomes to form the mitotic spindle. Prometaphase: Nuclear envelope breaks down; centrosomes move poleward. Metaphase: Kinetochore microtubules are attached to each kinetochore; sister chromatids are aligned to metaphase plane. Anaphase: Sister chromatids are separated and get pulled poleward by shortening kinetochore microtubules; Centrosomes move outwards. Telophase: Mitotic spindle disassembles; nuclear envelope starts to reform; contractile ring begins to form. Cytokinesis: Mitosis is completed; Nuclear envelope is complete; chromosomes start to decondense; the contractile ring forms the cleavage furrow. Modified after Morgen, 2007, and Mitchison and Salmon, 2001.

In higher plants however, the cell division proceeds differently compared to other eukaryotes. Microtubules in plants do not provide major structural support as in animal cells. Especially after the rigid cell wall is formed and determines the shape and ensures the structural integrity of the cell. Therefore, microtubules play a bigger role in organising the cell and transport mechanisms, requiring special microtubule arrays unique in plants throughout the mitotic cell cycle. These arrays are often missing in cell types without a rigid cell wall, such as endosperm cells and meiotic cells. Before mitosis microtubules are mostly arranged as a cortical interphase array, functioning as an orientation for cellulose microfibrils when new cell walls are synthesised, determining cell polarity and asymmetry³⁹⁻⁴¹. The cortical interphase array (**Figure 3, A and B**) is degraded before mitosis after DNA replication is finished. It is gradually replaced by the preprophase band, a dense ring of cortical microtubules around the nucleus with additional microtubules forming between the nucleus and cell cortex (**Figure 3, C and D**). The preprophase band determines the division plane and, later on, the localisation of the cell plate and the phragmoplast, even though it is dissolved after nuclear envelope breakdown during prometaphase and is not present later on. Studies indicate that this location “memory” is caused by endocytosis in the region of the preprophase band^{42,43}. After nuclear envelope breakdown the mitotic spindle is formed almost similar to animal cells (**Figure 3, E and F**). Since plants do not have any centrioles, plant spindles are less focused at the poles than animal spindles. The spindle poles are broader and contain several microtubule foci^{39,44,45}. After the separation of chromosomes is finished and the mitotic spindle disappears, the phragmoplast is formed near the equatorial plane of the cell. The phragmoplast is a plant unique microtubule array originating from the need to form a new cell wall between the two emerging daughter cells. The phragmoplast consists of two microtubule rings parallel to the equatorial plane and is built up partly from interzonal spindle microtubules and new polymerised microtubules (**Figure 3, G and H**). Along the microtubules of the phragmoplast, a lot of vesicle transport is taking place to form new membranes and the growing cell plate^{26,39,46,47}.

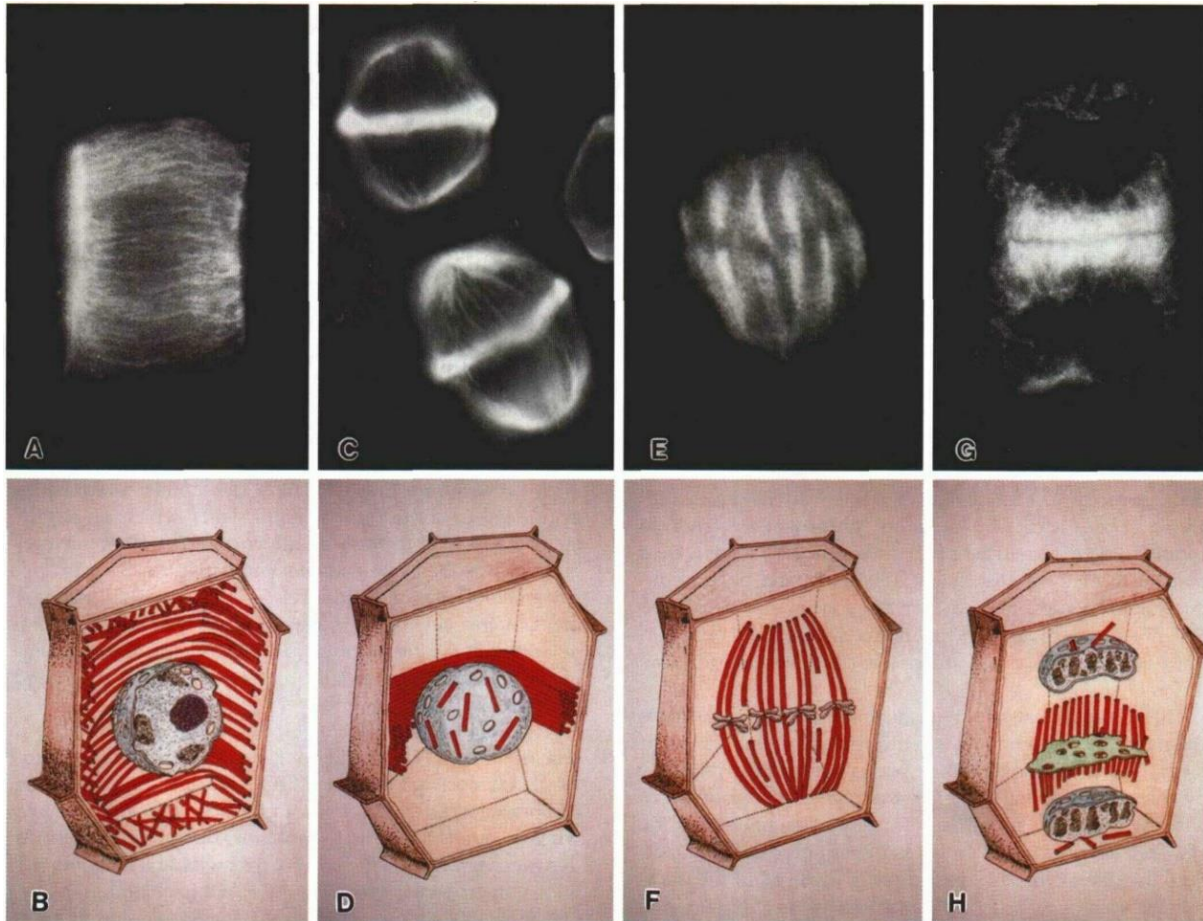


Figure 3: Microtubule arrays during plant mitosis.

Upper row (A, C, E, G) show immunofluorescence images of onion root tip cells labelled with tubulin antibodies and fluorescently conjugated secondary antibodies. Lower row (B, D, F, H) show simplified diagrams emphasising the role of microtubules (red). A and B picture the cortical microtubule array before the start of mitosis during interphase; C and D show the formation of the pre-prophase band and microtubules associated to the nuclear envelope; E and F show a metaphase spindle; G and H present the formation of a phragmoplast during cytokinesis, as well as new nuclear envelope-associated microtubules. Reprinted with permission from Goddard et al., 1994.

1.4 Microtubule interacting motor proteins – Kinesins

As mentioned above, the transport along microtubules and the organisation of microtubule arrays require special motor proteins that can interact with microtubules. In most eukaryotic cells two groups of motor proteins can move along microtubules; dynein, which is responsible for most of the transport towards the microtubule minus-end, and kinesin, which functions are far more diverse and which generally acts in the movement towards the plus-end of microtubules. As higher plants have lost dynein motors presumably with the loss of ciliated sperm during the evolution of angiosperms, accompanied by a loss of centrioles, minus-end directed kinesins that proliferated already in lower plants, are responsible for all minus-end directed transport in plants ⁴⁸⁻⁵².

The first kinesin, kinesin-1, was discovered in 1985 in a partial purification of proteins from squid giant axons⁵³. It was found that this protein is a heterotetramer, formed of two dimerised heavy chains and two associated light chains. The heavy chains can be classified in several functional domains: a globular head domain connected by a short flexible linker domain to a long stalk domain and by a small globular tail domain at the C-terminus that associates with a light chain⁵⁴ (**Figure 4**). Important for the motor protein function is the heavy chain dimer: The head domain contains the ATP-hydrolysing motor complex, which interacts with microtubules^{55,56}. The following neck linker domain ensures the flexibility of the head domain with respect to the stalk. This neck linker domain is responsible for the directionality of the whole motor protein^{57,58}. While the neck linker of plus-end directed kinesins, like kinesin-1, is located at the C-terminus of the head domain, they change their directionality if the neck linker is moved to the N-terminus of the head domain^{57,59}. Additionally, most neck linkers of minus-end directed kinesins contain a conserved motif, required for directionality⁶⁰. The stalk is important for the dimerisation of the two heavy chains. It consists of several coiled-coil domains⁶¹. The C-terminal tail domain is engaged in the interaction with receptors on the membrane of cargos⁶².

While most of these described domains occur in any member of the kinesin family, the order or the size of these domains can vary greatly. While the head domain with its motor function is highly conserved throughout evolution and has structural similarity and most likely an evolutionary link to the actin-based motor protein myosin^{63,64}, the other domains can differ greatly. The most variable domain in kinesins is the tail domain. This domain is specialised according to the function of the individual kinesin. The tail-domain can be responsible for self-interaction, binding to receptor proteins, interaction with microtubules or actin filaments, association to other MAPs, binding to DNA or membranes, and is often the target of post-translational modifications^{65,66}. For example, the kinesin-14 OsKCH1 can interact with actin filaments by its calponin homology domain and transport these actin filaments along microtubules⁶⁷. Most kinesins dimerise because they need two head domains to “walk” along microtubules (**Figure 4**).

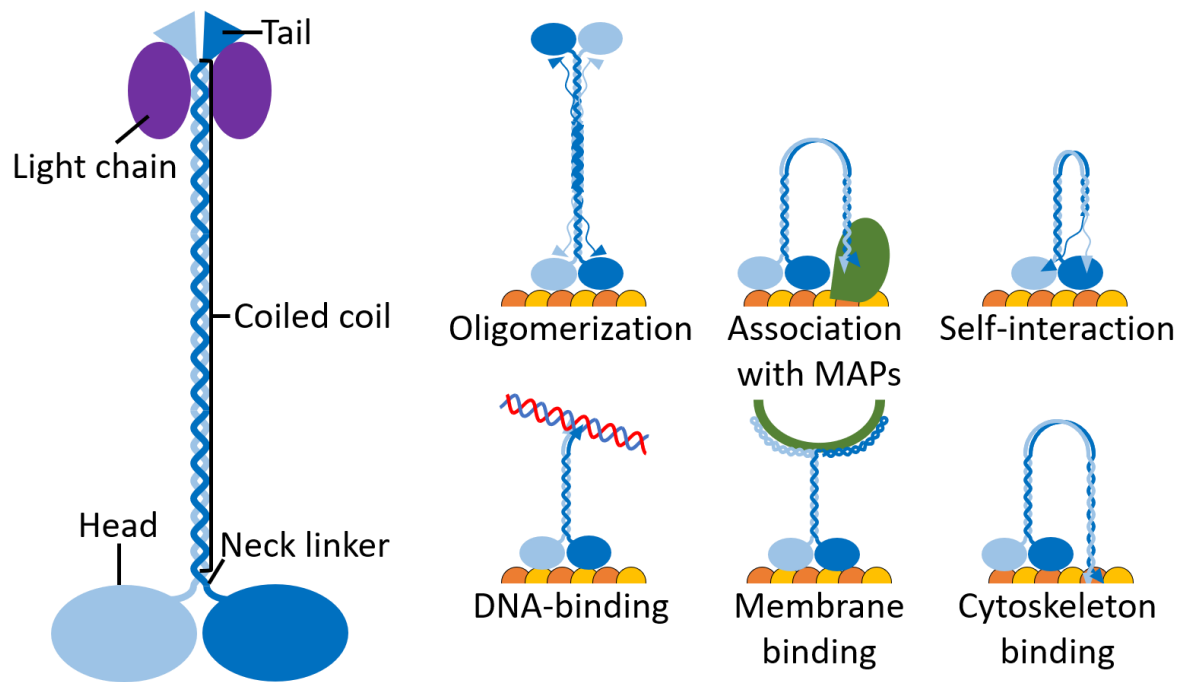


Figure 4: Schematic diagram of kinesin-1 and a variety of interactions from non-motor regions of different kinesins.

Schematic structure of 1985 discovered kinesin-1 and its functional domains. This kinesin consists of a head domain with motor function, a flexible neck linker domain, a coiled-coil domain for dimerization and a tail domain for interaction with other proteins, like the light chains in case of kinesin-1. Modified from Kosik et al. 1990.

Schematic diagram illustrating some of the various interactions of non-motor domains of kinesins and the wide array of functions deriving out of this diversity. While the highly conserved motor domain interacts mostly with microtubules. Non-motor domains can support the oligomerization of kinesins, or interact with MAPs or other domains of the molecule. Furthermore, they can support binding to DNA, phospholipid membranes or other parts of the cytoskeleton like actin or a second microtubule binding site. Modified from Welburn 2013.

The mechanism of kinesin movement along microtubules with its two head domains was discussed very controversially in the early years of kinesin research. It was found that kinesin moves forward 8.3 nm with each ATP-turnover, the exact size of a tubulin heterodimer⁶⁴. But two hypothetical ways seemed possible to move this distance: The “inchworm-type”, where the leading head moves forward on the microtubule and the rear one catches up. In this case the same head domain is always the leading one and the kinesin is “sliding” along the microtubule like an inchworm⁶⁸. The other mechanism is the “head-over-head-type”, in which the rear head domain moves past the leading head and becomes the new lead. Both head domains take their turn in leading and the kinesin is “walking” along the microtubule⁶⁹.

Studies showed strong indications for the “head-over-head” mechanism. Yildiz et al. (2004) showed impressively that the rear head domain moves forward 16.6 nm in a first ATP turnover and moves not at all in a second ATP turnover. The leading head domain (1) is able to bind to β -tubulin in its nucleotide-free state. Upon ATP binding, a conformational change within the neck-linker moves the rear head domain (2) forward 16.6 nm, where it binds weakly to

β -tubulin and releases ADP. The conformation of the neck-linker prevents immediate binding of ATP (Front-head gating). The hydrolysis of ATP in the former leading head (1) strengthens the binding of the new leading head (2) to β -tubulin and causes itself (1) to detach from the microtubule. This hydrolysis causes a conformational change in the neck linker and the new leading head (2) can then again bind ATP, starting the whole process again (**Figure 5**)⁷⁰⁻⁷³.

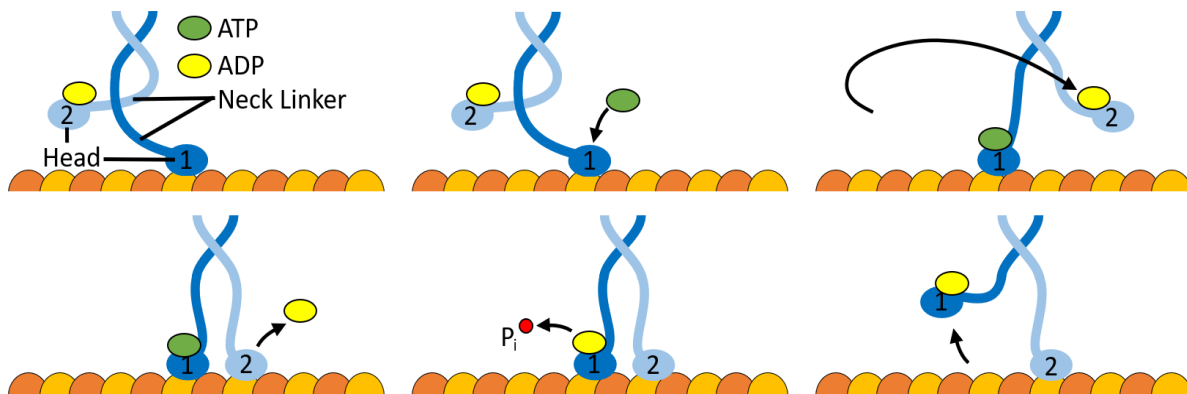


Figure 5: Principle of processive movement of kinesins along microtubules.

The process consists of several ATP/ADP states of both head domains and conformational changes of the neck linker: First, head 1 is bound tightly to the microtubule, while head 2 is unattached. The ATP binding of head 1 causes a conformational change in its neck linker domain, causing head 2 to move forward. Head 2 binds weakly to the microtubule and releases ADP. The hydrolysis of ATP at head 1 causes the detachment of head 1 from the microtubule and enhances the interaction of head 2 with the microtubule. Modified from Cassimeris et al. 2011.

In this way a single kinesin can “walk” processively along a microtubule, taking several hundreds or even thousands of steps before falling off the microtubule or reaching the end. During its walk, at least one head domain is always bound to the microtubule. However, not all kinesins move in a processive manner and they do not need to. Some kinesins detach from the microtubule after each step to allow other motor proteins to move the same substrate without constraining each other. These non-processive motors often work together in groups and large arrays, for example the kinesin ATK1 in the meiotic spindle of *A. thaliana*⁷⁴⁻⁷⁶.

Most kinesins are either plus-end directed or minus-end directed and cannot change their directionality unlike dynein⁷⁷⁻⁷⁹. It was thought that the direction of movement is determined by the position of the motor domain within the protein. All known minus-end directed kinesins are clustered in the family 14. Most of these kinesins contain either a C-terminal motor domain or an internal motor domain flanked by other domains. Most plus-end directed kinesins contain a N-terminal motor domain^{67,80}. Remarkably, kinesins seem to be not restricted to one direction and can in fact be bidirectional. So far, two kinesins have been found that are able to move to both sides of the microtubule: The *Drosophila* kinesin-14 motor Ncd that usually moves towards the minus-end, changes its direction to the plus-end by a

single amino acid change. This mutation is located in the neck region of Ncd, indicating that not the motor domain itself is responsible for the directionality but the formation of the neck^{57,81}. The other bidirectional kinesins were found in yeast. As a single molecule the kinesin-5s Cin8 and Cut7 move toward the minus-end, when they form clusters in the mitotic spindle though, Cin8 and Cut7 become plus-end directed⁸²⁻⁸⁵.

To this day, many different kinesins have been found in eukaryotic cells, displaying the high diversity in their structure and function. All these kinesins could be classified according to their structure and/or functionality into 17 families, of which 10 are present in *Arabidopsis thaliana* (**Figure 6**)⁸⁶⁻⁹⁰.

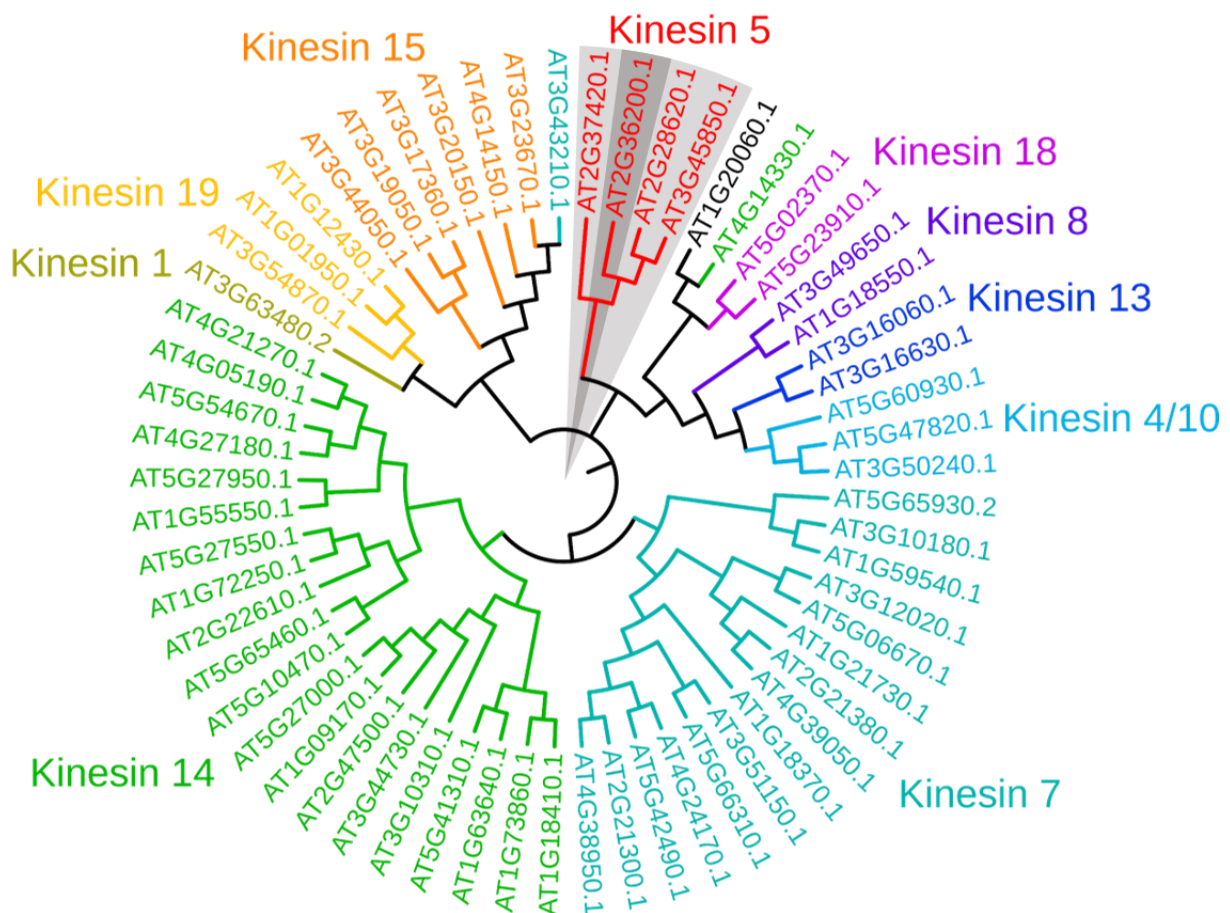


Figure 6: Phylogenetic tree of all 61 kinesins in *Arabidopsis thaliana*.

Phylogenetic tree coloured according to kinesin families proposed by Wickstead et al. 2010. The tree was calculated by “Clustal Omega” based on an alignment of the complete amino acid sequence of all annotated 61 kinesins in *A. thaliana*. The tree was annotated and coloured with “iTOL”. The kinesin 5 family and At2G36200.1 (AtKRP125b) are highlighted in grey.

A number of kinesins from several families are involved in mitosis. In *Arabidopsis thaliana* kinesins of the families 4, 5, 7, 13 and 14 are up-regulated and active during mitosis⁹¹. The kinesins of the families 4, 7 and 13 are mainly involved in chromosome movement. Kinesin-7, for example, is bound to the kinetochore and can attach to growing microtubules and thereby

link chromatids to the mitotic spindle. For the alignment of chromatids at the metaphase plate, kinesin-13 and kinesin-4 are responsible. Kinesin-13 is a microtubule depolymerase and shortens the microtubules on the side that is further away from the spindle pole, while the other side continues to grow. Kinesin-4 is located at the chromosome arms and is responsible for driving them away from the poles^{92,93}. For the assembly and maintenance of the mitotic spindle, kinesin-5 and 14 are of particular importance. The homotertrameric kinesin-5 can crosslink microtubules and slide anti-parallel microtubules apart. Kinesin-14 dimerises and can bind to microtubules with its tail-domain, as well as with its head domain, resulting in a crosslinking. As a minus-end directed motor, it seems to replace dynein and the dynein complex that is lost in the flowering plant lineage⁹⁴. These motor proteins work antagonistically and build opposing forces to maintain the spindle bipolarity and the focusing towards the spindle poles^{93,95}.

1.5 The kinesin-5 family

Kinesins of the kinesin-5 family are present in almost all eukaryotic organisms and are especially important in the formation and maintenance of the mitotic spindle. The loss or inhibition of kinesin-5 has a dramatic and often lethal effect on the organism. The bipolar spindle formation is severely compromised, forming uneven mono-polar spindles, resulting in disorganisation of chromatids and cell cycle arrest. Daughter cells are often misshaped and show aneuploidy⁹⁶⁻¹⁰³.

Kinesins of this family form a homotetramer, resulting in a bipolar structure with two head domains on each end of a central stalk. This structure allows kinesin-5s not only to interact with two microtubules but also to move along both of these microtubules at the same time. Other kinesins that are able to crosslink microtubules are fixed to one microtubule by an interaction with their tail-domain, while the motor dimer can move freely on the other microtubule¹⁰⁴. Though it is known that kinesins often dimerise by the interaction of coiled-coil domains along their stalk, a special form of coiled-coil structures can be found in kinesin-5s. This bipolar assembly (BASS) domain provides a mechanically stable junction to form the tetramer, transmits forces between the opposing motor dimers and ensures a uniform length of the kinesin-5 tetramer of about 79 nm (**Figure 7**)^{105,106}.

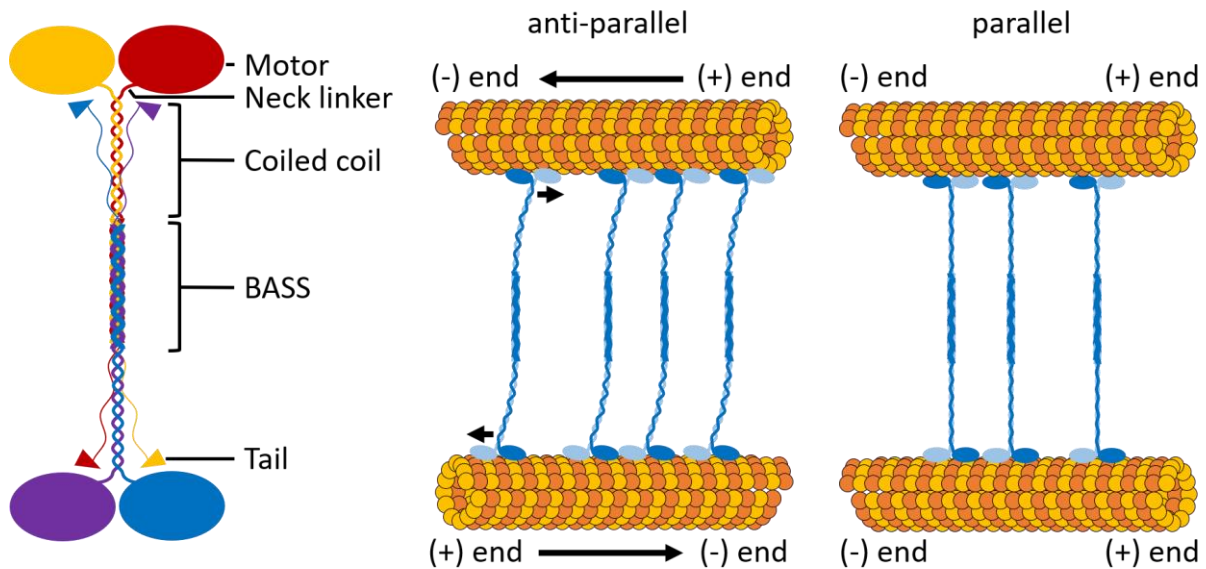


Figure 7: Structure and microtubule crosslinking of kinesin-5.

Kinesin-5 forms a homotetramer consisting of four identical subunits. Each subunit is classified in different functional domains: the motor domain with an ATP and microtubule binding site; a flexible neck linker, attaching the motor domain to the following domains; a coiled coil domain for dimerisation of two motor domains; a bipolar assembly (BASS) domain, ensuring a stiff connection of all four subunits in a protein microfilament, strong enough to transmit forces; and a tail domain that can interact with the motor domain of the opposite site and even neighbouring kinesin-5 tetramers, reducing the ATP hydrolysis of the motor domain.

Kinesin-5 is able to crosslink microtubules by its bipolar structure. Each end of the homotetramer is able to interact with a microtubule. Anti-parallel microtubules slide apart by each kinesin-5 end moving towards the plus-end of the respective microtubule. Parallel microtubules are crosslinked but the movement of kinesin-5 does not result in a movement of the microtubule. Modified from Scholey et al. 2014 and Bodrug et al. 2020.

Typical for kinesin-5 motor proteins is their slow velocity compared to other kinesins that are involved in transport functions. The velocity of kinesins can be determined best in highly controllable *in vitro* assays. While canonical kinesin-1 can achieve velocities of up to 800 nm s^{-1} , the vertebrate kinesin-5 Eg5 only reaches a mean velocity of about 20 nm s^{-1} ^{107,108}. In so-called sliding assays, where Eg5 can bind to microtubules with both its motor dimers, the velocity adds up to about 40 nm s^{-1} ¹⁰⁹. This sliding velocity fits remarkably to the speed of microtubules sliding apart at the equator of the metaphase spindle of $30\text{-}40 \text{ nm s}^{-1}$ ¹¹⁰. Similar velocities, as well as the doubled velocity under sliding conditions, could be observed in the drosophila kinesin-5 KLP61F ¹¹¹.

Over the past years, more and more studies showed how important the non-motor tail-domain of kinesin-5 is for the typical functions of this motor protein. If the tail of kinesin-5 is deleted, it moves much faster along microtubules but is not accumulating to the mitotic spindle compared to full-length kinesin-5. Without the tail-domain, the crosslinking of microtubules by kinesin-5 is decreased ^{112,113}. Recent cryogenic electron microscopy revealed that the tail-domain interacts with the head domain of a neighbouring kinesin-5 tetramer and

stabilises the nucleotide-free and ADP states of its head domain. This slows down the ATP hydrolysis and enhances the microtubule interaction. Therefore, the tail-domain is probably responsible for the typical slow velocity of kinesin-5 by reducing the ATP turnover, and by stabilising the interaction with microtubules; the tail-domain allows the generation of high forces at both motor dimers. This model elegantly explains the different behaviour of kinesin-5 when in clustered and non-clustered state ¹¹⁴. For example, the velocity of full-length kinesin-5 increased significantly more under high ionic conditions compared to the velocity of kinesin-5 with a deleted tail ^{113,115}. These conditions decrease protein-protein interactions like the proposed tail-head interaction, resulting in a behaviour similar to a kinesin-5 without a tail-domain. Further, as stated afore, the yeast kinesin-5s Cin8 and Cut7 can change their direction, depending on whether they are moving alone or are in a cluster with other kinesin-5 tetramers. This bidirectionality can again be explained by the influence of the kinesin-5 tail-domain of one tetramer with the head-domain of another tetramer. Cin8 with a deleted tail domain behaves like a single tetramer even when it is next to other tetramers. However, the exact mechanism of this bidirectionality remains unclear ^{84,85}.

A number of posttranslational modifications and interaction partners often regulate proteins that are involved in such crucial and perfectly timed processes, like mitosis. One of the most common posttranslational modifications is the phosphorylation, where a phosphate group is bound to the amino acid serine, threonine, tyrosine or histidine by a kinase. This reversible modification alters the structural conformation of the protein and can thereby change its activity or function. In almost all eukaryotic organisms, kinesin-5 is phosphorylated at a highly conserved threonine in the BimC box of the motor domain. This phosphorylation is important for the binding to the mitotic spindle ^{116,117}. Other phosphorylation sites are located to the tail domain of kinesin-5 and can increase the affinity towards microtubules and alter the velocity ¹¹⁸. Especially important for its function in mitosis, are several phosphorylation sites that are activated by the checkpoint kinase M-CDK and the cell cycle kinase Wee1, which both are regulated by each other during the cell cycle ¹¹⁹⁻¹²³. Although it is known that kinesin-5 in plants often contain CDK phosphorylation sites, little is known about other phosphorylation sites ⁹¹. Another prominent way to regulate proteins and alter their conformation is the interaction with other proteins. The spindle assembly factor TPX2 (Targeting protein for Xklp2) for example, was first discovered in *Xenopus* egg extracts and is involved in the formation of spindle poles. TPX2 itself is phosphorylated during mitosis and is involved in the localisation

of Xklp2, a kinesin-5 from *Xenopus*^{117,124,125}. Further research with the human homolog revealed an interaction between the C-terminus of TPX2 and Eg5. TPX2 is able to reduce the velocity of Eg5 and stabilises its colocalisation to the microtubule, which is critical for the correct organisation and stability of the mitotic spindle¹²⁶. This interaction is again influenced by other proteins like HSP70 (Heat shock protein 70)¹²⁷.

As kinesin-5 is especially important in dividing cells, it came up as a potential target in cancer therapy. As cancer cells undergo mitosis far more often than normal cells, the impact of kinesin-5 inhibition on them would be more extreme. In a phenotype-based screen monastrol was found, a small cell-permeable molecule that affected the bipolar spindle formation of mitotic cells. Further studies revealed that this drug is specifically affecting Eg5¹²⁸. Most known mitotic inhibitors interfere with tubulin, leading to severe side effects in non-dividing cells. Monastrol interferes with the ATPase activity of Eg5 and decreases the microtubule interaction dramatically. Monastrol presumably causes a conformational change in the motor domain of Eg5, resulting in a faster ADP release after ATP hydrolysis, reducing the time Eg5 is bound to the microtubule¹²⁹⁻¹³¹. Monastrol is highly specific for Eg5 and closely related kinesin-5s and does not interfere with other kinesins¹³².

The most studied function of kinesin-5, is without doubt, its role in the assembly and maintenance of the mitotic spindle. However, in recent years several studies revealed that kinesin-5 is not limited to its actions in the mitotic spindle. Kinesin-5 has been intensely studied in neurons in the course of cancer and Alzheimer's disease research. It was discovered that Eg5 is not only expressed during mitosis but also in postmitotic neurons¹³³. It is also important for the migration of neurons and the growth of dendrites and axons. Treatment of immature neurons with monastrol had a distinct impact on the growth of dendrites and axons, due to altered microtubule transportation of different microtubule classes, resulting in deranged microtubule networks¹³⁴⁻¹³⁶. An overexpression of Eg5 in this context caused shorter axons and a decrease in anterograde microtubule transport frequencies^{135,137}. A comparable function in the organisation of microtubules outside of mitosis could be observed in *Drosophila* embryos¹³⁸. The overexpression of Eg5 in mice had a severe impact on the spindle formation and caused genomic instability and tumour formation¹³⁹. Further, the amyloid-beta peptide, an important key factor in the pathogenesis of Alzheimer's disease, can inhibit Eg5 and thereby alter the localisation of neurotransmitter receptors to the cell surface¹⁴⁰. In line with that, studies showed Eg5s direct function in the transport of vesicles

from the trans-Golgi network to the cell surface¹⁴¹. Finally, artificially generated kinesin-5 dimers proved a microtubule polymerisation-promoting activity by stabilising the protofilament binding at the plus-end of microtubules¹⁴².

1.6 Kinesin-5 in plants

Although kinesin-5s are well studied in animals, especially in neurons, the knowledge about kinesin-5 in plants is still scarce. Similar to animals the most important function of kinesin-5 is the development and maintenance of the spindle during mitosis. As mentioned afore, the number of kinesins in the genome can vary enormously between organisms, especially in the plant kingdom (**Figure 6**)^{80,90}. Even the substantially reduced genome of the unicellular red algae *Cyanidioschyzon merolae*, probably one of the eukaryotic organisms with the most simplified mitosis, can establish a functioning spindle apparatus with only five kinesin genes in its genome^{143,144}. Among them is a copy of kinesin-5, showing the crucial role of kinesin-5 for mitosis⁸⁰. The fundamental role of kinesin-5 in mitosis of plants became apparent in the first study of a kinesin-5 *in planta* by Asada, et al. (1997) in *Nicotiana tabacum*. The kinesin-5 TKRP125 (TOBACCO KINESIN RELATED POLYPEPTIDE OF 125 kDa) was colocalised with spindle microtubules, especially towards the equatorial plane during segregation of chromosomes. The fact that TKRP125 was isolated from phragmoplasts of BY-2 cells showed already TKRP125s role in more than just mitosis¹⁴⁵. Apparently, TKRP125 localises evenly to the microtubules of the phragmoplast and helps in organising phragmoplast microtubules. Further, it was found that TKRP125 is also involved in the development of the preprophase band and is also present during S-phase and G₂-phase¹⁴⁶.

A comparable localisation to the spindle, preprophase band and phragmoplast could be observed in carrots (*Daucus carota*). The two kinesin-5 related proteins, DcKRP120-1 and DcKRP120-2 show additionally a colocalisation with cortical microtubules during interphase. DcKRP120-2 even showed a strong signal in the mid-line of the phragmoplast, where only weak signals could be observed in the case of TKRP125 and DcKRP120-1¹⁴⁷.

In contrast to the colocalisation with microtubules during the interphase, kinesin-5 in the brown alga *Silvetia compressa* is localised inside the nucleus during interphase. During mitosis though, kinesin-5 is localised to the spindle apparatus as expected^{148,149}.

Arabidopsis thaliana is one of the most important model organisms for higher plants and contains at least 61 kinesin genes, of which four code for a kinesin-5 (**Figure 6**). Out of these,

only AtKRP125c has been studied more closely yet. A point mutation in the fourth exon of *AtKRP125c* (*At2g28620*) leads to a root-swelling phenotype with reduced growth anisotropy. The mutant, therefore called *rsw7* (*radially swollen 7*) shows a normal microtubule distribution and cell wall organisation¹⁵⁰. However, the spindle structure, preprophase band and phragmoplast are severely compromised. The altered spindle structure resembles those of animals after the inhibition of kinesin-5, underlining that AtKRP125c works in spindle organisation as well as preprophase band and phragmoplast organisation, just as TKRP125 does in *N. tabacum*. Additionally, AtKRP125c is localised to cortical microtubules during interphase, indicating an additional function in the organisation of cortical microtubules. Interestingly, this localisation was also observed when AtKRP125c was ectopically expressed in animal epithelial cells, whereas Eg5 does not colocalise with microtubules during interphase. Finally, AtKRP125c seems not to be affected by the afore mentioned Eg-5 specific inhibitor monastrol, contrary to kinesin-5 in *Silvetia compressa*, where the spindle becomes disorganised upon monastrol treatment^{103,149}.

Taken together, kinesin-5 in plants plays a vital role in the organisation and maintenance of the mitotic spindle, in the same way as it is known for animals and fungi. Additionally, kinesin-5 is important to develop plant unique microtubule arrays such as the preprophase band and the phragmoplast. The localisation of kinesin-5, however, differs from species to species, possibly due to different functions besides its mitotic function. Most of the studies on kinesin-5 in plants rely mostly on microscopic visualisation, the biochemical and biophysical properties of the protein have not been studied yet. More and more additional functions of kinesin-5 are revealed in animals and most likely many functions are still unknown in plants.

1.7 *Arabidopsis thaliana* AtKRP125b

Little is known about the *Arabidopsis thaliana* kinesin-5 AtKRP125b (ARABIDOPSIS THALIANA KINESIN RELATED PROTEIN 125b). It shows high homology to other plant kinesin-5s like tobacco TKRP125⁹⁰. The gene coding for AtKRP125b is one of four known kinesin-5 genes in *Arabidopsis* and located on the second chromosome, as are its two close homologs *AtKRP125a* and *AtKRP125c*. According to Klepikova et al. (2016), *AtKRP125b* is expressed predominantly in flowering organs, especially during the transition from SAM (shoot apical meristem) to inflorescence meristem and in the final inflorescence meristem. Additionally, a rather high expression was found in the carpels of young flowers. In leaves and seed development, the

expression of *AtKRP125b* was higher than in roots and seedling, particularly in the petioles but way lower than in flowering organs and meristems. In senescent organs, almost none expression for *AtKRP125b* was found¹⁵¹. The expression pattern of *AtKRP125b* is highly comparable to the expression pattern of *AtKRP125a* and *AtKRP125c*, the two other kinesin-5 genes on chromosome 2. Only the expression pattern of the fourth kinesin-5 gene *AtF16L2.60* is clearly different, showing a lower expression in flower meristems but therefore a much higher expression in leaves, sepals, petals and siliques. These analyses fit the findings of Vanstraelen et al. (2006) who also found an upregulation of *AtKRP125a*, *AtKRP125b* and *AtKRP125c* during mitosis. Further, they identified mitosis activation motifs (MSA) in the promoter region of all three upregulated kinesin-5 genes but not in *AtF16L2.60*⁹¹.

Brieske (2017) found *AtKRP125b* in a search for interaction partners of the E3 ubiquitin ligase SAUL1 (SENESCENCE-ASSOCIATED E3 UBIQUITIN LIGASE 1). Two independent tandem-affinity purification experiments in cooperation with the University of Ghent, one including the U-Box of SAUL1 and one excluding it, found several possible interaction partners of SAUL1, predominantly nucleus located proteins. The only protein present in all experiments was *AtKRP125b*. The interaction of *AtKRP125b* and SAUL1 was confirmed *in planta* by bimolecular fluorescent complementation (BiFC) in *A. thaliana* protoplasts. The interaction was visible in the cytoplasm and the nucleus¹⁵². Which parts of SAUL1 and *AtKRP125b* are interacting is still unknown, only an interaction of *AtKRP125b* with the U-Box of SAUL1 can be excluded, due to the results of the tandem-affinity-purification.

SAUL1, also known as PUB44 (PLANT U-BOX TYPE E3 UBIQUITINATION LIGASE 44), is part of the vast plant ubiquitination system. In this system, ubiquitin, a small protein of 8.5 kDa, is ligated to a target protein as a posttranslational modification leading to various fates for the target protein¹⁵³. The ubiquitination system consists mainly of three protein families, the ubiquitin-activating enzymes (E1), the ubiquitin-conjugating enzymes (E2), and the ubiquitin ligases (E3). E1 activates ubiquitin using ATP, which causes a conformational change of ubiquitin that allows it to bind to E2. The ubiquitin loaded E2 can then associate with E3¹⁵⁴. E3 can not only interact with E2 but is also associated with the target protein, making E3 to the most variable member of the ubiquitination system with a vast number of subfamilies such as the PLANT U-BOX TYPE E3 UBIQUITINATION LIGASES (PUBs)¹⁵⁵. Studies showed that the fate of the target protein is determined by the length of the ubiquitination chain added to the target protein by E2 and by posttranslational modification of ubiquitin itself, recognised

by special ubiquitin receptors^{154,156,157}. Depending on the ubiquitination, the target protein can either be degraded in the 26S proteasome¹⁵⁸, function in cell signalling such as kinase activation or DNA repair¹⁵⁹, or be labelled for transport and localisation^{160,161}.

SAUL1 is a member of the afore-mentioned PUBs consisting of a U-Box domain, for the interaction with E2¹⁶² and several ARMADILLO (ARM) repeats, known for their role in protein-protein interaction and association to the plasma membrane¹⁶³⁻¹⁶⁵. PUB genes are often differentially expressed under the influence of various stress treatments¹⁶⁶. In this context, *SAUL1* was found to be differentially expressed in an ABA experiment¹⁶⁷. Further studies revealed that SAUL1 is associated to the plasma membrane via the five C-terminal ARM repeats^{163,168}. The investigation of knockout mutants revealed that SAUL1 plays a vital role in plant immunity. The SAUL1 deficient mutant *saul1-1* showed an impressive autoimmune phenotype: If the ambient temperature was lower than 24 °C or if the relative humidity was below 80 %, *saul1-1* seedlings, as well as older plants started a simultaneous yellowing of all above-ground organs and an immediate growth arrest, while under normal growth conditions the mutant was indistinguishable from the wild type^{169,170}. Further studies linked this autoimmune phenotype with the SA pathway¹⁷¹ and pathogen-related (PR) genes were strongly up-regulated in *saul1-1*, indicating that the mutant phenotype is related to plant immunity¹⁶⁹. However, it was not clear if SAUL1 is involved in PTI (pattern triggered immunity) or ETI (effector-triggered immunity).

A temperature-dependent autoimmune phenotype could also be observed in mutants of CHS1 (CHILLING SENSITIVE 1),¹⁷². Both mutants, *saul1-1* and *chs1-2*, could be rescued by a knockout of *SOC3* (SUPPRESSOR OF CHS1-2, 3)¹⁷³, suggesting that all three proteins are involved in the same pathway. In fact, *SOC3* and *CHS1* are not only neighbouring each other on chromosome 1, their proteins, SOC3 and CHS1 interact and form a heteromeric NLR (Nod-like receptor) complex¹⁷⁴. It is hypothesised that the complex of SOC3 and CHS1 is in close proximity to SAUL1 and guards SAUL1, causing an ETI response when SAUL1 is knocked out or manipulated by pathogen effectors^{173,175}. SAUL1 itself is able to ubiquitinate a yet unknown target protein, most likely a negative regulator of the immune response¹⁷⁶.

Recent studies suggested additional functions of SAUL1 apart from ubiquitination. Tao et al. (2019) connected an unusual localisation of SAUL1, where it is localised in patch-like structures at the plasma membrane, to the tethering of MVB (multi-vesicular bodies)^{163,177}. These patches were formed after inducing the immune response and when only the last five ARM

repeats were expressed fused to a fluorescent tag. Interestingly, these patches colocalised with markers for MVB tethering.

As it is known, kinesin-5 not only maintains the spindle apparatus during mitosis but is also able to move vesicles along microtubules to the plasma membrane¹⁴¹, it is hypothesised that AtKRP125b plays a part in the newly discovered role of SAUL1 in MVB tethering.

During my master thesis, I started the characterisation of AtKRP125b. I performed *in vitro* assays with recombinant AtKRP125b from *Escherichia coli* and determined first motor characteristics: A crosslinking of microtubules and sliding events could be observed in sliding assays (SLA) and the gliding velocity could be estimated to be around 20 nm s⁻¹. However, only a small number of events could be obtained, due to problems with long-term motor functionality¹⁷⁸. Further, I was able to establish two T-DNA insertion lines, *kin5b-1* and *kin5b-2* and performed temperature shift experiments to compare those mutant lines with *saul1-1*. Finally, I narrowed down the intracellular localisation of AtKRP125b to the nucleus. However, not all results of the thesis were reproducible, which leads to the aim of this doctoral thesis.

Aim of the Doctoral Thesis

The highly conserved motor protein family kinesin-5 mainly acts in cell division processes such as the maintenance of the mitotic spindle or the formation of the phragmoplast. In recent years, additional functions of kinesin-5s, apart from cell division have been suggested, for example the transport of vesicles from the trans-Golgi network to the cell surface. The newfound interaction of AtKRP125b, one out of four Kinesin-5s in *Arabidopsis thaliana*, and the E3 ubiquitin ligase SAUL1, a protein involved in plant defence, led to the question of new possible functions of kinesin-5s within the plant kingdom. Therefore, this thesis aims at investigating the putative functions of AtKRP125b by applying (I) *in vitro* and (II) *in vivo* methods.

(I) Motility assays will be utilised to determine the biochemical and biophysical properties of AtKRP125b *in vitro*. In order to perform these assays, the reproducible production of recombinant motor protein is of major importance to guarantee sufficient amounts of pure protein. By optimising existing bacterial expression systems and establishing new eukaryotic expression systems, motility assays can be conducted and optimised to determine properties, such as the direction of movement or the velocity of AtKRP125b.

(II) Physiological functions of AtKRP125b will be examined, by using reporter gene constructs in order to determine the expression pattern of *AtKRP125b*. Furthermore, T-DNA insertion lines will be studied to gain knowledge about the involvement of AtKRP125b in physiological and developmental processes. Findings from the analysis of the T-DNA insertion lines shall be confirmed with the generation of new kinesin-5 knockout lines by using the CRISPR/Cas9 technology. Finally, the subcellular localisation of AtKRP125b will be determined by using fluorescently labelled fusion proteins in *A. thaliana* protoplasts and *Nicotiana benthamiana* leaf pavement cells.

In summary, these experiments will lead to the characterisation of AtKRP125b on multiple levels and give insight into new possible functions for Kinesin-5s in plants.

2 Results and Discussion

2.1 Results of *in vitro* experiments

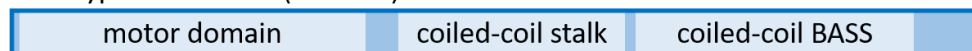
Ideally, biological processes are studied in their native environment. However, these environments are of high complexity and many components affect each other. To study the characteristics of a single component of a complex system it is often helpful to investigate them uncoupled from its cellular background in controlled *in vitro* experiments.

To study the biochemical and biophysical properties of kinesin motor proteins, certain *in vitro* experiments are well established and have been used to characterise many different kinesins^{67,179-181}. Advanced knowledge of these properties can give important information about the functions of the investigated motor protein.

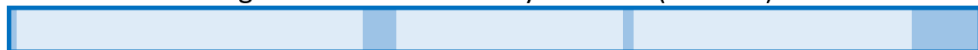
2.1.1 Expression and purification of AtKRP125b in *Escherichia coli*

In order to conduct *in vitro* experiments, it is necessary to provide sufficient protein of interest in appropriate concentration and purity. To obtain this, recombinant protein is expressed in special expression systems like several strains of *Escherichia coli*.

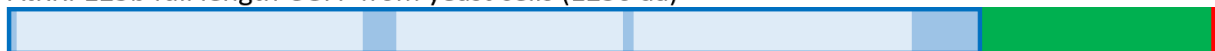
Wild type AtKRP125b (1009 aa)



AtKRP125b full length from bacterial and yeast cells (1015 aa)



AtKRP125b full length-eGFP from yeast cells (1250 aa)



AtKRP125b full length from insect cells (1026 aa)

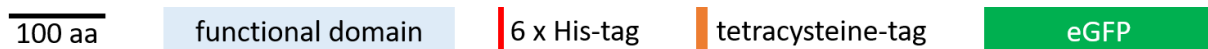
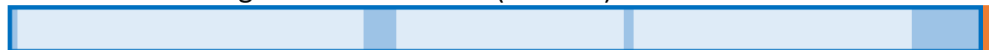


Figure 8: Schematic representation of the domain organisation of AtKRP125b.

The 1009 amino acids of AtKRP125b can be clustered into several functional domains, such as the motor domain at the N-terminus, a coiled-coil stalk domain for dimerisation and a coiled-coil BASS domain for tetramerisation. A 6 x His-tag was added for purification in all recombinant proteins. Additionally, a GFP-tag was added in a recombinant version from yeast. Recombinant protein from insect cells had an additional tetracysteine-tag for fluorescent labelling with FAsH. Domains were defined using “Conserved Domains” and “Wagawagga”.

Previously, the cDNA of *AtKRP125b* was cloned into the bacterial expression vector pQE80L via overlap extension cloning (OEC, see 4.3.9), adding a C-terminal 6 x His-tag to the sequence in the process (**Figure 8**)¹⁷⁸. Whereas a first expression in the *E. coli* strain BL21 pRARE was

successful, and the purification yielded sufficient functional protein that could be used in first *in vitro* assays, this was not the case in following expression experiments.

In this work, the expression construct from Strauß (2016) was therefore used to optimise the expression conditions in *E. coli* and the purification process. In a first attempt, an expression test was performed by transforming five *E. coli* strains with the construct and testing the expression under eight different conditions (see 4.5.4). Coomassie-stained PAGE gels showed an expected band of 115 kDa in several conditions and strains. The most prominent bands were received in BL21 pRARE cells and expression conditions of 18 °C in TB (terrific broth) media with either 20 or 200 µM IPTG (isopropyl β-D-1-thiogalactopyranoside), respectively.

A large-scale expression was carried out (see 4.5.5), followed by French-press-mediated cell lysis and affinity purification. Along with several smaller bands, a band of 115 kDa could be detected, correlating to the His-tagged AtKRP125b (**Figure 9 A**). The motor protein though was not functional in *in vitro* motility assays, presumably due to too harsh conditions during the cell lysis.

Another expression, followed by lysozyme-mediated cell lysis and affinity purification, revealed a similar picture: A band of the right size was found in a Coomassie-stained PAGE gel, along with several smaller bands, resulting in non-functional motor-protein (**Figure 9 B**).

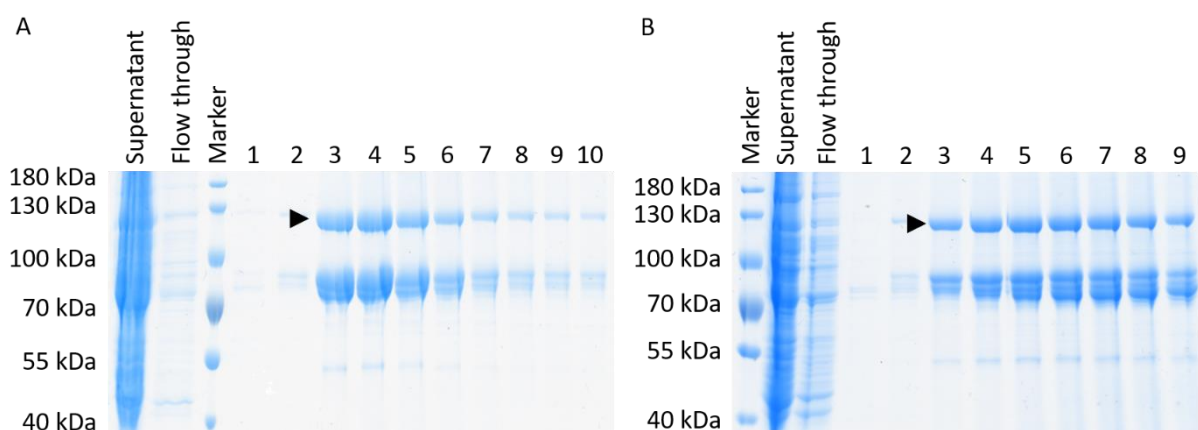


Figure 9: SDS-PAGE of AtKRP125b, purified from BL21pRARE after French press and lysozyme lysis.

A: Coomassie-stained SDS-PAGE gel of different fractions after affinity purification of AtKRP125b from BL21 pRARE cells, expressed in TB-medium at 18 °C and 0.2 mM IPTG (AtKRP125b at a size of 115 kDa, arrowhead). Cells were lysed by French press homogenising.

B: Coomassie-stained SDS-PAGE gel of different fractions after affinity purification of AtKRP125b from BL21 pRARE cells, expressed in TB-medium at 18 °C and 0.2 mM IPTG (AtKRP125b at a size of 115 kDa, arrowhead). Cells were lysed, using 1 mg ml⁻¹ lysozyme (Sigma-Aldrich/Merck).

To rule out a possible negative effect of the smaller bands on motor activity, a size exclusion chromatography (SEC) was conducted after affinity chromatography. Although SEC removed smaller peptides, there were still several larger bands that could not be separated even with

slow flow rates such as 0.1 ml min^{-1} (**Figure 10**). It is possible that these bands represent fragments of AtKRP125b that were not completely synthesised by the bacterial cell but could still interact with other kinesin-5 monomers to form tetramers. Such a tetramer of different AtKRP125b fractions could not be separated by SEC and would explain why no functional motor protein could be expressed in bacterial cells. In order to separate smaller fragments nevertheless, the tetramer would have to be dissociated into monomers first, for example by a controlled dialysis with molar quantities of urea ¹⁸². Preliminary experiments in this direction did, however, not yield the expected results. Another downside of SEC was the dilution of the protein sample resulting in a protein concentration that was too low for *in vitro* assays.

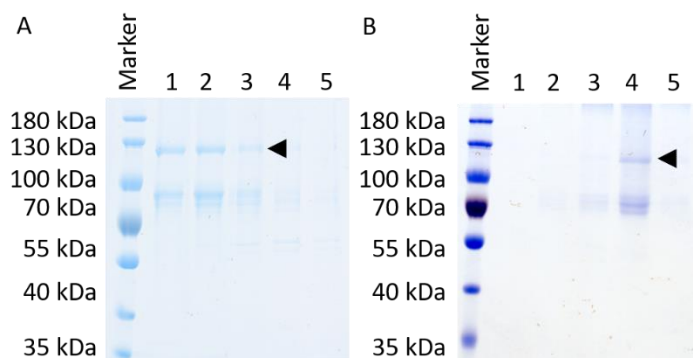


Figure 10: SDS-PAGE of AtKRP125b, purified from BL21 pRARE, after SEC.

A: Coomassie-stained SDS-PAGE gel of different fractions after affinity purification of AtKRP125b from BL21 pRARE cells, following SEC at 1 ml min^{-1} (AtKRP125b at a size of 115 kDa, arrowhead). Even after SEC bands of different size are present in each fraction.

B: Coomassie-stained SDS-PAGE gel of different fractions after affinity purification of AtKRP125b from BL21 pRARE cells, following SEC at 0.1 ml min^{-1} (AtKRP125b at a size of 115 kDa, arrowhead).

To enhance the protein yield of expression cultures and to compensate for the dilution of SEC, 3 % ethanol was added to the culture media after inoculation ¹⁸³. Although ethanol did boost the yield and concentration of the following expression (**Figure 11**), the protein was again not functional in *in vitro* assays.

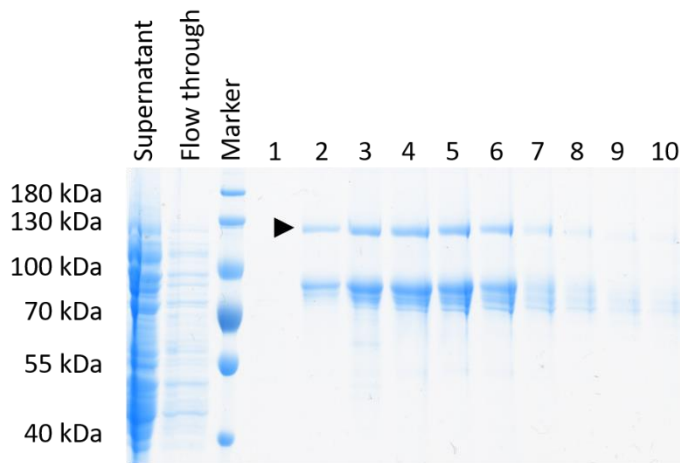


Figure 11: SDS-PAGE of AtKRP125b, purified from BL21pRARE, expressed with 3 % ethanol.

Coomassie-stained SDS-PAGE gel of different fractions after affinity purification of AtKRP125b from BL21 pRARE cells, expressed in TB-medium at 18 °C containing 0.2 mM IPTG and 3 % ethanol (AtKRP125b at a size of 115 kDa, arrowhead). Cells were lysed by French press homogenising.

In a last attempt to retrieve functional protein from *E. coli*, another cell lysis method was tested. When using high pressure homogenisation the cell is ruptured comparable to the procedure in a French press but much faster, thereby avoiding an overheating of the sample and reducing possible denaturation of the protein. Although this method worked well for other kinesin-proteins in the laboratory of Prof. Wim Walter (unpublished data), it did not work with AtKRP125b.

2.1.2 Expression of AtKRP125b in *Pichia pastoris*

The expression of eukaryotic proteins in prokaryotic expression systems like *E. coli* often leads to premature translation termination, or misfolding of proteins, due to missense substitutions^{184,185}. As there were many smaller bands visible in protein purifications from bacterial expression cultures, a eukaryotic expression system could help to gain a more functional recombinant kinesin-5 protein. The methylotrophic yeast *Pichia pastoris* has been used for heterologous protein expression for many years and is easy to cultivate. The *P. pastoris* expression system used the inducible promoter of the alcohol oxidase *Aox1* and *Aox2*, which was activated by the presence of methanol as a carbon source^{186,187}.

Two constructs were cloned from *AtKRP125b* cDNA into the *P. pastoris* expression vector pPICZαA by OEC. One full length construct with a secretion signal in the N-terminus and a C-terminal 6 x His-tag for affinity purification; and one full length construct with a C-terminal eGFP-tag for single-molecule tracking in stepping motility assays, additionally to the secretion signal and the purification-tag (**Figure 8**). These constructs were successfully introduced into

the yeast-strain X-33 and several recombinants were isolated by zeocin selection (see 4.5.6). It was even possible to isolate some clones from plates with high zeocin concentrations, which probably had integrated the construct into their genome several times, promising a higher yield than single integrations. Optimisation of cultivation and expression conditions, for example, the analysis of several time points after induction, or the testing of different methanol concentrations of the expression media, was controlled by SDS-PAGE and Western blot. However, no recombinant AtKRP125b could be detected by using α -His-antibodies neither in the sediment fraction nor in the supernatant, even though a positive control with His-tagged AtKRP125b from bacteria cells was easily detected. One reason for this could be a problem with the translation of AtKRP125b, as this gene was not codon-optimised, and the codon usage of yeast and plants can be very different in some parts^{188,189}. Another frequent problem with the *Pichia* expression system is the premature termination of transcripts due to AT-rich regions. In such a case, the detection of protein residues would be complicated with an anti-His antibody that uses the His-tag at the very end of the protein for interaction^{190,191}. Finally, the production of a functional kinesin-5 in such high amounts could be toxic for the yeast cells, even though the protein should be secreted, and could thereby cause their death or the activation of appropriate counter measurements like gene silencing^{139,192,193}. However, in such a case even small amounts of AtKRP125b should be detectable in the highly sensitive Western blot.

2.1.3 Expression and purification of AtKRP125b in insect cells

As the expression in yeast did not yield the desired results, another eukaryotic expression system was tested. As Korten et al. (2016) impressively showed, the long-term stability and motor performance are significantly increased when kinesins were expressed in insect cells instead of bacterial cells¹⁰⁷. Since the cultivation of insect cells is a very time-consuming and fragile task, the resources to maintain such a culture in the molecular plant physiology group could not be established¹⁹⁴. Thankfully, a cooperation with Dr. Astrid Sydow and Dr. Gunnar Baermann from the group of Prof. Dr. Aepfelbacher at the Universitätsklinikum Eppendorf in Hamburg opened the possibility to test the heterologous expression of kinesins in insect cells. For that purpose, the cDNA of *AtKRP125b* was cloned into the insect cell expression vector pFastBac1 by OEC, adding a 6 x His-tag and a tetracysteine-tag for fluorescent labelling to the C-terminus in the process (**Figure 8**). This construct was successfully introduced into bacmid

DNA, required for transfection of insect cells and production of recombinant baculovirus particles. In a first attempt, the expression was carried out in Sf9-cells from ovarian tissue of the fall armyworm *Spodoptera frugiperda*¹⁹⁵. Problems in the purification process and a general low yield made it impossible to detect any protein apart from the positive control from bacterial cells (**Figure 12**).

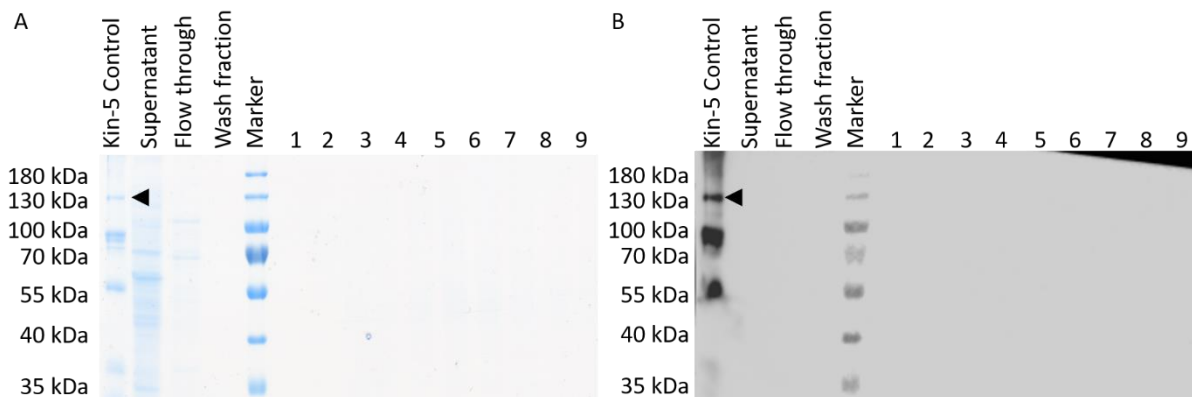


Figure 12: SDS-PAGE and western blot of AtKRP125b, purified from Sf9-cells.

A: Coomassie-stained SDS-PAGE gel of different fractions after affinity purification of AtKRP125b from Sf9 insect cells. Apart from control (AtKRP125b at a size of 115 kDa, arrowhead), no bands of the right size are visible.

B: Western blot of the same purification, detected with anti-His antibodies. Except from the control, no bands were detected.

In a second attempt, another strain of insect cells, High Five (BTI-TN-5B1-4) cells originating from the ovary cells of the cabbage looper *Trichoplusia ni* were used, promising a higher production of recombinant protein than Sf9-cells^{196,197}. In fact, after cell disruption by high pressure homogenising, followed by affinity purification, a clear band of 115 kDa could be observed in Coomassie-stained SDS-PAGE gels, as well as in Western blots (**Figure 13**). The purified protein proved to be functional at last and was used in the following motility assays.

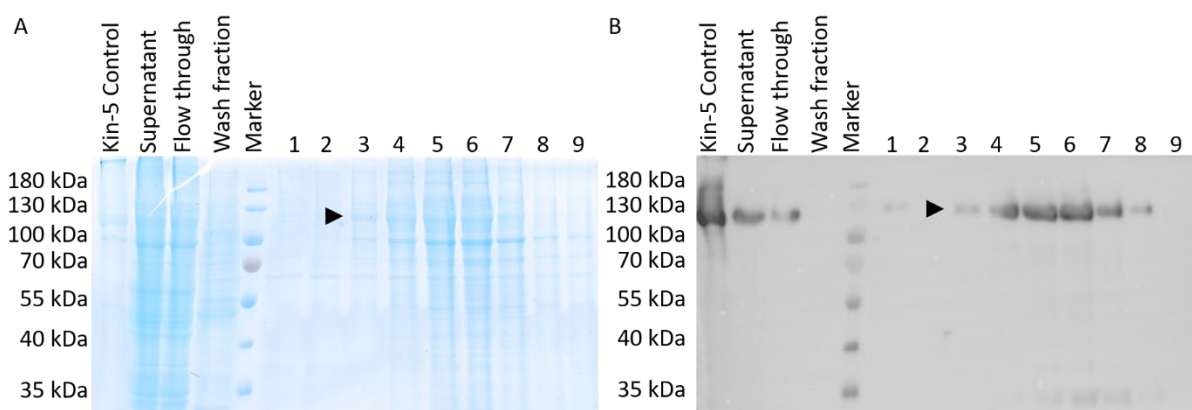


Figure 13: SDS-PAGE and western blot of AtKRP125b, purified from High Five cells.

A: Coomassie-stained SDS-PAGE gel of different fractions after affinity purification of AtKRP125b from High Five insect cells. Bands are visible at a size of approximately 115 kDa (arrowhead), the according size of AtKRP125b.

B: Western blot of the same purification, detected with anti-His antibodies. Bands are visible at a size of approximately 115 kDa (arrowhead), the same size as the Kin-5 control from an earlier purification.

2.1.4 KIN5b moves along microtubules towards the plus-end at a low velocity.

One of the most important properties of motor proteins, regarding their function, is to move in a certain direction at a distinct velocity. Whereas the position of the motor domain and the structure of the neck linker indicate a plus-end directed movement for most kinesin-5s, studies showed that the yeast kinesin-5 motor proteins Cin8 and Cut7 were able to move into both directions of the microtubule⁸²⁻⁸⁴. To determine the direction of AtKRP125b movement along microtubules and to evaluate the velocity of this movement, gliding motility assays were performed (see 4.6.3). In these assays, fluorescently labelled, polarity-marked microtubules glide along a glass surface coated with AtKRP125b by anti-His antibodies. The movement of microtubules was captured by epifluorescent microscopy (**Figure 14**).

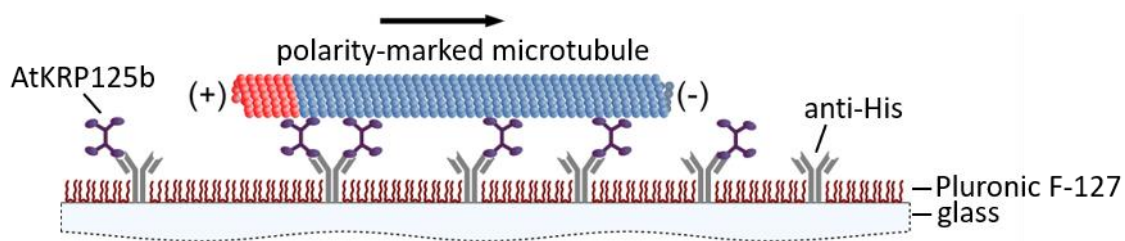


Figure 14: Schematic representation of a gliding motility assay.

Recombinant AtKRP125b is immobilized to a hydrophobic glass surface by anti-His antibodies. Polarity-marked fluorescent microtubules can slide along the surface, moved by AtKRP125b. Glass surface is blocked with Pluronic F-127 to reduce unspecific binding. Scheme kindly provided by Wim Walter.

Gliding assays showed that AtKRP125b was able to bind and transport microtubules. AtKRP125b moved polarity-marked microtubules in a unidirectional manner with a trailing plus-end, confirming the plus-end directed movement of AtKRP125b (**Figure 15 A and B**). The movement of 507 microtubule filaments was tracked with FIESTA and statistical analysis with MATLAB revealed a mean velocity of $17 \pm 8.8 \text{ nm s}^{-1}$ (mean \pm SD, **Figure 15 C**).

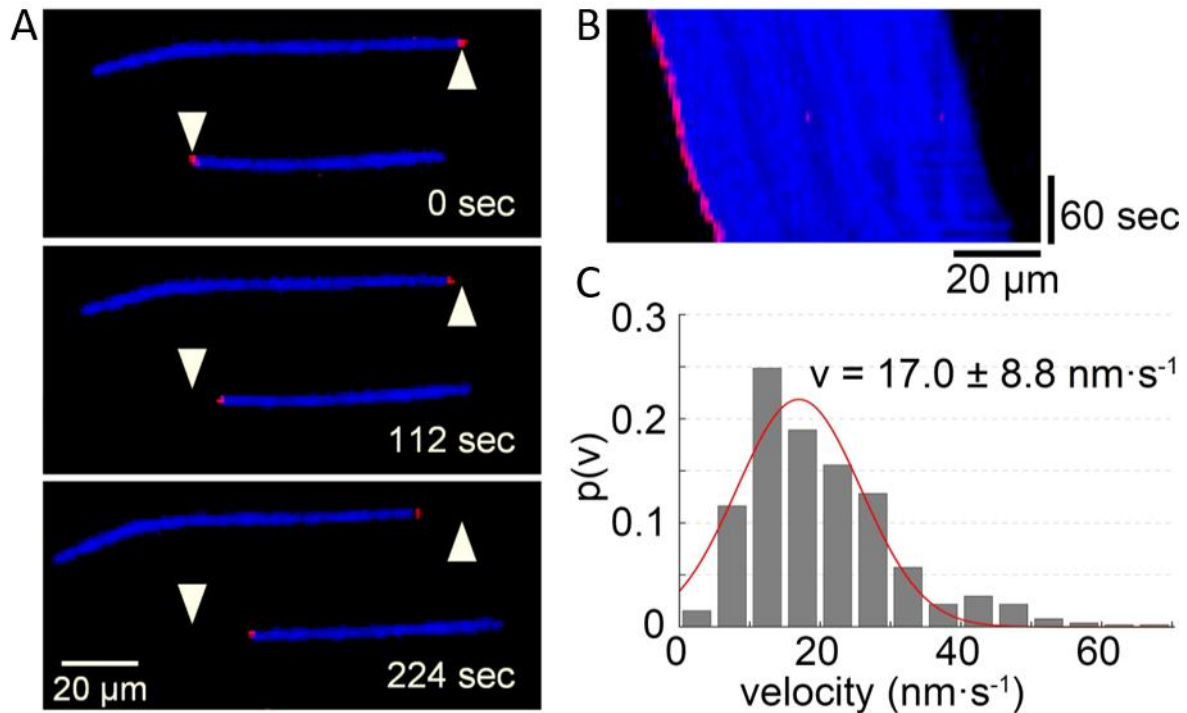


Figure 15: Gliding assay and velocity analysis of AtKRP125b.

A: Fluorescent micrographs of polarity-marked microtubules gliding along a AtKRP125b coated surface at different time points. The microtubule plus-end is labelled red, while the rest of the microtubule is blue. Arrowheads mark the starting point of each microtubule at time point 0 sec.

B: Kymograph of the lower microtubule shown in A.

C: Histogram of the mean transport velocities for 507 gliding microtubule filaments, transported by AtKRP125b in BRB80 at pH 6.9. A gaussian fit (red line) shows a velocity of $17 \pm 8,8 \text{ nm s}^{-1}$ (mean \pm SD).

This slow velocity is typical for kinesin-5 family members. Comparable studies on animal kinesin-5, showed a mean velocity of about 20 nm s^{-1} ^{109,198}. Of these, Eg5 from *Xenopus laevis* was determined to be plus-end directed as well¹⁰⁹.

2.1.5 Single AtKRP125b molecules move in a processive manner.

Another important property of motor proteins is their processivity, the way they are moving along microtubules. It has been intensively discussed, whether kinesin-5 is a processive or non-processive motor protein. A study with an artificially truncated version of human Eg5, resulting in a dimerised kinesin-5 version, showed that this protein is barely processive. Other forms of kinesin-5, however, showed a processive movement¹⁹⁹. As it is not required to be processive to slide microtubules apart²⁰⁰⁻²⁰³, the processivity of AtKRP125b is of high interest, because a processive motor would allow more diverse functions, such as long-range transport of cargo.

To determine the processivity of AtKRP125b, stepping assays were performed, in which single molecules of AtKRP125b are visualised by TIRF microscopy as they interact with microtubules

(**Figure 16**). To be able to detect single molecules in this assay, it was necessary to label AtKRP125b with a fluorescent tag. A truncated AtKRP125b version with an eGFP-tag was not functional in preliminary studies, probably due to the size of the tag¹⁷⁸. Other methods of labelling with smaller fluorophores were tested, such as Alexa Fluor 488. Alexa Fluor 488-NHS is an amine-reactive fluorophore and forms covalent bonds between the protein and the fluorophore²⁰⁴. However, AtKRP125b was not functional after the labelling process. The exchange of buffers during the labelling process probably damaged the fragile kinesin-5. To cope with these problems, we used a precise labelling technique with the small fluorophore FIASH, a biarsenic reagent, which binds to the cysteine residues of a specific tetracysteine-tag²⁰⁵⁻²⁰⁷. This tetracysteine-tag was integrated into the expression construct for insect cells (see 4.6.4).

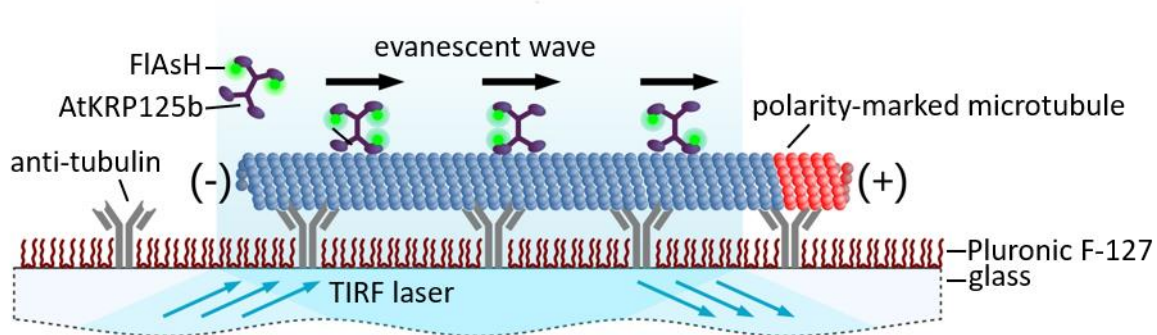


Figure 16: Schematic representation of a stepping motility assay.

Polarity-marked microtubules are immobilized to a hydrophobic glass surface by anti-tubulin antibodies. Recombinant AtKRP125b was fluorescently labelled with FIASH and binds to and “walks” along the microtubule. Single molecules can be detected in an evanescent wave with a special TIRF laser. Glass surface is blocked with Pluronic F-127 to reduce unspecific binding. Scheme kindly provided by Wim Walter.

These stepping assays revealed that single AtKRP125b molecules were moving along the microtubule in a processive manner without detaching for several micrometres, equalling several hundreds of steps (**Figure 17 A and B**). Additionally, the observation from the gliding assays, regarding the directionality of AtKRP125b was confirmed. All observed AtKRP125b molecules moved towards the plus-end of polarity-marked microtubules. As before, the movement of 122 single molecules were tracked in FIESTA and evaluated with MATLAB to determine a mean velocity of $11.3 \pm 12.5 \text{ nm s}^{-1}$ (mean \pm SD, **Figure 17 C**).

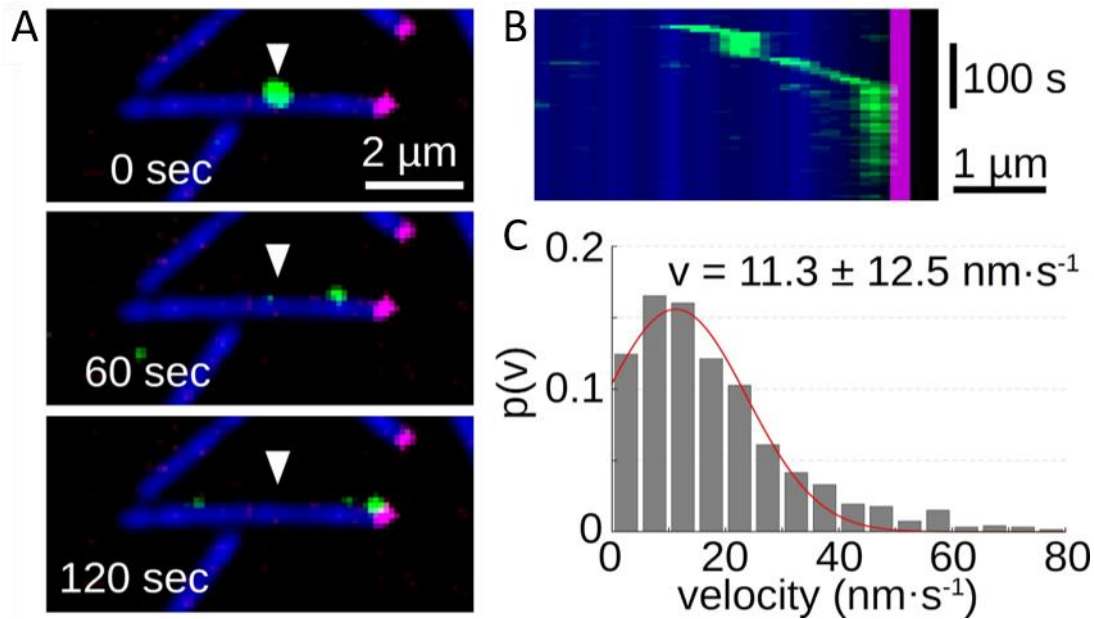


Figure 17: Stepping assay and velocity analysis of AtKRP125b.

A: Fluorescent micrographs of a single AtKRP125b molecule (green) stepping along an immobilized polarity-marked microtubule at different time points. The microtubule plus-end is labelled magenta, while the rest of the microtubule is blue. The arrowhead marks the starting point of the AtKRP125b molecule at time point 0 sec.

B: Kymograph of the stepping event shown in A.

C: Histogram of the mean transport velocities for 122 single-molecule stepping events in BRB80 at pH 6.9. A gaussian fit (red line) shows a velocity of $11.3 \pm 12.5 \text{ nm s}^{-1}$ (mean \pm SD).

These stepping assays show that AtKRP125b is able to move processively along microtubules in BRB80 with a pH of 6.9. Studies with Eg5 from *Xenopus laevis* showed that kinesin-5 is only processive at conditions with low ionic strength. At higher ion concentrations kinesin-5 starts to behave non-processively and gets diffusive¹¹⁵. Furthermore, it was found that the tail region of kinesin-5 is critical for a proper microtubule interaction¹¹³. If the tail domain is cleaved off, kinesin-5 shows a low processivity under normal ionic conditions, but is still able to move along the microtubule for several consecutive steps. In conditions with higher ionic strength, this tailless version of kinesin-5 is barely able to bind to microtubules at all and cannot move processively along them, indicating the importance of the tail domain and explaining why truncated versions of AtKRP125b were not functional.

2.1.6 AtKRP125b crosslinks microtubules and slides them apart.

Due to its bipolar structure with two motor domains at each end of a stalk, kinesin-5 can crosslink microtubules and slide them apart. To investigate whether AtKRP15b is able to crosslink microtubules and therefore have a role in the bipolar organisation of the mitotic spindle, sliding motility assays were carried out. In these assays, the motion of differently

labelled microtubules was observed in the presence of recombinant full length AtKRP125b under epifluorescence microscopy (**Figure 18**).

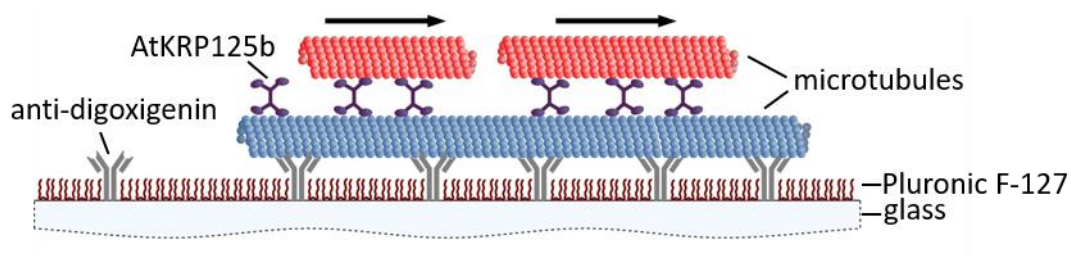


Figure 18: Schematic representation of a sliding motility assay.

Fluorescently labelled digoxigenin microtubules are immobilized to a hydrophobic glass surface by anti-digoxigenin antibodies. Recombinant AtKRP125b can bind to the immobilized microtubules and slide fluorescently labelled microtubules along the immobilized digoxigenin microtubules. The glass surface is blocked with Pluronic F-127 to reduce unspecific binding. Scheme kindly provided by Wim Walter.

In the presence of AtKRP125b, the movement of short microtubules along long, immobilised digoxigenin microtubules could be observed. Therefore, AtKRP125b crosslinks microtubules and slides them apart (**Figure 19 A and B**). 121 moving microtubules were tracked with FIESTA and a mean velocity of $11.7 \pm 5.2 \text{ nm s}^{-1}$ (mean \pm SD) was calculated with MATLAB (**Figure 19 C**).

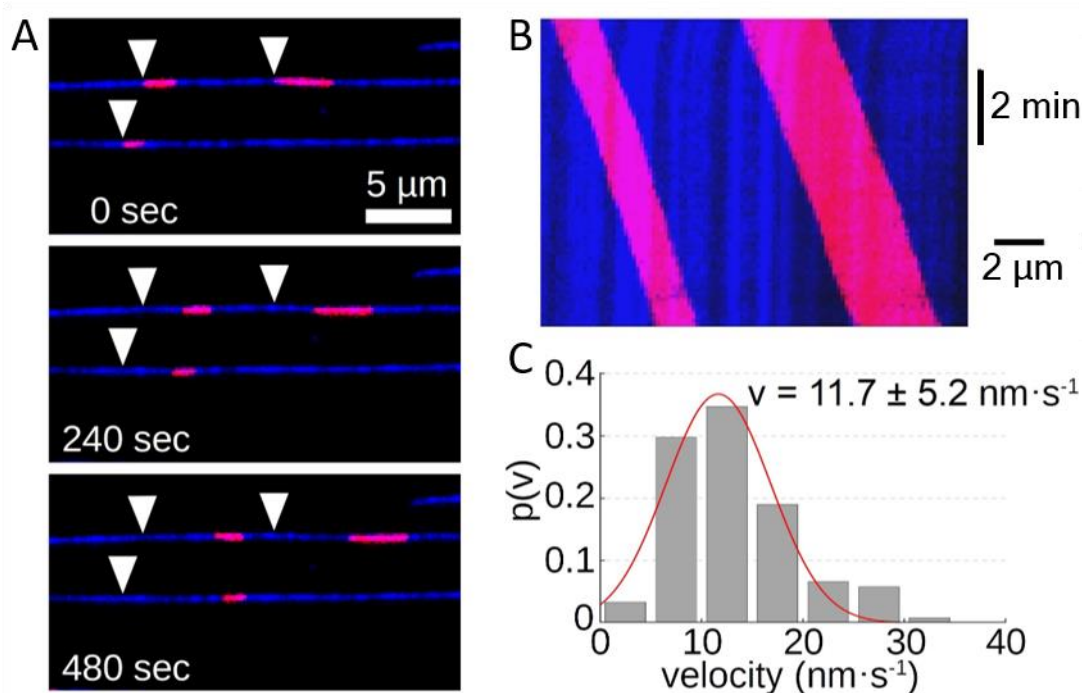


Figure 19: Sliding assay and velocity analysis of AtKRP125b.

A: Fluorescent micrographs of short microtubules (red) sliding along long, immobilized microtubules (blue) at different time points. Arrowheads mark the starting point of each short microtubule at time point 0 sec.

B: Kymograph of the upper blue microtubule shown in A.

C: Histogram of the mean transport velocities for 121 sliding microtubule filaments, transported by AtKRP125b in BRB80 at pH 6.9. A gaussian fit (red line) shows a velocity of $11.7 \pm 5.2 \text{ nm s}^{-1}$ (mean \pm SD).

It could be observed that not all cross-linked microtubules moved along the immobilised long microtubules. Some were just locked in place for the time of the observation or moved very slowly. Rare flipping events showed the reason for moving and non-moving microtubules: While most microtubules detached at the end of an immobilised microtubule, some flipped back onto the immobilised microtubule, thereby changing their orientation with regard to the long microtubule. After the flipping event, short microtubules stopped their movement almost immediately (**Figure 20**). This finding indicates that AtKRP125b crosslinks microtubules regardless of their orientation to each other but can move apart only those in a certain orientation to each other. It is likely that AtKRP125b continued to move between parallel microtubules towards their plus-end. However, since these are no longer in opposite directions, AtKRP125b gradually moves towards the same side with both motor dimers¹⁹⁸. The remaining shift, which can be observed in the assay can be explained by roadblocks on one of the microtubules caused by non-functional motor protein.

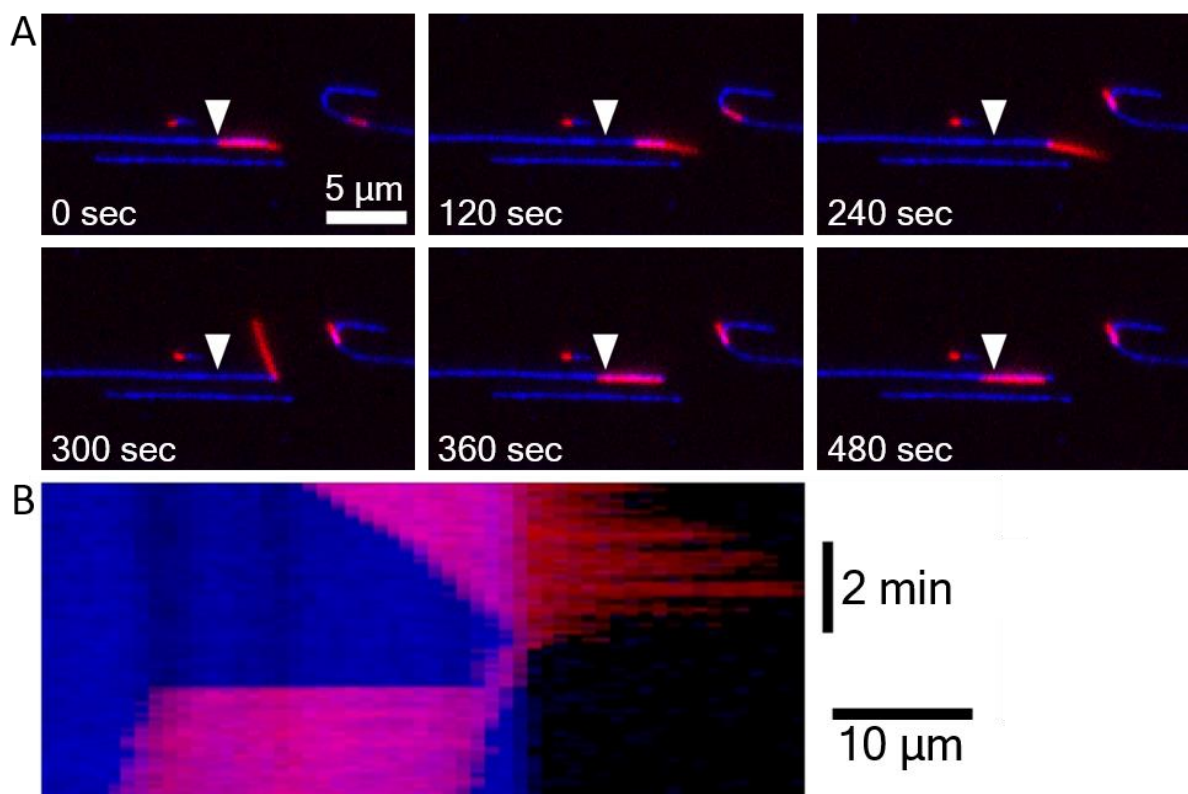


Figure 20: Flipping event during sliding assay.

A: Fluorescent micrographs of short microtubules (red) sliding along long, immobilized microtubules (blue) at different time points. The short microtubule moves to the end of the long microtubule and flips back onto it after 300 seconds. After the flipping event the short microtubule does not move at the same velocity anymore. The arrowhead marks the starting point of the short microtubule at time point 0 sec.

B: Kymograph of the event shown in A.

These findings match with studies of Kapitein et al. (2005), in which sliding assays with polarity-marked microtubules revealed that those microtubules are moved by kinesin-5 that are orientated in an anti-parallel fashion¹⁰⁹. As kinesin-5 is a plus-end directed motor protein, a dislocation of crosslinked microtubules only occurs if each end of the bipolar kinesin-5 moves in the opposite direction of the other. This leads to the rise of pushing forces in anti-parallel microtubules orientation and resisting forces in parallel orientation¹⁹⁸. This also suits the role of kinesin-5 within the mitotic spindle, where it can slide apart anti-parallel microtubules in the midzone and bundle parallel microtubules near the spindle poles.

Regarding the velocity measured in sliding assays with AtKRP125b, a higher velocity was expected. Since two gliding events take place simultaneously at both ends of the bipolar kinesin-5 in a sliding assay, the velocity was expected to be doubled in comparison to gliding assays as well. A doubled velocity of about 40 nm s^{-1} in sliding events was found in the aforementioned study with Eg5 from *Xenopus laevis*¹⁰⁹. This velocity also matches the speed of microtubules sliding apart at the equator of the metaphase spindle in cell free extracts from *Xenopus laevis* eggs of about $30 - 50 \text{ nm s}^{-1}$ ²⁰⁸. The results in this thesis showed an even slower velocity in sliding assays than in gliding or stepping assays.

The recent findings of Bodrug et al. (2020), regarding the function of the kinesin-5 tail domain, allowed an interesting hypothesis for kinesin-5 self-regulation that explains several contradicting findings in context with the velocity and processivity of kinesin-5s. Cryo-EM structure analysis revealed that the tail domain of one kinesin-5 tetramer interacts with the opposing motor domain of a neighbouring tetramer. Thereby, the tail slows down the ATP binding of the motor domain, resulting in a prolonged interaction between the motor domain and microtubule and a slower velocity¹¹⁴. This explains the often-observed velocity increase and loss of processivity under conditions with high ionic strength^{113,115}. Such conditions could weaken the interaction between the motor domain and tail domain. Further, the bidirectionality of kinesin-5 in yeast could be explained by this interaction and the clustering in microtubule overlap regions^{82-84,112}. In the case of AtKRP125b, an interaction between the motor domain and tail domain that slows down the ATP throughput of the motor domain could explain the extremely slow velocity measured in sliding assays. In gliding and stepping assays, molecules are too far away from each other to form clusters and interact, resulting in a higher velocity. In sliding assays, the tail-motor interaction can display its full potential and reduces the velocity even further. A slow velocity can bring interesting advantages. A study by

Shimamoto et al. 2018 showed a correlation between force production and velocity of Eg5 clusters. The slower the kinesin-5s move along a microtubule, the higher their generated pushing force¹⁹⁸. Due to their slow velocity the interaction time with the microtubule is increased compared to faster motor proteins. Therefore, kinesin-5 motor proteins can distribute the resulting forces very well among several motor proteins in a cluster and prevent the detachment of individual molecules¹⁹⁸.

Other reasons for the slow sliding velocity might be missing posttranslational modification due to the heterologous expression in insect cells. Muretta et al., 2018 showed how important posttranslational modifications are in regard to the “fine-tuning” of motor protein functions, such as force generation and velocity²⁰⁹.

Taken together, the *in vitro* data showed that AtKRP125b fulfils the canonical role of a kinesin-5 motor protein. It moves along microtubules towards the plus-end in a processive manner at a typically slow velocity of about 17 nm s⁻¹, comparable to studies on kinesin-5 from other species. Furthermore, AtKRP125b can crosslink microtubules and slides anti-parallel microtubules apart, while it bundles parallel microtubules, just as it is needed for the maintenance of the spindle apparatus during mitosis.

Due to limited protein amounts of AtKRP125b and its limited stability, it was not possible to study the direct interaction between SAUL1 and AtKRP125b in motility assays. To see, if SAUL1 is directly transported by AtKRP125b along microtubules or if SAUL1 alternates the biochemical and biophysical properties of AtKRP125b, has to be part of future studies.

2.2 Results of *in vivo* experiments

The just described *in vitro* experiments elucidated fundamental properties of the AtKRP125b protein. Whereas these properties will be important in the context of its role in *Arabidopsis*, the physiological functions of AtKRP125b still have to be uncovered by *in vivo* experiments.

2.2.1 *At2g36200/AtKRP125b* is not expressed in mitotic tissue.

One of the most essential strategies to learn more about the physiological function of a protein is to identify the tissues, in which the corresponding gene is expressed. To determine the expression pattern of *AtKRP125b* in the plant, the promoter activity was investigated with a reporter gene under the control of the *AtKRP125b* promoter region. For this purpose, the 851 bp in front of the start codon of *AtKRP125b*, in which the promoter region was

predicted²¹⁰, were cloned by means of OEC into the β -glucuronidase-containing vector pMDC162. This region represents the intergenomic region between *AtKRP125b* and *AT2G36210*, a small auxin responsive gene in front of *AtKRP125b*, as well as the 5' UTR of *AtKRP125b*. The construct was used to transform *A. thaliana* Col-0 plants via agrobacteria-mediated transformation. Selection with hygromycin resulted in ten transgenic lines that contained the construct and showed β -glucuronidase activity, indicated by blue staining.

The promoter activity was investigated at several developmental stages and in all organs. In one-day-old *pAtKRP125b::GUS* seedlings, most lines showed no promoter activity at all (**Figure 21 A and B**). At this early time point, only two lines showed very limited activity in the vascular tissue of the hypocotyl (**Figure 21 C**). Already one day later, blue staining could be observed in almost all lines, starting in the vascular tissue of the hypocotyl towards the vascular tissue of the root (**Figure 21 D and F**), as well as in the vascular tissue of cotyledons (**Figure 21 E**). In these young developmental stages, there was no promoter activity visible in meristematic tissue, where most of the mitosis takes place.

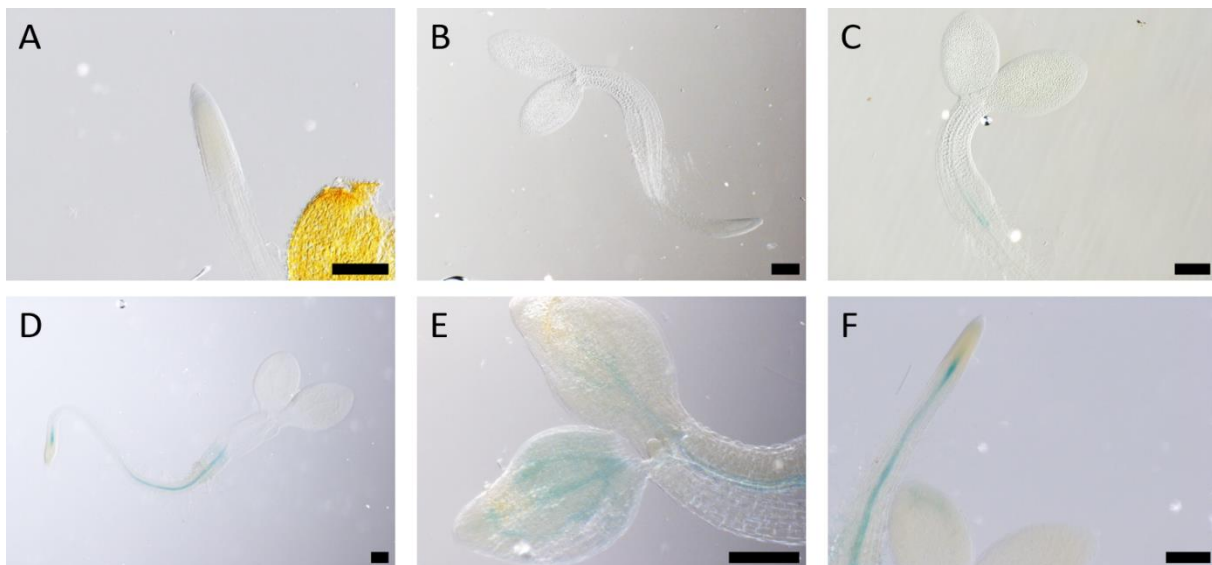


Figure 21: Macroscopic imaging of β -glucuronidase (GUS) activity under control of *AtKRP125b* promoter in young seedlings 1 and 2 days after germination.

GUS staining of young seedlings of *A. thaliana*, stained for 90 min at 37 °C with X-Gluc. One day after germination no promoter activity is present in any meristematic tissue (A, B). Only a very faint GUS staining is visible in the vascular tissue of the hypocotyl in some lines (C). After two days, more promoter activity is visible in the vascular tissue of the root (D, F) and the vascular tissue of the cotyledons (E). Scale bar represents 200 μ m in all images. Control staining of Col-0 WT is attached in Figure S9 in the supplement (see 6).

Eight days after germination, the promoter activity was visible in all 10 transgenic lines to some degree in a uniform manner. More specifically, an activity could be observed in the vascular tissue of roots and emerging lateral roots (**Figure 22 A-C**), starting at the root tip, near the elongation zone. The meristematic zones at the very tip of the main and lateral roots

remained unstained. Additional promoter activity was visible in the basal region of the hypocotyl as well as in the vascular tissue of neighbouring adventitious roots (**Figure 22 D**). In above-ground organs, activity was found at the stipulae of emerging leaves (**Figure 22 E**), the apex of cotyledons and true leaves and in their vascular tissue (**Figure 22 F-I**). Again, no staining was present in leaf tissues with high mitotic activity²¹¹.

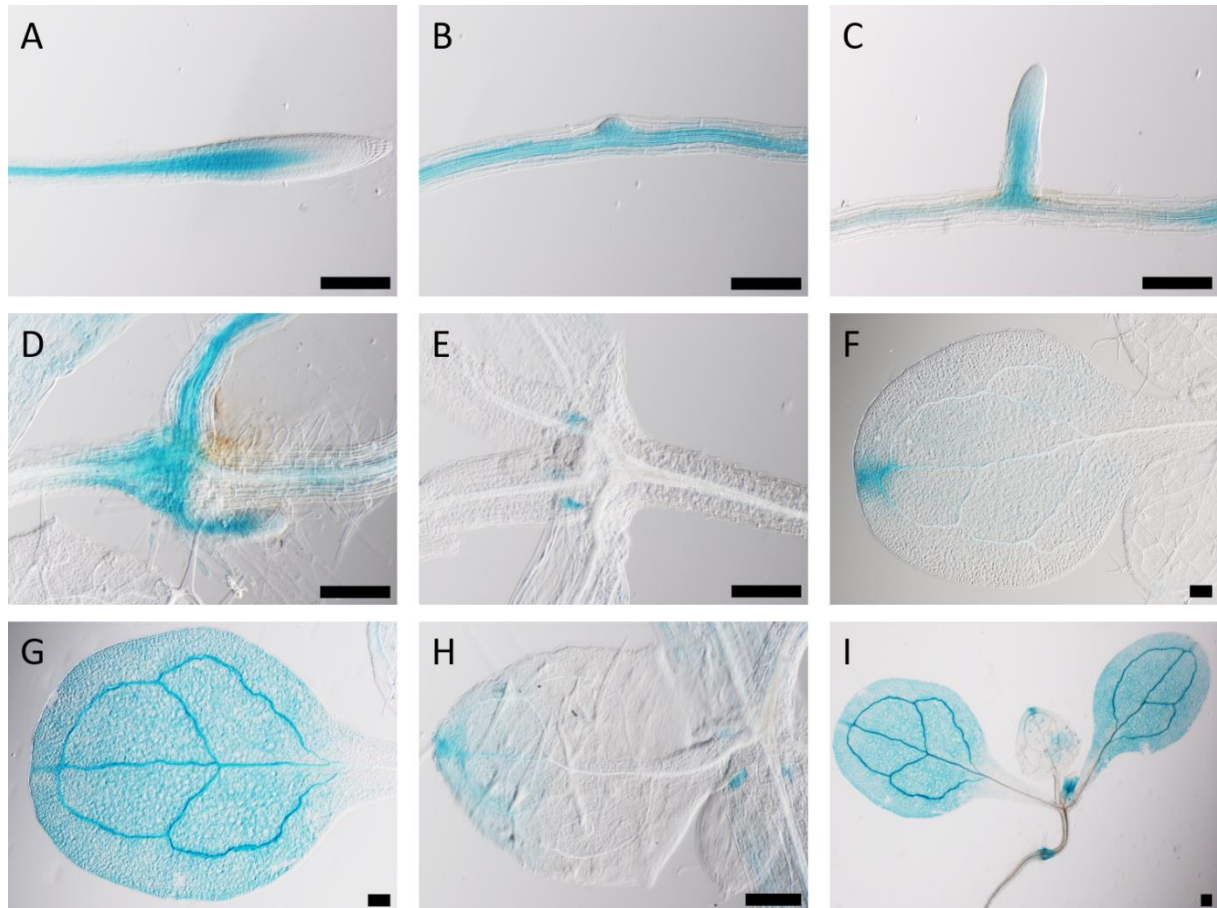


Figure 22: Macroscopic imaging of β -glucuronidase (GUS) activity under control of *AtKRP125b* promoter in vegetative organs, 8 days after germination.

GUS staining of vegetative organs of 8-day old *A. thaliana* plants, stained for 90 min at 37 °C with X-Gluc. An intensive GUS staining is visible in the vasculature of root tips (A) and emerging lateral roots (B, C), starting in the elongation zone. No promoter activity is visible in the root apical meristem and in lateral root meristems. The basal region of the hypocotyl, as well as adventitious roots shows intense *AtKRP125b* promoter activity (D, I). Further, promoter activity was visible in the stipulae of emerging true leaves (E, I), in the apex and vascular tissue of cotyledons (F, G, I) and true leaves (H, I). Scale bar represents 200 μ m in all images. Control staining of Col-0 WT is attached in Figure S9 in the supplement (see 6).

In a next step, the promoter activity of *AtKRP125b* in flowers and young siliques was observed in 24 day-old *pAtKRP125b::GUS* plants. There was no GUS-staining visible in the flowering meristems and the youngest inflorescence buds (**Figure 23 A-B**). Flowers in pre-anthesis though showed a clear staining in the vascular tissue of sepals (**Figure 23 A-E**). The promoter activity in sepals increased with the ongoing bud development. The developing stamen and pistil showed no promoter activity at this time point (**Figure 23 E**). After anthesis, the signal in

the vascular tissue of sepals decreased with the maturing of the flower and a clear signal emerged at the stigma of pistils, the connective tissue of anthers and in filaments of the stamen (**Figure 23 F and G**). The promoter activity in the stigma remained active even after the formation of the silique progressed (**Figure 23 H**). Additionally, a very noticeable activity could be observed in the connective tissue between silique and internode (**Figure 23 H**). Lateral buds showed a similar promoter activity pattern as the main inflorescence, with a strong signal in the vascular tissue of the cauline leaf and the sepals of older buds (**Figure 23 I**).

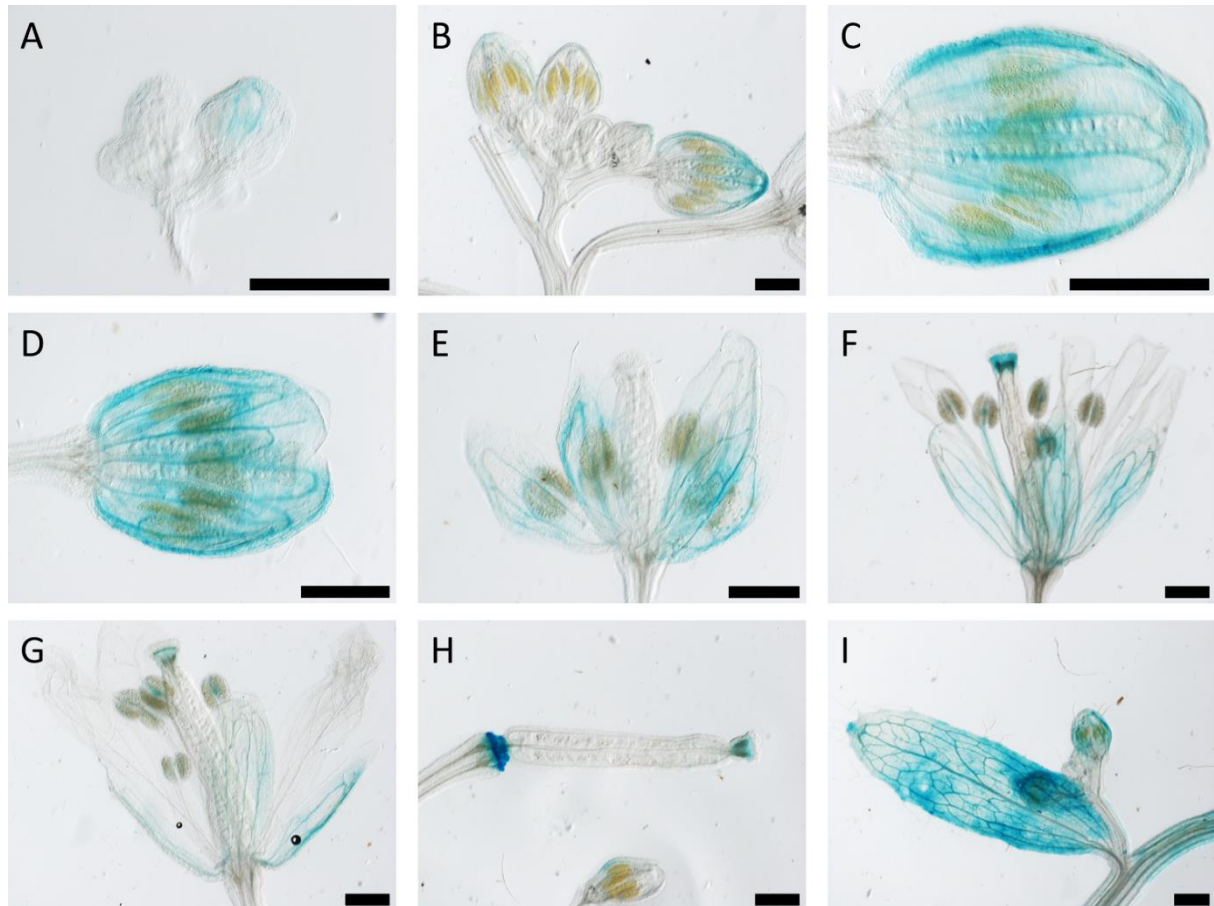


Figure 23: Macroscopic imaging of β -glucuronidase (GUS) activity under control of *AtKRP125b* promoter in flowering organs, 24 days after germination.

GUS staining of flowering organs of 24-day old *A. thaliana* plants, stained for 90 min at 37 °C with X-Gluc. Flowering meristems and youngest inflorescence buds show no promoter activity. With progressive development of buds, a faint GUS-staining is visible at the vasculature of the petals (A, B). The vascular staining of petals intensifies in pre-anthesis flowers (C-E), whereas, other flower organs show no promoter activity (E). Flowers after anthesis show a clear promoter activity in the stigma of the pistil and the connective tissue in the stamen (F, G). Young siliques present an intense Gus-staining in the internode between silique and pedicel, as well as a staining in the residues of the stigma (H). Axillary buds showed the same activity as the main buds. Cauline leaves presented a similar staining in the vasculature as true leaves in earlier stages (I). Scale bar represents 200 μ m in all images. Control staining of Col-0 WT is attached in Figure S9 in the supplement (see 6).

In all observed developmental stages of the plant, no promoter activity was present in mitotically active tissues, such as the root apical meristem or the flowering meristem, despite kinesin-5's canonical role in mitosis. These results strongly indicated that *AtKRP125b* may have

functions other than spindle organisation and phragmoplast development. However, these findings were also in contrast to the observed up-regulation of *AtKRP125b* during mitosis on a transcriptomic level in other studies^{91,151}. This discrepancy is possibly caused by missing regulatory elements in the used promoter sequence. Often regulatory elements can be found not only in the DNA in front of the start-codon but also within the first introns and exons. As it was not possible to transform agrobacteria with a construct containing the promoter region, followed by genomic *AtKRP125b* fused to GUS, the regulatory effect of intron-derived motifs or exon transcription factor binding sites could not be investigated²¹²⁻²¹⁵. Another reason for the up-regulation during mitosis might be an increase in transcript stability rather than an increase in promoter activity²¹⁶, although no staining was found at all in the respective tissues. However, it is not possible to infer potential functions from expression patterns alone. The expression pattern from transcriptome analysis of *AtKRP125c* is pretty similar to that of *AtKRP125a* and *AtKRP125b*, with the highest expression in flowering meristems and flowering organs¹⁵¹. Nevertheless, the *AtKRP125c* mutant *rsw7* exclusively showed a phenotype in the morphology of the roots, where the expression was below average¹⁰³.

2.2.2 T-DNA insertion lines of *AtKRP125b*

To investigate possible developmental abnormalities in the regions with promoter activity, two *AtKRP125b*-deficient mutant lines, namely *kin5b-1* and *kin5b-2*, were established and their phenotypes were observed.

Previously, it was shown that both lines were deficient of *AtKRP125b* mRNA¹⁷⁸. Here, the two T-DNA insertion lines were investigated in more detail. The line *kin5b-1* contained a T-DNA insertion in the fourth exon, whereas the line *kin5b-2* had an insertion within the promoter region of *AtKRP125b* (**Figure 24 A**). A repetition of the RT-PCR with the shoot and root RNA isolated separately, showed that line *kin5b-2* still contained the transcript of *AtKRP125b* and was thereby not a knockout mutant that could be considered in further experiments. The other line *kin5b-1* showed no expression of *AtKRP125b* at all, neither in the shoot nor the root (**Figure 24**). This knockout mutant was examined in detail with regard to its phenotype.

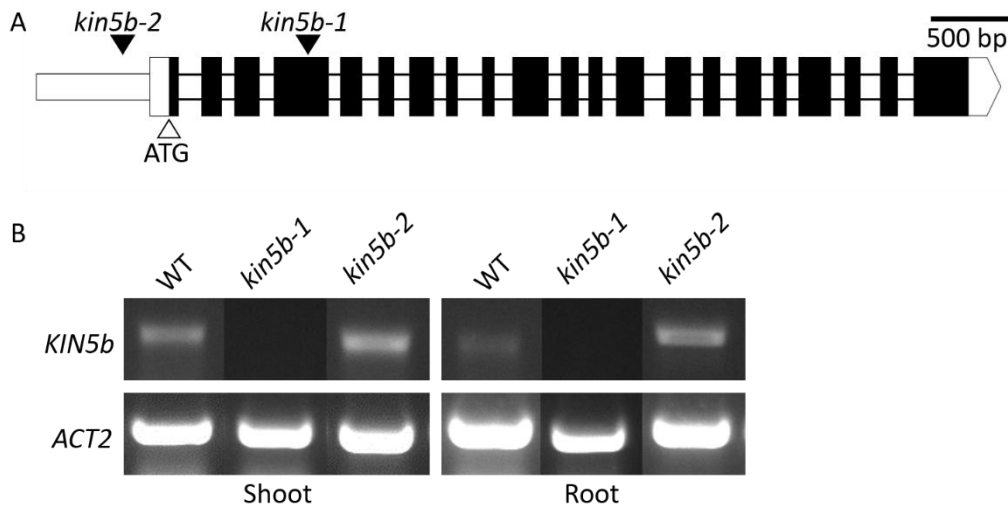


Figure 24: Position and RT-PCR of *AtKRP125b* T-DNA insertion lines.

A: Exon-Intron structure of *AtKRP125b*, including 5' UTR and intergenic region. Positions of T-DNA insertions are marked with black arrowheads. T-DNA insertion of *kin5b-1* is present in the fourth exon, and in the intergenic region in front of *AtKRP125b* for *kin5b-2*, respectively.

B: RT-PCR of T-DNA insertion lines performed with RNA, isolated from shoot and root. No transcript was detected for *kin5b-1*, but for *kin5b-2* a clear band is visible in both root and shoot RNA. Primers for *ACTIN2* were used as a positive control.

2.2.3 The knockout of *AtKRP125b* in *kin5b-1* did not result in distinct phenotypes.

In first experiments the general growth and development of *kin5b-1* plants were compared to WT plants during normal long-day growth conditions at 22 °C ambient temperature. Problems during mitosis often manifest themselves through a delayed or disproportional growth, due to aneuploidy or misshaped cells^{217,218}. This could not be observed for *kin5b-1*. The mutant line grew entirely within the natural variances of the WT, over several weeks (**Figure 25**).



Figure 25: Comparison of WT and *kin5b-1* plants during vegetative growth.

Col-0 WT and *AtKRP125b*-deficient *kin5b-1* plants were grown for 3 weeks on soil under long-day conditions at 22 °C. *kin5b-1* shows no growth delays or other abnormalities.

The inconspicuous growth could also be observed in subsequent stages of development. After five weeks under normal growth conditions, the plants had switched into reproductive growth

by bolting and developing flowers and first siliques. There was no visible difference between WT and *kin5b-1* in all organs (**Figure 26**). In summary, *kin5b-1* showed no abnormal phenotype in all aboveground organs under normal growth conditions.

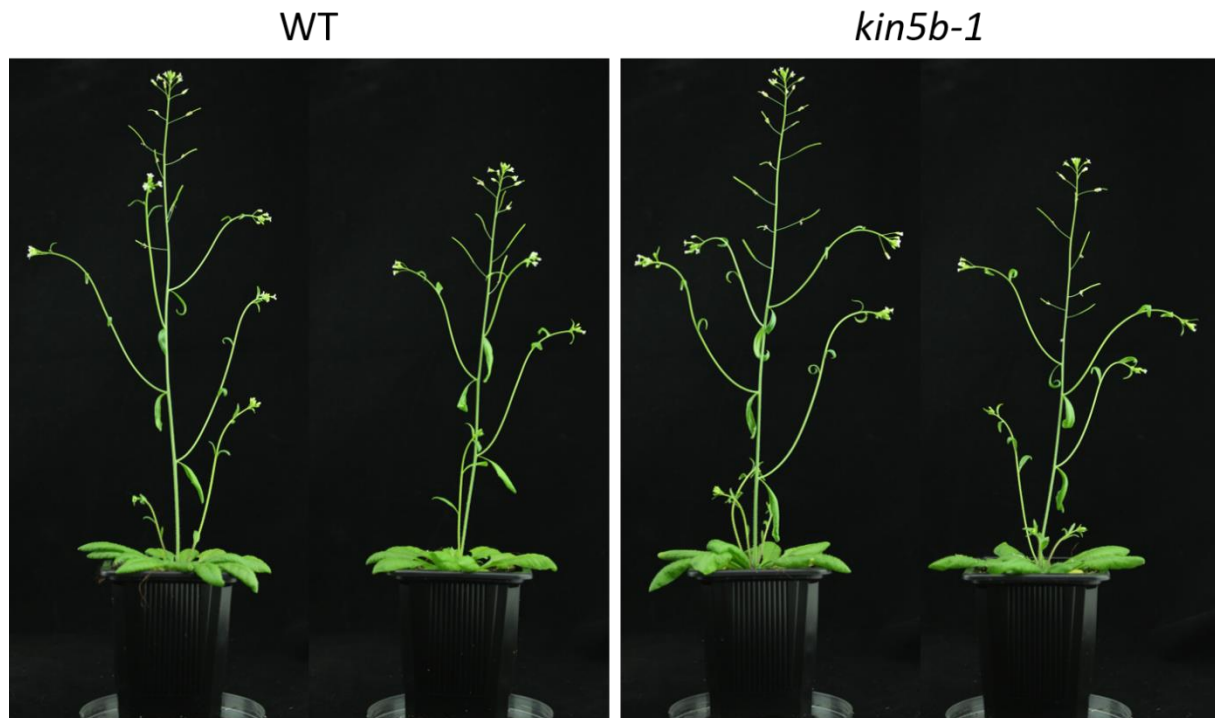


Figure 26: Comparison of WT and *kin5b-1* plants during reproductive growth.

Col-0 WT and *kin5b-1* plants were grown for 5 weeks on soil under long-day conditions at 22 °C. *kin5b-1* shows a normal growth after bolting. The formation of flowers and siliques is highly comparable to WT.

In the following, the root growth of *kin5b-1* was examined more closely, as a point mutation of *AtKRP125c* showed a root phenotype, too and *AtKRP125b* was expressed in roots (**Figure 21** and **Figure 22**)¹⁰³.

Furthermore, an attempt was made to induce a phenotype by applying abiotic stress. Salt stress is a well-studied and easy to apply abiotic stress that has especially severe consequences on the development of the root²¹⁹. As the root growth of *kin5b-1* was responding to salt stress in small-scale preliminary tests, the experiment was scaled-up. Therefore, 90 seeds of *kin5b-1* and its segregating WT were each sown in two rows on MS-medium plates and grown for seven days under normal growth conditions at 22 °C. Seven days after germination, the seedlings were carefully shifted in sterile conditions to new plates, containing 150 mM NaCl. In this way, all roots laid on the surface of the MS-medium and their growth could be investigated. For each plate, ten *kin5b-1* plants were placed in two rows next to ten plants of the WT, allowing a direct comparison between mutant and WT on each plate. In order to distinguish between salt stress and stress caused by the plant shifting itself, 30

additional plants of each line were transferred to normal MS-medium as a control. The plants continued to grow for another seven days and were documented on a flatbed scanner daily. It could be observed that the plants exposed to salt stress immediately restricted their growth substantially. After two days on the saline medium, the most WT plants had started to develop lateral roots, while the mutant remained without lateral roots. On the control medium, more mutant plants formed lateral roots compared to the saline medium (**Figure 27**). Mutant and WT plants cultivated on the control medium grew more uniformly and no difference could be observed at later time points. As the number of plants of the control group was too small and they started to grow into the second row of plants or the rim of the plate after three days on the new medium (**Figure 27**) these plants could not be used for a reliable comparison.

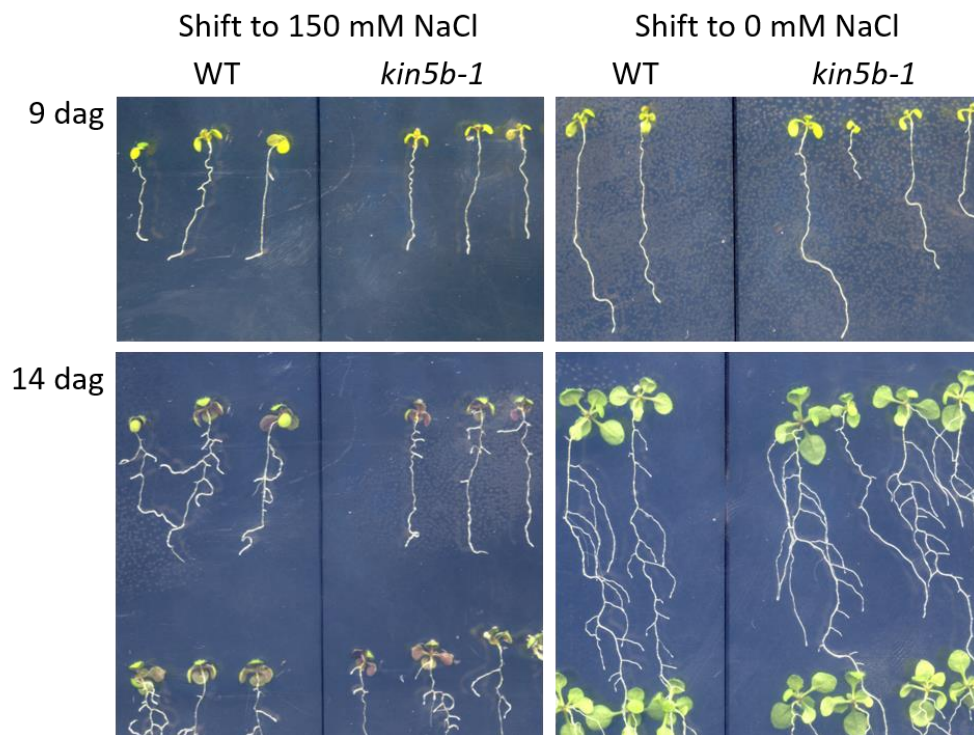


Figure 27 Comparison of WT and *kin5b-1* root growth after shift to salt stress.

90 plants of *kin5b-1* and its segregating WT were grown on MS-medium plates for 7 days at long-day conditions at 22 °C and were then shifted to new MS-medium plates containing 150 mM NaCl. As a control, 30 plants of each line were shifted to new MS-medium plates without additional salt (0 mM NaCl). 9 dag (2 days on the new plates) WT plants showed longer roots compared to the mutant when grown on MS-medium without salt. After 7 days on the new plates (14 dag) WT plants developed more lateral roots on the salt-plates. Mutant plants shifted to plates without salt seemed to grow as the WT.

A second experiment was conducted, placing the plants in only one row per plate. Again, 90 plants of *kin5b-1* and its segregating WT were each shifted to MS-medium containing 150 mM NaCl and 90 plants were shifted to normal MS-medium as a control. The plates were documented in the same way as in the first experiment on a flatbed scanner. After two days on the new medium, lateral and adventitious root started to emerge in WT and *kin5b-1* plants.

As observed in the first experiment, the root growth on the salt containing medium was rather erratic, with numerous directional changes and seemingly an absence of gravitropism. Both plant lines were severely affected by the saline medium, but the mutant showed even less root growth as the WT (**Figure 28**). On the contrary, the plants transplanted to fresh MS-medium continued to grow normally. Two days after the shift to new medium, the first lateral roots began to emerge in these plants, too. At this time, the main roots were already almost twice as long as those of the plants on the saline medium. In contrast to the first experiment, the mutant plants grew slightly slower compared to WT plants. Their leaves were smaller, the main root was shorter and the lateral roots started to emerge about one day later. This impression intensified after further days of growth: The main and lateral roots remained shorter in the mutant, the number of lateral roots was slightly lower and the size of the leaves was slightly smaller, compared to the WT (**Figure 28**). However, several mutant plants deviated from this overall picture and showed a similarly root growth as the WT plants.

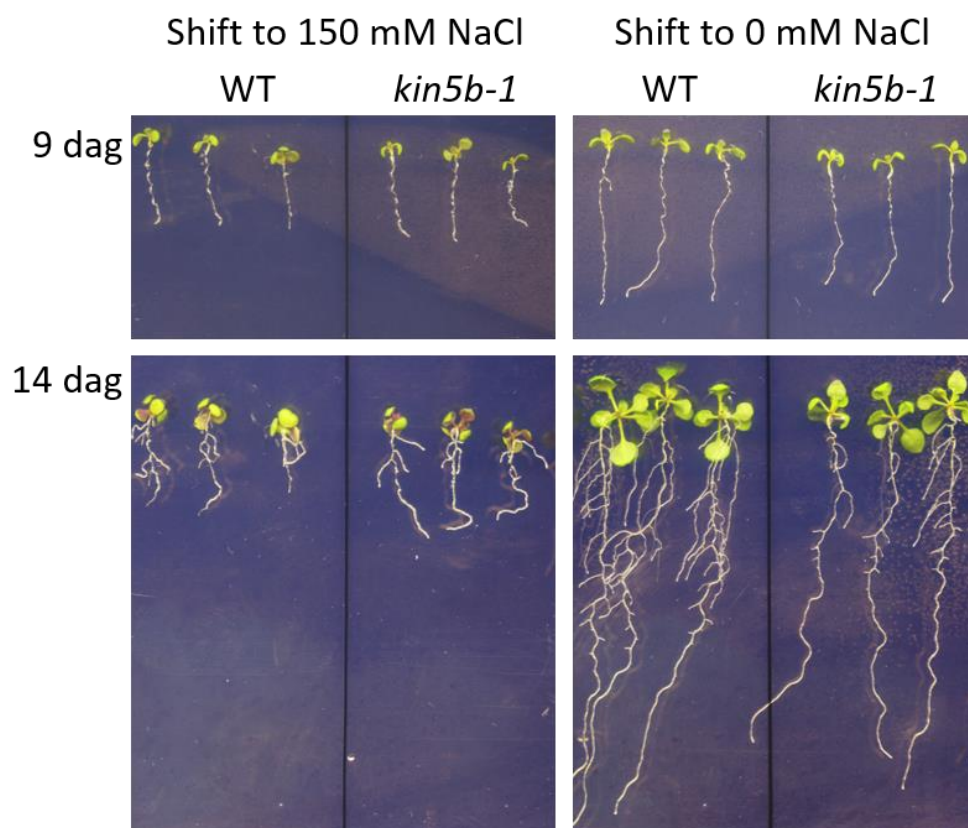


Figure 28: Comparison of WT and *kin5b-1* root growth after shift to salt stress in a second experiment.

90 plants of *kin5b-1* and its segregating WT were grown on MS-medium plates for 7 days at long-day conditions at 22 °C and were then shifted to new MS-medium plates containing 150 mM NaCl. As a control, the same number of plants was shifted to new MS-medium plates without additional salt (0 mM NaCl). 9 dag (2 days on the new plates) WT plants showed longer roots compared to the mutant when grown on MS-medium without salt. After 7 days on the new plates (14 dag) WT plants developed more lateral on the salt-plates. Mutant plants shifted to plates without salt seemed to have fewer and shorter lateral roots and shorter main roots, compared to the WT.

The evaluation of the total root size for each plant (see 4.4.9) showed a significant difference in the relative root size of WT and *kin5b-1*, under control conditions as well as under salt stress (**Figure 29**). Even directly after transferring the young seedlings onto fresh MS medium 7 days after germination, a significant size difference was measured in the root size of WT and mutant plants. The difference increased substantially over the course of the experiment.

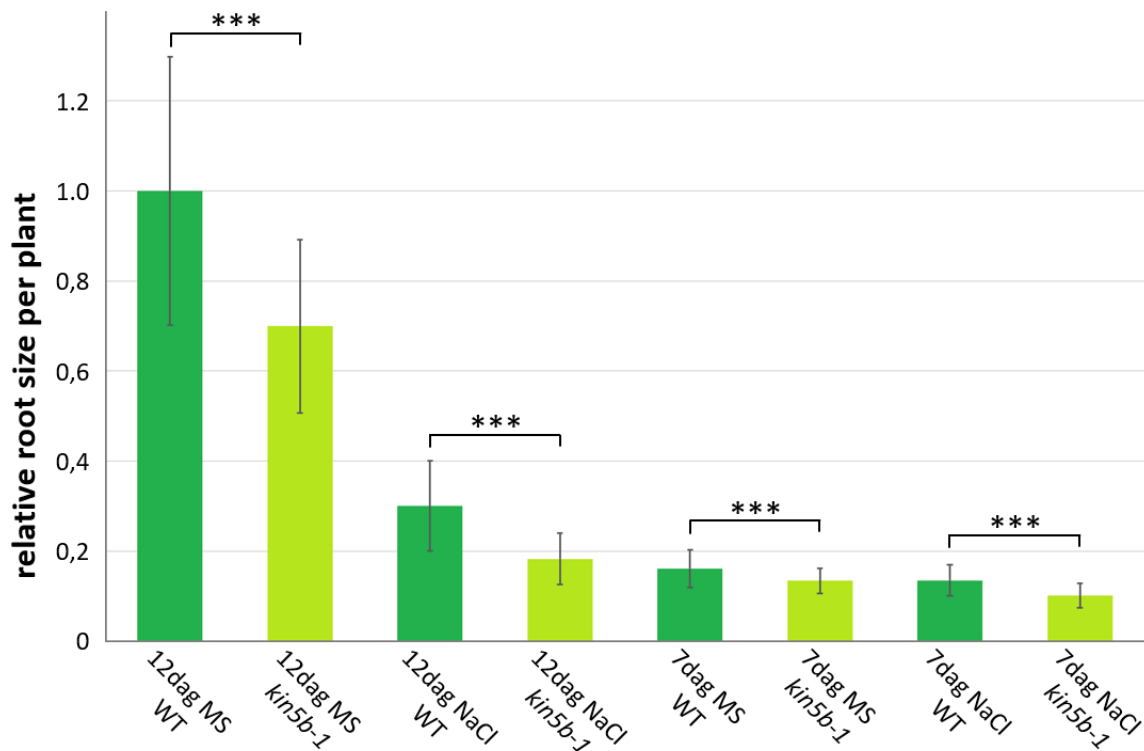


Figure 29: Relative root size per plant for WT and *kin5b-1* plants under salt stress.

The relative root size per plant was calculated for both plant lines and each treatment after 7 dag, directly after shifting to new medium, and after 12 dag, at the end of the experiment. A significant difference in root size could be evaluated between WT and *kin5b-1*. Even directly after the shift, the root size differed. The difference increased with the course of the experiment. Significance is indicated by ***, $p \leq 0.001$ (Welch test). For each time point and condition, the following number of plants were evaluated: 12 dag MS WT: 86, 12 dag MS *kin5b-1*: 78, 12 dag NaCl WT: 86, 12 dag NaCl *kin5b-1*: 81, 7 dag MS WT: 86, 7 dag MS *kin5b-1*: 82, 7 dag NaCl WT: 86, 7 dag NaCl *kin5b-1*: 80.

As *kin5b-1* showed a significant growth reduction of the roots compared to the wild type even without applying the immense salt stress, other conditions were tested to evaluate their impact regarding the root development of the mutant. In a small-scale preliminary experiment, it was found that a reduction of the ambient temperature had an effect on the growth of lateral roots, too, though not as severe as the saline MS-medium. Therefore, plants grown on MS-medium for seven days at 22 °C and long-day conditions, were transplanted to new MS-medium and then cultivated either at 17 °C or 22 °C. For each condition 90 plants of each line were transferred onto new MS-medium plates, by placing three seedlings of each line in a row. The root growth was again documented on a flatbed scanner. However, the plant

size differed already seven days after germination, when the plants were shifted, in WT and *kin5b-1* plants due to cultivation problems. The results of this experiment could not be used to investigate the possible phenotype of *kin5b-1*. Therefore, the temperature experiment was repeated again with 72 plants of each line per temperature at the same conditions. In the second experiment the plants grew more uniformly (**Figure 30**). It could be observed that the plants at 17 °C grew slower than those at 22 °C, as expected. Two days after the shift to new MS-medium, plants at 22 °C started to grow lateral roots, while those at 17 °C did not and had shorter main roots as well. But there was no difference in root length visible between WT and mutant plants, neither at 17 °C, nor at 22 °C. Seven days after the temperature shift and 14 days after germination, the difference between both temperatures became even bigger. While at this time point no distinct difference between WT and mutant plants was visible at 17 °C, a difference between these lines could be observed in some plants grown at 22 °C. The lateral roots did emerge later in the mutant line and were shorter at the end of the experiment. The same could be observed for the size of the leaves. Surprisingly this difference was not as uniform as in the previous phenotyping experiment. Some mutant plants grew a dense network of lateral roots, similar to WT plants. Similar to that, some WT plants developed fewer lateral roots compared to other WT plants (**Figure 30**).

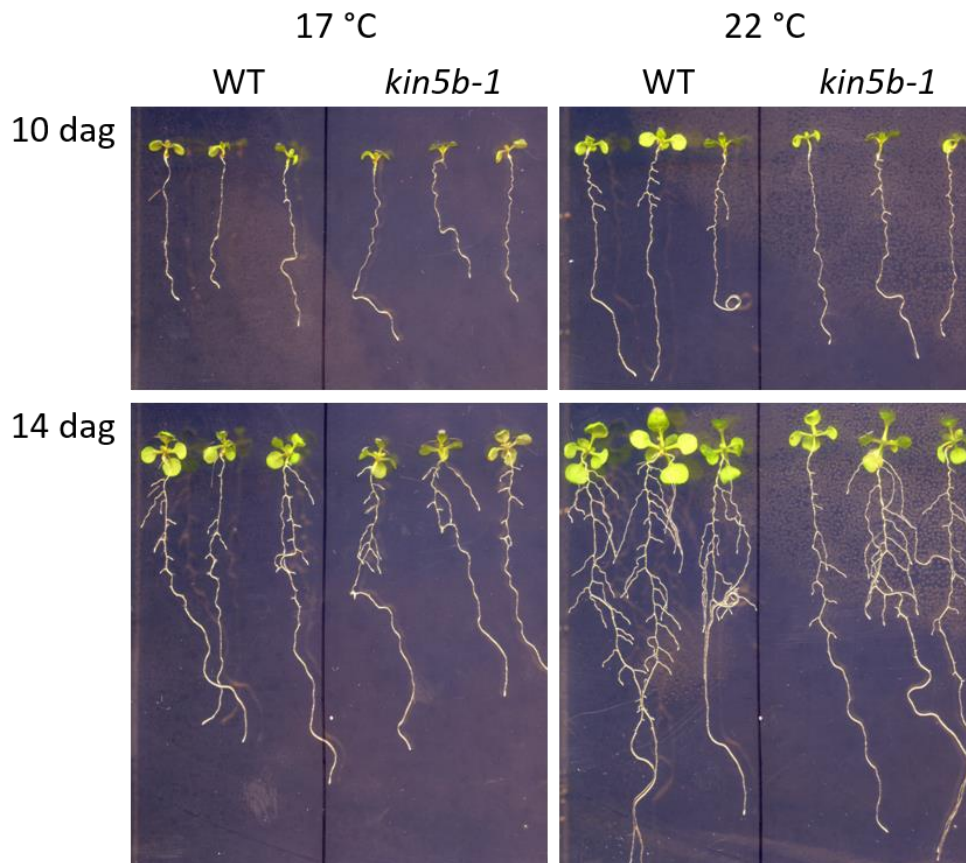


Figure 30: Comparison of WT and *kin5b-1* root growth after shift to 17 °C.

72 plants of *kin5b-1* and its segregating WT were grown on MS-medium plates for 7 days at long-day conditions at 22 °C and were then shifted to new MS-medium plates and cultivated at 17 °C. As a control, the same number of plants was shifted to new MS-medium plates cultivated at 22 °C. 10 dag (3 days at the lower temperature) WT and mutant plants show no differences in the temperature treatment. Although the control plants at 22 °C grew fewer lateral roots. 7 days after the temperature shift, the mutant plants were a bit smaller compared to the WT. Mutant plants in the control shift, seemed to have fewer and shorter lateral roots, compared to the WT.

This observation could be confirmed after measuring the relative root size per plant for each treatment and both plant lines, 7 and 12 days after germination (see 4.4.9). Although a significant difference between the two growth conditions at 17 °C and 22 °C could be evaluated, no significant difference between WT and *kin5b-1* was determined after 12 days, neither within the control group at 22 °C, nor in the treated plants at 17 °C. The only difference in the relative root size per plant could be evaluated between WT and *kin5b-1* directly after the shift to fresh MS-medium (**Figure 31**).

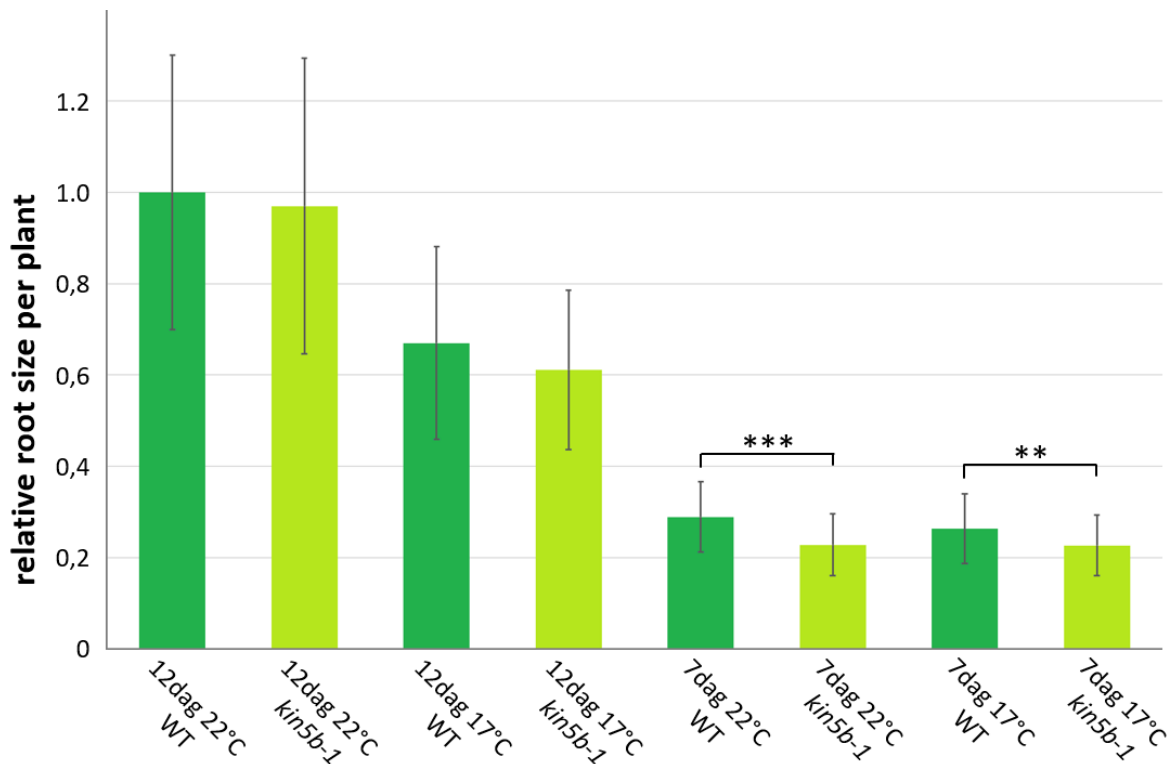


Figure 31: Relative root size per plant for WT and *kin5b-1* plants under different temperature conditions.

The relative root size per plant was calculated for both plant lines and each treatment after 7 dag, directly after the shift to new medium, and after 12 dag. A significant difference in root size could be evaluated between 17 °C and 22 °C, though no difference could be determined between WT and *kin5b-1*. Directly after the shift, the root size differed between WT and mutant. Significance is indicated by **, $p \leq 0.01$; ***, $p \leq 0.001$ (Students t-test/Welch test). For each time point and condition, the following number of plants were evaluated: 12 dag 22 °C WT: 66, 12 dag 22 °C *kin5b-1*: 66, 12 dag 17 °C WT: 71, 12 dag 17 °C *kin5b-1*: 70, 7 dag 22 °C WT: 72, 7 dag 22 °C *kin5b-1*: 72, 7 dag 17 °C WT: 72, 7 dag 17 °C *kin5b-1*: 72.

These results were in contrast to those determined in the salt experiment. Especially, the difference in the control groups of all experiments was inexplicable. These plants were treated the same way in all experiments and grew on the same MS-medium under the same conditions at 22 °C. Another problem in all experiments was the size difference between WT and *kin5b-1* plants directly after the shift. The mutant seems to be smaller seven days after germination compared to the WT, indicating a growth retardation in *kin5b-1* even before the start of the abiotic stress experiments.

Since the results of these experiments differed to much from each other, especially in the control groups, it was not possible to draw an exact conclusion about a possible phenotype of *kin5b-1*. Therefore, the knockout mutant was tested for its susceptibility towards oryzalin and monastrol. As mentioned afore, oryzalin is a microtubule depolymerising compound that only interacts with plant tubulin. A treatment with 300 nM oryzalin increased the root diameter in *Arabidopsis* at least threefold²²⁰ In the AtKRP125c point mutant *rsw7* this effect could be observed already at concentrations of 30 nM¹⁰³. A mutant that already lacks one of its four

kinesin-5s seems to be more susceptible to a microtubule depolymerising drug. The same could apply for a kinesin-5 inhibitor like monastrol. Monastrol binds to a specific loop in the kinesin-5 protein and allosterically impedes the ATPase activity of the motor domain by inhibiting the release of ADP. The mechanism of action of monastrol has been discovered in animal cells and the influence of monastrol on Eg5 is well documented^{102,128}. However, it is controversial whether the homologies between kinesin-5 from animals and plants are sufficiently high for monastrol to be effective in plants. It is known that monastrol inhibits the kinesin-5 in the brown alga *Silvetia compressa*^{148,149}. But it does not impact the *Arabidopsis* kinesin-5 AtKRP125c¹⁰³.

In the case of oryzalin, plants germinated and grew for nine days at long-day conditions at 22 °C on MS-medium containing the drug. A final concentration of 100 nM oryzalin in the medium had only a small effect on the growth of the plants with a slightly reduced growth of the main root and lateral roots. A concentration of 200 nM though, had an impressive impact on the root growth²²¹. The main root did not exceed a length of 2 cm and the lateral root growth was completely inhibited. Although oryzalin had a clear effect on the examined plants, there was no difference visible between WT and *kin5b-1* (**Figure 32**).

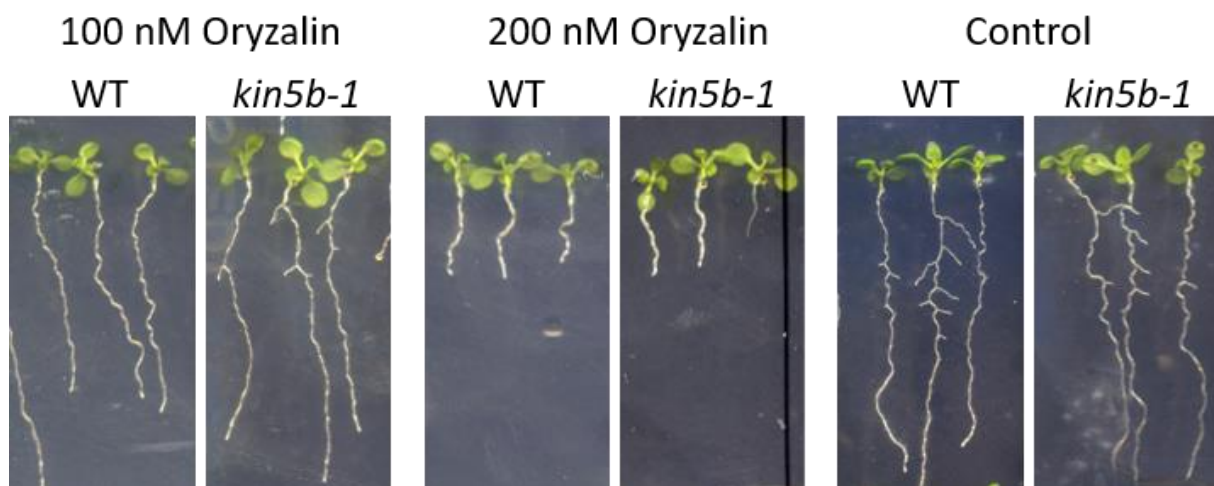


Figure 32: Influence of oryzalin on WT and *kin5b-1* after 9 days.

Col-0 WT and *kin5b-1* plants were grown on MS-medium with 100 nM and 200 nM oryzalin. As a control plants were grown on medium without oryzalin but the same amount of DMSO as the 200 nM oryzalin plates, as oryzalin is solved in DMSO. Plants were cultivated in long-day conditions at 22 °C. 100 nM oryzalin caused a small growth retardation, while 200 nM oryzalin impeded the root growth more severely. No difference in growth is visible between WT and mutant.

Monastrol, on the other hand, had to be applied in a different way than oryzalin. As it is not clear how stable this drug is in the presence of light, and a rather high concentration of 200 µM is needed to cause a reaction in other organisms, monastrol was not added directly into the MS-medium but was applied by spraying a 200 µM monastrol solution directly onto the plants,

every day, starting five days after germination. As a control, plants were sprayed with a mock solution, containing the same amount of DMSO as the monastrol solution. Throughout the experiment, no difference was found between the monastrol treatment and the control treatment. The WT started to develop slightly more lateral roots than could be observed in earlier abiotic stress experiments (**Figure 33**).

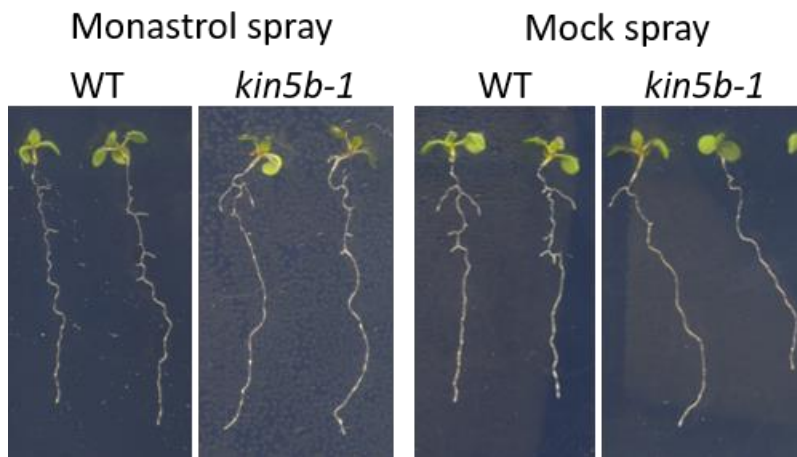


Figure 33: Influence of monastrol on WT and *kin5b* plants after 9 days.

kin5b-1 and its segregating WT were grown on MS-medium and sprayed daily, either with 200 μ M monastrol or with a mock spray containing the same amount of DMSO. The monastrol treatment had no effect on mutant, or WT plants. The WT developed slightly more lateral roots 9 dag compared to the mutant.

Although monastrol is highly specific for kinesin-5s, it needs to be applied in relatively high concentrations of up to 200 μ M to trigger a reaction. Due to the application with a spray onto the plants, these high concentrations may have never been reached. Another more promising way to test the susceptibility of AtKRP125b to monastrol would be in *in vitro* motility assays. In these assays, the concentration could be controlled much better and the effect could be observed directly by a change of the motor protein motility.

To sum up the investigation of the AtKRP125b deficient mutant line *kin5b-1*, an impaired growth could be detected under certain conditions. Under normal growth conditions on soil, the mutant showed no difference at all compared to the WT. Formation of flowers and siliques were without deviations. In experiments with applied salt stress, a significant growth reduction of the roots could be observed compared to WT, in the treated group as well as in the control group. This growth reduction was already measurable directly after the start of the experiment seven days after germination. However, this phenotype was not consistent in further experiments. Some minor growth retardations could be observed in some plants but these were ambiguous and not significant and could even be observed in some WT plants. Also, the application of mitotic drugs like oryzalin or monastrol did not affect the growth of

kin5b-1 at all, in comparison to WT plants. Due to the inconsistent phenotype of *kin5b-1* especially under the same control conditions at 22 °C, this T-DNA insertion line is not suitable to determine the physiological effect that the loss of AtKRP125b may cause. It was not possible to distinguish between the control conditions in the salt experiments (**Figure 27** and **Figure 28**) and the temperature experiment (**Figure 30**). In all experiments the control group was cultivated on the same MS-medium, at the same temperature of 22°C, and the same light conditions. Even though a significant growth pattern could be observed in these groups. In all these experiments During the evaluation of the root size per plant in the salt and temperature experiment, it was noticed that *kin5b-1* plants were already smaller directly after the shift, indicating a small growth retardation of the mutant from the beginning of the germination. Further studies on the germination behaviour of *kin5b-1* could provide additional explanations for this inconsistent phenotype.

2.2.4 Generation of knockout mutants via CRISPR/Cas9

As the investigation of the T-DNA insertion line *kin5b-1* did not yield any new insights into possible functions of *AtKRP125b*, and no other T-DNA insertion lines were available to knockout AtKRP125b completely, additional knockout should be generated by using CRISPR/Cas9 genome editing (see 4.4.9). The CRISPR/Cas9 system was discovered as a part of the bacterial adaptive immunity²²². In recent years, molecular techniques have been developed to use this system as a precise tool for genome editing in various organisms²²³⁻²²⁷. This technique allows manipulating DNA strands at a specific target sequence, determined by an sgRNA²²². Usually, double-strand breaks induced by Cas9 are repaired immediately by non-homologous end joining, which often results in the formation of point mutations, such as deletions or insertions of one base pair at the respective site^{228,229}. Such small mutations are often sufficient to cause the knockout of a certain gene but unfortunately, they are very difficult to detect. In most cases, it is necessary to sequence the target area of hundreds of plants to find such a small mutation, because gel electrophoresis methods are not sensitive enough to detect a size difference of just one base pair. Therefore, it was attempted to remove the entire gene by cutting the DNA at two sgRNA target sites in the front of the gene and two target sites in the back (**Figure 34**)²³⁰. Such a large deletion of several thousand base pairs could be reliably detected with a classic PCR approach. A comparable approach with a deletion of several kilobases has already been successfully used in soybean²³¹. A strategy for genome

editing was developed to produce single knockout lines of all four kinesin-5s in *A. thaliana*. Later on, this system could be upgraded to generate double or triple knockout mutants. Target sites for sgRNAs were determined and all sgRNA target sequences were cloned successfully into the pDGE2-vector and transferred into agrobacteria for plant transformation. Three *Arabidopsis* plant lines, Col-0 WT, and the two reporter gene lines H2B-mTuquoise2 and TagRFP-T-TUA5 were successfully transformed with each construct, respectively. Transformed plants were identified by phosphinothricin selection and tested by PCR for the integrated vector construct. Several hundred plants of the twelve resulting plant lines were investigated in the following three generations for a deletion in the respective kinesin-5 gene by PCR. It was not possible to verify a single deletion event in all investigated plants, even though all plants still contained the Cas9-construct.

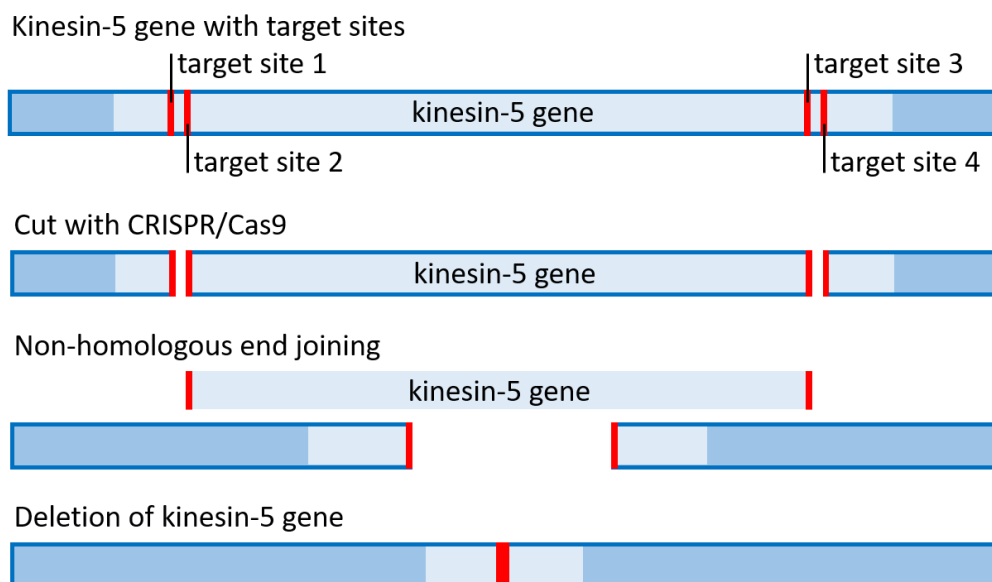


Figure 34: Schematic representation of the CRISPR/Cas9 strategy.

Four target sequences were determined for four respective sgRNAs. Cas9 induced double-strand breaks at these target sequences and cause non-homologous end joining of the blunt ends of the DNA. In some cases, the outer ends should be re-joined without in inner part of the kinesin-5 gene, thereby causing a large deletion.

Therefore, another CRISPR/Cas9 method was tested to introduce two sgRNA target sites for *AtKRP125b* into Col-0 WT plants. Again, one of the target sites was located in the front of *AtKRP125b*, whereas the other one was located at the end, comparable to **Figure 34** (see 4.4.9)²³². Transgenic plant lines could be generated that indeed contained the Cas9 sequence, but no deletion event of *AtKRP125b* could be verified in the following two generations.

It is very well possible that the introduced CRISPR/Cas9 constructs generated point mutations or the deletion or insertion of a few base pairs, but these alterations could not be detected

with the chosen PCR method. As the non-homologous end-joining is a fast repair mechanism, the double-strand breaks at both ends of the gene must take place at roughly the same moment. However, the activity of the introduced constructs is highly dependent on the integration site in the plant genome. One way to increase the efficiency of genome editing with the CRISPR/Cas9 system is to induce heat stress in the transformed plants. Studies showed that heat stress at 37 °C enhanced the activity of Cas9 to induce double-strand breaks compared to 22 °C²³³. With an increased Cas9 activity, a simultaneous double-strand break at both ends of the gene is considerably more likely. However, it may not even be necessary to delete the whole gene from the genome. Even small mutations at the target site could be enough to cause a frame-shift and as a result, a complete knockout of the gene. A new technique for the detection of small genome modifications has been developed that allows screening hundreds of plants with a limited effort and at moderate costs. The high-resolution melting curve analysis utilises the small temperature difference in the DNA melting temperature between a homoduplex strand consisting of wild type DNA or mutant DNA and a heteroduplex strand consisting of both, wild type and mutated DNA²³⁴. This technique can be applied rather easily with most qPCR-thermocyclers and corresponding fluorescent dyes that intercalate double-stranded DNA²³⁵. With this method, new single and multiple knockout mutants of kinesin-5 genes in *A. thaliana* could be established in the future and investigated for a more consistent phenotype.

2.2.5 GFP-AtKRP125b is not exclusively localised inside the nucleus.

Since the promoter of *AtKRP125b* showed no activity in mitotically active cells, the putative intracellular localisation of AtKRP125b could provide crucial information about its function and site of action. For that purpose, a *2x35S::GFP-AtKRP125b* reporter construct with the reporter gene GFP was designed and cloned into the plasmid pMDC43 by Gateway cloning²³⁶. The construct under the control of a double 35S-promoter was transiently expressed in *A. thaliana* mesophyll protoplasts (see 4.4.3), and the fluorescence was investigated by confocal laser scanning microscopy²³⁷. In all transformed protoplasts, a strong GFP fluorescence was detected in a nuclear-like structure. This structure could be determined to be indeed the nucleus of the cell by a colocalisation with the DNA-stain Hoechst 33342 (**Figure 35 A**). Additionally, in about 50 % of the transformed protoplasts, the GFP-AtKRP125b protein was also present within the cytosol (**Figure 35 B**), thus indicating that AtKRP125b may

have a function outside the nucleus during the interphase. Since AtKRP125b is a microtubule interacting motor protein, the localisation of GFP-AtKRP125b was observed in mesophyll protoplasts, isolated from a tubulin marker-line to investigate the interaction with microtubules. In this line TUA-5-RFP is constitutively expressed and fluorescently labelled. Indeed, a colocalisation of tubulin and GFP-AtKRP125b could be observed in the cytosol of a few protoplasts (**Figure 35 C**). However, it was not possible to observe polymerised microtubules in these protoplasts and therefore a colocalisation of AtKRP125b could not be observed.

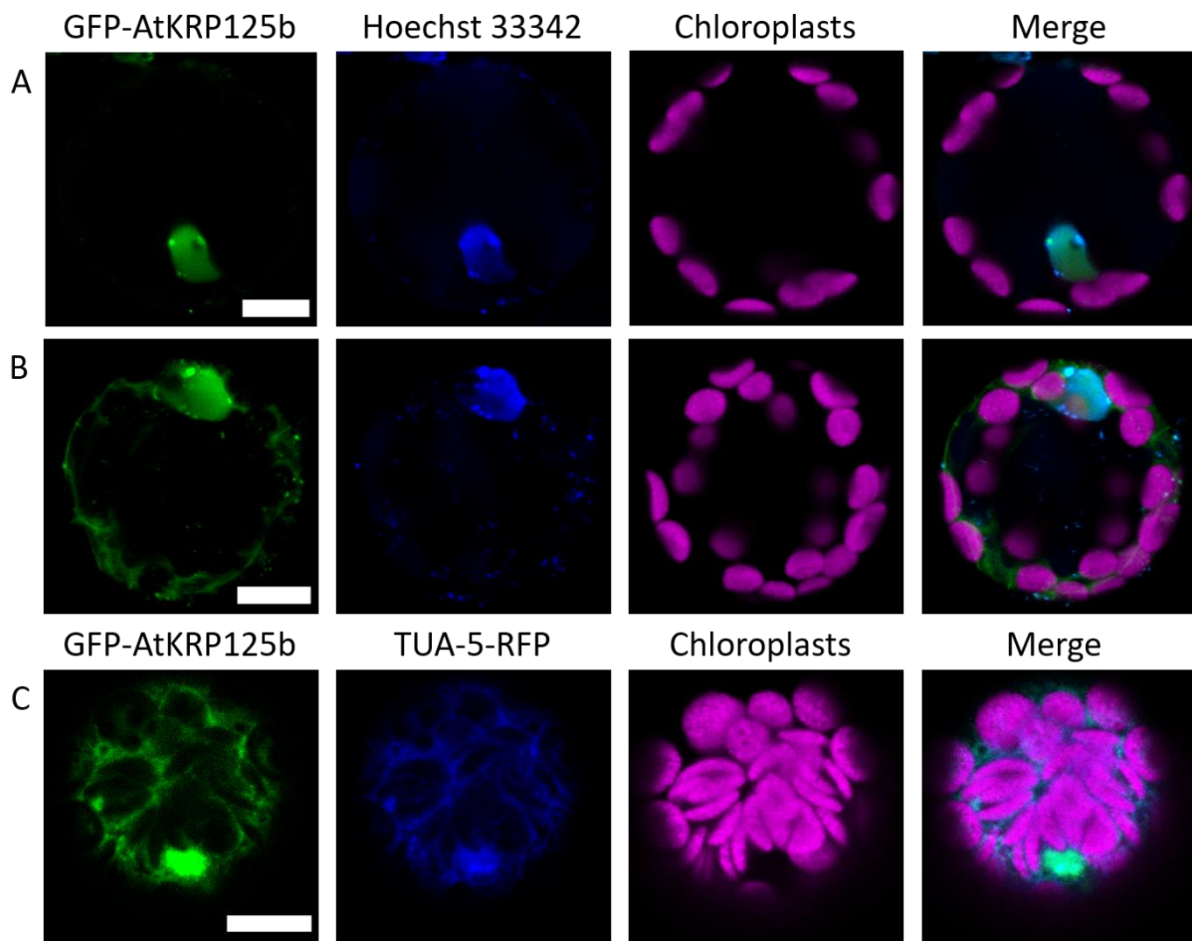


Figure 35: GFP-AtKRP125b is localised in the nucleus and cytoplasm in *A. thaliana* protoplasts.

A: Colocalisation of GFP-AtKRP125b and nucleus in *A. thaliana* mesophyll protoplasts. Fluorescent micrographs show transient expressed GFP-AtKRP125b (green), nuclei staining with Hoechst 33342 (blue), chloroplast autofluorescence (magenta), and a merge of all three channels. The GFP-signal is limited to the nucleus.

B: A maximum intensity projection in the same order as (A). Additionally, to the signal in the nucleus, a GFP-signal in the cytosol is visible.

C: A partial colocalisation of GFP-AtKRP125b and tubulin TUA-5-RFP in the cytosol of mesophyll protoplasts from a tubulin-RFP reporter-line. Maximum projection of transient expressed GFP-AtKRP125b (green), constitutive expressed TUA-5-RFP (blue), chloroplast autofluorescence (magenta), and a merge of all three channels.

The scale bar represents 10 μm .

To confirm the nuclear localisation signal observed in *Arabidopsis* protoplasts, the reporter construct was introduced into *Nicotiana benthamiana* leaf pavement cells as well. Therefore,

leaves of *N. benthamiana* were infected with agrobacteria that had been transformed with the *2x35S::GFP-AtKRP125b* construct (see 4.4.5), and the fluorescence of the expressed fusion protein was investigated by confocal laser scanning microscopy. A bright GFP fluorescence was observed exclusively in the nucleus (**Figure 36 A**). As a control, another leaf of the same plant was infected with agrobacteria carrying a free GFP construct, which produced a clearly different fluorescence pattern, with a strong signal in the cytoplasm and the nucleus (**Figure 36 B**).

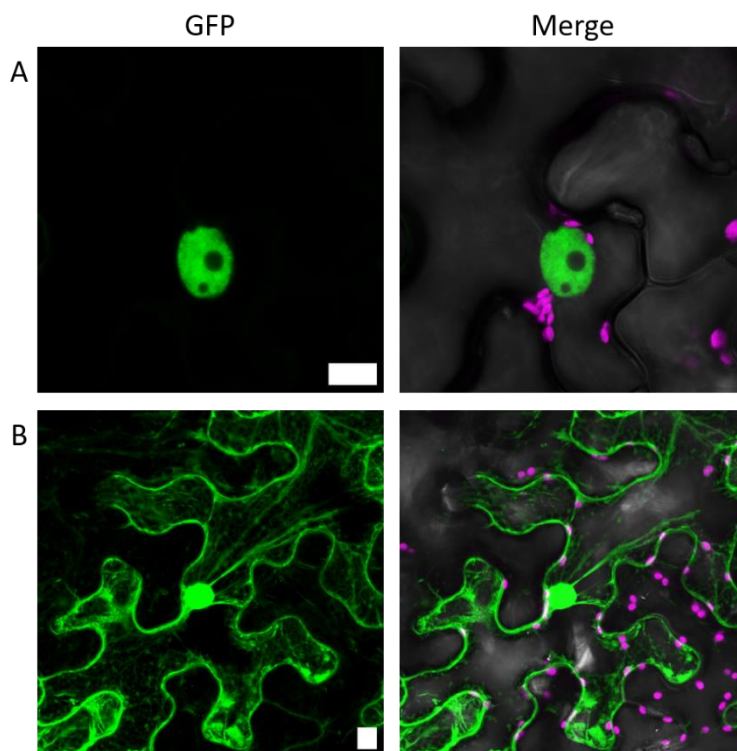


Figure 36: GFP-AtKRP125b is localised in the nucleus in *Nicotiana benthamiana* leaf pavement cells.

A: Images show fluorescent micrographs of transient expression of GFP-AtKRP125b (green). Second image shows a merge of three channels: GFP-AtKRP125b (green), chloroplast autofluorescence (magenta), and bright field (grey). A clear GFP-signal is visible in the nucleus.

B: Fluorescent image of transient expressed free GFP as a comparison to A.

The scale bar represents 10 μm .

As mentioned before, AtKRP125b showed a direct interaction with the E3 ubiquitin ligase SAUL1¹⁵². This interaction was present mainly in the cytoplasm and the nucleus in BiFC experiments. To see whether the absence of one interaction partner influences the localisation of the other, protoplasts were isolated from the respective mutant lines and transiently transformed with a GFP construct of its interaction partner. SAUL1-GFP expressed in the AtKRP125b-deficient T-DNA insertion line *kin5b-1* showed a clear localisation to the plasma membrane (**Figure 37 A**). This localisation has always been observed for SAUL1, and

was also observed in protoplasts generated from the segregating WT of *kin5b-1* (**Figure 37 B**)^{163,168}.

Subsequently, the localisation of GFP-AtKRP125b in the SAUL1 deficient mutant *saul1-1* was investigated. GFP-AtKRP125b could be detected inside the nucleus (**Figure 37 C**), similar to earlier experiments (**Figure 35** and **Figure 36**). It could be noticed that the general GFP-signal in all investigated *saul1-1* protoplasts was relatively weak. This could be explained by the process of protoplast isolation, which can be quite stressful for the plant cells. This could lead to an activation of the autoimmune phenotype of the mutant. Nonetheless, the lack of SAUL1 in the protoplast did not change the localisation of GFP-AtKRP125b and vice versa.

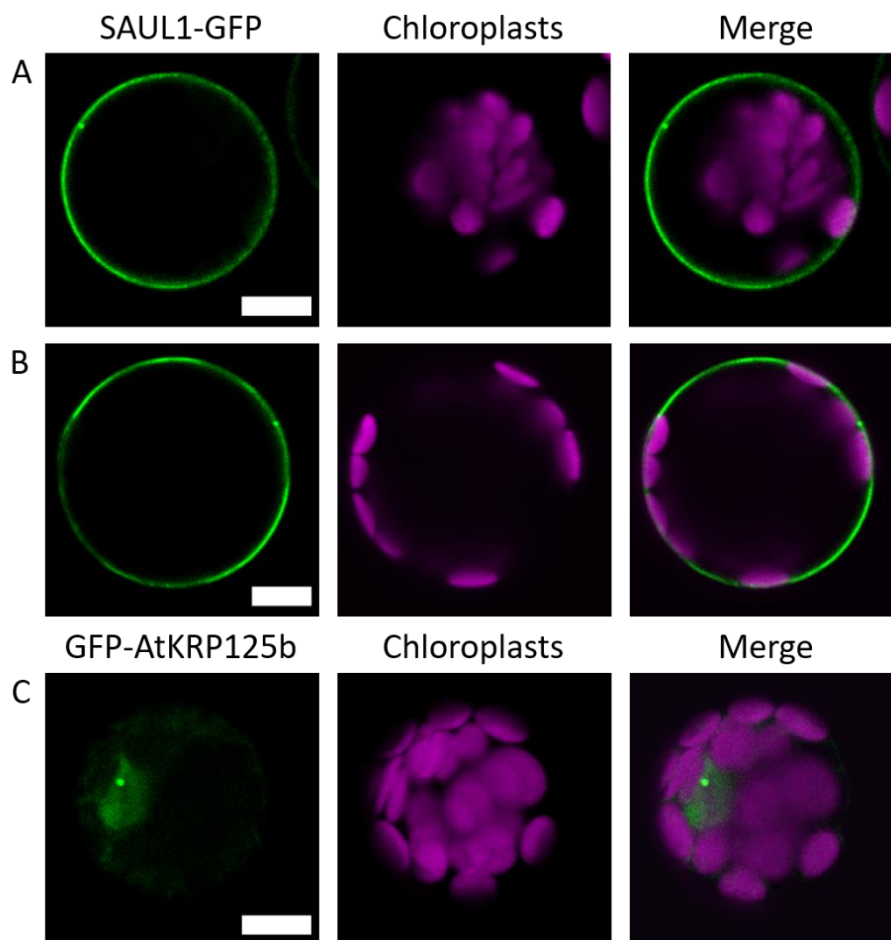


Figure 37: Localisation of SAUL1-GFP and GFP-AtKRP125b in *A. thaliana* mutant and WT protoplasts.

A: Localisation of SAUL1-GFP in *kin5b-1* protoplasts. Fluorescent micrographs show transient expressed SAUL1-GFP (green), chloroplast autofluorescence (magenta) and a merge of these two channels. SAUL1-GFP is located to the plasma membrane.

B: Localisation of SAUL1-GFP in segregating WT of *kin5b-1* protoplasts. Fluorescent micrographs are in the same order as in (A). SAUL1-GFP shows the same localisation as in protoplasts generated from the mutant line.

C: Localisation of GFP-KIN5b in *saul1-1* protoplasts. Fluorescent micrographs of transient expressed GFP-KIN5b (green), chloroplast autofluorescence (magenta) and a merge of these two channels. GFP-KIN5b shows the same localisation in the nucleus afore mentioned (**Figure 35**).

The scale bar represents 10 μm .

Although protoplasts and *N. benthamiana* cells are well-established systems to study the subcellular localisation of proteins in plants, they do not resemble the natural environment of the protein completely: Protoplasts are produced with relatively harsh methods to be transformed and often are quite stressed, and *N. benthamiana* is an entirely different, not even closely related species. Especially, the observation of cells during mitosis is very difficult in these systems. Therefore, the GFP-construct was stably integrated into Col-0 WT plants and eight transgenic lines could be selected. Each of these lines was tested for the successful, stable integration of the construct into its genome by PCR. Although all eight lines were tested positive for the DNA of the construct, no line showed a GFP-signal under a fluorescent microscope. This could be explained by an auto-inactivation of the gene expression, due to the powerful promoter from the cauliflower mosaic virus^{238,239}. The gene-silencing of the CaMV35S-promoter seems to be a common reaction to the infection with this virus, as it evolved a protein to suppress the gene silencing mechanisms of the plant²⁴⁰. This shows that using the CaMV35S-promoter has its advantages and disadvantages. On the one hand, it creates a strong expression, which is needed to detect the fluorescence of the reporter protein, on the other hand, this expression can cause deviations from the natural localisation and trigger gene silencing.

To circumvent the gene-silencing and confirm the localisation in the nucleus, another construct was cloned under the control of the native promoter region of *AtKRP125b*. The construct *pAtKRP125b::YFP-AtKRP125b* was generated, using the promoter-GUS vector *pAtKRP125b::GUS* as a basis and exchanging the GUS-gene with *YFP-AtKRP125b* by OEC. The construct was tested in *Arabidopsis* mesophyll protoplasts but no fluorescent signal could be obtained. Probably, the expression level was too low, either because the promoter is not very active in the leaves as it was shown in section 2.2.1, or the expression conditions in the highly stressed protoplasts are not favourable. Protoplasts are in general not a very suitable environment to study a possible interaction with cortical microtubules, as these are frequently disorganised or even are depolymerised by the removal of the cell wall²⁴¹⁻²⁴³. The high calcium concentrations during the transformation of protoplasts can destabilise microtubule arrays further²⁴⁴. High calcium concentrations can enhance the activity of microtubule-destabilising proteins, such as MDP25 (MICROTUBULE-DESTABILIZING PROTEIN 25)²⁴⁵. Especially between parallel-arranged cortical microtubule arrays, AtKRP125b could take on an important function and create order by connecting and shifting these microtubules. Studies on AtKRP125c

showed that cortical microtubules became disorganised in root cells of the point mutant *rsw7*¹⁰³. To observe the reporter protein in a more natural environment, the construct was additionally stably transfected into Col-0, TagRFP-T-TUA5 and H2B-mTurquoise2 plants by agrobacteria-mediated transformation. Although 21 transgenic plant lines were obtained, no fluorescent protein could be observed in the roots or leaf apex, where a significant promoter activity was detected before in the promoter-GUS experiments.

One way to investigate the localisation of AtKRP125b in *A. thaliana* plants further could be the use of inducible promoters that activate the expression of the reporter protein right before the localisation experiment²⁴⁶, or the co-transformation with a gene-silencing suppressor, as it was done in the transient GFP-AtKRP125b expression in *N. benthamiana*²⁴⁷.

After all, it would be of great interest to see where AtKRP125b is localised during mitosis and cell division. A heterologous expression of GFP-AtKRP125b in *Nicotiana tabacum* BY2-cells, a fast-growing cell culture with high numbers of mitotic cells, could be used to visualise a possible interaction with the spindle apparatus or the phragmoplast, as it was done with AtKRP125c^{103,248}. The examination of mitotic cells in living *Arabidopsis* plants is best performed near the root meristem, because the autofluorescence of chloroplasts and other plant pigments does not interfere there²⁴⁹. First experiments with the mentioned fluorescently labelled tubulin and histone marker lines did not show cells with a developed spindle apparatus or an ongoing cell division.

2.3 General discussion

The canonical functions of kinesin-5 in the organisation and maintenance of the spindle apparatus during cell division are extensively described and well researched. However, recent studies continue to indicate new functions for kinesin-5 proteins beyond their canonical functions, which can be divided into two categories: First, functions in the transport of vesicles through the cell, and second, functions in the displacement and transport of microtubule arrays.

2.3.1 Functions of kinesin-5 in vesicle transport

While proteins from many different kinesin families are involved in the transport of vesicles, the role of kinesin-5 in this context is quite surprising. Until now, such kinesins have been characterised by a high velocity and processivity. Many of these kinesins contain special

domains for the interaction with proteins that are associated to these vesicles. Most of the vesicle transport in animal cells is carried out by kinesins from the families 1,2, and 3²⁵⁰. Such as the transport of Rab6-positive secretory vesicles from the Golgi apparatus to the cell periphery by kinesin-1 KIF5B and kinesin-3 KIF13B²⁵¹. Recent experiments showed, that both kinesin motor proteins are involved in the transport of these vesicles. While KIF13B is the faster motor protein, it tends to move in the front of the vesicle, followed by KIF5B, which seems to be the major player in the transport of vesicles because it detaches less frequently under load. Since the movement of KIF5B is strongly dependent on MAP7, which is more abundant on older microtubules, KIF13B seems to be especially important for the transportation at the dynamic tip of the microtubule^{23,252,253}.

As kinesins from these families are not present in most plant species (**Figure 6**)⁸⁰, kinesins from other families perform the vesicle transport. Such as the highly processive kinesin-4 FRA1 (FRAGILE FIBER 1). This kinesin transports pectin and hemicellulose filled vesicles along the cortical microtubules to the plasma membrane²⁵⁴⁻²⁵⁷. Additionally, FRA1 interacts with, and influences the localisation of proteins that maintain the positional and lateral stability of cortical microtubules²⁵⁸. FRA1 walks towards the microtubule plus-end with a velocity of about 400 nm s⁻¹ in a highly processive manner with an average run length of 3.45 μm. This high processivity seems to be crucial for its physiological function²⁵⁹.

Although kinesin-5 is indeed a processive motor protein, which was confirmed by the characterisation of AtKRP125b in this thesis, it is one of the slowest kinesins known²⁶⁰.

Studies with animal kinesin-5s, such as vertebrate Eg5 and *Drosophila* KLP61F, showed that kinesin-5 is directly involved in the transport of CARTS, vesicles that are used for the transport of specific secretory and integral membrane proteins, such as PAUF (PANCREATIC ADENOCARCINOMA UP-REGULATED FACTOR), from the trans-Golgi network to the cell surface²⁶¹. *Drosophila* S2 cells with a knockdown of KLP61F secreted less vesicles with a HRP (HORSERADISH PEROXIDASE) signal sequence compared to control cells. The HRP signal sequence accumulated within the cells, indicating a problem in the transport of HRP from the trans-Golgi network to the cell surface. Further, the knockdown of Eg5 in HeLa cells by siRNA and its inhibition by monastrol showed a reduced secretion of PAUF, while the organisation of cytoplasmic microtubules and the Golgi apparatus remained unaffected¹⁴¹. The knockdown of other kinesins had no impact on the secretion of PAUF, but it was possible to colocalise GFP-Eg5 decorated microtubules with RFP-PAUF filled vesicles, indicating that kinesin-5 is

directly involved in the transport of CARTS. However, it is still unknown how kinesin-5 and these vesicles interact.

A similar process had been observed in the transport of neurotrophin and neurotransmitter receptors to the cell surface in the context of Alzheimer's disease. A key factor of the neuronal dysfunction in the course of Alzheimer's disease is the amyloid beta peptide ($A\beta$). $A\beta$ is known for its devastating effect on the mitotic spindle by interacting and inhibiting mitotic kinesins like Eg5, the kinesin-4 KIF4A, and the kinesin-13 motor protein MCAK²⁶². It was shown that the inhibition of Eg5 by $A\beta$ does not only affect the mitotic spindle but also disrupts the localisation of neurotrophin and neurotransmitter receptors to the cell surface comparable to a monastrol treatment¹⁴⁰. The inhibition of Eg5 by $A\beta$ and the resulting problems in vesicular transport could also explain other abnormal localisations of neurotransmitter receptors or transmembrane proteins in the course of Alzheimer's disease, such as LDLR (LOW-DENSITY LIPOPROTEIN RECEPTOR) and NMDA-receptors²⁶³⁻²⁶⁶.

Although Eg5 seems to be involved in the transport of vesicles in several different cells and has an important role in the localisation of receptor proteins in neurons, it remains unclear in which way Eg5 is connected to these vesicles. Studies showed that the trafficking of amyloid precursor protein APP is critical for the generation of $A\beta$. APP contains a transmembrane domain by which it is associated to membrane-limited organelles and vesicles^{267,268}. Further, APP is transported in Golgi-derived vesicles to the cell surface²⁶⁹. Localisation studies in squid giant axons with the squid homolog of APP showed that this protein is localised at the interphase between organelles and microtubules²⁷⁰. These organelles move towards the microtubule plus-end, attach to microtubules in the absence of ATP and detach in its presence, indicating that these proteins interact with a kinesin motor protein. Interestingly, APP interacts with members of the kinesin families 1 and 2 via adaptor proteins²⁷¹⁻²⁷⁴. A comparable interaction with other kinesins, such as Eg5, could explain the observed vesicle transport of CARTS and receptor proteins.

However, not much is known about possible interaction partners of kinesin-5. Although some interactions have been discovered that primarily serve the regulation of kinesin-5, such as the MAP TPX2, which substantially reduces the velocity of Eg5^{125,126,275,276}. A recent study showed the interaction of Eg5 with TRIM8 (TRIPARTITE MOTIF 8), a E3 ubiquitin ligase that is involved in various pathological processes, such as hypertrophy, antiviral defence, and cancer development²⁷⁷⁻²⁸⁰. TRIM8 is associated to several structures of the mitotic spindle, such as

the midbody and centrosomes. The silencing of *TRIM8* delayed the progression of mitosis and caused the formation of micronuclei, a phenotype of chromosome instability. However, the function of the interaction between TRIM8 and Eg5 remains unclear.

To date none of the interaction partners of kinesin-5 that have been discovered indicate a connection to vesicles. In the case of AtKRP125b the interaction with SAUL1 could enable such a connection¹⁵². Although, SAUL1 had not been colocalised with vesicles directly, it is known, that SAUL1 is associated to plasma membranes with its C-terminal ARM domains and seems to be involved in the tethering of multivesicular bodies to the plasma membrane^{163,177}. A transportation of SAUL1 by AtKRP125b could be tested in further *in vitro* motility assays with fluorescently labelled SAUL1 or in *in vitro* vesicle transport assays²⁸¹.

Additionally, it could be possible that AtKRP125b is involved in a cooperative cargo transport with a second, faster kinesin, similar to the vesicle transport by KIF5B and KIF13B^{251,282,283}. Mixed population of kinesin motor proteins in transport processes could harness the advantages of different classes of motor proteins^{284,285}. One of the big advantages of kinesin-5 over other kinesins is its relative insensitivity to detach from microtubules even when extensive loads are applied, due to its strong microtubule interaction²⁸⁶⁻²⁸⁸.

2.3.2 Functions of kinesin-5 in microtubule organisation

The function of kinesin-5 in the organisation and maintenance of the mitotic spindle is well studied from many different perspectives. With its bipolar structure and the ability to crosslink microtubules, kinesin-5 is perfectly suited for a function in overlapping microtubule arrays.

It has been extensively shown that kinesin-5 is of great importance for the organisation of microtubule arrays before and after mitosis in plants. The formation of the preprophase band and the development of the phragmoplast requires kinesin-5 in several plant species, such as *Nicotiana tabacum*, *Daucus carota*, and *Arabidopsis thaliana*^{103,146,147}. In all these species kinesin-5 was colocalised to the respective microtubule array during cell division. As the development of the preprophase band and the phragmoplast are indispensable components of the cell division in plants and some of the spindle microtubules even remain to form the phragmoplast, these functions were not surprising³⁹. However, in *D. carota* and *A. thaliana* kinesin-5 also decorated cortical microtubules during the interphase, indicating additional functions beyond cell division.

In this line, the subcellular localisation of GFP-AtKRP125b during interphase not only inside the nucleus but also in the cytosol and the expression in vascular tissue of roots, leaves, and sepals, supports the hypothesis of possible new functions, either in the vesicle transport of cell wall material comparable to FRA1 or the organisation of cortical microtubules itself²⁵⁸. These microtubule arrays often change depending on developmental, physiological and environmental parameters²⁸⁹. They are crucial for the formation of the cell wall and determine the cell shape. In vascular tissues, cortical microtubules are especially important for the regular positioning of secondary cell wall thickenings of xylem tissue²⁹⁰⁻²⁹². The organisation of cortical microtubules requires a coordinated transport of microtubules along other microtubules²⁹³. With the ability to slide anti-parallel microtubules apart and crosslink parallel microtubules, AtKRP125b could play an important role in microtubule-bundling that is necessary for the proper organisation of cortical microtubules.

It has been shown that kinesin-5 has a substantial role in the organisation of microtubule networks in axons and dendrites of animal cells^{30,134-137}. The growth and maintenance of the axon requires a large array of microtubules, which extends over the entire length of the axon, starting at the cell body. It has been observed that the length of microtubules in these arrays varies greatly²⁹⁴. While long microtubules of up to 100 μm are mostly immobile, function as a transport route and maintain the structural integrity of the axon, short microtubules are highly mobile and are transported along the long microtubules^{295,296}. A substantial part of these transport processes are performed by cytoplasmic dynein, although it has been shown, that mitotic kinesins play a vital part in the microtubule transport as well²⁹⁷. Neurons, treated with the kinesin-5-specific inhibitor monastrol developed longer axons, while an overexpression of Eg5 produced shorter axons^{135,136}. Additionally, the knockdown of Eg5 resulted in a higher axonal branching frequency¹³⁷. The reason for this behaviour seemed to be an imbalance between the anterograde and retrograde transport of short microtubules in the axon. Eg5 restricts the transport of short microtubules by other motor proteins, especially in the anterograde direction. The forces generated by Eg5 antagonize the forces generated by cytoplasmic dynein¹³⁷. This process shows some similarities to the maintenance of the mitotic spindle, where kinesin-5 as a plus-end directed motor protein opposes the forces of minus-end directed motor proteins, like dynein or kinesin-14.

In plants, it has further been shown that kinesins can play a role in the cytoplasm and the nucleus at the same time, which would fit to the localisation of AtKRP125b, shown in this

thesis. The FRA1 homologue in rice OsBC12 (BRITTLE CULM 12) is localised in the cytoplasm and the nucleus and has functions in the deposition of cellulose microfibrils, is associated to microtubule arrays during cell division, and can bind to the promoter region of a gibberellin biosynthesis gene^{298,299}. Similar to OsBC12, OsDLK (DUAL LOCATED KINESIN) is localised in the nucleus and the cytoplasm and is involved in the sliding of microtubules in the mitotic spindle and phragmoplast. Its localisation, however, changed in response to cold, where it is imported inside the nucleus⁵⁰. Further localisation studies in intact plant tissue or dividing cells, like BY2-cells could raise new information on the interaction of AtKRP125b with interphase- and mitotic-microtubule arrays.

Interestingly, three out of four kinesin-5s in *A. thaliana* show great homology in the protein structure and expression pattern^{91,151}. This could indicate that AtKRP125a, AtKRP125b, and AtKRP125c share common functions. Despite the great homologies between these three kinesins, AtKRP125b is the only Kinesin-5 that directly interacts with SAUL1. Further insights regarding the physiological function of AtKRP125b and kinesin-5 in *A. thaliana* have to be produced by the investigation of multiple kinesin-5 knockouts.

The large number of new functions for kinesin-5 motor proteins beyond cell division that were discovered in recent years suggests many possible functions for AtKRP125b. By its processive motion, its expression outside of mitotic tissue, and its localisation in the cytosol during interphase, AtKRP125b could serve a role in the transport of vesicles and cargo, as well as in the organisation of overlapping microtubule structures. Further research on the interaction with SAUL1, the localisation at interphase microtubule arrays, and its connection to the other three kinesin-5 homologs in *A. thaliana* could help to understand if AtKRP125b can fulfil any of these suggested functions.

3 Conclusion

In this thesis, the kinesin-5 motor protein AtKRP125b was characterised directly on a biophysical and biochemical level with several (I) *in vitro* approaches, as well as on a physiological level by (II) *in vivo* experiments.

(I) The combination of different *in vitro* assays showed that AtKRP125b is a processive plus-end directed motor protein that moves along microtubules with a mean velocity of about 17 nm s^{-1} . Additionally, it was shown that AtKRP125 crosslinks microtubules and slides apart anti-parallel microtubules with a reduced velocity of about 12 nm s^{-1} . This reduced velocity may be explained by a proposed interaction of tail-domains with the motor-domains of neighbouring kinesin-5 molecules within overlapping regions of microtubules. These findings, suggested that AtKRP125b is able to fulfil the canonical functions of the kinesin-5 family. Additionally, its processive movement would allow the transport of cargo such as vesicles along microtubules through the cell.

(II) *In vivo* approaches showed that *AtKRP125b* is presumably not expressed in mitotic tissue, but in the vascular tissue of roots, leaves, and sepals. Additionally, with a subcellular localisation not only inside the nucleus but in the cytosol as well during interphase, this may indicate that AtKRP125b has a function beyond mitosis and cell division, for example in the organisation of cortical microtubule arrays, due to its ability to crosslink microtubules. The study of T-DNA knockout mutants, however, did not show any distinct phenotype that would indicate a specific physiological function. Due to the great homology of AtKRP125a, AtKRP125b, and AtKRP125c and great similarities in the expression pattern, it is likely that the knockout of one kinesin-5 is not sufficient to cause a phenotype in *A. thaliana*. Therefore, for further research on new functions of kinesin-5 in plants, the generation and characterisation of mutants with multiple kinesin-5 knockouts will be required. With the CRISPR/Cas9 approaches undertaken in this study, no deletion of the corresponding genes could be detected. Nevertheless, numerous Cas9-constructs could be stably transferred into WT plants and reporter lines.

In summary, this thesis showed the canonical biophysical and biochemical characteristics of AtKRP125b and suggested possible new functions for kinesin-5s in plants. Further analysis of the interaction between SAUL1 and AtKRP125b and the physiological role of AtKRP125b could specify these possible functions.

4 Material and Methods

4.1 Organisms

4.1.1 Bacterial strains

Table 1: *E. coli* strains used in this thesis.

Strain	Genotype	Reference
BL21 Gold (DE3)	B F ⁻ ompT hsdS(r _B ⁻ m _B ⁻) dcm ⁺ Tet ^r gal λ(DE3) endA I	Agilent Technologies (Santa Clara, USA)
BL21 pRARE (DE3)/ Rosetta 2 (DE3)	F-ompT Ion hsdSB (r _B ⁻ m _B ⁻) gal dcm (DE3) pRARE2 (Cam ^R)	Novagen/Merck (Darmstadt, Germany)
BL21 RIPL (DE3)	B F ⁻ ompT hsdS(r _B ⁻ m _B ⁻) dcm ⁺ Tet ^r gal λ(DE3) endA The (argU proL Cam ^R) (argU ileY leuW Strep/Spec ^R)	Agilent Technologies (Santa Clara, USA)
BL21 Rosetta Gami2 (DE3)	Δ(ara-leu)7697 ΔlacX74 ΔphoA PvuII phoR araD139 ahpC 73ale galK rpsL(DE3) F'(lac ⁺ lacI ^q pro) gor522::Tn10 trxB pRARE2 (Cam ^R , Str ^R , Tet ^R)	Novagen/Merck (Darmstadt, Germany)
DH5α	B F ⁻ endA1 glnV44 thi-1 recA1 relA1 gyrA96 deoR nupG purB20 φ80lacZ ΔM15 Δ(lacZYA- argF) U169, hsdR17(r _K ⁻ m _K ⁺), λ ⁻	Hanahan (1983) ³⁰⁰
DH10Bac	F-mcrA Δ(mrr-hsdRMS-mcrBC) Φ80lacZΔM15 ΔlacX74 recA1 endA1 araD139 Δ(ara, leu)7697 galU galK λ-rpsL nupG/pMON14272/pMON7124	Invitrogen (Santa Clara, USA)
OneShot Top10	F- mcrA Δ(mrr-hsdRMS-mcrBC) φ80lacZ ΔM15 ΔlacX74 recA1 araD139 Δ(ara-leu)7697 galU galK rpsL (Str ^R) endA1 nupG	Invitrogen (Santa Clara, USA)

Table 2: *A. tumefaciens* strains used in this thesis.

Strain	Genotype	Reference
C58C1	C58	Deblaere, et al. (1985) ³⁰¹
GV3101	C58 (Rif ^R), pMP90 (Gent ^R)	Ashby, et al. (1988) ³⁰²

Table 3: *P. pastoris* strains used in this thesis.

Strain	Genotype	Distributor
X-33	Wild type ^{303,304}	Invitrogen (Santa Clara, USA)

Table 4: Insect cell lines used in this thesis.

Cell line	Origin	Distributor
Sf9	Ovarian tissue of <i>Spodoptera frugiperda</i> ^{195,305}	Invitrogen (Santa Clara, USA)
BTI-Tn-5B1-4 (High Five)	Ovarian tissue of <i>Trichoplusia ni</i> ^{196,197}	Invitrogen (Santa Clara, USA)

4.1.2 Plant lines

The following *A. thaliana* plant lines were used and generated in this thesis. As a comparison for mutant lines and for the establishment of new transgenic lines, the wild type Col-0³⁰⁶ was used. T-DNA insertion lines were obtained from the Nottingham Arabidopsis Stock Centre (NASC).

Table 5: List of *A. thaliana* T-DNA insertion lines used in this thesis.

Line	Stock-ID	Affected Gene	Reference
<i>kin5b-1/</i> ML096	GK011.H10	At2g36200	GABI-Kat ³⁰⁷ Strauß (2016) ¹⁷⁸
<i>kin5b-2/</i> ML098	SALK_152139	At2g36200	SIGnAL ³⁰⁸ Strauß (2016) ¹⁷⁸
<i>saul1-1</i>	SALK-063974	At1g20780	Raab et al. (2009) ¹⁷⁰

Table 6: List of *A. thaliana* transgenic lines used or established in this thesis.

Line	Purpose	Affected Gene	Reference
<i>H2B-mTurquoise2</i>	Reporter line	At5g22880	Prusicki et al. (2019) ³⁰⁹
<i>TagRFP-T-TUA5</i>	Reporter line	At5g19780	Komaki et al. (2020) ³¹⁰
<i>pkin5b::GUS #1-3, 5-8, 11-13</i>	Reporter line	pAt2g36200	This thesis
<i>2x35S::GFP-KIN5b</i>	Reporter line	At2g36200	This thesis
<i>35::YFP-KIN5b</i>	Reporter line	At2g36200	This thesis
<i>35::YFP-KIN5b</i> in <i>H2B-mTurquoise2</i>	Reporter line	At2g36200	This thesis
<i>35::YFP-KIN5b</i> in <i>TagRFP-T-TUA5</i>	Reporter line	At2g36200	This thesis
<i>2x35S::GFP-KIN5b</i> in <i>kin5b-1</i>	Complementation	At2g36200	This thesis
<i>CRISPR KIN5b T1-T3</i> in <i>H2B-mTurquoise2</i>	Genome editing	At2g36200	This thesis
<i>CRISPR KIN5b T3-T1</i> in <i>H2B-mTurquoise2</i>	Genome editing	At2g36200	This thesis
<i>CRISPR KIN5b T1-T3</i> in Col-0	Genome editing	At2g36200	This thesis
<i>CRISPR KIN5b T3-T1</i> in Col-0	Genome editing	At2g36200	This thesis
<i>CRISPR KIN5b T1-T3</i> in <i>TagRFP-T-TUA5</i>	Genome editing	At2g36200	This thesis
<i>CRISPR KIN5b T3-T1</i> in <i>TagRFP-T-TUA5</i>	Genome editing	At2g36200	This thesis
<i>CRISPR Kin5AI-IV</i> in Col-0	Genome editing	At2g37420	This thesis
<i>CRISPR Kin5AI-IV</i> in <i>TagRFP-T-TUA5</i>	Genome editing	At2g37420	This thesis
<i>CRISPR Kin5AI-IV</i> in <i>H2B-mTurquoise2</i>	Genome editing	At2g37420	This thesis

<i>CRISPR Kin5BI-IV</i> in Col-0	Genome editing	At2g36200	This thesis
<i>CRISPR Kin5BI-IV</i> in <i>TagRFP-T-TUA5</i>	Genome editing	At2g36200	This thesis
<i>CRISPR Kin5BI-IV</i> in <i>H2B-mTurquoise2</i>	Genome editing	At2g36200	This thesis
<i>CRISPR Kin5CI-IV</i> in Col-0	Genome editing	At2g28620	This thesis
<i>CRISPR Kin5CI-IV</i> in <i>TagRFP-T-TUA5</i>	Genome editing	At2g28620	This thesis
<i>CRISPR Kin5CI-IV</i> in <i>H2B-mTurquoise2</i>	Genome editing	At2g28620	This thesis
<i>CRISPR Kin5DI-IV</i> in Col-0	Genome editing	At3g45850	This thesis
<i>CRISPR Kin5DI-IV</i> in <i>TagRFP-T-TUA5</i>	Genome editing	At3g45850	This thesis
<i>CRISPR Kin5DI-IV</i> in <i>H2B-mTurquoise2</i>	Genome editing	At3g45850	This thesis

4.2 Material

4.2.1 Vectors

A map of every vector that was used or generated in this thesis is presented in the supplement (see 6).

Table 7: Vectors used in this thesis.

Vector	Promoter	Resistance	Reference
pQE80L	T7	ampicillin	Qiagen (Hilden, Germany)
pENTR™/D-TOPO®	T7	kanamycin	Invitrogen (Santa Clara, USA)
pMDC43	2x35S	kanamycin, chloramphenicol, hygromycin	Karimi, et al. (2007) ³¹¹

pMDC163	-	kanamycin, chloramphenicol, hygromycin	Karimi, et al. (2007) ³¹¹
pEarleyGate104	35S	kanamycin, phosphinothricin	Earley, et al. (2006) ³¹²
pDGE5, 7, 9, 11	-	ampicillin, chloramphenicol	Ordon, et al. (2017) ²³⁰
pDGE2	35S	spectinomycin, chloramphenicol, phosphinothricin	Ordon, et al. (2017) ²³⁰
pEN-C1-1	-	ampicillin	Schimpl, et al. (2016) ³¹³
pDE-Cas9	PcUbi	spectinomycin, phosphinothricin	Schimpl, et al. (2016) ³¹³

4.2.2 Chemicals

The chemicals and reagents, used in this thesis, were obtained from one of the following suppliers, if not stated otherwise: Th. Geyer (Renningen, Germany), Sigma Aldrich/Millipore/Merck (Darmstadt, Germany), Carl Roth (Karlsruhe, Germany), PanReac AppliChem (Darmstadt, Germany), SERVA (Heidelberg, Germany), VWR International (Darmstadt, Germany), Bernd Kraft (Duisburg, Germany), Jena Bioscience (Jena, Germany).

4.2.3 Kits

Table 8: Kits used in this thesis.

Kit	Manufacturer
Bac-to-Bac™ Baculovirus Expression System	Thermo Fisher Scientific (Waltham, USA)
EasySelect™ <i>Pichia</i> Expression Kit	Invitrogen (Santa Clara, USA)
Gateway® BP Clonase II enzyme mix	Invitrogen (Santa Clara, USA)
HiYield® PCR Clean-up/Gel Extraction Kit	SLG® (Gauting, Germany)
HiYield® Plasmid Mini DNA Isolating Kit	SLG® (Gauting, Germany)
NucleoBond™ Xtra Midi Kit	Macherey-Nagel (Düren, Germany)
pENTR™/D-TOPO® Cloning Kit	Invitrogen (Santa Clara, USA)
RevertAid™ First Strand cDNA synthesis Kit	Thermo Fisher Scientific (Waltham, USA)

4.2.4 Antibodies

Table 9: Antibodies used in this thesis.

Antibody	Manufacturer
Anti-biotin antibody (from mouse)	Invitrogen (Santa Clara, USA)
Anti-digoxigenin antibody (from sheep)	Roche (Penzberg, Germany)
Anti-mouse-HRP antibody (from goat)	Abcam (Cambridge, Great Britain)
Anti-Penta-His antibody (from mouse)	Qiagen (Hilden, Germany)
Anti- β -Tubulin antibody (from mouse)	SigmaAldrich/Merck (Darmstadt, Germany)

4.2.5 Enzymes

Table 10: Enzymes used in this thesis.

Enzyme	Manufacturer
Antarctic Phosphatase	NEB (Ipswich, USA)
BamHI (FastDigest)	Thermo Fisher Scientific (Waltham, USA)
Benzonase	Th. Geyer (Renningen, Germany)
Bpil (FastDigest)	Thermo Fisher Scientific (Waltham, USA)
Bsal	NEB (Ipswich, USA)
Bsu36I	NEB (Ipswich, USA)
Catalase	Calbiochem®/Merck (Darmstadt, Germany)
Cellulase	SERVA (Heidelberg, Germany)
DpnI (FastDigest)	Thermo Fisher Scientific (Waltham, USA)
DreamTaq DNA polymerase	Thermo Fisher Scientific (Waltham, USA)
EcoRI (FastDigest)	Thermo Fisher Scientific (Waltham, USA)
EcoRV	Thermo Fisher Scientific (Waltham, USA)
Glucose oxidase	SigmaAldrich/Merck (Darmstadt, Germany)
Macerozym	SERVA (Heidelberg, Germany)
MluI-HF	NEB (Ipswich, USA)
Phusion High-Fidelity DNA polymerase	Thermo Fisher Scientific (Waltham, USA)
PstI (FastDigest)	Thermo Fisher Scientific (Waltham, USA)
T4-DNA ligase	Thermo Fisher Scientific (Waltham, USA)
Universal Nuclease	Thermo Fisher Scientific (Waltham, USA)

4.2.6 DNA-Oligonucleotides

DNA oligonucleotides (primers) for specific methods are attached to the corresponding method.

Table 11: List of primers used for genotyping and sequencing of plants and bacterial colonies.

ID	Name	Sequence (5' to 3')
CB3	pQE_for	GTATCACGAGGCCCTTTCGTCT
CB32	nosT_101f	GTATAATTGCGGGACTCTAATCAT
CB33	GFP_374r	GACACCCTCGTCAACAGGATCGAG
CB4	pQE_rev	CATTACTGGATCTATCAACAGGAG
ED29	RP_saul1	TGAGGCCAATCAAATGATTTTC
ED30	LP_saul1	TTTCCCCATTCATGAGTGAAG
H413	SeqPrNN-YFP-HA	TCTTCAAGGACGACGGCAACTAC
H414	SeqPrNN-YFP-MYC	ACCACTACCAGCAGAACAC
H443	KINSeq1f	GGCAAGCTCAACTTGGTTGAC
H444	KINSeq2f	CCACAAACGAGGAATTGAAG
H445	KINSeq3f	GGTATACGCTTCCCGTGAG
H447	KINSeq4f	CAGCATTGACGACTTC
H454	ML096_011H10_fwd	ATATATTTTCTGACCCTGCCAAGT
H455	ML096_011H10_rev	TTATATGTTGAACACAGGTGTTTGGA
H458	ML098LP	ATCCTTCTGTTGTGCTGATGG
H459	ML098RP	TCAGAAGCTTGTCTCGAATCG
H627	M13uni(-21)	TGTA AACGACGGCCAGT
H628	M13rev(-29)	CAGGAAACAGCTATGACC
H729	KIN5bSeq5f	GTA CTTGTTCCA ACTTGAC
H730	KIN5bSeq6f	CAGAGCGCACCTTGTGGAGGTC
H731	KIN5bSeq7f	CTCGGCTGCAAACATTGTC
W3	LBa1primer	TGGTTCACGTAGTGGGCCATCG
W15	TDNAGKprimer	CCATTTGGACGTGAATGTAGACAC
W278	qPCRforKin5Ex2	CCCAAACATCGCTGGGAAG
W279	qPCRrevKin5Ex3	ACAAATCCTTCTGTTGTGCTGA
W280	qPCRforKin5Ex17	AGCCAGAGAAGGTGCTGATT

W281	qPCRrevKin5Ex18	ATTCCGCATGACCCACAGAT
W638	KIN Seq8f Tobi	TCTCTTTGCGAGGGAAGT
W639	Kin5b-Prom_ GT_fw	CGCCGGTGAGACAGAATAAG
W766	pFastBac_fw	TCCGGATTATTCATACCGTCCC
W767	pFastBac_rv	CCTCTACAAATGTGGTATGGCTG

4.3 Molecular biological methods

4.3.1 Isolation of genomic DNA from *Arabidopsis thaliana*

To extract genomic DNA (gDNA) from *A. thaliana*, about 50 mg of leaf tissue or one leaf of *A. thaliana* was harvested and transferred into a 1.5 ml reaction tube. 200 µl lysis buffer (200 mM Tris-HCl (pH 7.8), 250 mM NaCl, 25 mM EDTA, 0.5 % SDS) was added and ground up with a pestle. To remove cell debris, the mixture was centrifuged for 5 min at 14000 x g at RT (Heraeus Fresco 21, Heraeus, Hanau, Germany). The supernatant was mixed thoroughly with 150 µl 2-propanol in a new reaction tube and incubated for 10 min at -20 °C. After centrifugation at 14000 x g for 8 min at RT the precipitated DNA formed a sediment at the bottom of the tube and the supernatant was removed. The precipitate was washed with 500 µl of 70 % ethanol, vigorously mixed and then centrifuged for 5 min at 14000 x g at RT. Ethanol was removed completely and the precipitated DNA dried at 50 °C for 10 min on a block heater (Thermomixer compact, Eppendorf, Hamburg, Germany). The DNA was dissolved in 50 µl ddH₂O and stored at 4 °C.

4.3.2 DNA amplification by polymerase chain reaction (PCR)

Polymerase chain reaction (PCR) is used to amplify a certain section of DNA, for example a gene from the genome. The following reaction mixture with polymerase, dNTP-mix and buffer solutions (Thermo Fisher Scientific, Waltham, USA) was pipetted on ice (Table 12). The listed thermocycler PCR protocol (Table 13) was used and carried out in peqSTAR 2X Cyler (Pqlab, VWR International, Darmstadt, Germany) or T-Gradient and T-Professional Thermocycler (Biometra, Goettingen, Germany). Annealing temperature was chosen according to the primer melting temperature (T_m) and elongation time according to the length of the amplification product.

DNA amplification for cloning purposes was performed with Phusion DNA polymerase (Phusion High-Fidelity DNA Polymerase, Thermo Fisher Scientific), as it has an additional

proof-reading function that prevents base exchanges. The composition of the PCR reaction mix (Table 12) was adjusted accordingly to the manufacturer's instructions. The primer annealing temperature for thermocycler protocols was calculated, using the T_m Calculator (NEB, Ipswich, USA). The elongation time could be reduced to 30 s kb^{-1} .

Table 12: Composition of PCR reaction mix using Dream Taq polymerase.

Component	Volume
Dream Taq Green Buffer 10 x	2.0 μl
dNTP-mix (10 mM each)	0.4 μl
Primer fw (10 μM)	1.0 μl
Primer rev (10 μM)	1.0 μl
Template DNA	2.0 μl
Dream Taq DNA-Polymerase (5 U/ μl)	0.1 μl
dd H ₂ O	up to 20 μl

Table 13: Thermocycler protocol used in PCRs with Dream Taq polymerase.

Step	Temperature	Duration
Initial denaturation	95 °C	3 min
Denaturation	95 °C	30 s
Annealing	T_m	30 s
Elongation	72 °C	1 min/kb
Final Elongation	72 °C	5 min
Store	10 °C	∞

← 30 x

4.3.3 Colony PCR

To conclude if a bacterial colony contains the desired plasmid, a colony-PCR was performed by picking a colony from plate and diluting it in 10 μl sterile water. 2 μl of this bacterial suspension was used as template DNA in a standard PCR (see 4.3.2). The duration of the initial denaturation was extended to 5 min in order to disrupt the cells.

4.3.4 Agarose gel electrophoresis

DNA-fragments from PCR (see 4.3.2) or DNA restriction (see 4.3.8) were separated according to their size by agarose gel electrophoresis. For larger fragments (more than 1 kb) 1 % agarose was dissolved in 1 x TAE buffer (50 x TAE Buffer: 2 M Tris-HCl, 0.5 M EDTA, 1 M Glacial acetic acid, pH 8.5) by heating in a microwave. For RNA and smaller DNA fragments 1.5 % agarose gels were prepared accordingly. 4 µl ethidium bromide (Carl Roth, Karlsruhe, Germany) was added per 100 ml of hot agarose mixture and poured into a gel caster (Peqlab). The solidified gel was transferred into an electrophoresis tank, filled with 1 x TAE buffer until the gel slab was completely covered. Samples were loaded into the wells of an agarose gel along with a defined marker (Gene Ruler DNA Ladder Mix, Thermo Fisher Scientific). Electrophoresis was performed at 120 mV for 30-60 min and visualised afterwards under UV-light (E-Box VX2, Thermo Fisher Scientific).

If necessary distinct fragments were cut from the gel under UV-light and extracted, using the HiYield PCR Clean-up/Gel Extraction Kit (SLG, Gauting, Germany), according to the manufacturer's instructions.

4.3.5 Isolation of total RNA from *Arabidopsis thaliana*

For RNA extraction, about 100 mg plant tissue was harvested into a 2 ml reaction tube containing two 4.5 mm steel beads. The tissue was frozen in liquid nitrogen, pulverised with a vibration mill (Retsch „TissueLyser“, Quiagen, Hilden, Germany) at 30 Hz for 3 min and kept in liquid nitrogen afterwards. One ml TriFast (peqGold TriFast, Peqlab) was added to the frozen tissue powder and homogenised on a Vortex shaker for 5 min at RT. Then 200 µl chloroform was added and everything was mixed briefly. After 8 min incubation at RT the mixture was vigorously mixed again and then centrifuged for 10 min at 4 °C and 18000 x g for phase separation (MIKRO 22 R Centrifuge, Hettich, Tuttlingen, Germany). The upper, aqueous phase was transferred into a new 2 ml reaction tube, together with 500 µl 2-propanol and gently inverted. After precipitation on ice for 10 min the mixture was centrifuged for 10 min at 4 °C and 18000 x g to collect the precipitated RNA in a sediment. After removal of the supernatant, the precipitated RNA was washed two times with 1 ml of 70 % ethanol and then centrifuged for 5 min at 4 °C and 18000 x g. The ethanol was removed completely and the precipitate was dried on a block heater at 50 °C for 5 min. The precipitate was then dissolved in 50 µl RNase free water and used immediately or stored at -20 °C. Quality control of RNA isolation was done

by mixing 2 μ l RNA with 5 μ l 2 x RNA Loading Dye (Thermo Fisher Scientific) and 3 μ l ddH₂O, heating the mixture for 10 min at 70 °C, following separation by agarose gel electrophoresis (see 4.3.4). All work with TriFast and chloroform was carried out under a fume hood.

4.3.6 Synthesis of cDNA

RNA (1 pg up to 1 μ g) was transcribed to cDNA with QuantiTect Reverse Transcription Kit (Qiagen). Therefore, the RNA yield was measured with a NanoDrop 2000 Spectrophotometer (Thermo Fisher Scientific) at a wavelength of 260 nm. The transcription process was performed according to the manufacturer's instructions.

4.3.7 Reverse transcriptase-PCR (RT-PCR)

In order to analyse, whether expression of a particular gene is compromised in knockout mutant lines, RT-PCR was performed by using 1 μ l cDNA as template DNA in a standard PCR mix as described in 4.3.2. The thermocycler protocol was set to 10, 20, 30 and 40 cycles. Samples were further analysed by agarose gel electrophoresis (see 4.3.4).

All designed primers flanked several exon-intron regions, in order to confirm purity of the cDNA. While most genomic DNA contains introns, cDNA does not contain intronic regions and thus, can be distinguished from possible genomic DNA contamination by a size difference after gel electrophoresis. Actin2 was used as a positive control and standard (Table 14).

Table 14: List of primers used in this thesis for RT-PCR.

ID	Name	Sequence (5' to 3')
W278	qPCRforKin5Ex2	CCCAAACATCGCTGGGAAG
W286	RTPCRrevKin5Ex6	GTAAGGAACGTGTCCAAGATG
W898	RT-ACTIN2_for	ACTCTCCCCTATGTATGTC
W899	RT-ACTIN2_rev	CCACTGAGCACAATGTTACC

4.3.8 Restriction and ligation cloning

Inserts for this cloning method were generated by Phusion PCR, separated by agarose gel electrophoresis and purified with PCR clean-up Kit. The purified insert and designated vector plasmid were cut with restriction enzymes (New England Biolabs Inc.) according to the manufacturer's specifications and separated by agarose gel electrophoresis. Additionally, the vector was dephosphorylated with Antarctic phosphatase for one hour in 1 x Antarctic Buffer (Thermo Fisher Scientific Inc.) before separation. DNA band of expected size was cut and purified. Insert and vector were mixed in a ratio of 3:1, 5:1 and 7:1 and ligated with a T4 ligase and matching buffer (Thermo Fisher Scientific Inc.) overnight at 16 °C. Ligase products were transformed into DH5α *E. coli* cells by heat shock method (see 4.3.12).

4.3.9 Overlap extension cloning (OEC)

Overlap extension cloning is a way of cloning without DNA ligation, using two consecutive PCRs³¹⁴. The insert is generated in a first PCR with long chimeric primers, which contain areas complementary to the template DNA and to the final vector (Table 19). The reaction mix (Table 15) was divided into two PCR reaction tubes (50 µl each) for better thermal transfer before thermocycling (Table 16). The use of a DNA-Polymerase with proof-reading function is necessary to avoid point mutation in the further process.

Table 15: Composition of first PCR reaction mix for OEC.

Component	Volume
HF or GC Phusion Buffer 5 x	20 µl
dNTP-mix (10 mM each)	2 µl
Primer fw (100 µM)	0.5 µl
Primer rev (100 µM)	0.5 µl
DMSO	2 µl
Template DNA (100 ng/µl)	1 µl
Phusion DNA-Polymerase (2 U/µl)	0.5 µl
dd H ₂ O	up to 100 µl

Table 16: Thermocycler protocol used for first PCRs of OEC.

Step	Temperature	Duration
Initial denaturation	100 °C	2 min
Denaturation	95 °C	30 s
Annealing	45-72 °C	30 s
Elongation	70 °C	2.5 min
Final Elongation	70 °C	10 min
Store	10 °C	∞

← x 35

The PCR product was mixed with 6 x loading dye and separated by agarose gel electrophoresis. The product of the according size was excised and extracted from the agarose gel (see 4.3.4). This purified PCR product was then used in a second PCR to integrate the insert into the desired vector plasmid, thereby generating a new plasmid. Therefore, the following PCR reaction mix (Table 17) was used and divided into two PCR reaction tubes. In one of these tubes 0.5 µl Phusion DNA polymerase was added before thermocycling (Table 18), the other one was used as a negative control.

Table 17: Composition of second PCR reaction mix for OEC.

Component	Volume
HF or GC Phusion Buffer 5 x	20 µl
dNTP-mix (10 mM each)	2 µl
DMSO	2 µl
Purified DNA insert from first PCR	35 µl
Vector DNA (60 ng/µl)	0.5 µl
dd H ₂ O	40 µl
Total	99.5 µl

Table 18: Thermocycler protocol used for second PCRs of OEC.

Step	Temperature	Duration
Initial denaturation	100 °C	1 min
Denaturation	95 °C	30 s
Annealing	50 °C	30 s
Elongation	70 °C	12 min
Final Elongation	70 °C	12 min
Store	10 °C	∞

← x 20

To eliminate template vector DNA, 0.5 µl DpnI restriction enzyme (20 U/µl, New England Biolabs, Ipswich, USA) was added to the mixture and incubated for 2 h at 37 °C. DpnI specifically digests DNA that is methylated at its recognition site. Due to the *in vitro* synthesis of the final vector, no methylation occurred, thus, only the template DNA is digested. After DpnI treatment, both 1 µl and 10 µl of the final PCR product were used to transform DH5α *E. coli* cells by heat shock method (see 4.3.12).

Table 19: List of primer used in this thesis for OEC.

ID	Name	Sequence (5' to 3')
W348	AtKin5a_OEC_for	ATTCACACAGAATTCATTAAGAGGAGAAATTA ACTATGT CTAGCCGCCATGACAAAGAGAAAGGC
W349	AtKin5a_OEC_rev	CTATCAACAGGAGTCCAAGCTCAGCTAATTAATGGTGATG ATGGTGATGGACTTGTGAGAGAGGCGACCGTGTTAG
W387	For Kin5bProm-GU	GAGGATCCCCGGGTACCGAGCTCGAATTATCGTGTTTCCT AGCCTTCTTTTGACCTTAACG
W388	Rev Kin5bProm-GU	CACGGGTTGGGGTTTCTACAGGACGTAACATCGGCGAAC GGACGGCGAATCCAGTGAGACTG
W431	OEC_K5b_fw_Pichia	GGTATCTCTCGAGAAAAGAGAGGCTGAAGCTTCTAGCCGC CATGACAAAGAGAAAGGCGTC
W432	OEC_K5bFL_rv_Pichia	GGCTACAACTCAATGATGATGATGATGATGGACTTGTGA GAGAGGCGACCGTGTTAGCTG
W433	OEC_K5b- eGFP_rv_Pichia	GGCTACAACTCAATGATGATGATGATGATGTTTGTATAG TTCATCCATGCCATGTGTAATC

W434	OEC_K5bFL_eGFP_rv	CTCCAGTGAAAAGTTCTTCTCCTTTACTGACTTGTGAGAGA GGCGACCGTGTTAG
W456	OEC_fw_kin5b- Promoter-eYFP-KIN5b	CAGTCTCACTGGATTCGCCGTCGGTTCGCCGATGGGCAAG GGCGAGGAGCTGTTC
W457	OEC_rv_kin5b- Promoter-eYFP-KIN5b	ATGGTGCGCCAGGAGAGTTGTTAGTTGACTTGTGAGAGA GGCGACC
W762	OEC_fw_pFB1-KIN5b	CGCGGAATTCAAAGGCCTACATGTCTAGCCGCATGACAA AGAG
W763	OEC_rv_KIN5BFL-pFB1	AAGCTTGGTACCGCATGCCTTAATGGTGATGATGGTGATG GGGCTCCATGCAGCAGCCGGGGCAGCAGTTCAGGAAGAC TTGTGAGAGAGGCCGACCGTGTTAG

4.3.10 Gateway cloning

Gateway cloning is a reliable cloning method to integrate an insert into a wide array of specific destination vectors. Gateway cloning is performed in two major steps. First, the PCR product is cloned into the entry vector and in a second step transferred into the destination vector. For the establishment of entry-clones, inserts were generated by PCR with special forward primers containing a CACC sequence at the 5'-end. This sequence is needed to integrate the insert into the entry-vector by a so called TOPO reaction. This reaction was performed by gently mixing 0.5 µl pENTR/D-TOPO vector, 0.5 µl salt mixture (pENTR/D-TOPO Cloning Kit, Thermo Fisher Scientific), and 2 µl of purified PCR product (see 4.3.4) and subsequent incubation of the mixture for 1 h at RT. The whole mixture was then transformed into chemically competent DH5α *E. coli* cells by heat shock method (see 4.3.12). Colonies were tested by colony PCR (4.3.3) and sequencing. For cloning the desired sequence into the destination vector, plasmid DNA was extracted from positive clones (see 4.3.16) and 150 ng of this plasmid was mixed with 150 ng of destination vector, 1 µl L/R Clonase II (Thermo Fisher Scientific Inc.) and filled up to 10 µl with TE buffer. L/R reaction was incubated overnight at 16 °C and transformed into DH5α *E. coli* cells again using heat shock method.

Table 20: List of primers used in this thesis for Gateway cloning.

ID	Name	Sequence (5' to 3')
W355	At2g36200g+_-11 (Kin5_GUS_long-fw)	CACCATTCCGACTTCTTCTTCATA
W356	At2g36200g+_-85 (Kin5_GUS-fw)	CACCGTGTTTCCTAGCCTTCTTTT
W357	At2g36200g-_-12 (Kin5_GUS-rev)	GAACGGACGGCGAATCCAGTGAGA
W458	GW_fw+CACC_KIN5b FL	CACCATGTCTAGCCGCCATGACAAAG
W459	GW_rv_KIN5b FL	GTTGACTTGTGAGAGAGGCGACCG

4.3.11 Preparation of chemically competent *Escherichia coli* cells

To prepare *E. coli* cells for the uptake of plasmid DNA, they were made competent by chemical treatment^{315,316}. Therefore, a pre-culture was grown overnight in 20 ml LB-medium (10 g l⁻¹ tryptone, 5 g l⁻¹ yeast extract, and 10 g l⁻¹ NaCl, pH 7.0) at 37 °C, shaken at 180 rpm (Incubator shaker MAXQ 5000/6000, Thermo Fisher Scientific). 50 ml main-culture was inoculated with 1 ml pre-culture and incubated at 37 °C until reaching an OD₆₀₀ of 0.5 (Eppendorf BioPhotometer, Eppendorf). The culture was centrifuged at 2000 x g for 10 min at 4 °C (Centrifuge 5810R, Eppendorf). After discarding the supernatant, the sedimented bacteria were kept on ice and resuspended in 10 ml transformation buffer I (TfbI; Table 21) After 10-minute incubation on ice, the mixture was centrifuged for 5 min at 1500 x g at 4 °C and supernatant was removed again. The sediment was resuspended in 2 ml transformation buffer II (TfbII; Table 21) and divided into 100 µl aliquots in 1.5 ml reaction tubes, frozen in liquid nitrogen and stored at -80 °C.

Table 21: Solution for the preparation of chemically competent *E. coli*.

Buffer	Components	Comments
Tfb I	30 mM KAc, 50 mM MgCl ₂ , 100 mM KCl, 15 % glycerol, set to pH 5.8 with acetic acid	Sterile filtered, stored at 4 °C

Tfb II	10 mM MOPS, 10 mM KCl, 75 mM CaCl ₂ , 15 % glycerol, set to pH 7 with NaOH	Sterile filtered, stored at 4 °C
--------	---	----------------------------------

4.3.12 “Heat shock” transformation of chemically competent cells

Transformation of chemically competent *E. coli* cells was performed by heat shock method^{315,316}. Chemically competent cells were thawed on ice and mixed carefully with plasmid DNA or ligation product and incubated for 30 min on ice. Heat shock was applied with a heating block at 42 °C for 90 s (Eppendorf Thermomixer compact, Eppendorf). Bacteria were immediately transferred on ice. For recovery, 200 µl LB media was added to the bacteria cells, following incubation at 37 °C for 30 min with slow shaking at 550 rpm. Finally, cells were plated onto LB plates (LB-medium solidified with 15 g l⁻¹ agar) containing the appropriate antibiotics and incubated overnight at 36 °C. Positive clones were determined by colony PCR (see 4.3.3).

4.3.13 Preparations of electrocompetent *Agrobacterium tumefaciens* cells

To prepare agrobacteria for electroporation, a flask with 100 ml LB-medium was inoculated with *Agrobacterium tumefaciens* and incubated at 28 °C overnight. The culture was transferred into 50 ml falcon tubes and stored on ice for 30 min. Cells were kept on ice for all of the following steps. The culture was centrifuged at 4000 x g for 10 min at 4 °C (Eppendorf Centrifuge 5810 R, Eppendorf) and the supernatant was discarded afterwards. The bacterial sediment was then resuspended in 20 ml sterile 10 % glycerol and again centrifuged. After resuspension in 15 ml 10 % glycerol the process was repeated two more times with a further reduction of the resuspension volume to 10 ml and finally 2 ml 10 % glycerol. Electrocompetent cells were divided in 80 µl aliquots, frozen in liquid nitrogen and stored at -80 °C³¹⁷.

4.3.14 Transformation of electrocompetent cells

For electroporation of agrobacteria, electrocompetent cells were thawed on ice and carefully mixed with about 100 ng plasmid DNA. This mixture was transferred into a cuvette for electroporation (PqLab) and electroshocked in an electroporator (Eppendorf Eporator, Eppendorf) for 5 ms at 1440 V. 400 µl LB-medium was added to the bacterial cells and the suspension was transferred into a new 1.5 ml reaction tube. Agrobacteria recovered at 28 °C for 2 h while slowly shaking. Cells were finally plated onto LB plates containing the appropriate antibiotics and incubated for 2-3 days at 28 °C³¹⁷.

4.3.15 Generation of glycerol stocks

For long-term storage of bacterial cells, glycerol stocks were prepared and kept at -80 °C. In order to prepare these, 800 µl of a well grown overnight culture was filled into a sterile 2 ml screw cap micro tube. Then, 800 µl of 80 % sterile glycerol was added and mixed thoroughly. Glycerol stocks were frozen in liquid nitrogen and stored at -80 °C.

In order to start new cultures from a glycerol stock, a small bit of the still frozen glycerol stock was picked with a sterile pipet tip and dropped into LB-media supplemented with the appropriate antibiotics and grown overnight at the appropriate temperature, shaking at 180 rpm.

4.3.16 Plasmid extraction from bacteria

For extraction of plasmid DNA from *E. coli* the alkaline extraction procedure was used³¹⁸. First, 5 ml of liquid LB-media was inoculated by picking a colony and growing the culture overnight at 37 °C shaking at 180 rpm. About 4 ml of the overnight culture was centrifuged for 1 min at 10000 x g at RT (Heraeus Fresco 21, Heraeus) and the bacterial sediment was then resuspended in 300 µl S1 buffer (50 mM Tris-HCl, 10 mM EDTA, 100 µg/ml RNase A, pH 8.0). For cell lysis 300 µl of buffer S2 (200 mM NaOH, 1 % SDS) was added to the mixture, gently inverted and incubated at RT for 5 min. To neutralise the alkaline conditions, 300 µl S3 buffer (2.8 M K-acetate, pH 5.1) was added and again gently inverted, incubated for 5 min at RT and then centrifuged for 5 min at 14000 x g. The supernatant was transferred into a new 1.5 ml reaction tube and 500 µl 2-propanol was added to precipitate the plasmid DNA. After mixing thoroughly and centrifugation for 10 min at 14000 x g a DNA precipitate could be isolated. After washing the precipitate with 500 µl of 70 % ethanol and centrifugation for 5 min at

14000 x g, the ethanol was removed and the precipitate dried on a block heater (Eppendorf Thermomixer compact, Eppendorf) at 50 °C for 10 min. The precipitate was then dissolved in 50 µl ddH₂O.

In some cases, plasmid DNA was isolated by using plasmid DNA purification kits to obtain greater amounts of plasmid DNA or to increase the purity (HiYield Plasmid Mini DNA Isolating Kit, SLG, Gauting, Germany or NucleoBond Xtra Midi/Maxi, Macherey-Nagel, Düren, Germany). These kits were used according to the manufacturer's instructions.

DNA yield of plasmid extractions was measured with a NanoDrop 2000 Spectrophotometer at 260 nm (Thermo Fisher Scientific).

4.3.17 Sanger Sequencing

Sequencing samples were prepared as recommended and send to Eurofins Genomics (Eurofins, Ebersberg, Germany) for sequencing. Sequencing results were analysed with Clone Manager Professional 9 (Sci Ed Software, Westminster, USA).

4.4 Plant handling

4.4.1 Growth conditions

Arabidopsis thaliana plants were grown under different conditions according to the requirement of the experiment. For seed production and plant proliferation, plants were grown on soil consisting of 60 % Fruhstorfer Pikiersubstrat (Wilsaflor, Neulehe, Germany), 30 % coarse-grained sand and 10 % expanded clay (Fibo ExClay, Lahmstedt, Germany) in climate chambers (Weiss Klimatechnik, Reiskirchen-Lindenstruth, Germany) or GroBanks® (Brightboy, CLF Plant Climatics, Wertingen, Germany) under long-day conditions with 16 h light and 8 h dark, at around 22 °C. For the production of protoplasts, plants were grown in GroBanks® under short-day conditions with 8 h light and 16 h dark at around 22 °C. In all cases, light intensity was set between 90 and 120 µmol m⁻² s⁻¹.

For phenotyping experiments and plant selection, *A. thaliana* were cultivated in sterile conditions on complete Murashige and Skoog-medium³¹⁹ (MS, M0221, Duchefa Biochemie, Haarlem, Netherlands, supplemented with 1 % sucrose and 0.8 % phyto agar, P1003, Duchefa; set pH 5.6 with KOH). After autoclaving, MS-medium was cast into square petri dishes with vents (Greiner BIO-ONE, Kremsmünster, Austria) under sterile conditions at a laminar flow cabinet. Plants on MS-medium were cultivated in an upright position in climate cabinets

(Percival, Percival Scientific, Perry, USA) under long-day conditions with light intensity set between 90 and 120 $\mu\text{mol m}^{-2} \text{s}^{-1}$ at 22 °C or 17 °C according to the experiment.

Nicotiana benthamiana plants for localisation studies were grown on soil consisting of two parts Einheitserde Classic Typ-P (Einheitserde Werkverband, Sinntal-Altengronau, Germany) and one part coarse-grained sand in a green house at 22 °C at day and 20 °C at night. Light conditions were set to 300 $\mu\text{mol m}^{-2} \text{s}^{-1}$ for 14 h. Especially in the summer temperature and light conditions varied.

4.4.2 Sterilisation, stratification and sowing of *Arabidopsis thaliana* seeds

Before *Arabidopsis* seeds could be sown on soil, the dormancy had to be broken first. For this purpose, they were stratified in a 1.5 ml reaction tube with water for at least 48 h at 4 °C in the dark. Before sowing, the soil was first treated for at least 2 h with Biomükk® WDG (1 ml l⁻¹; Biofa, Münsingen, Germany) to prevent fly infestation and afterwards with Previcur® Energy (2.5 ml l⁻¹; Bayer CropScience, Langenfeld, Germany) to prevent damping-off disease caused by fungi. Once the seeds were sown, a hood was placed on top of the plant pot for 2-3 days to keep the seeds moist while they germinated in a growth chamber.

For cultivation on MS-medium, the seed surface had to be sterilised. Two methods for surface sterilisation were used on dry seeds before stratification: In the first method chlorine gas was used. Therefore, a beaker with 25 ml sodium hypochlorite was placed into a desiccator. Chlorine gas was produced by adding 2 ml hydrochloric acid to the sodium hypochlorite. The seeds were exposed to the chlorine gas for at least 5 h. After outgassing under a laminar flow cabinet for half an hour, the seeds were ready for stratification. In the second method, the seeds were washed thoroughly with ethanol. First, the seeds were filled into a spin column (from HiYield® Plasmid Mini DNA Isolating Kit or HiYield® PCR Clean-up/Gel Extraction Kit, SLG®) and incubated for 5 min in 700 μl 70 % ethanol while shaking at 900 rpm on a thermomixer (Eppendorf thermomixer compact, Eppendorf). Following the incubation, the ethanol was removed by spinning the column in a centrifuge at 10000 x g for 1 min (Eppendorf Centrifuge 5424 R, Eppendorf). The flow through was removed and 700 μl pure ethanol was added to the seeds and immediately removed by centrifugation as before. After removal of the flow-through, seeds were dried by centrifugation for up to 3 min at 10000 x g to completely remove all residues of ethanol. The seeds were finally transferred into a sterile 1.5 ml reaction tube and were ready for stratification.

4.4.3 Isolation and transformation of *Arabidopsis thaliana* leaf protoplasts

Protoplasts were isolated from 6-8-week-old *A. thaliana* plants grown under short day conditions (see 4.4.1) ^{173,237}. First, about 40 leaves were cut into 2 mm stripes with a sharp razor blade and transferred into a square petri dish (100 mm x 100 mm, Sarstedt, Nümbrecht, Germany) filled with 0.5 x MCP buffer (Table 22). The liquid was then removed with a pipette and replaced with 20 ml digestion buffer (Table 22) and incubated for 2 h at 26 °C shaking at 60 rpm (Unimax 1010, Heidolph Instruments, Schwabach, Germany) in the dark. To release the protoplast from the leaf skeleton the petri dish was shaken at 80 rpm for 1 min. A 50 µm nylon mesh was fixed to a funnel and moistened with MaMg buffer (Table 22). The protoplasts were carefully sifted through the mesh into a 50 ml reaction tube and the mesh was rinsed with MaMg buffer. To remove the digestion buffer, protoplasts were centrifuged at 100 x g and 23 °C for 3 min in a swing-out rotor (Eppendorf Centrifuge 5810 R, Eppendorf) with slow acceleration (set to 4) and deceleration (set to 1) to reduce shearing forces. Supernatant was removed and protoplast were resuspended in 20 ml MaMg buffer by slowly and carefully turning the reaction tube sideways. The protoplasts were centrifuged again as mentioned above and resuspended in 1 ml MaMg buffer and were ready for immediate transformation. Transformation of protoplasts was achieved by carefully mixing 150 µl of protoplasts with 20 µg DNA and 165 µl PEG-Ca buffer (Table 22) in a 13 ml reaction tube (Sarstedt). Reaction tubes were slowly rotated in order to gently, but thoroughly mix the solution, followed by incubation for 30 min at RT in the dark. To remove PEG-Ca buffer, 500 µl, 1 ml and 1.5 ml of W5 buffer (Table 22) were added to the mixture in an interval of 5 min. The mixture was gently mixed by turning the reaction tube sideways after each step. Protoplasts were then centrifuged as above mentioned and resuspended in 3 ml W5 buffer by turning the reaction tube sideways slowly. This step was repeated once, to wash out residues of PEG-Ca buffer. The transformed protoplasts were transferred into a small petri dish (Ø 3 cm; Sarstedt) and stored overnight at RT in the dark. Transformation was investigated using a confocal laser scanning microscope (see 4.4.6).

Table 22: Buffers used for protoplast isolation and transformation.

Buffer	Components	Comments
MCP	500 mM sorbitol, 1 mM CaCl ₂ , 10 mM MES (2-(N-morpholino)-ethanesulfonic acid); set to pH 5.6 with KOH	Autoclaved
Enzyme solution	0.25 % macerozyme 1 % cellulase	In MCP buffer
MaMg	450 mM sorbitol, 15 mM MgCl ₂ , 5 mM MES; set to pH 5.6 with KOH	Autoclaved
PEG-Ca	61.5 % (w/w) PEG 4000 (Fluka/Merck), 300 mM mannitol, 150 mM CaCl ₂	In ddH ₂ O
W5	154 mM NaCl, 125 mM CaCl ₂ , 5 mM KCl, 5 mM glucose, 2 mM MES; set to pH 5.6 with KOH	Autoclaved

4.4.4 Agrobacteria-mediated transformation of *Arabidopsis thaliana*

To introduce transgenic material into *A. thaliana*, agrobacteria were used as a vector³²⁰. Therefore, *A. tumefaciens* (Table 2) containing a T-DNA binary vector with the desired insert were cultivated in 10 ml LB-medium for 2 days at 28 °C shaking at 180 rpm (Unimax 1010, Heidolph Instruments). The bacterial culture was centrifuged at 4000 x g and RT for 5 min (Eppendorf Centrifuge 5810 R, Eppendorf). Supernatant was removed and the pale pink sediment was resuspended in 10 ml infiltration-solution (5 % sucrose, 0.05 % Silwet L-77, Momentive Performance Materials, Waterford, USA) and recovered for 2 h at 28 °C. Plants

were prepared for painting by cutting off all siliques and opened flowers leaving behind only the flower buds. The bacterial suspension was then applied on all flower buds with a brush three consecutive times. This way the infiltration is much more sparing than dipping the whole plant into a beaker filled with bacterial suspension. Painted plants were carefully covered with a plastic bag and kept in the dark for 1 – 2 days. After removal of the bags, the plants grew under normal conditions until seeds were harvested.

4.4.5 Agrobacteria-mediated transformation of *Nicotiana benthamiana*

In order to determine the localisation of fluorescent fusion proteins in *Nicotiana benthamiana*, agrobacteria-mediated transformation was used to transmit the desired plasmids. Therefore, 50 ml LB-medium was inoculated with agrobacteria containing the desired plasmid from an overnight pre-culture with the according antibiotics. Additionally, a culture was inoculated with agrobacteria containing a plasmid for the P19 gene silencing-inhibitor from tombusvirus²⁴⁷. All cultures grew overnight at 28 °C, shaking at 180 rpm (Unimax 1010, Heidolph Instruments) and were concentrated by centrifugation at 4000 x g at 4 °C for 10 min (Eppendorf Centrifuge 5810 R, Eppendorf). The supernatant was discarded and the pinkish sediment was resuspended in 10 ml infiltration-solution (20 mM MgCl₂, 0.01 mM acetosyringone, SigmaAldrich/Merck, in 0.1 M sodium phosphate buffer pH 6.1). This bacterial suspension was then used to resuspend an agrobacteria sediment containing the P19 gene silencing-inhibitor. After regeneration for 2 h at 28 °C, the bacterial suspension was filled into a 2 ml syringe and injected into the stomata of well-watered *N. benthamiana* plants. Therefore, the syringe was pressed against the underside of a leaf. A darkening of the leaf could be observed around the injection site, due to the bacterial liquid entering the intercellular space through opened stomata. The area of injection was marked and plants recovered for two days, before the leaf tissue was examined by confocal laser scanning microscopy (see 4.4.6).

4.4.6 Confocal laser scanning microscopy

To determine the subcellular localisation of fluorescently labelled proteins in living plant cells, confocal laser scanning microscopy, using the Leica TCS SP8 Confocal Platform (Leica Microsystems, Wetzlar, Germany) was performed. All images were obtained using a HC PL APO CS2 63 x /1.2 water objective (Leica Microsystems). Emission of fluorescent molecules

were recorded with Leica HyD (Leica Microsystems) detectors and bright field emission with a photomultiplier (PMT). Excitation and emission parameters are listed below (Table 23).

Table 23: List of fluorophores used in this thesis with their respective excitation and emission wavelength.

Fluorophore	Excitation	Emission	Detector
Chlorophyll autofluorescence	Any laser line	660-675 nm	HyD
GFP (green fluorescent protein)	488 nm	502-512 nm	HyD
Hoechst 33342	405 nm	445-465 nm	HyD
mTurquoise2	458 nm	470-480 nm	HyD
tagRFP (red fluorescent protein)	561 nm	575-595 nm	HyD
YFP (yellow fluorescent protein)	514 nm	522-532 nm	HyD

4.4.7 Selection of transformed plants

By successfully transforming the plants with the desired vector (see 4.4.4), the transgenic plants also gained a herbicide resistance, which could be used to exclude untransformed plants. Transgenic plant lines were selected either by treatment with phosphinothricin or hygromycin, regarding the resistance on the transmitted vector.

In case of phosphinothricin-resistance^{321,322}, plants were grown on soil (see 4.4.2) until all cotyledons emerged completely. Phosphinothricin was then applied by spraying a phosphinothricin-solution (1 mM Basta®, Bayer CropScience, Langenfeld, Germany) onto the young seedlings. After a few days, plants without the resistance started to die and the remaining thriving plants were shifted to new soil and genotyped accordingly. If necessary, phosphinothricin-treatment was repeated several times if plants did not react to the treatment immediately.

In case of hygromycin resistance³²³, seeds were surface sterilised and sown on sterile MS-medium (see 4.4.2) complemented with hygromycin-B (15 µg ml⁻¹, SigmaAldrich/Merck, Darmstadt, Germany). Following stratification, the seeds were cultivated at 22 °C and light, in order to stimulate germination. After 6 h in the light, plates with seeds were wrapped in aluminium foil and kept in the dark at 22 °C for 48 h, before normal long-day growth conditions continued. Hygromycin resistant plants could now easily be distinguished from not transformed plants by their elongated hypocotyl³²⁴. Resistant plants were then shifted to soil and genotyped accordingly.

4.4.8 β -glucuronidase (GUS) staining

For the analysis of gene activity in *A. thaliana*, plants were transformed with a promoter- β -glucuronidase (GUS) construct, selected accordingly (see 4.4.4 and 4.4.7) and stained in a solution containing 5-Bromo-4-chloro-3-indolyl- β -D-glucuronide (X-Gluc)³²⁵. Therefore, plants were grown on MS-medium to the desired developmental stage and then transferred into a 24-well plate filled with 1 ml 0.1 M sodium phosphate buffer (pH 7.0). After all plants were harvested, the phosphate buffer was discarded and replaced with 1 ml X-Gluc-solution (20 mM sodium phosphate buffer, 3 mM ferrocyanide, 0.5 % Triton X-100 and 1 mg ml⁻¹). After vacuum infiltration for up to 10 minutes (Eppendorf Concentrator plus, Eppendorf), the plants were incubated at 37 °C for 90 min to reach an optimal staining. The bacterial enzyme GUS can hydrolyse X-Gluc at 37 °C, which leads to the formation of a very stable blue indigo dye in the presence of oxygen. To remove chlorophyll and other plant pigments, the X-Gluc-solution was removed and 2 ml ethanol-glacial acidic acid (1:1) was added for 30 min. The ethanol-glacial acidic acid was exchanged several times, until all chlorophyll was removed. The GUS-stained plants were cleared, using either Hoyer's clearing solution (58 g of chloral hydrate is solved in a warm mixture of 15 ml ddH₂O and 2.5 ml glycerol)³²⁶ or ClearSee (10 % xylitol, 15 % deoxycholate, 25 % urea in ddH₂O)³²⁷. Cleared plants were investigated at a microscope using the Olympus cellSens Standard software (Olympus MVX10, Objective: MV PLAPO 1X or MV PLAPO 2XC, Camera: DP73; Olympus, Tokyo, Japan).

4.4.9 Evaluation of root size by coloured pixel counting

In order to establish a mutant phenotype for *kin5b-1*, several phenotyping experiments were conducted and the root growth was observed and documented with a flatbed scanner (Epson Perfection V700 PHOTO, Epson). As the measuring of the combined root size could not be determined manually, especially at later time points of these experiments, a method was developed to determine the root size by counting every pixel that belonged to a part of the root network. Therefore, all scanned pictures from one time point were loaded into FIJI and transformed into a two-colour picture using the same threshold for all pictures. To count the root pixels with the FIJI plugin "Color Pixel Counter", the colour of every picture was turned to green and the area of the root network of every plant was marked individually (**Figure 38**).

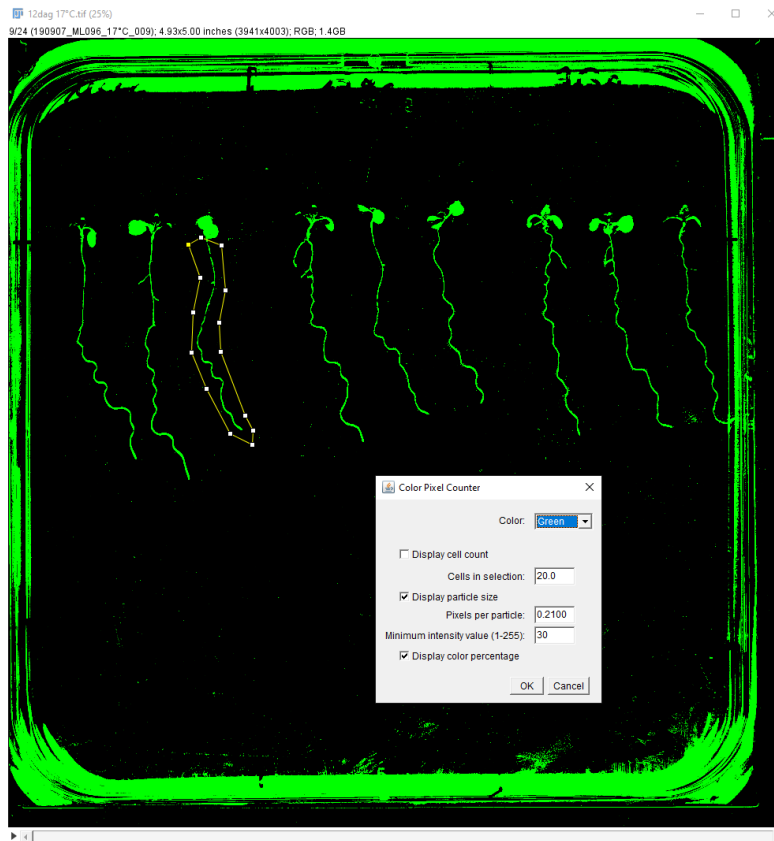


Figure 38: Example of measuring the number of root pixels per flatbed scan.

The measured pixel data was further analysed using excel, in order to calculate the mean root pixel number per plant, as well as the variance and the standard deviation. The differences between certain groups were tested with a Students t-test or Welch test for its significance and a corresponding p-value was determined.

4.4.10 CRISPR/Cas9

In order to obtain *A. thaliana* knockout mutants that lack the ability to produce one or even multiple kinesin-5s, two CRISPR/Cas9 genome editing approaches were tested. Cas9 is a nuclease that is able to interact with small RNA sequences that bind DNA and determine the cleavage site or target sequence of Cas9. It was found that a single-guide RNA (sgRNA) is sufficient for the cleavage of DNA. These double-strand breaks can lead to point mutations or even deletions upon repairing. In this way, inheritable genome modifications can be realised in a highly precise manner. Aim of the genome editing was to remove most of the open reading frame of the respective kinesin-5 gene.

In order to set up a cloning strategy, potential target sequences near protospacer adjacent motifs (PAM) were determined with the online-software CC-Top^{328,329}. This software also

rated the cleavage efficiency and showed potential off target sites. Further, it provided DNA oligo sequences for the introduction of the sgRNA sequence into the respective vector. For the beginning of the respective kinesin-5 gene, two target sites were chosen in relatively close proximity (about 20-40 bp) to one another. The same was done for the end of the gene. As the two approaches used the same functional principle and target generation, they differed in the used vectors and target sequences.

CRISPR/Cas9 genome editing following Stuttmann^{230,330}:

One of the big advantages of the vectors offered by Johannes Stuttmann, is the possibility to transfer up to eight sgRNA sequences into the plant genome with a single vector. To introduce more than one sgRNA sequence into the genome editing vector pDGE2, each sgRNA sequence had to be loaded into a shuttle vector first. Therefore, the two DNA oligos (Table 24) for each sgRNA sequence were hybridised by mixing 5 µl of oligo 1 (100 µM; fw) and 5 µl oligo 2 (100 µM; rev) with 40 µl ddH₂O and denaturing at 98 °C for 5 min. The oligo mix was cooled slowly at RT. Hybridised oligos were set to a final concentration of 50 fmol µl⁻¹ by mixing 2 µl hybridised oligos with 398 µl ddH₂O. Each hybridised oligo pair was loaded into another shuttle vector (pDGE5, 7, 9 and 11) with a one-step cut/ligation reaction. Therefore, 50 fmol hybridised oligos was mixed with 20 fmol shuttle vector and 1 µl 10 x ligation buffer (Thermo Fisher Scientific), 1 µl 10 x BSA (1 mg ml⁻¹), 0.5 µl Bpil restriction enzyme (Thermo Fisher Scientific), 0.5 µl T4 DNA ligase (Thermo Fisher Scientific), set to 10 µl with ddH₂O and treated in a thermocycler (2 min at 37 °C, followed by 5 min at 16 °C, repeated 20 times, then 10 min at 50 °C and 10 min at 80 °C). The cut/ligation reaction was transferred into chemically competent Top10 cells (see 4.3.11 and 4.3.12) and plated on LB-medium plates supplemented with ampicillin (100 µg ml⁻¹) and incubated over night at 37 °C. Two colonies were used to inoculate an overnight culture for plasmid preparation (4.3.16). The plasmids of all four sgRNA sequences were used in another cut/ligation reaction. The mixture (20 fmol pDGE2, 20 fmol of each shuttle vector, 2 µl 10 x ligation buffer, 2 µl 10 x BSA, 1 µl Bsal, 1 µl T4 DNA ligase, set to 20 µl with ddH₂O) was incubated in a thermocycler (2 min at 37 °C, followed by 5 min at 16 °C, repeated 40 times, then 10 min at 50 °C and 10 min at 80 °C) and transferred into chemically competent Top10 cells. The cells were streaked on LB-medium plates supplemented with spectinomycin (100 µg ml⁻¹) and incubated overnight at 37 °C. Four colonies were used to start an overnight culture for plasmid preparation. As a control the plasmids were restricted with PstI and EcoRV, analysed by agarose gel electrophoresis (4.3.4)

and sequenced, using the primer W133 and W136 (Table 24). This procedure was conducted for all four kinesin-5 genes of *A. thaliana* with the primers listed in Table 24. The four vectors were transferred into agrobacteria C58C1 (4.3.14) and painted onto *A. thaliana* plants (see 4.4.4; Col-0, H2B-mTurquoise2, TagRFP-T-TUA5, Table 6). Transformed plants were selected with phosphinothricin (see 4.4.7).

Plants were tested for several generations for a deletion of the respective kinesin-5 and the presence of Cas9 by PCR of gDNA (Table 25).

Table 24: List of primers used for cloning and analysis of CRISPR/Cas9 constructs following Stüttmann.

ID	Name	Sequence (5' to 3')
W133	JS811	GAATATCATCCGGTGCAGC
W136	pPMR	AGCGAAACCCTATAAGAA
W139	Kin5a_fw_I	ATTGCAGGAAACAGAGCCGAATCC
W140	Kin5a_rev_I	AAACGGATTCGGCTCTGTTTCCTG
W141	Kin5a_fw_II	ATTGGATTAGGGTAAGTAACCGTT
W142	Kin5a_rev_II	AAACAACGGTTACTTACCCTAATC
W143	Kin5a_fw_III	ATTGGTCTCTCATAAAAGACTATC
W144	Kin5a_rev_III	AAACGATAGTCTTTTATGAGAGAC
W145	Kin5a_fw_IV	ATTGATCCATAAATGTGCCAAGCC
W146	Kin5a_rev_IV	AAACGGCTTGGCACATTTATGGAT
W147	Kin5b_fw_I	ATTGTGAATTTAGGAATTGTTCGA
W148	Kin5b_rev_I	AAACTCGAACAATTCCTAAATTCA
W149	Kin5b_fw_II	ATTGATTTTTAAACGGCGAACGGA
W150	Kin5b_rev_II	AAACTCCGTTCCGCCGTTTAAAAT
W151	Kin5b_fw_III	ATTGGGCGACCGTGTTAGCTGTTG
W152	Kin5b_rev_III	AAACCAACAGCTAACACGGTCGCC
W153	Kin5b_fw_IV	ATTGTACATGGAGTATGAGCCCAC
W154	Kin5b_rev_IV	AAACGTGGGCTCATACTCCATGTA
W155	Kin5c_fw_I	ATTGCGGTAGCACAAAATATAGCT
W156	Kin5c_rev_I	AAACAGCTATATTTTGTGCTACCG
W157	Kin5c_fw_II	ATTGCTGCAGACCGTTTAATTCAG
W158	Kin5c_rev_II	AAACCTGAATTAAACGGTCTGCAG

W159	Kin5c_fw_III	ATTGAGAATCGACATCGCTTAAAG
W160	Kin5c_rev_III	AAACCTTTAAGCGATGTGCGATTCT
W161	Kin5c_fw_IV	ATTGACGAACGCAGTTTTCTTCCG
W162	Kin5c_rev_IV	AAACCGGAAGAAAAGTGCCTTCGT
W163	Kin5d_fw_I	ATTGTCAGCGAGTAGTACTTTTCC
W164	Kin5d_rev_I	AAACGGAAAAGTACTACTCGCTGA
W165	Kin5d_fw_II	ATTGCTTCTCTTAATACCGATGAC
W166	Kin5d_rev_II	AAACGTCATCGGTATTAAGAGAAG
W167	Kin5d_fw_III	ATTGCTGCTGCTTTGCATCCCCAT
W168	Kin5d_rev_III	AAACATGGGGATGCAAAGCAGCAG
W169	Kin5d_fw_IV	ATTGTCAATGCTTGGTATGTCGAT
W170	Kin5d_rev_IV	AAACATCGACATACCAAGCATTGA

Table 25: List of primers used for genotyping of plants containing CRISPR/Cas9 constructs.

ID	Name	Sequence (5' to 3')
W385	Cas9 CRISPR fw	ACCGACGACCAGGACTTGAC
W386	Cas9 CRISPR rv	CCTCTTGCGTTCATTCTCG
W389	Kin5a_GT_for	GGAGTAGCCCATAGACTAAG
W390	Kin5a_GT_wt_rev	CTCTATCGAGACGGTTAGAG
W391	Kin5a_GT_mut_rv	TCGTCACCAGTGACGGATTC
W392	Kin5b_GT_for	ACCACGCAGTTCACGCTAAG
W393	Kin5b_GT_wt_rev	TCCACAAGGTGCGCTCTGTC
W394	Kin5b_GT_mut_rv	GGCACAGTGACTCTGATTTC
W395	Kin5c_GT_for	TCAAACCTCCACGTTTCGACTG
W396	Kin5c_GT_wt_rev	GCTGAACCTTTCTCCAAGAC
W397	Kin5c_GT_mut_rv	GCTTCTCCGTTCTGCATTTG
W398	Kin5d_GT_for	CCCAAACCTAAACCGCTAACC
W399	Kin5d_GT_wt_rev	CACCTGCAACGCAATATGAC
W400	Kin5d_GT_mut_rv	ACTCGTGGTGTGTCTTCTC
W417	Kin5b_GT_mut_rv2	TTTCTGAGTGGCACAGTGAC
W418	Kin5b_GT_mut_rv3	CTCATGGGAAGTGAGAAAG
W419	Kin5b_GT_for2	TACTTGCCGATGACGACTCC

W420	Kin5c_GT_wt_rv2	CTCTGCTGTGCGTCTCTTAG
W421	Kin5c_GT_wt_rv3	ACACCACCTTTGCCATCTTC
W953	Kin5b_GT_mut_rv5	CAGAGGTGGTTCCTTAGTTG

CRISPR/Cas9 genome editing following Puchta ³¹³:

In another system, generated by Holger Puchta, it is only possible to generate a vector with up to two sgRNA sequences. Therefore, the corresponding DNA oligos were hybridised as mentioned before (Table 26). The entry-vector pEN-C1-1 was restricted with BpsI for 1.5 h at 37 °C and separated by agarose gel electrophoresis. The fragment of around 3700 bp was cut from the gel, purified with a gel extraction kit (HiYield® PCR Clean-up/Gel Extraction Kit, SLG) and set to a concentration of 5 ng µl⁻¹. For each sgRNA sequence one entry vector was generated by ligating 2 µl digested entry vector with 3 µl of the hybridised DNA oligos in a reaction with 1 µl T4 ligation buffer, 3 µl ddH₂O and 1 µl T4 ligase at RT for 2 h. Top10 cells were transformed with 5 µl ligation reaction and plated on LB-medium plates supplemented with ampicillin (100 mg l⁻¹) and incubated at 37 °C overnight. Colonies were tested by colony PCR (forward sgRNA oligo, W532; Table 26, see 4.3.2). Overnight cultures of two positive clones were cultivated for plasmid preparation (see 4.3.16). The entry plasmids were verified by sequencing with primer W529 (see 4.3.17). In a next step the first sgRNA sequence was introduced into the vector pDE-Cas9 by ligation. Therefore, 1 µg of both vectors were each restricted with MluI and Bsu36I (NEB) at 37 °C for 1.5 h. In case of the sgRNA vector, the resulting fragments were separated by agarose gel electrophoresis and the fragment with the size of about 530 bp was purified from the gel and used in the next step along with the cleaned pDE-Cas9 vector. Both restricted vector parts were ligated, using 5 µl of each vector, 2 µl T4 ligation buffer, 1 µl T4 ligase and 6 µl ddH₂O at RT for 3 h. Top10 cells were transformed with the ligation reaction and plated on LB-medium plates supplemented with spectinomycin (100 mg l⁻¹). Positive clones were identified by colony PCR (see 4.3.3) using the primers W529 and W928 (Table 26). The plasmid of one positive clone was prepared and adjusted to 50 ng µl⁻¹. The second sgRNA sequence plasmid was set to a concentration of 100 ng µl⁻¹. Both plasmids were used in a Gateway-reaction with 2 µl sgRNA sequence plasmid, 3 µl destination vector containing the first sgRNA sequence, 4 µl TE-buffer and 1 µl LR Clonase II (Thermo Fisher Scientific). The Gateway-reaction was incubated at 17 °C overnight and incubated with 1 ml Proteinase K (Thermo Fisher Scientific) for 10 min at 37 °C. The complete Gateway-

reaction was transformed into Top10 cells and plated on LB-medium plates, containing spectinomycin. Positive clones were tested by colony PCR (W531 and W927; Table 26) and plasmid DNA was prepared from positive clones. The final plasmid was sequenced (W926, Table 26) and transformed into agrobacteria C58C1. *A. thaliana* plants (Col-0, H2B-mTurquoise2, TagRFP-T-TUA5, Table 6) were painted with the agrobacteria containing the final vector and where selected with phosphinothricin. Plants were tested for several generations for a deletion of the respective kinesin-5 and the presence of Cas9 by PCR of gDNA (Table 25).

Table 26: List of primers for cloning and analysis of CRISPR/Cas9 constructs following Puchta.

ID	Name	Sequence (5' to 3')
W385	Cas9 CRISPR fw	ACCGACGACCAGGACTTGAC
W386	Cas9 CRISPR rv	CCTCTTGCGTTCATTCTCG
W529	SS42_Melanie_CRISPR	TCCCAGGATTAGAATGATTAGG
W530	SS43_Melanie_CRISPR	CGACTAAGGGTTTCTTATATGC
W531	SS61_Melanie_CRISPR	GAGCTCCAGGCCTCCCAGCTTTCG
W532	SS129_Melanie_CRISPR	CACAGGAAACAGCTATGAC
W900	CRISPR-KIN5b-T2fw	ATTGTTCAAGTCCTCCTCCGATGC
W901	CRISPR-KIN5b-T2rv	AAACGCATCGGAGGAGGACTTGAA
W902	CRISPR-KIN5b-T3fw	ATTGGCTGTTTCCCAAACATCGC
W903	CRISPR-KIN5b-T3rv	AAACGCGATGTTTTGGGAAACAGC
W916	CRISPR-KIN5b-Exon21-T1fw	ATTGGGCGACCGTGTTAGCTGTTG
W917	CRISPR-KIN5b-Exon21-T1rev	AAACCAACAGCTAACACGGTCGCC
W926	SS144	GTCCGGACGTCTTAATTAACC
W927	SS143	CAAGAAAGCTGGGTCCTCAG
W928	SS102	CACCATGTTATCACATCAATCC
W929	SS72	CTTCTATCGCCTTCTTGACG

4.5 Protein biochemical methods

4.5.1 Sodium dodecyl sulphate-polyacrylamide gel electrophoresis (SDS-PAGE)

To separate proteins according to their size, sodium dodecyl sulphate-polyacrylamide gel electrophoresis (SDS-PAGE) was used. For this purpose, a polyacrylamide gel was prepared in a gel caster (Mini-PROTEAN Tetra Handcast Systems, Bio-Rad Laboratories, Hercules, USA) by pouring a 10 % separating gel (Table 27) between a spacer plate with 0.75 mm integrated spacers and a short plate. To ensure a plane surface of the separating gel, the gel was overlaid with isopropanol. After the separating gel was fully polymerised, isopropanol was removed and a stacking gel (Table 27) was mixed and poured on top of the separating gel. Sample wells were formed by inserting a 10- or 15-well comb into the still liquid stacking gel. Once the whole gel was polymerised, the comb was removed and the gel was stored in a damp paper towel at 4 °C until use.

Table 27: Composition of separating and stacking gel for SDS-PAGE

Buffer	Components
10 % Separating gel	382 mM Tris-HCl pH 8.8, 10 % acryl/bisacrylamide mix (37.5:1), 0.1 % sodium dodecyl sulfate (SDS), 0.1 % ammonium persulfate (APS), 0.001 % tetramethylethylenediamine (TEMED)
5 % Stacking gel	130 mM Tris-HCl pH 6.8, 5.1 % acryl/bisacrylamide mix (37.5:1) 0.1 % SDS 0.1 % APS 0.001 % TEMED

For the electrophoresis, the glass slides with the acrylamide gel were clamped into a vertical electrophoresis tank (Bio-Rad) and the tank was filled with SDS-running buffer (25 mM Tris, 192 mM glycine, 0.1 % SDS). Protein samples from expression tests or protein purifications were mixed with 6 x loading buffer (375 mM Tris-HCl pH 6.8, 6 % SDS, 48 % glycerol, 0.03 % bromophenol blue, 60 mM dithiothreitol (DTT)) and heated to 95 °C for 5 min. 15 or 20 µl protein sample was filled into each sample well, as well as 5 µl pre-stained protein ladder

(PageRuler 10 to 180 kDa, Thermo Fisher Scientific) as a size standard. Electrophoresis was performed at constant 120 V for 15 min and constant 150 V until the lowest band of protein ladder reached the end of the gel.

4.5.2 Coomassie staining

To visualise the protein on a polyacrylamide gel, the gel was washed three times for 15 min with ddH₂O and then incubated in a colloidal Coomassie-staining solution (0.02 % Coomassie Brilliant Blue G-250, 5 % aluminium sulphate-(14-18)-hydrate, 10 % ethanol, 2 % phosphoric acid) for at least one hour, up to 24 hours³³¹. To remove excess staining, the gel was bathed in ddH₂O until bands were clearly visible and documented on a flatbed scanner (Epson Perfection V700 PHOTO, Epson, Nagano, Japan).

4.5.3 Western blot

In order to detect specific proteins, even at low concentrations, semi-dry Western blots were conducted after SDS-PAGE (see 4.5.1). For this purpose, an SDS-PAGE gel was washed with ddH₂O and incubated for 5 min in Western blot transfer buffer (WTB; 192 mM glycine, 25 mM TRIS-HCl pH 8.3, 2 % freshly added methanol). A sheet of polyvinylidene fluoride membrane (Immobilon-P Transfer, Millipore/Merck) of the size of the gel was incubated in methanol for 5 min. The blot was built up in the following order from the cathode to the anode: two chromatography Whatman papers (a little larger than the gel) were soaked with WTB. Air bubbles were removed by carefully rolling a glass pipette over the papers. Next, the membrane was placed on top of the papers, only touching the membrane with a tweezer at one side. On top of the membrane the SDS-PAGE gel was placed and air bubbles were carefully removed as mentioned before. Finally, the stack was overlaid with two chromatography Whatman papers soaked in WTB and air bubbles were removed again. After closing the blotting equipment with the anode, the blotting was performed for 65 min at constant 60 mA per gel.

After the blot was carefully disassembled, the membrane was transferred with a tweezer into a small basin filled with blocking buffer (TBS-T (0.05 M Tris-HCl pH 7.5, 0.15 M NaCl, 0.05 % Tween-20) complimented with 2 % skim milk powder) and incubated overnight at 4 °C on a shaker (Compact Digital Waving Rotator, Thermo Fisher Scientific) at 80 rpm. The next day, the membrane was incubated with the primary antibody diluted in blocking buffer (1:1000;

anti-Penta-His Antibody, Qiagen) for at least 1 h at RT, shaking at 80 rpm. Excess antibody was removed by washing the membrane in fresh blocking buffer three times for 10 min each. Secondary antibody diluted in blocking buffer (1:1000; anti-mouse-HRP antibody, Abcam, Cambridge, UK) was applied to the membrane for at least 1 h, while shaking at RT. Finally, the membrane was washed three times with TBS-T buffer for 10 min each.

The blot was then ready for imaging. Therefore, it was carefully placed with a tweezer into a plastic foil and wetted with a freshly prepared chemiluminescent solution consisting of 1 ml solution A (100 mM Tris-HCl pH 8.6 and 250 $\mu\text{g l}^{-1}$ Luminol (SigmaAldrich/Merck)), 100 μl solution B (22.7 mg ml^{-1} trans-4-hydroxycinnamic acid, solved in DMSO), and 0.3 μl H_2O_2 . After incubation in the dark for 2 min, chemiluminescence was detected with a ChemiDoc Imaging System (Bio-Rad) for 360 s with a picture taken every 60 s.

4.5.4 Protein expression test

In order to test the expression level of the different *E. coli* strains and to determine the optimal expression conditions, small scale protein expression tests were conducted. For this, several *E. coli* strains were transformed with the desired construct and selected on LB-medium plates containing the appropriate antibiotics. Growing colonies were tested by colony PCR (see 4.3.3) and positive clones were used to inoculate a 20 ml overnight pre-culture for every strain, which grew at 37 °C while being shaken at 180 rpm. The next day, several main cultures were prepared for each strain in LB-medium and TB-medium (24 g l^{-1} yeast extract, 20 g l^{-1} tryptone, 0.4 ml l^{-1} glycerol, 17 mM potassium dihydrogen phosphate, and 72 mM di-potassium hydrogen phosphate), by inoculating 30 ml of medium, containing the appropriate antibiotics, with 800 μl of the respective overnight pre-culture. Once the main cultures reached an OD_{600} of 0.6, each culture was processed in the following manner. 1 ml of the main culture was stored as a pre-induction sample and four culture tubes were filled with 3 ml of the culture. Each tube was treated in a different way: Two were induced with 20 μM IPTG and cultivated either for 3 h at 37 °C or overnight at 18 °C, the other two were induced with 200 μM IPTG and cultivated for either 3 h at 37 °C or overnight at 18 °C. All culture tubes were shaken at 180 rpm to ensure adequate aeration of the culture. At the end of each expression 1 ml from each culture was collected and prepared for SDS-PAGE (see 4.5.1). SDS-PAGE gels were stained (see 4.5.2) and documented and evaluated for the highest amount of the desired protein.

4.5.5 Protein expression in *Escherichia coli*

For expression of recombinant protein in *Escherichia coli*, a positive transformed bacteria colony was picked from a plate and grown overnight in 50 ml TB-medium with appropriate antibiotic at 37 °C and 180 rpm as a pre-culture (Incubator shaker MAXQ 5000 or 6000, Thermo Fisher Scientific). 5 to 10 ml of this culture was used to inoculate 1 l of TB-medium. The culture grew at 37 °C and 180 rpm until an OD₆₀₀ of 0.6 was reached (Eppendorf BioPhotometer, Eppendorf). 200 µM isopropyl β-D-1-thiogalactopyranoside (IPTG) was added to the culture to start the expression at 17 °C and 180 rpm (Shaker 3015, GFL, Burgwedel, Germany) overnight. In some experiments, the bacterial culture grew until an OD₆₀₀ of 1.2 was reached. In this case the culture was diluted with 1 l fresh TB-medium before the start of expression with IPTG.

4.5.6 Protein expression in *Pichia pastoris*

As an easy to cultivate eukaryotic expression system, *Pichia pastoris* was used for heterologous expression of recombinant AtKRP125b^{186,332}. Two constructs were designed and cloned into pPICZα A expression vector (Invitrogen, Santa Clara, USA) by OEC (4.3.9): One full length construct containing all 1009 aa of AtKRP125b, and one full length construct, augmented with an eGFP. Both constructs AtKRP125b sequences were integrated without the start and stop codon. The pPICZα A vector provided a polyhistidine-tag for purification at the C-terminus and the required N-terminal secretion α-factor.

Table 28: List of primers used for cloning and analysis of constructs for *P. pastoris* expression system

ID	Name	Sequence (5' to 3')
W363	pPICZ_for	GACTGGTTCCAATTGACAAGC
W364	pPICZ_rev	GCAAATGGCATTCTGACATCC
W431	OEC_K5b_fw_Pichia	GGTATCTCTCGAGAAAAGAGAGGCTGAAGCTTCTA GCCGCCATGACAAAGAGAAAGGCGTC
W432	OEC_K5bFL_rv_Pichia	GGCTACAAACTCAATGATGATGATGATGATGGACTT GTGAGAGAGGCGACCGTGTTAGCTG
W433	OEC_K5b-eGFP_rv_Pichia	GGCTACAAACTCAATGATGATGATGATGATGTTTGT ATAGTTCATCCATGCCATGTGTAATC

W434	OEC_K5bFL_eGFP_rv	CTCCAGTGAAAAGTTCTTCTCCTTTACTGACTTGTGA GAGAGGCGACCGTGTTAG
------	-------------------	---

Constructs were transformed into chemical competent *E. coli* TOP10F' cells and grew on low salt LB plates (Table 29) containing 25 mg l⁻¹ zeocin (InvivoGen, San Diego, USA) for selection. Colonies were tested by colony PCR (4.3.3) with primers W363 and W364 (Table 28). As a large amount of linearised DNA is needed for the integration into *P. pastoris* genome via recombination, a midi-plasmid preparation (see 4.3.16) was conducted from positive *E. coli* clones grown in low salt LB media with 25 mg l⁻¹ zeocin. 10 µg plasmid DNA was linearised by restriction with SacI (Fast Digest, Thermo Fisher Scientific) for 30 min at 37 °C to ensure complete linearisation. The restriction was stopped by heat inactivation for 5 min at 65 °C. The vector was cleaned with a phenol/chloroform extraction and precipitated with ethanol. The resulting precipitate was washed with 70 % ethanol, dried until all ethanol evaporated and resuspended in 10 µl sterile ddH₂O.

In order to prepare *P. pastoris* X33 cells for transformation, an overnight culture was grown in 5 ml YPD medium (Table 29) in a 50 ml conical flask at 30 °C and 180 rpm. Up to 0.5 ml overnight culture were used to inoculate 500 ml YPD medium. The culture was grown in a 2 l conical flask at 30 °C and 180 rpm to an OD₆₀₀ of 1.3, divided into centrifugation tubes and centrifuged at 1500 x g for 5 min at 4 °C. The precipitate was resuspended in 500 ml ice-cold, sterile ddH₂O, centrifuged again as before and resuspended in 250 ml ice-cold, sterile ddH₂O. After another centrifugation, the precipitate was resuspended in 20 ml ice-cold, sterile 1 M sorbitol and centrifuged a final time. The cells were resuspended in 1 ml ice-cold, sterile 1 M sorbitol and were ready for immediate transformation.

For the transformation, 80 µl competent X-33 cells was mixed thoroughly with the 10 µl linearised plasmid and transferred into an electroporation cuvette (VWR) on ice. The cells were electroporated at 1500 V for 5 ms in an Eppendorf Eporator (Eppendorf) and treated with 1 ml ice-cold, sterile 1 M sorbitol immediately after the electroshock. The cell suspension was recovered in a 15 ml tube for 2 h at 30 °C without shaking. After recovery the transformed yeast suspension was spread out onto YPDS plates (Table 29) supplemented with different concentration of zeocin to select clones with multiple insertions of the plasmid. 10, 25, 50, 100, and 200 µl yeast suspension was spread out on plates containing 100 or 500 µg ml⁻¹ zeocin and 100, and 200 µl yeast suspension was spread out on plates with 1000 or

2000 $\mu\text{g ml}^{-1}$ zeocin. The plates were cultivated for 3 to 10 days at 30 °C until colonies started to form. About 10 colonies were picked from each plate and tested for the integrated inserts and expression of recombinant protein.

For the verification of an insertion of the plasmid into the genome of *P. pastoris* a modified colony PCR was performed in order to break up the cells. Therefore, a few cells were picked from a colony with a pipette tip and mixed in 25 μl 20 mM NaOH and boiled at 99 °C on a heating block for 15 min. Afterwards a standard PCR could be performed with the primers W363 and W364 and reviewed by agarose gel electrophoresis.

To test whether a clone expressed AtKRP125b, small scale expression tests were performed. For that purpose, 25 ml of MGY in a 250 ml baffled flask was inoculated with cells from a single colony that was tested positive for the insert. The culture was grown at 30 °C at 250 rpm until an OD_{600} of 2-6 was reached. For optimal expression the cells had to be in log-phase growth before induction. As the aeration is critical for protein expression in *P. pastoris*, baffled flasks were used, shaken at high rpm and closed with a cap that allowed enough air circulation. Before induction of expression with methanol, the culture was centrifuged at 1500 x g for 5 min at RT and the cell sediment was resuspended in fresh MM medium (Table 29) and set to an OD_{600} of 1.0. The culture continued to grow as before and was treated with 5 ml 100 % methanol every 24 h to maintain the induction. Samples to test for possible protein expression were taken at various time points. At the beginning (0 h) and after 6, 12, 24, 36, 48, 60, 72, 84, 96 h 1 ml of culture was extracted from the baffled flask and transferred into a 1.5 ml reaction tube. All samples were centrifuged at 21000 x g for 3 minutes at RT (Heraeus FRESCO 21), in order to separate the supernatant from cells. As AtKRP125b should be secreted the supernatant and the cell sediment were frozen in liquid nitrogen and kept at -80 °C until all samples were gathered. Expression was evaluated by SDS-PAGE (see 4.5.1 and 4.5.2) and Western blot with an anti penta-His antibody (see 4.5.3). As all tested clones were negative for the expression of AtKRP125b, some of these were cultivated again with higher concentrations of methanol (1 %, 2 % and 4 %). As these conditions did not result in any expression, a large-scale expression followed by protein purification was not performed.

Table 29: Composition of media and buffers used for the transformation, selection and cultivation of *P. pastoris*.

Medium/Buffer	Components	Comments
Low salt LB medium	1 % tryptone, 0.5 % yeast extract, 0.5 % NaCl, pH 7.5 with NaOH	For plates, 1 % agar where added
YPD medium	1 % yeast extract, 2 % peptone, 2 % dextrose (glucose)	Glucose was added from sterile filtered 20 % stock after autoclaving
YPDS plates	1 % yeast extract, 2 % peptone, 2 % dextrose (glucose), 1 M sorbitol, 2 % agar	Glucose was added from sterile filtered 20 % stock after autoclaving
10 x YNB (yeast nitrogen base)	13.4 % YNB (Invitrogen)	
MGY (minimal glycerol medium)	1.34 % YNB, 1 % glycerol, 4 x 10 ⁻⁵ % biotin	
MM (minimal methanol medium)	1.34 % YNB, 1 % glycerol, 4 x 10 ⁻⁵ % biotin, 0.5 % methanol	

4.5.7 Protein expression in insect cells

For the expression of recombinant AtKRP125b from insect cells, an expression construct was cloned into pFastBac1, including a tetracysteine-tag for fluorescent labelling and a 6 x His-tag for affinity purification, using OEC (see 4.3.9). The generated vector was transferred into DH10Bac cells to produce recombinant bacmid-DNA that was needed for the transfection of insect cells. A Midi- plasmid preparation was used to produce enough high purity recombinant bacmid DNA. The cultivation of insect cells and production of cells with recombinant protein was carried out thanks to a cooperation in the lab of Prof. Dr. Martin Aepfelbacher by Dr.

Astrid Sydow and Dr. Gunnar Baermann after the Bac-to-Bac baculovirus expression system guidelines (Bac-to-Bac™ Baculovirus Expression System, Thermo Fisher Scientific).

4.5.8 Cell lysis of bacteria, yeast and insect cells

Cells were centrifuged for 20 min at 10000 x g and 4 °C in a JA10 rotor (Avanti J-E, Beckman Coulter, Brea, USA) and resuspended in 10 ml 2 x PBS (Table 30) adding 1 µl Benzonase. Cells were then either disrupted in a French press in three consecutive cycles. Or lysed, by solving 50 mg lysozyme (Pierce Lysozyme, Thermo Scientific (Waltham, USA)) in the resuspended cell solution and incubating it for 30 min at RT. Or disrupted in a high-pressure homogeniser (IKA, Staufen im Beisgau, Germany) at 700-1000 bar. Lysate was centrifuged in a JA25.50 rotor at 40000 x g and 4 °C for 20 min (Avanti J-E centrifuge) to remove cell debris from the lysate. Insect cells were always lysed in a high-pressure homogeniser.

4.5.9 Protein purification by affinity chromatography

Protein containing supernatant from cell lysis was mixed with 3 % elution buffer and kept on ice, while a Ni-column (HisTrap FF Crude, GE Healthcare Life Sciences, Little Chalfont, UK) was equilibrated with 10 ml equilibration buffer (Table 30). Supernatant was loaded onto the column with a peristaltic pump (Peristaltic Tubing Pump FH10, Thermo Fisher Scientific) and washed with 10 ml washing buffer (Table 30). Proteins with His-tag were eluted with elution buffer (Table 30) in fractions of 250 µl (ca. 10 droplets). Protein concentration was measured with a NanoDrop 2000 Spectrophotometer (Thermo Fisher Scientific). Ni-column was washed with remaining elution buffer, flowed by 15 ml ddH₂O and stored in 20 % ethanol at 4 °C.

Table 30: Composition of buffers used for the purification by affinity chromatography.

Buffer	Components	Comments
6 x PBS	822 mM NaCl, 16.2 mM KCl, 48.6 mM Na ₂ HPO ₄ , 10.56 mM KH ₂ PO ₄ , 6 mM MgCl ₂ , pH 7.4	

Equilibration Buffer	2 x PBS, 6 % elution buffer	1 mM ATP and 1 mM DTT were added right before use
Washing Buffer	6 x PBS, 6 % elution buffer	1 mM ATP and 1 mM DTT were added right before use
Elution Buffer	2 x PBS, 500 mM imidazole, pH 8.0	1 mM ATP and 1 mM DTT were added right before use

4.5.10 Tubulin purification from porcine brain

In order to polymerise microtubules for *in vitro* kinesin motility assays, high grade tubulin had to be purified. Since the purification of tubulin from plants is not yet possible in the required quantity and quality, tubulin was isolated from porcine brain. The purification takes advantage of the unique ability of tubulin to polymerise into microtubules in the presence of GTP in a warm environment and to depolymerise again under cold conditions. In this way, the tubulin can be separated from other components of the brain in two polymerisation-depolymerisation cycles and thereby be purified and concentrated³³³. For this purpose, about 1 kg of porcine brain (5-6 brains) was transported to the laboratory directly after slaughter, stored in ice-cold PBS (Table 31) with PBS ice cubes. The porcine brains were cleaned from clotted blood and meninges inside a cooling chamber. About 400 g cleaned brain was mixed with 400 ml depolymerisation buffer (Table 31) supplemented with 0.24 mM AEBSF (PanReac AppliChem, Darmstadt, Germany) and 2 mM DTT and homogenised with a hand blender thoroughly. The brain mixture was divided evenly into two 500 ml centrifuge beakers and centrifuged at 9000 rpm for 30 min at 4 °C (JA10 rotor, Avanti J-E Centrifuge) to remove cell debris. The solution was cleared further by ultra-centrifugation of the supernatant at 30000 rpm for 30 min at 4 °C (50.2 Ti rotor, Optima XE ultra-centrifuge, Beckman Coulter). The volume of the supernatant was determined (V1) and mixed with the same volume of 2 x HM-PIPES (Table 31) complemented with 0.1 mM GTP (Jena Bioscience, Jena, Germany) and 1 mM ATP (Jena Bioscience). The mixture was divided into 50.2 Ti centrifugation tubes and incubated for 60 min at 35 °C in a water bath to induce microtubule polymerisation. The incubated mixture was centrifuged in a warm 50.2 Ti rotor at 40000 rpm for 30 min at 35 °C, to concentrate the polymerised microtubules in a sediment. The supernatant was discarded and the microtubule sediment was resuspended in 0.1 x V1 ice-cold depolymerisation buffer

supplemented with 0.12 mM AEBSF and 1 mM DTT. To homogenise the sediment completely, the mixture was processed in an ice-cold Dounce homogeniser. The homogenised mixture was divided into centrifugation tubes, depolymerised on ice for 30 min and then centrifuged in a cooled 50.2 Ti rotor at 30000 rpm at 4 °C for 30 min. The volume of the supernatant was determined (V2) and the same volume 2 x HM-PIPES complemented with 0.5 mM GTP and 1 mM ATP was added. This mixture was divided into centrifugation tubes and incubated at 35 °C for 30 min in a water bath. After a final centrifugation in a warm 50.2 Ti rotor at 40000 rpm at 35 °C, the purified tubulin sediment was either frozen in liquid nitrogen and stored at -80 °C or used immediately for tubulin labelling.

Table 31: Buffer and solutions used for purification of tubulin from porcine brain

Buffer	Components	Comments
PBS (phosphate buffered saline)	0.137 M NaCl, 2.7 mM KCl, 10 mM Na ₂ HPO ₄ , 1.8 mM KH ₂ PO ₄ , pH 7.4	
Depolymerisation buffer	50 mM MES, 1 mM CaCl ₂ , pH 6.6	
2 x HM-PIPES	1 M PIPES, 10 mM MgCl ₂ , 20 mM EGTA	20 % DMSO are added right before use

4.5.11 Tubulin labelling

For *in vitro* motility assays the tubulin had to be either labelled with a fluorescent dye like Cy5 or DyLight594; or with a molecular probe like biotin or digoxigenin for specific antibody binding (Table 32). All labelling agents were bound to tubulin in a covalent fashion with their N-Hydroxysuccinimide (NHS) ester group to an amine group of the protein³³⁴. In order to label the tubulin, it had to be transferred into a suitable buffer for the NHS ester reaction. Therefore, the purified tubulin (see 4.5.10) was depolymerised and homogenised with 0.06 x V1 ice-cold BRB80 (Table 33) supplemented with 0.12 mM AEBSF and 1 mM DTT in a chilled

Dounce homogeniser for 30 min. The homogenised tubulin mixture was divided into centrifugation tubes and centrifuged for 30 min at 40000 rpm in a 50.2 Ti rotor at 4 °C. The volume and concentration of the tubulin in the supernatant was determined and mixed with the same volume of 2 x HM-PIPES (Table 31) supplemented with 0.5 mM MgCl₂ and 100 mM GTP. The mixture was divided into centrifugation tubes and incubated for 30 min at 35 °C in a water bath. The tubulin mixture was sub-layered with 20 ml warm high pH cushion (Table 33) in each tube and centrifuged in a JA 25.50 rotor at 40000 x g for 45 min at 35 °C (Avanti J-E). The liquid phases were removed carefully and the microtubule sediment was resolved in 1 ml warm labelling buffer (Table 33). For the labelling, a 5-fold molar excess of labelling agents was added and incubated for 1 h at 35 °C in a water bath. The incubation was continued for 5 min after an equal volume of quenching solution (Table 33) was added to the labelling mixture. The mixture was placed on top of a centrifugation tube, filled with 2 ml warm low pH cushion (Table 33) and was centrifuged at 40000 x g for 30 min at 35 °C in a JA 25.50 rotor. The supernatant was carefully removed and the sediment was resuspended in 1 ml ice-cold injection buffer (Table 33). Microtubules were depolymerised on ice for 30 min in a Dounce homogeniser. After centrifugation for 10 min at 80000 rpm in a TLA110 rotor (Optima MAX-XP ultracentrifuge, Beckmann Coulter) at 2 °C, the supernatant was mixed with the same volume 2 x BRB80 supplemented with 4 mM MgCl₂ and 1 mM GTP and the mixture was incubated at 35 °C for 30 min in a water bath. The polymerised microtubules were laid on top of a 2 ml low pH cushion in a centrifugation tube and centrifuged at 40000 x g in a JA 25.50 rotor for 30 min at 35 °C. The supernatant and the remaining cushion were removed carefully and the microtubule sediment was resuspended in ice-cold injection buffer and depolymerised on ice for 30 min. After a final centrifugation at 80000 rpm in a TLA110 rotor at 2 °C for 10 min, volume and concentration of the labelled tubulin were determined by spectrophotometry (NanoDrop 2000 Spectrophotometer, Thermo Fisher Scientific) and set to 4 mg ml⁻¹ with injection buffer, divided into 5 µl aliquots (in 0.6 ml Maxymum Recovery snaplock tubes, Axygen/Corning) frozen in liquid nitrogen and stored at -80 °C.

Table 32: Fluorescent dyes and molecular probes used for labelling of tubulin.

Component	Manufacturer
Cyanine 5-NHS ester	Enzo Life Science, Lörrach, Germany
Digoxigenin NHS ester	Enzo Life Science, Lörrach, Germany
DyLight 594 NHS Ester	Thermo Fisher Scientific, Waltham, USA
EZ-Link NHS-Biotin	Thermo Fisher Scientific, Waltham, USA

Table 33: Buffer and solutions used for labelling of tubulin.

Buffer	Components	Comments
1 x BRB80	80 mM PIPES, 1 mM MgCl ₂ , 1 mM EGTA, pH 6.8	
High pH cushion	0.1 mM NaHEPES, 1 mM MgCl ₂ , 1 mM EGTA, pH 8.6	60 % glycerol were added right before use
Labelling buffer	0.1 mM NaHEPES, 1 mM MgCl ₂ , 1 mM EGTA, pH 8.6	40 % glycerol were added right before use
Quenching solution	2 x BRB80, 100 mM K-glycinate, 40 % glycerol	
Low pH cushion	1 x BRB80, 60 % glycerol	
Injection buffer	100 mM K-glycinate, 5 mM MgCl ₂	

4.5.12 Preparation of microtubules

For *in vitro* assays, different kinds of microtubules were needed, regarding the layout of the experiment. For all motility assays, normal fluorescently labelled microtubules were used. They were prepared by mixing 5 μ l Cy5- or DyLight 594-labelled tubulin with 1.25 μ l

microtubule polymerisation mix (BRB80 pH 6.9 containing 5 % DMSO, 4 mM MgCl₂, 1 mM GTP). This mixture was incubated for 30 min at 37 °C in order to polymerise microtubules. To stop the polymerisation, 100 µl warm BRB80 supplemented with 10 µM taxol (Paclitaxel, Enzo Life Sciences) was added and centrifuged at 21000 x g for 10 min at 25 °C (Heraeus FRESCO 21 Centrifuge). The supernatant was discarded and the microtubule sediment was resuspended in 200 µl warm BRB80 with taxol.

For sliding assays, biotinylated or digoxigenin labelled microtubules were prepared with only a small amount of fluorescent tubulin. For these microtubules 5 µl digoxigenin-labelled tubulin or biotinylated tubulin were mixed with 1 µl Cy5- or DiLight 594-labelled tubulin and 2.5 µl microtubule polymerisation mix. Incubation and centrifugation were performed as mentioned previously. The concentration of microtubules was approximately 400 nM. The length of microtubules could be increased by extending the incubation at 37 °C for up to 10 min and shortened by grinding the reaction tube along half the length of a reaction tube rack.

For gliding and stepping assays, polarity-marked microtubules were needed³³⁵. Therefore, 5 µl Cy5-labelled tubulin was mixed with 3.3 µl GMPCPP microtubule polymerisation mix (BRB80 pH 6.9 containing 0.25 mM GTP, 0.75 mM GMPCPP) and incubated for 20 min at 37 °C. In the meantime, a fresh stock solution of 50 mM NEM was prepared and used in an elongation mixture (BRB80 pH 6.9 containing 14 µM NEM, 1 mM GMPCPP, 1 mM MgCl₂). Once the Cy5-tubulin mixture was ready, 1.5 µl of DyLight 594-labelled tubulin was mixed with 97.8 µl elongation mixture and heated for 30 s at 37 °C, to produce DyLight microtubule seeds. These seeds were mixed with 6 µl of Cy5 tubulin mixture and incubated for another 20 min at 37 °C. The polymerisation was stopped by adding 100 µl warm BRB80 complemented with 10 µM taxol and microtubules were centrifuged at 21000 x g for 10 min (Heraeus FRESCO 21 Centrifuge). The sediment was carefully resuspended in 100 µl warm BRB80 with 10 µM taxol. All taxol stabilised microtubules were stored in the dark at RT.

4.6 Methods for characterisation of kinesin motor proteins

4.6.1 Cleaning and silanisation of cover slips

For the construction of flow cells for *in vitro* assays, glass coverslips had to be prepared in a special way to ensure a clean, hydrophobic surface. Therefore, two kinds of coverslips (22 x 22 cm and 18 x 18 cm, Marienfeld, Lauda Königshofen, Germany) were sorted in special racks and put into 100 ml beakers. In a first step, the beakers were filled with 50 ml 5 M NaOH to clean the glass surface and to activate the silicon-dioxide for the interaction with silane. The NaOH filled beakers were treated for 15 min in an ultrasonic bath (Ultrasonic Cleaner USC-T, VWR). After the treatment, the NaOH was discarded and the cover slips were rinsed with deionised water for 1 min. Next, the cover slip racks were placed into new beakers and treated with 50 ml methanol in an ultrasonic bath for 15 min. The methanol was discarded, and residues of methanol evaporated under the fume hood after a few minutes. The cover slips were rinsed with deionised water and carefully dried with compressed air. The dry coverslips were placed in a plasma cleaner (Zepto Model 1, Diener Electronics, Ebhausen, Germany) and treated with plasma for 2 min. Afterwards, the cover slip racks were placed in clean beakers and incubated in 50 ml silane (Repel-silane ES, 2 % dimethyldichlorosilane dissolved in octamethylcyclooctasilane, SigmaAldrich/Merck) for 1 h under a fume hood. The silane was discarded and the beakers filled with deionised water and treated in an ultrasonic bath for 1 min. The water was discarded into waste for halogens and the beaker and coverslips were rinsed for 1 min with deionised water. This washing procedure was repeated until the water stayed clear after sonification. The cover slips were carefully dried with compressed air and stored in a dry box with silica gel.

4.6.2 Preparation of flow cell chambers

To construct flow cells with two channels, three parafilm strips (cut into 2 x 25 mm pieces, Bemis Company, Neenah, USA) were placed on a cleaned 22 x 22 mm cover slip (see 4.6.1). A smaller 18 x 18 mm cover slip was put on top (**Figure 39**) and the whole setup was heated on a heating plate set to 60 °C (IKA C-MAG HS4, IKA Werke) until the parafilm started melting. When the flow cell had cooled down, excess parafilm on the sides of the smaller cover slip was removed with a sharp razorblade. The flow cell chamber was mounted to a custom-made aluminium carrier and was ready for use in motility assays.

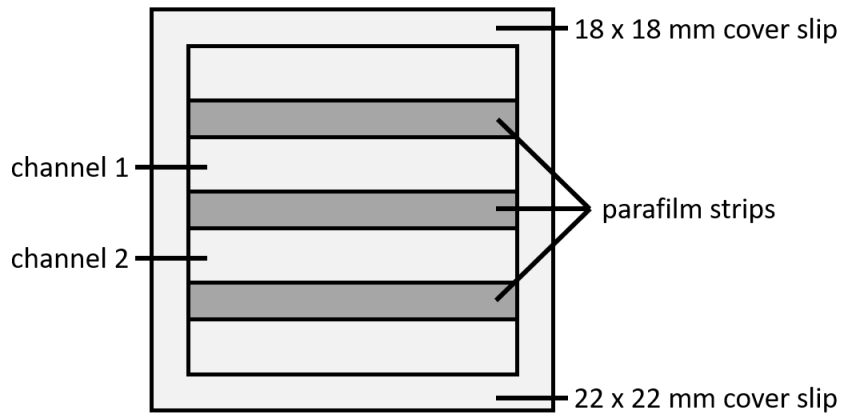


Figure 39: Schematic model of a flow cell chamber with two channels

4.6.3 Gliding assay

To determine the velocity and directionality of motor proteins, gliding assays were conducted. Therefore, each channel of a flow cell chamber (see 4.6.2) was coated with 40 μl anti-Penta-His antibodies (20 $\mu\text{g ml}^{-1}$, Qiagen) in 1 x BRB80 pH 6.9 (80 mM PIPES pH 6.9, 1 mM MgCl_2 , 1 mM EGTA) for five minutes at RT and blocked for one hour at RT with Pluronic F127 (1 % Pluronic F127, Sigma Aldrich/Merck in 1 x BRB80 pH 6.9). After washing out the blocking solution with 1 x BRB80 pH 6.9, 10 – 20 μl His-tagged motor protein (about 50-500 $\mu\text{g ml}^{-1}$ in 1 x BRB80 containing 1 mM ATP and 10 mM DTT) was flushed into a channel. Unattached motor protein was washed out with 20 μl 1 x BRB80 pH 6.9 and 5 – 10 μl of polarity marked, taxol stabilised microtubules (see 4.5.12) was flushed into the channel and incubated for 30 seconds at RT. Excess microtubules were washed out with 20 μl imaging solution (1 x BRB80 pH 6.9 containing 10 μM taxol, 10 mM DTT, 1 mM ATP, 40 mM glucose, 40 $\mu\text{g ml}^{-1}$ glucose oxidase and 16 $\mu\text{g ml}^{-1}$ catalase) to prevent bleaching of fluorophores³³⁶ and to start the transport processes.

4.6.4 Stepping assay

To analyse the processivity and velocity of single motor protein molecules, stepping assays were performed. Therefore, motor protein had to be fluorescently labelled with FIAsh. Motor protein was incubated for one hour on ice with FIAsh-EDT₂ (5 μM , Thermo Fisher Scientific) to ensure a binding to the tetracysteine-tag of the protein^{207,337}. The optimised tetracysteine-tag was designed, consisting of the amino acid sequence “FLNCCPGCCMEP”²⁰⁵ and added to the cDNA of *AtKRP125b* during the cloning process with the reverse primer of the OEC (4.3.9),

using the optimal codon-usage for *Drosophila melanogaster* as a close relative of the expression system organism *Trichoplusia ni*. For the actual assay, a flow cell channel (see 4.6.2) was coated with 40 μl anti-tubulin antibodies (25 $\mu\text{g ml}^{-1}$ in 1 x BRB80 pH 6.9; Sigma Aldrich/Merck, Darmstadt, Germany), incubated for 5 minutes at RT and then blocked for one hour at RT with Pluronic F127 (1 % Pluronic F127 in 1 x BRB80 pH 6.9) and afterwards with casein (1 mg ml^{-1}) for five minutes to avoid unspecific binding of motor protein. After washing the flow channel with 1 x BRB80 pH 6.9, to remove unbound casein, 10 μl of polarity-marked microtubules (see 4.5.12) was flushed into the flow cell and incubated for 30 seconds. The microtubule solution was washed out with 20 μl 1 x BRB80 pH 6.9 with 10 μM taxol, and 20 μl imaging solution with diluted motor protein (1 x BRB80 pH 6.9 containing 10 μM taxol, 10 mM DTT, 1 mM ATP, 0.05 % n-propyl gallate^{338,339}, and about 5 $\mu\text{g ml}^{-1}$ recombinant motor protein) was flushed into the channel.

4.6.5 Sliding assay

In order to investigate the typical kinesin-5 function of microtubule crosslinking, a sliding assay was conducted. Therefore, a flow cell channel (4.6.2) was coated with 40 μl anti-digoxigenin antibodies (20 $\mu\text{g ml}^{-1}$ in 1 x BRB80 pH 6.9; Roche, Penzberg, Germany), incubated for 5 minutes at RT and then blocked with Pluronic F127 (1% in 1 x BRB80 pH 6.9) for one hour at RT. After washing the flow channel with 1 x BRB80 pH 6.9, 10 μl digoxigenin labelled, long microtubules (see 4.5.12) was flushed into the flow channel and incubated for 30 seconds. 10 to 20 μl motor protein (about 500-50 $\mu\text{g ml}^{-1}$ diluted in 1 x BRB80 pH 6.9 containing 1 mM DTT and 10 μM taxol) was flushed in and washed out after 20 seconds three times with 20 μl 1 x BRB80 pH 6.9 containing 10 μM taxol. Finally, 10 μl short microtubules (see 4.5.12) was injected into the flow channel and removed with 20 μl imaging solution (1 x BRB80 pH 6.9 containing 10 μM taxol, 10 mM DTT, 1 mM ATP, 40 mM glucose, 40 $\mu\text{g ml}^{-1}$ glucose oxidase and 16 $\mu\text{g ml}^{-1}$ catalase) after 30 seconds incubation.

4.6.6 Imaging of motility assays

Images were acquired by NIS software (Nikon, Tokio, Japan), using an EMCCD camera (iXon DV 897, Andor/Oxford Instruments, Belfast, UK) mounted on an inverted fluorescence microscope (Ti-Eclipse, Nikon) with an CFI Apochromat 100 x/1.49 oil immersion objective (Nikon), heated to 28 °C (TempController 2000-1, Pecon, Erbach, Germany). For gliding and

sliding assays, a 1.0 x relay optical system (Nikon) was used, and acquisition rate was set to 1 frame per 10 seconds and the acquisition time was set to 10 minutes. For a stepping assay, a 1.5 x relay optical system was used, and acquisition rate was set to 1 frame per 5 seconds. Fluorescently labelled microtubules were visualised using epi-illumination: Cy5-labelled tubulin at 640 nm wavelength, and DyLight 594-labelled tubulin at 560 nm. Single FIAsh-labelled motor protein molecules in stepping assays, were visualised using a motorised TIRF slider (Nikon) and a 488 nm laser (Nikon) and an emission wavelength of 509 nm.

4.7 Software and Databases

4.7.1 Tracking of filaments and single molecules and analysis of velocity

Filaments observed in GA, SLA and single molecules recorded in STA were tracked with FIESTA (fluorescent image evaluation software for tracking and analysis)³⁴⁰. Filaments and molecules were recognised automatically and sorted by hand to identify correct moving tracks. Velocity of tracks was analysed using a MATLAB (Math Works, Natick, USA) program, kindly provided by Saskia Schattner.

4.7.2 Software and databases used in this thesis

Resource	Reference
Arabidopsis Gene Regulatory Information Server (agris; https://agris-knowledgebase.org/AtcisDB/)	Yilmaz et al. (2011) ²¹⁰
CC-Top (CRISPR/Cas9 target online predictor; https://cctop.cos.uni-heidelberg.de:8043/index.html)	Stemmer et al. (2015) ³²⁸ Labuhn et al. (2017) ³²⁹
Clone Manager Professional 9	Sci Ed Software (Westminster, USA)
Clustal Omega (https://www.ebi.ac.uk/Tools/msa/clustalo/)	Madeira et al. (2019) ³⁴¹
Codon Usage Database (www.kazusa.or.jp/codon)	Nakamura et al. (2000) ¹⁸⁹
Conserved Domains (https://www.ncbi.nlm.nih.gov/Structure/cdd/wrpsb.cgi)	Marchler-Bauer et al. (2017) ³⁴²
Exon-Intron Graphic Maker (www.wormweb.org/exonintron)	Nikhil Bhatla

Expasy ProtParam (https://web.expasy.org/protparam/)	Gasteiger et al. (2003) ³⁴³
FIESTA (fluorescent image evaluation software for tracking and analysis)	Ruhnnow, et al. (2011) ³⁴⁰
Fiji (Fiji Is Just ImageJ)	Schindelin et al. (2012) ³⁴⁴
iTOL (Interactive Tree of Life; https://itol.embl.de)	Letunic et al. (2019) ³⁴⁵
LAS X	Leica (Wetzlar, Germany)
MATLAB	Math Works (Natick, USA)
SnapGene Software	GDL Biotech (San Diego, USA)
TAIR (The Arabidopsis Information Resource; www.arabidopsis.org)	Lamesch et al. (2011) ³⁴⁶
Tm Calculator v1.13.0 (https://tmcalculator.neb.com/#!/main)	NEB (Ipswich, USA)
TRAVA (Transcriptome Variation Analysis; http://travadb.org/)	Klepikova, et al. (2015) ¹⁵¹
Waggawagga (coiled-coil prediction; https://waggawagga.motorprotein.de/)	Simm et al. (2015) ³⁴⁷

5 References

- 1 Stalder, D. & Gershlick, D. C. Direct trafficking pathways from the Golgi apparatus to the plasma membrane. *Semin Cell Dev Biol* (2020).
- 2 Wada, M. Chloroplast movement. *Plant Sci* **210**, 177-182 (2013).
- 3 Dogterom, M. & Koenderink, G. H. Actin-microtubule crosstalk in cell biology. *Nat Rev Mol Cell Biol* **20**, 38-54 (2019).
- 4 Yamada, M. & Goshima, G. The KCH Kinesin Drives Nuclear Transport and Cytoskeletal Coalescence to Promote Tip Cell Growth in *Physcomitrella patens*. *Plant Cell* **30**, 1496-1510 (2018).
- 5 Cammarata, G. M., Bearce, E. A. & Lowery, L. A. Cytoskeletal social networking in the growth cone: How +TIPs mediate microtubule-actin cross-linking to drive axon outgrowth and guidance. *Cytoskeleton (Hoboken)* **73**, 461-476 (2016).
- 6 Coles, C. H. & Bradke, F. Coordinating neuronal actin-microtubule dynamics. *Curr Biol* **25**, R677-691 (2015).
- 7 Vale, R. D. The molecular motor toolbox for intracellular transport. *Cell* **112**, 467-480 (2003).
- 8 Chalfie, M. & Thomson, J. N. Organization of neuronal microtubules in the nematode *Caenorhabditis elegans*. *J Cell Biol* **82**, 278-289 (1979).
- 9 Mickolajczyk, K. J., Geyer, E. A., Kim, T., Rice, L. M. & Hancock, W. O. Direct observation of individual tubulin dimers binding to growing microtubules. *Proc Natl Acad Sci U S A* **116**, 7314-7322 (2019).
- 10 Cassimeris, L. U., Walker, R. A., Pryer, N. K. & Salmon, E. D. Dynamic instability of microtubules. *Bioessays* **7**, 149-154 (1987).
- 11 Vorobjev, I. A., Rodionov, V. I., Maly, I. V. & Borisy, G. G. Contribution of plus and minus end pathways to microtubule turnover. *J Cell Sci* **112** (Pt 14), 2277-2289 (1999).
- 12 Mandelkow, E. M., Mandelkow, E. & Milligan, R. A. Microtubule dynamics and microtubule caps: a time-resolved cryo-electron microscopy study. *J Cell Biol* **114**, 977-991 (1991).
- 13 Desai, A. & Mitchison, T. J. Microtubule polymerization dynamics. *Annu Rev Cell Dev Biol* **13**, 83-117 (1997).
- 14 Cassimeris, L. Microtubule assembly: lattice GTP to the rescue. *Curr Biol* **19**, R174-176 (2009).
- 15 Tropini, C., Roth, E. A., Zanic, M., Gardner, M. K. & Howard, J. Islands containing slowly hydrolyzable GTP analogs promote microtubule rescues. *PLoS One* **7**, e30103 (2012).

- 16 Vorobjev, I. A., Svitkina, T. M. & Borisy, G. G. Cytoplasmic assembly of microtubules in cultured cells. *J Cell Sci* **110** (Pt 21), 2635-2645 (1997).
- 17 Keating, T. J., Peloquin, J. G., Rodionov, V. I., Momcilovic, D. & Borisy, G. G. Microtubule release from the centrosome. *Proc Natl Acad Sci U S A* **94**, 5078-5083 (1997).
- 18 Lambert, A. M. Microtubule-organizing centers in higher plants. *Curr Opin Cell Biol* **5**, 116-122 (1993).
- 19 Hashimoto, T. A ring for all: gamma-tubulin-containing nucleation complexes in acentrosomal plant microtubule arrays. *Curr Opin Plant Biol* **16**, 698-703 (2013).
- 20 Yagi, N., Matsunaga, S. & Hashimoto, T. Insights into cortical microtubule nucleation and dynamics in Arabidopsis leaf cells. *J Cell Sci* **131** (2018).
- 21 Schmidt, S. & Smertenko, A. Identification and characterization of the land-plant-specific microtubule nucleation factor MACET4. *J Cell Sci* **132** (2019).
- 22 Gigant, E. *et al.* Inhibition of ectopic microtubule assembly by the kinesin-13 KLP-7 prevents chromosome segregation and cytokinesis defects in oocytes. *Development* **144**, 1674-1686 (2017).
- 23 Tymanskyj, S. R. & Ma, L. MAP7 Prevents Axonal Branch Retraction by Creating a Stable Microtubule Boundary to Rescue Polymerization. *J Neurosci* **39**, 7118-7131 (2019).
- 24 Ogawa, T., Nitta, R., Okada, Y. & Hirokawa, N. A common mechanism for microtubule destabilizers-M type kinesins stabilize curling of the protofilament using the class-specific neck and loops. *Cell* **116**, 591-602 (2004).
- 25 Cassimeris, L., Lingappa, V., R. & Plopper, G. in *Lewin's cells* Ch. 11 Microtubules, 503-556 (Jones and Bartlett Publishers, 2011).
- 26 Lodish, H. *et al.* in *Molecular cell biology* Ch. 18 Cell organization and movement II: Microtubules and intermediate filaments, 757-800 (W.H. Freeman and Company, 2008).
- 27 Schiff, P. B. & Horwitz, S. B. Taxol stabilizes microtubules in mouse fibroblast cells. *Proc Natl Acad Sci U S A* **77**, 1561-1565 (1980).
- 28 Borisy, G. G. & Taylor, E. W. The mechanism of action of colchicine. Colchicine binding to sea urchin eggs and the mitotic apparatus. *J Cell Biol* **34**, 535-548 (1967).
- 29 Morejohn, L. C., Bureau, T. E., Mole-Bajer, J., Bajer, A. S. & Fosket, D. E. Oryzalin, a dinitroaniline herbicide, binds to plant tubulin and inhibits microtubule polymerization in vitro. *Planta* **172**, 252-264 (1987).
- 30 Dostal, V. & Libusova, L. Microtubule drugs: action, selectivity, and resistance across the kingdoms of life. *Protoplasma* **251**, 991-1005 (2014).
- 31 Delye, C., Menchari, Y., Michel, S. & Darmency, H. Molecular bases for sensitivity to tubulin-binding herbicides in green foxtail. *Plant Physiol* **136**, 3920-3932 (2004).

-
- 32 Bajer, A. S. & Mole-Bajer, J. Drugs with colchicine-like effects that specifically disassemble plant but not animal microtubules. *Ann N Y Acad Sci* **466**, 767-784 (1986).
- 33 Lyons-Abbott, S. *et al.* alpha-Tubulin mutations alter oryzalin affinity and microtubule assembly properties to confer dinitroaniline resistance. *Eukaryot Cell* **9**, 1825-1834 (2010).
- 34 Heald, R. & Khodjakov, A. Thirty years of search and capture: The complex simplicity of mitotic spindle assembly. *J Cell Biol* **211**, 1103-1111 (2015).
- 35 Mitchison, T. J. Microtubule dynamics and kinetochore function in mitosis. *Annu Rev Cell Biol* **4**, 527-549 (1988).
- 36 Movsisyan, N. & Pardo, L. A. Kv10.1 Regulates Microtubule Dynamics during Mitosis. *Cancers (Basel)* **12** (2020).
- 37 Morgan, D. O. in *The Cell Cycle* (ed Eleanor Lawrence) Ch. 5 Early Mitosis: Preparing the Chromosomes for Segregation, 87-90 (New Science Press Ltd, 2007).
- 38 Mitchison, T. J. & Salmon, E. D. Mitosis: a history of division. *Nat Cell Biol* **3**, E17-21 (2001).
- 39 Goddard, R. H., Wick, S. M., Silflow, C. D. & Snustad, D. P. Microtubule Components of the Plant Cell Cytoskeleton. *Plant Physiol* **104**, 1-6 (1994).
- 40 Hush, J. M. & Overall, R. L. Re-orientation of cortical F-actin is not necessary for wound-induced microtubule re-orientation and cell polarity establishment *Protoplasma* **196**, 97-106 (1992).
- 41 Thitamadee, S., Tuchiara, K. & Hashimoto, T. Microtubule basis for left-handed helical growth in Arabidopsis. *Nature* **417**, 193-196 (2002).
- 42 Karahara, I., Staehelin, L. A. & Mineyuki, Y. A role of endocytosis in plant cytokinesis. *Commun Integr Biol* **3**, 36-38 (2010).
- 43 Karahara, I. *et al.* The preprophase band is a localized center of clathrin-mediated endocytosis in late prophase cells of the onion cotyledon epidermis. *Plant J* **57**, 819-831 (2009).
- 44 Smirnova, E. A. & Bajer, A. S. Spindle poles in higher plant mitosis. *Cell Motil Cytoskeleton* **23**, 1-7 (1992).
- 45 Mazia, D. Centrosomes and mitotic poles. *Exp Cell Res* **153**, 1-15 (1984).
- 46 Smertenko, A. *et al.* Phragmoplast microtubule dynamics - a game of zones. *Journal of cell science* **131** (2018).
- 47 Tang, H. *et al.* Exocyst subunit Sec6 is positioned by microtubule overlaps in the moss phragmoplast prior to cell plate membrane arrival. *J Cell Sci* **132** (2019).

-
- 48 Lawrence, C. J., Morris, N. R., Meagher, R. B. & Dawe, R. K. Dyneins have run their course in plant lineage. *Traffic* **2**, 362-363 (2001).
- 49 Wickstead, B. & Gull, K. Dyneins across eukaryotes: a comparative genomic analysis. *Traffic* **8**, 1708-1721 (2007).
- 50 Xu, X., Walter, W. J., Liu, Q., Machens, I. & Nick, P. A rice class-XIV kinesin enters the nucleus in response to cold. *Scientific reports* **8**, 3588 (2018).
- 51 Gicking, A. M., Swentowsky, K. W., Dawe, R. K. & Qiu, W. Functional diversification of the kinesin-14 family in land plants. *FEBS Lett* **592**, 1918-1928 (2018).
- 52 Yamada, M., Tanaka-Takiguchi, Y., Hayashi, M., Nishina, M. & Goshima, G. Multiple kinesin-14 family members drive microtubule minus end-directed transport in plant cells. *J Cell Biol* **216**, 1705-1714 (2017).
- 53 Vale, R., Reese, T. & Sheetz, M. Identification of a novel force-generating protein, kinesin, involved in microtubule-based motility. *Cell* **42**, 39-50 (1985).
- 54 Kosik, K. S., Orecchio, L. D., Schnapp, B., Inouye, H. & Neve, R. L. The primary structure and analysis of the squid kinesin heavy chain. *J Biol Chem* **265**, 3278-3283 (1990).
- 55 Scholey, J. M., Heuser, J., Yang, J. T. & Goldstein, L. S. Identification of globular mechanochemical heads of kinesin. *Nature* **338**, 355-357 (1989).
- 56 Sack, S., Kull, F. J. & Mandelkow, E. Motor proteins of the kinesin family. Structures, variations, and nucleotide binding sites. *Eur J Biochem* **262**, 1-11 (1999).
- 57 Endow, S. A. Determinants of molecular motor directionality. *Nat Cell Biol* **1**, E163-167 (1999).
- 58 Vale, R. D. & Fletterick, R. J. The design plan of kinesin motors. *Annu Rev Cell Dev Biol* **13**, 745-777 (1997).
- 59 Rank, K. C. & Rayment, I. Functional asymmetry in kinesin and dynein dimers. *Biol Cell* **105**, 1-13 (2013).
- 60 Endow, S. A. & Waligora, K. W. Determinants of kinesin motor polarity. *Science* **281**, 1200-1202 (1998).
- 61 de Cuevas, M., Tao, T. & Goldstein, L. S. Evidence that the stalk of *Drosophila* kinesin heavy chain is an alpha-helical coiled coil. *J Cell Biol* **116**, 957-965 (1992).
- 62 Skoufias, D. A., Cole, D. G., Wedaman, K. P. & Scholey, J. M. The carboxyl-terminal domain of kinesin heavy chain is important for membrane binding. *J Biol Chem* **269**, 1477-1485 (1994).
- 63 Kull, F. J., Sablin, E. P., Lau, R., Fletterick, R. J. & Vale, R. D. Crystal structure of the kinesin motor domain reveals a structural similarity to myosin. *Nature* **380**, 550-555 (1996).

-
- 64 Vale, R. D. & Milligan, R. A. The way things move: looking under the hood of molecular motor proteins. *Science* **288**, 88-95 (2000).
- 65 Welburn, J. P. The molecular basis for kinesin functional specificity during mitosis. *Cytoskeleton (Hoboken)* **70**, 476-493 (2013).
- 66 Goldstein, L. S. & Philp, A. V. The road less traveled: emerging principles of kinesin motor utilization. *Annu Rev Cell Dev Biol* **15**, 141-183 (1999).
- 67 Walter, W. J., Machens, I., Rafieian, F. & Diez, S. The non-processive rice kinesin-14 OsKCH1 transports actin filaments along microtubules with two distinct velocities. *Nature plants* **1**, 15111 (2015).
- 68 Hua, W., Chung, J. & Gelles, J. Distinguishing inchworm and hand-over-hand processive kinesin movement by neck rotation measurements. *Science* **295**, 844-848 (2002).
- 69 Rice, S. *et al.* A structural change in the kinesin motor protein that drives motility. *Nature* **402**, 778-784 (1999).
- 70 Yildiz, A., Tomishige, M., Vale, R. D. & Selvin, P. R. Kinesin walks hand-over-hand. *Science* **303**, 676-678 (2004).
- 71 Asenjo, A. B., Weinberg, Y. & Sosa, H. Nucleotide binding and hydrolysis induces a disorder-order transition in the kinesin neck-linker region. *Nat Struct Mol Biol* **13**, 648-654 (2006).
- 72 Dogan, M. Y., Can, S., Cleary, F. B., Purde, V. & Yildiz, A. Kinesin's front head is gated by the backward orientation of its neck linker. *Cell Rep* **10**, 1967-1973 (2015).
- 73 Andreasson, J. O. *et al.* Examining kinesin processivity within a general gating framework. *Elife* **4** (2015).
- 74 Stewart, R. J., Semerjian, J. & Schmidt, C. F. Highly processive motility is not a general feature of the kinesins. *Eur Biophys J* **27**, 353-360 (1998).
- 75 deCastro, M. J., Fondecave, R. M., Clarke, L. A., Schmidt, C. F. & Stewart, R. J. Working strokes by single molecules of the kinesin-related microtubule motor ncd. *Nat Cell Biol* **2**, 724-729 (2000).
- 76 Marcus, A. I., Ambrose, J. C., Blickley, L., Hancock, W. O. & Cyr, R. J. Arabidopsis thaliana protein, ATK1, is a minus-end directed kinesin that exhibits non-processive movement. *Cell Motil Cytoskeleton* **52**, 144-150 (2002).
- 77 Schnapp, B. J. & Reese, T. S. Dynein is the motor for retrograde axonal transport of organelles. *Proc Natl Acad Sci U S A* **86**, 1548-1552 (1989).
- 78 Ambrose, J. C., Li, W., Marcus, A., Ma, H. & Cyr, R. A minus-end-directed kinesin with plus-end tracking protein activity is involved in spindle morphogenesis. *Mol Biol Cell* **16**, 1584-1592 (2005).

-
- 79 Walter, W. J., Koonce, M. P., Brenner, B. & Steffen, W. Two independent switches regulate cytoplasmic dynein's processivity and directionality. *Proceedings of the National Academy of Sciences of the United States of America* **109**, 5289–5293 (2012).
- 80 Richardson, D. N., Simmons, M. P. & Reddy, A. S. N. Comprehensive comparative analysis of kinesins in photosynthetic eukaryotes. *BMC genomics* **7**, 18 (2006).
- 81 Sciambi, C. J., Komma, D. J., Skold, H. N., Hirose, K. & Endow, S. A. A bidirectional kinesin motor in live *Drosophila* embryos. *Traffic* **6**, 1036–1046 (2005).
- 82 Roostalu, J. *et al.* Directional switching of the kinesin Cin8 through motor coupling. *Science* **332**, 94–99 (2011).
- 83 Singh, S. K., Pandey, H., Al-Bassam, J. & Gheber, L. Bidirectional motility of kinesin-5 motor proteins: structural determinants, cumulative functions and physiological roles. *Cellular and molecular life sciences : CMLS* **75**, 1757–1771 (2018).
- 84 Edamatsu, M. Bidirectional motility of the fission yeast kinesin-5, Cut7. *Biochem Biophys Res Commun* **446**, 231–234 (2014).
- 85 Shapira, O., Goldstein, A., Al-Bassam, J. & Gheber, L. A potential physiological role for bi-directional motility and motor clustering of mitotic kinesin-5 Cin8 in yeast mitosis. *J Cell Sci* **130**, 725–734 (2017).
- 86 Lawrence, C. J. *et al.* A standardized kinesin nomenclature. *J Cell Biol* **167**, 19–22 (2004).
- 87 Kim, A. J. & Endow, S. A. A kinesin family tree. *Journal of cell science* **113 Pt 21**, 3681–3682 (2000).
- 88 Wickstead, B., Gull, K. & Richards, T. A. Patterns of kinesin evolution reveal a complex ancestral eukaryote with a multifunctional cytoskeleton. *BMC Evol Biol* **10**, 110 (2010).
- 89 Zhu, C. & Dixit, R. Functions of the Arabidopsis kinesin superfamily of microtubule-based motor proteins. *Protoplasma* **249**, 887–899 (2012).
- 90 Reddy, A. S. & Day, I. S. Kinesins in the Arabidopsis genome: a comparative analysis among eukaryotes. *BMC genomics* **2**, 2 (2001).
- 91 Vanstraelen, M., Inzé, D. & Geelen, D. Mitosis-specific kinesins in Arabidopsis. *Trends in plant science* **11**, 167–175 (2006).
- 92 Cleveland, D. W., Mao, Y. & Sullivan, K. F. Centromeres and kinetochores: from epigenetics to mitotic checkpoint signaling. *Cell* **112**, 407–421 (2003).
- 93 Yamada, M. & Goshima, G. Mitotic Spindle Assembly in Land Plants: Molecules and Mechanisms. *Biology* **6** (2017).
- 94 Jonsson, E., Yamada, M., Vale, R. D. & Goshima, G. Clustering of a kinesin-14 motor enables processive retrograde microtubule-based transport in plants. *Nat Plants* **1** (2015).

-
- 95 Goshima, G., Nedelec, F. & Vale, R. D. Mechanisms for focusing mitotic spindle poles by minus end-directed motor proteins. *J Cell Biol* **171**, 229-240 (2005).
- 96 Sawin, K. E., LeGuellec, K., Philippe, M. & Mitchison, T. J. Mitotic spindle organization by a plus-end-directed microtubule motor. *Nature* **359**, 540-543 (1992).
- 97 Heck, M. M. *et al.* The kinesin-like protein KLP61F is essential for mitosis in *Drosophila*. *J Cell Biol* **123**, 665-679 (1993).
- 98 Sawin, K. E. & Mitchison, T. J. Mutations in the kinesin-like protein Eg5 disrupting localization to the mitotic spindle. *Proc Natl Acad Sci U S A* **92**, 4289-4293 (1995).
- 99 Kashina, A. S. *et al.* A bipolar kinesin. *Nature* **379**, 270-272 (1996).
- 100 Endow, S. A. Microtubule motors in spindle and chromosome motility. *Eur J Biochem* **262**, 12-18 (1999).
- 101 Sharp, D. J. *et al.* The bipolar kinesin, KLP61F, cross-links microtubules within interpolar microtubule bundles of *Drosophila* embryonic mitotic spindles. *J Cell Biol* **144**, 125-138 (1999).
- 102 Kapoor, T. M., Mayer, T. U., Coughlin, M. L. & Mitchison, T. J. Probing spindle assembly mechanisms with monastrol, a small molecule inhibitor of the mitotic kinesin, Eg5. *J Cell Biol* **150**, 975-988 (2000).
- 103 Bannigan, A. *et al.* A conserved role for kinesin-5 in plant mitosis. *J Cell Sci* **120**, 2819-2827 (2007).
- 104 McDonald, H. B., Stewart, R. J. & Goldstein, L. S. The kinesin-like *ncd* protein of *Drosophila* is a minus end-directed microtubule motor. *Cell* **63**, 1159-1165 (1990).
- 105 Acar, S. *et al.* The bipolar assembly domain of the mitotic motor kinesin-5. *Nat Commun* **4**, 1343 (2013).
- 106 Scholey, J. E., Nithianantham, S., Scholey, J. M. & Al-Bassam, J. Structural basis for the assembly of the mitotic motor Kinesin-5 into bipolar tetramers. *eLife* **3**, e02217 (2014).
- 107 Korten, T., Chaudhuri, S., Tavkin, E., Braun, M. & Diez, S. Kinesin-1 Expressed in Insect Cells Improves Microtubule in Vitro Gliding Performance, Long-Term Stability and Guiding Efficiency in Nanostructures. *IEEE transactions on nanobioscience* **15**, 62-69 (2016).
- 108 Agayan, R. R. *et al.* Optimization of isopolar microtubule arrays. *Langmuir* **29**, 2265-2272 (2013).
- 109 Kapitein, L. C. *et al.* The bipolar mitotic kinesin Eg5 moves on both microtubules that it crosslinks. *Nature* **435**, 114-118 (2005).
- 110 Sawin, K. E. & Scholey, J. M. Motor proteins in cell division. *Trends Cell Biol* **1**, 122-129 (1991).

-
- 111 van den Wildenberg, S. M. *et al.* The homotetrameric kinesin-5 KLP61F preferentially crosslinks microtubules into antiparallel orientations. *Curr Biol* **18**, 1860-1864 (2008).
- 112 Duselder, A. *et al.* Deletion of the Tail Domain of the Kinesin-5 Cin8 Affects Its Directionality. *J Biol Chem* **290**, 16841-16850 (2015).
- 113 Weinger, J. S., Qiu, M., Yang, G. & Kapoor, T. M. A nonmotor microtubule binding site in kinesin-5 is required for filament crosslinking and sliding. *Curr Biol* **21**, 154-160 (2011).
- 114 Bodrug, T. *et al.* The kinesin-5 tail domain directly modulates the mechanochemical cycle of the motor domain for anti-parallel microtubule sliding. *eLife* **9** (2020).
- 115 Kapitein, L. C. *et al.* Microtubule cross-linking triggers the directional motility of kinesin-5. *J Cell Biol* **182**, 421-428 (2008).
- 116 Blangy, A. *et al.* Phosphorylation by p34cdc2 regulates spindle association of human Eg5, a kinesin-related motor essential for bipolar spindle formation in vivo. *Cell* **83**, 1159-1169 (1995).
- 117 Waitzman, J. S. & Rice, S. E. Mechanism and regulation of kinesin-5, an essential motor for the mitotic spindle. *Biol Cell* **106**, 1-12 (2014).
- 118 Cahu, J. *et al.* Phosphorylation by Cdk1 increases the binding of Eg5 to microtubules in vitro and in Xenopus egg extract spindles. *PLoS One* **3**, e3936 (2008).
- 119 McGowan, C. H. & Russell, P. Cell cycle regulation of human WEE1. *EMBO J* **14**, 2166-2175 (1995).
- 120 Avunie-Masala, R. *et al.* Phospho-regulation of kinesin-5 during anaphase spindle elongation. *J Cell Sci* **124**, 873-878 (2011).
- 121 Chee, M. K. & Haase, S. B. B-cyclin/CDKs regulate mitotic spindle assembly by phosphorylating kinesins-5 in budding yeast. *PLoS Genet* **6**, e1000935 (2010).
- 122 Garcia, K., Stumpff, J., Duncan, T. & Su, T. T. Tyrosines in the kinesin-5 head domain are necessary for phosphorylation by Wee1 and for mitotic spindle integrity. *Curr Biol* **19**, 1670-1676 (2009).
- 123 Russell, P. & Nurse, P. Negative regulation of mitosis by *wee1+*, a gene encoding a protein kinase homolog. *Cell* **49**, 559-567 (1987).
- 124 Wittmann, T., Boleti, H., Antony, C., Karsenti, E. & Vernos, I. Localization of the kinesin-like protein Xklp2 to spindle poles requires a leucine zipper, a microtubule-associated protein, and dynein. *J Cell Biol* **143**, 673-685 (1998).
- 125 Wittmann, T., Wilm, M., Karsenti, E. & Vernos, I. TPX2, A novel xenopus MAP involved in spindle pole organization. *J Cell Biol* **149**, 1405-1418 (2000).

-
- 126 Ma, N., Titus, J., Gable, A., Ross, J. L. & Wadsworth, P. TPX2 regulates the localization and activity of Eg5 in the mammalian mitotic spindle. *The Journal of cell biology* **195**, 87–98 (2011).
- 127 Fang, C. T., Kuo, H. H., Hsu, S. C. & Yih, L. H. HSP70 regulates Eg5 distribution within the mitotic spindle and modulates the cytotoxicity of Eg5 inhibitors. *Cell Death Dis* **11**, 715 (2020).
- 128 Mayer, T. U. *et al.* Small molecule inhibitor of mitotic spindle bipolarity identified in a phenotype-based screen. *Science* **286**, 971-974 (1999).
- 129 Cochran, J. C., Gatial, J. E., 3rd, Kapoor, T. M. & Gilbert, S. P. Monastrol inhibition of the mitotic kinesin Eg5. *J Biol Chem* **280**, 12658-12667 (2005).
- 130 Maliga, Z., Kapoor, T. M. & Mitchison, T. J. Evidence that monastrol is an allosteric inhibitor of the mitotic kinesin Eg5. *Chem Biol* **9**, 989-996 (2002).
- 131 Kwok, B. H. *et al.* Allosteric inhibition of kinesin-5 modulates its processive directional motility. *Nat Chem Biol* **2**, 480-485 (2006).
- 132 DeBonis, S. *et al.* Interaction of the mitotic inhibitor monastrol with human kinesin Eg5. *Biochemistry* **42**, 338-349 (2003).
- 133 Ferhat, L. *et al.* Expression of the mitotic motor protein Eg5 in postmitotic neurons: implications for neuronal development. *J Neurosci* **18**, 7822-7835 (1998).
- 134 Baas, P. W. The role of motor proteins in establishing the microtubule arrays of axons and dendrites. *J Chem Neuroanat* **14**, 175-180 (1998).
- 135 Falnikar, A., Tole, S. & Baas, P. W. Kinesin-5, a mitotic microtubule-associated motor protein, modulates neuronal migration. *Mol Biol Cell* **22**, 1561-1574 (2011).
- 136 Yoon, S. Y. *et al.* Monastrol, a selective inhibitor of the mitotic kinesin Eg5, induces a distinctive growth profile of dendrites and axons in primary cortical neuron cultures. *Cell Motil Cytoskeleton* **60**, 181-190 (2005).
- 137 Myers, K. A. & Baas, P. W. Kinesin-5 regulates the growth of the axon by acting as a brake on its microtubule array. *J Cell Biol* **178**, 1081-1091 (2007).
- 138 Lv, Z., Rosenbaum, J., Aspelmeier, T. & Grosshans, J. A 'molecular guillotine' reveals the interphase function of Kinesin-5. *J Cell Sci* **131** (2018).
- 139 Castillo, A., Morse, H. C., 3rd, Godfrey, V. L., Naeem, R. & Justice, M. J. Overexpression of Eg5 causes genomic instability and tumor formation in mice. *Cancer Res* **67**, 10138-10147 (2007).
- 140 Ari, C., Borysov, S. I., Wu, J., Padmanabhan, J. & Potter, H. Alzheimer amyloid beta inhibition of Eg5/kinesin 5 reduces neurotrophin and/or transmitter receptor function. *Neurobiol Aging* **35**, 1839-1849 (2014).

-
- 141 Wakana, Y. *et al.* Kinesin-5/Eg5 is important for transport of CARTS from the trans-Golgi network to the cell surface. *The Journal of cell biology* **202**, 241–250 (2013).
- 142 Chen, Y. & Hancock, W. O. Kinesin-5 is a microtubule polymerase. *Nat Commun* **6**, 8160 (2015).
- 143 Nozaki, H. *et al.* A 100%-complete sequence reveals unusually simple genomic features in the hot-spring red alga *Cyanidioschyzon merolae*. *BMC Biol* **5**, 28 (2007).
- 144 Imoto, Y., Yoshida, Y., Yagisawa, F., Kuroiwa, H. & Kuroiwa, T. The cell cycle, including the mitotic cycle and organelle division cycles, as revealed by cytological observations. *J Electron Microsc (Tokyo)* **60 Suppl 1**, S117-136 (2011).
- 145 Asada, T. & Shibaoka, H. Isolation of polypeptides with microtubule-translocating activity from phragmoplasts of tobacco BY-2 cells. *J Cell Sci* **107 (Pt 8)**, 2249-2257 (1994).
- 146 Asada, T., Kuriyama, R. & Shibaoka, H. TKRP125, a kinesin-related protein involved in the centrosome-independent organization of the cytokinetic apparatus in tobacco BY-2 cells. *Journal of cell science* **110 (Pt 2)**, 179–189 (1997).
- 147 Barroso, C. *et al.* Two kinesin-related proteins associated with the cold-stable cytoskeleton of carrot cells: characterization of a novel kinesin, DcKRP120-2. *Plant J* **24**, 859-868 (2000).
- 148 Peters, N. T. & Kropf, D. L. Kinesin-5 motors are required for organization of spindle microtubules in *Silvetia compressa* zygotes. *BMC Plant Biol* **6**, 19 (2006).
- 149 Peters, N. T., Miller, A. C. & Kropf, D. L. Localization and function of Kinesin-5-like proteins during assembly and maintenance of mitotic spindles in *Silvetia compressa*. *BMC Res Notes* **2**, 106 (2009).
- 150 Wiedemeier, A. M. *et al.* Mutant alleles of *Arabidopsis* RADIALLY SWOLLEN 4 and 7 reduce growth anisotropy without altering the transverse orientation of cortical microtubules or cellulose microfibrils. *Development* **129**, 4821-4830 (2002).
- 151 Klepikova, A. V., Kasianov, A. S., Gerasimov, E. S., Logacheva, M. D. & Penin, A. A. A high resolution map of the *Arabidopsis thaliana* developmental transcriptome based on RNA-seq profiling. *Plant J* **88**, 1058-1070 (2016).
- 152 Brieske, C. *Proteinbiochemische und molekularbiologische Analysen pflanzlicher PUB-ARM E3 Ubiquitinligasen*, Universität Hamburg, (2017).
- 153 Hershko, A. & Ciechanover, A. The ubiquitin system. *Annu Rev Biochem* **67**, 425-479 (1998).
- 154 Trujillo, M. News from the PUB: plant U-box type E3 ubiquitin ligases. *J Exp Bot* **69**, 371-384 (2018).
- 155 Chen, L. & Hellmann, H. Plant E3 ligases: flexible enzymes in a sessile world. *Mol Plant* **6**, 1388-1404 (2013).

-
- 156 Swatek, K. N. & Komander, D. Ubiquitin modifications. *Cell Res* **26**, 399-422 (2016).
- 157 Kulathu, Y. & Komander, D. Atypical ubiquitylation - the unexplored world of polyubiquitin beyond Lys48 and Lys63 linkages. *Nat Rev Mol Cell Biol* **13**, 508-523 (2012).
- 158 Vierstra, R. D. The ubiquitin-26S proteasome system at the nexus of plant biology. *Nat Rev Mol Cell Biol* **10**, 385-397 (2009).
- 159 Chen, Z. J. & Sun, L. J. Nonproteolytic functions of ubiquitin in cell signaling. *Mol Cell* **33**, 275-286 (2009).
- 160 Johnson, A. & Vert, G. Unraveling K63 Polyubiquitination Networks by Sensor-Based Proteomics. *Plant Physiol* **171**, 1808-1820 (2016).
- 161 Romero-Barrios, N. & Vert, G. Proteasome-independent functions of lysine-63 polyubiquitination in plants. *New Phytol* **217**, 995-1011 (2018).
- 162 Azevedo, C., Santos-Rosa, M. J. & Shirasu, K. The U-box protein family in plants. *Trends Plant Sci* **6**, 354-358 (2001).
- 163 Drechsel, G. *et al.* C-terminal armadillo repeats are essential and sufficient for association of the plant U-box armadillo E3 ubiquitin ligase SAUL1 with the plasma membrane. *J Exp Bot* **62**, 775-785 (2011).
- 164 Jung, C. *et al.* PLANT U-BOX PROTEIN10 Regulates MYC2 Stability in Arabidopsis. *Plant Cell* **27**, 2016-2031 (2015).
- 165 Mudgil, Y., Shiu, S. H., Stone, S. L., Salt, J. N. & Goring, D. R. A large complement of the predicted Arabidopsis ARM repeat proteins are members of the U-box E3 ubiquitin ligase family. *Plant Physiol* **134**, 59-66 (2004).
- 166 Yee, D. & Goring, D. R. The diversity of plant U-box E3 ubiquitin ligases: from upstream activators to downstream target substrates. *J Exp Bot* **60**, 1109-1121 (2009).
- 167 Hoth, S. *et al.* Genome-wide gene expression profiling in Arabidopsis thaliana reveals new targets of abscisic acid and largely impaired gene regulation in the *abi1-1* mutant. *J Cell Sci* **115**, 4891-4900 (2002).
- 168 Vogelmann, K. *et al.* Plasma membrane-association of SAUL1-type plant U-box armadillo repeat proteins is conserved in land plants. *Front Plant Sci* **5**, 37 (2014).
- 169 Disch, E. M. *et al.* Membrane-Associated Ubiquitin Ligase SAUL1 Suppresses Temperature- and Humidity-Dependent Autoimmunity in Arabidopsis. *Mol Plant Microbe Interact* **29**, 69-80 (2016).
- 170 Raab, S. *et al.* Identification of a novel E3 ubiquitin ligase that is required for suppression of premature senescence in Arabidopsis. *Plant J* **59**, 39-51 (2009).

-
- 171 Vogelmann, K. *et al.* Early senescence and cell death in *Arabidopsis saul1* mutants involves the PAD4-dependent salicylic acid pathway. *Plant Physiol* **159**, 1477-1487 (2012).
- 172 Wang, Y., Zhang, Y., Wang, Z., Zhang, X. & Yang, S. A missense mutation in CHS1, a TIR-NB protein, induces chilling sensitivity in *Arabidopsis*. *Plant J* **75**, 553-565 (2013).
- 173 Tong, M. *et al.* E3 ligase SAUL1 serves as a positive regulator of PAMP-triggered immunity and its homeostasis is monitored by immune receptor SOC3. *New Phytol* **215**, 1516-1532 (2017).
- 174 Zhang, Y. *et al.* Temperature-dependent autoimmunity mediated by *chs1* requires its neighboring TNL gene SOC3. *New Phytol* **213**, 1330-1345 (2017).
- 175 Liang, W., van Wersch, S., Tong, M. & Li, X. TIR-NB-LRR immune receptor SOC3 pairs with truncated TIR-NB protein CHS1 or TN2 to monitor the homeostasis of E3 ligase SAUL1. *New Phytol* **221**, 2054-2066 (2019).
- 176 Knop, J. *Structure and Function of a guarded Arabidopsis Immune Signaling Ubiquitin Ligase*, Univesität Hamburg, (2019).
- 177 Tao, K., Waletich, J. R., Wise, H., Arredondo, F. & Tyler, B. M. Tethering of Multi-Vesicular Bodies and the Tonoplast to the Plasma Membrane in Plants. *Front Plant Sci* **10**, 636 (2019).
- 178 Strauß, T. *Characterization of a SAUL1-interacting kinesin-5* Master of Science thesis, Universität Hamburg, (2016).
- 179 Walter, W. J., Beránek, V., Fischermeier, E. & Diez, S. Tubulin acetylation alone does not affect kinesin-1 velocity and run length in vitro. *PloS one* **7**, e42218 (2012).
- 180 Kerssemakers, J., Howard, J., Hess, H. & Diez, S. The distance that kinesin-1 holds its cargo from the microtubule surface measured by fluorescence interference contrast microscopy. *Proc Natl Acad Sci U S A* **103**, 15812-15817 (2006).
- 181 Varga, V., Leduc, C., Bormuth, V., Diez, S. & Howard, J. Kinesin-8 motors act cooperatively to mediate length-dependent microtubule depolymerization. *Cell* **138**, 1174-1183 (2009).
- 182 Toba, S. & Toyoshima, Y. Y. Dissociation of double-headed cytoplasmic dynein into single-headed species and its motile properties. *Cell Motil Cytoskeleton* **58**, 281-289 (2004).
- 183 Chhetri, G., Kalita, P. & Tripathi, T. An efficient protocol to enhance recombinant protein expression using ethanol in *Escherichia coli*. *MethodsX* **2**, 385-391 (2015).
- 184 Kurland, C. & Gallant, J. Errors of heterologous protein expression. *Curr Opin Biotechnol* **7**, 489-493 (1996).
- 185 Schmidt, F. R. Recombinant expression systems in the pharmaceutical industry. *Appl Microbiol Biotechnol* **65**, 363-372 (2004).

-
- 186 Daly, R. & Hearn, M. T. Expression of heterologous proteins in *Pichia pastoris*: a useful experimental tool in protein engineering and production. *J Mol Recognit* **18**, 119-138 (2005).
- 187 Macauley-Patrick, S., Fazenda, M. L., McNeil, B. & Harvey, L. M. Heterologous protein production using the *Pichia pastoris* expression system. *Yeast* **22**, 249-270 (2005).
- 188 Gustafsson, C., Govindarajan, S. & Minshull, J. Codon bias and heterologous protein expression. *Trends Biotechnol* **22**, 346-353 (2004).
- 189 Nakamura, Y., Gojobori, T. & Ikemura, T. Codon usage tabulated from international DNA sequence databases: status for the year 2000. *Nucleic Acids Res* **28**, 292 (2000).
- 190 Zaret, K. S. & Sherman, F. Mutationally altered 3' ends of yeast *CYC1* mRNA affect transcript stability and translational efficiency. *J Mol Biol* **177**, 107-135 (1984).
- 191 Henikoff, S. & Cohen, E. H. Sequences responsible for transcription termination on a gene segment in *Saccharomyces cerevisiae*. *Mol Cell Biol* **4**, 1515-1520 (1984).
- 192 Steakley, D. L. & Rine, J. On the Mechanism of Gene Silencing in *Saccharomyces cerevisiae*. *G3 (Bethesda)* **5**, 1751-1763 (2015).
- 193 Vieira Gomes, A. M., Souza Carmo, T., Silva Carvalho, L., Mendonca Bahia, F. & Parachin, N. S. Comparison of Yeasts as Hosts for Recombinant Protein Production. *Microorganisms* **6** (2018).
- 194 Miller, L. K. Insect baculoviruses: powerful gene expression vectors. *Bioessays* **11**, 91-95 (1989).
- 195 Vaughn, J. L., Goodwin, R. H., Tompkins, G. J. & McCawley, P. The establishment of two cell lines from the insect *Spodoptera frugiperda* (Lepidoptera; Noctuidae). *In Vitro* **13**, 213-217 (1977).
- 196 Wickham, T. J., Davis, T., Granados, R. R., Shuler, M. L. & Wood, H. A. Screening of insect cell lines for the production of recombinant proteins and infectious virus in the baculovirus expression system. *Biotechnol Prog* **8**, 391-396 (1992).
- 197 Wickham, T. J. & Nemerow, G. R. Optimization of growth methods and recombinant protein production in BTI-Tn-5B1-4 insect cells using the baculovirus expression system. *Biotechnol Prog* **9**, 25-30 (1993).
- 198 Shimamoto, Y., Forth, S. & Kapoor, T. M. Measuring Pushing and Braking Forces Generated by Ensembles of Kinesin-5 Crosslinking Two Microtubules. *Dev Cell* **34**, 669-681 (2015).
- 199 Crevel, I. M., Lockhart, A. & Cross, R. A. Kinetic evidence for low chemical processivity in *ncd* and *Eg5*. *J Mol Biol* **273**, 160-170 (1997).
- 200 Braun, M. *et al.* Changes in microtubule overlap length regulate kinesin-14-driven microtubule sliding. *Nat Chem Biol* **13**, 1245-1252 (2017).

- 201 Hentrich, C. & Surrey, T. Microtubule organization by the antagonistic mitotic motors kinesin-5 and kinesin-14. *J Cell Biol* **189**, 465-480 (2010).
- 202 Hepperla, A. J. *et al.* Minus-end-directed Kinesin-14 motors align antiparallel microtubules to control metaphase spindle length. *Dev Cell* **31**, 61-72 (2014).
- 203 Mitra, A. *et al.* Kinesin-14 motors drive a right-handed helical motion of antiparallel microtubules around each other. *Nat Commun* **11**, 2565 (2020).
- 204 Arttamangkul, S., Alvarez-Maubecin, V., Thomas, G., Williams, J. T. & Grandy, D. K. Binding and internalization of fluorescent opioid peptide conjugates in living cells. *Mol Pharmacol* **58**, 1570-1580 (2000).
- 205 Martin, B. R., Giepmans, B. N. G., Adams, S. R. & Tsien, R. Y. Mammalian cell-based optimization of the biarsenical-binding tetracysteine motif for improved fluorescence and affinity. *Nature biotechnology* **23**, 1308–1314 (2005).
- 206 Roberti, M. J., Bertoncini, C. W., Klement, R., Jares-Erijman, E. A. & Jovin, T. M. Fluorescence imaging of amyloid formation in living cells by a functional, tetracysteine-tagged alpha-synuclein. *Nature methods* **4**, 345–351 (2007).
- 207 Griffin, B. A., Adams, S. R., Jones, J. & Tsien, R. Y. Fluorescent labeling of recombinant proteins in living cells with FIAsh. *Methods Enzymol* **327**, 565-578 (2000).
- 208 Sawin, K. E. & Mitchison, T. J. Poleward microtubule flux mitotic spindles assembled in vitro. *J Cell Biol* **112**, 941-954 (1991).
- 209 Muretta, J. M. *et al.* A posttranslational modification of the mitotic kinesin Eg5 that enhances its mechanochemical coupling and alters its mitotic function. *Proc Natl Acad Sci U S A* **115**, E1779-E1788 (2018).
- 210 Yilmaz, A. *et al.* AGRIS: the Arabidopsis Gene Regulatory Information Server, an update. *Nucleic Acids Res* **39**, D1118-1122 (2011).
- 211 Fox, S. *et al.* Spatiotemporal coordination of cell division and growth during organ morphogenesis. *PLoS Biol* **16**, e2005952 (2018).
- 212 Gallegos, J. E. & Rose, A. B. An intron-derived motif strongly increases gene expression from transcribed sequences through a splicing independent mechanism in *Arabidopsis thaliana*. *Sci Rep* **9**, 13777 (2019).
- 213 Stergachis, A. B. *et al.* Exonic transcription factor binding directs codon choice and affects protein evolution. *Science* **342**, 1367-1372 (2013).
- 214 Ahituv, N. Exonic enhancers: proceed with caution in exome and genome sequencing studies. *Genome Med* **8**, 14 (2016).
- 215 Mascarenhas, D., Mettler, I. J., Pierce, D. A. & Lowe, H. W. Intron-mediated enhancement of heterologous gene expression in maize. *Plant Mol Biol* **15**, 913-920 (1990).

- 216 Narsai, R. *et al.* Genome-wide analysis of mRNA decay rates and their determinants in *Arabidopsis thaliana*. *Plant Cell* **19**, 3418-3436 (2007).
- 217 Sollner, R. *et al.* Cytokinesis-defective mutants of *Arabidopsis*. *Plant Physiol* **129**, 678-690 (2002).
- 218 Li, H. *et al.* *Arabidopsis* MAP65-4 plays a role in phragmoplast microtubule organization and marks the cortical cell division site. *New Phytol* **215**, 187-201 (2017).
- 219 Jiang, K., Moe-Lange, J., Hennet, L. & Feldman, L. J. Salt Stress Affects the Redox Status of *Arabidopsis* Root Meristems. *Front Plant Sci* **7**, 81 (2016).
- 220 Baskin, T. I., Beemster, G. T., Judy-March, J. E. & Marga, F. Disorganization of cortical microtubules stimulates tangential expansion and reduces the uniformity of cellulose microfibril alignment among cells in the root of *Arabidopsis*. *Plant Physiol* **135**, 2279-2290 (2004).
- 221 Komaki, S. *et al.* Nuclear-localized subtype of end-binding 1 protein regulates spindle organization in *Arabidopsis*. *J Cell Sci* **123**, 451-459 (2010).
- 222 Jinek, M. *et al.* A programmable dual-RNA-guided DNA endonuclease in adaptive bacterial immunity. *Science* **337**, 816-821 (2012).
- 223 Friedland, A. E. *et al.* Heritable genome editing in *C. elegans* via a CRISPR-Cas9 system. *Nat Methods* **10**, 741-743 (2013).
- 224 Jiang, W., Bikard, D., Cox, D., Zhang, F. & Marraffini, L. A. RNA-guided editing of bacterial genomes using CRISPR-Cas systems. *Nat Biotechnol* **31**, 233-239 (2013).
- 225 Mali, P. *et al.* RNA-guided human genome engineering via Cas9. *Science* **339**, 823-826 (2013).
- 226 Shan, Q. *et al.* Targeted genome modification of crop plants using a CRISPR-Cas system. *Nat Biotechnol* **31**, 686-688 (2013).
- 227 Li, J. F. *et al.* Multiplex and homologous recombination-mediated genome editing in *Arabidopsis* and *Nicotiana benthamiana* using guide RNA and Cas9. *Nat Biotechnol* **31**, 688-691 (2013).
- 228 Ma, X. *et al.* A Robust CRISPR/Cas9 System for Convenient, High-Efficiency Multiplex Genome Editing in Monocot and Dicot Plants. *Mol Plant* **8**, 1274-1284 (2015).
- 229 Pan, C. *et al.* CRISPR/Cas9-mediated efficient and heritable targeted mutagenesis in tomato plants in the first and later generations. *Sci Rep* **6**, 24765 (2016).
- 230 Ordon, J. *et al.* Generation of chromosomal deletions in dicotyledonous plants employing a user-friendly genome editing toolkit. *Plant J* **89**, 155-168 (2017).
- 231 Cai, Y. *et al.* CRISPR/Cas9-Mediated Deletion of Large Genomic Fragments in Soybean. *Int J Mol Sci* **19** (2018).

- 232 Fauser, F., Schiml, S. & Puchta, H. Both CRISPR/Cas-based nucleases and nickases can be used efficiently for genome engineering in *Arabidopsis thaliana*. *Plant J* **79**, 348-359 (2014).
- 233 LeBlanc, C. *et al.* Increased efficiency of targeted mutagenesis by CRISPR/Cas9 in plants using heat stress. *Plant J* **93**, 377-386 (2018).
- 234 Denbow, C. J. *et al.* Gateway-Compatible CRISPR-Cas9 Vectors and a Rapid Detection by High-Resolution Melting Curve Analysis. *Front Plant Sci* **8**, 1171 (2017).
- 235 Wittwer, C. T., Reed, G. H., Gundry, C. N., Vandersteen, J. G. & Pryor, R. J. High-resolution genotyping by amplicon melting analysis using LCGreen. *Clin Chem* **49**, 853-860 (2003).
- 236 Curtis, M. D. & Grossniklaus, U. A gateway cloning vector set for high-throughput functional analysis of genes in planta. *Plant Physiol* **133**, 462-469 (2003).
- 237 Yoo, S.-D., Cho, Y.-H. & Sheen, J. *Arabidopsis* mesophyll protoplasts: a versatile cell system for transient gene expression analysis. *Nature protocols* **2**, 1565–1572 (2007).
- 238 Meyer, P. *et al.* Endogenous and environmental factors influence 35S promoter methylation of a maize A1 gene construct in transgenic petunia and its colour phenotype. *Mol Gen Genet* **231**, 345-352 (1992).
- 239 Mishiba, K. *et al.* Consistent transcriptional silencing of 35S-driven transgenes in gentian. *Plant J* **44**, 541-556 (2005).
- 240 Love, A. J. *et al.* Cauliflower mosaic virus protein P6 is a suppressor of RNA silencing. *J Gen Virol* **88**, 3439-3444 (2007).
- 241 Hasezawa, S., Hogetsu, T. & Syono, K. Rearrangement of Cortical Microtubules in Elongating Cells derived from Tobacco Protoplasts — A Time-course Observation by Immunofluorescence Microscopy —. *Journal of plant physiology* **133**, 46-51 (1988).
- 242 Lloyd, C. W., Slabas, A. R., Powell, A. J. & Lowe, S. B. Microtubules, protoplasts and plant cell shape : An immunofluorescent study. *Planta* **147**, 500-506 (1980).
- 243 Akashi, T., Kawasaki, S. & Shibaoka, H. Stabilization of cortical microtubules by the cell wall in cultured tobacco cells : Effects of extensin on the cold-stability of cortical microtubules. *Planta* **182**, 363-369 (1990).
- 244 Cyr, R. J., Bustos, M. M., Guiltinan, M. J. & Fosket, D. E. Developmental modulation of tubulin protein and mRNA levels during somatic embryogenesis in cultured carrot cells. *Planta* **171**, 365-376 (1987).
- 245 Qin, T., Li, J., Yuan, M. & Mao, T. Characterization of the role of calcium in regulating the microtubule-destabilizing activity of MDP25. *Plant Signal Behav* **7**, 708-710 (2012).
- 246 Zuo, J., Niu, Q. W. & Chua, N. H. Technical advance: An estrogen receptor-based transactivator XVE mediates highly inducible gene expression in transgenic plants. *Plant J* **24**, 265-273 (2000).

-
- 247 Danielson, D. C. & Pezacki, J. P. Studying the RNA silencing pathway with the p19 protein. *FEBS Lett* **587**, 1198-1205 (2013).
- 248 Kumagai-Sano, F., Hayashi, T., Sano, T. & Hasezawa, S. Cell cycle synchronization of tobacco BY-2 cells. *Nat Protoc* **1**, 2621-2627 (2006).
- 249 Rahni, R. & Birnbaum, K. D. Week-long imaging of cell divisions in the Arabidopsis root meristem. *Plant Methods* **15**, 30 (2019).
- 250 Yang, R. *et al.* A novel strategy to visualize vesicle-bound kinesins reveals the diversity of kinesin-mediated transport. *Traffic* **20**, 851-866 (2019).
- 251 Serra-Marques, A. *et al.* Concerted action of kinesins KIF5B and KIF13B promotes efficient secretory vesicle transport to microtubule plus ends. *Elife* **9** (2020).
- 252 Hooikaas, P. J. *et al.* MAP7 family proteins regulate kinesin-1 recruitment and activation. *J Cell Biol* **218**, 1298-1318 (2019).
- 253 Monroy, B. Y. *et al.* A Combinatorial MAP Code Dictates Polarized Microtubule Transport. *Dev Cell* **53**, 60-72 e64 (2020).
- 254 Kong, Z. *et al.* Kinesin-4 Functions in Vesicular Transport on Cortical Microtubules and Regulates Cell Wall Mechanics during Cell Elongation in Plants. *Mol Plant* **8**, 1011-1023 (2015).
- 255 Zhong, R., Burk, D. H., Morrison, W. H., 3rd & Ye, Z. H. A kinesin-like protein is essential for oriented deposition of cellulose microfibrils and cell wall strength. *Plant Cell* **14**, 3101-3117 (2002).
- 256 Zhu, C. & Dixit, R. Single molecule analysis of the Arabidopsis FRA1 kinesin shows that it is a functional motor protein with unusually high processivity. *Mol Plant* **4**, 879-885 (2011).
- 257 Zhu, C. *et al.* The fragile Fiber1 kinesin contributes to cortical microtubule-mediated trafficking of cell wall components. *Plant Physiol* **167**, 780-792 (2015).
- 258 Ganguly, A., Zhu, C., Chen, W. & Dixit, R. FRA1 Kinesin Modulates the Lateral Stability of Cortical Microtubules through Cellulose Synthase-Microtubule Uncoupling Proteins. *Plant Cell* **32**, 2508-2524 (2020).
- 259 Ganguly, A., DeMott, L. & Dixit, R. The Arabidopsis kinesin-4, FRA1, requires a high level of processive motility to function correctly. *J Cell Sci* **130**, 1232-1238 (2017).
- 260 Howard, J. Molecular motors: structural adaptations to cellular functions. *Nature* **389**, 561-567 (1997).
- 261 Wakana, Y. *et al.* A new class of carriers that transport selective cargo from the trans Golgi network to the cell surface. *EMBO J* **31**, 3976-3990 (2012).

- 262 Borysov, S. I., Granic, A., Padmanabhan, J., Walczak, C. E. & Potter, H. Alzheimer Abeta disrupts the mitotic spindle and directly inhibits mitotic microtubule motors. *Cell Cycle* **10**, 1397-1410 (2011).
- 263 Abisambra, J. F. *et al.* LDLR expression and localization are altered in mouse and human cell culture models of Alzheimer's disease. *PLoS One* **5**, e8556 (2010).
- 264 Snyder, E. M. *et al.* Regulation of NMDA receptor trafficking by amyloid-beta. *Nat Neurosci* **8**, 1051-1058 (2005).
- 265 Shah, S. B. *et al.* Examination of potential mechanisms of amyloid-induced defects in neuronal transport. *Neurobiol Dis* **36**, 11-25 (2009).
- 266 Almeida, C. G. *et al.* Beta-amyloid accumulation in APP mutant neurons reduces PSD-95 and GluR1 in synapses. *Neurobiol Dis* **20**, 187-198 (2005).
- 267 Owen, D. J. & Collins, B. M. Vesicle transport: a new player in APP trafficking. *Curr Biol* **20**, R413-415 (2010).
- 268 Groemer, T. W. *et al.* Amyloid precursor protein is trafficked and secreted via synaptic vesicles. *PLoS One* **6**, e18754 (2011).
- 269 Yamazaki, T., Koo, E. H. & Selkoe, D. J. Trafficking of cell-surface amyloid beta-protein precursor. II. Endocytosis, recycling and lysosomal targeting detected by immunolocalization. *J Cell Sci* **109 (Pt 5)**, 999-1008 (1996).
- 270 Stevenson, J. W. *et al.* The Amyloid Precursor Protein of Alzheimer's Disease Clusters at the Organelle/Microtubule Interface on Organelles that Bind Microtubules in an ATP Dependent Manner. *PLoS One* **11**, e0147808 (2016).
- 271 Muresan, V. & Muresan, Z. Is abnormal axonal transport a cause, a contributing factor or a consequence of the neuronal pathology in Alzheimer's disease? *Future Neurol* **4**, 761-773 (2009).
- 272 Setou, M., Nakagawa, T., Seog, D. H. & Hirokawa, N. Kinesin superfamily motor protein KIF17 and mLin-10 in NMDA receptor-containing vesicle transport. *Science* **288**, 1796-1802 (2000).
- 273 Inomata, H. *et al.* A scaffold protein JIP-1b enhances amyloid precursor protein phosphorylation by JNK and its association with kinesin light chain 1. *J Biol Chem* **278**, 22946-22955 (2003).
- 274 Matsuda, S., Matsuda, Y. & D'Adamio, L. Amyloid beta protein precursor (AbetaPP), but not AbetaPP-like protein 2, is bridged to the kinesin light chain by the scaffold protein JNK-interacting protein 1. *J Biol Chem* **278**, 38601-38606 (2003).
- 275 Eckerdt, F., Eysers, P. A., Lewellyn, A. L., Prigent, C. & Maller, J. L. Spindle pole regulation by a discrete Eg5-interacting domain in TPX2. *Current biology : CB* **18**, 519-525 (2008).
- 276 Balchand, S. K., Mann, B. J., Titus, J., Ross, J. L. & Wadsworth, P. TPX2 Inhibits Eg5 by Interactions with Both Motor and Microtubule. *J Biol Chem* **290**, 17367-17379 (2015).

- 277 Chen, L. *et al.* Tripartite Motif 8 Contributes to Pathological Cardiac Hypertrophy Through Enhancing Transforming Growth Factor beta-Activated Kinase 1-Dependent Signaling Pathways. *Hypertension* **69**, 249-258 (2017).
- 278 Li, Q. *et al.* Tripartite motif 8 (TRIM8) modulates TNFalpha- and IL-1beta-triggered NF-kappaB activation by targeting TAK1 for K63-linked polyubiquitination. *Proc Natl Acad Sci U S A* **108**, 19341-19346 (2011).
- 279 Okumura, F., Matsunaga, Y., Katayama, Y., Nakayama, K. I. & Hatakeyama, S. TRIM8 modulates STAT3 activity through negative regulation of PIAS3. *J Cell Sci* **123**, 2238-2245 (2010).
- 280 Venuto, S. *et al.* TRIM8 interacts with KIF11 and KIFC1 and controls bipolar spindle formation and chromosomal stability. *Cancer Lett* **473**, 98-106 (2020).
- 281 Machens, I. *Characterization of two novel kinesin-14 subfamilies from Arabidopsis thaliana*, Universität Hamburg, (2018).
- 282 Gross, S. P., Vershinin, M. & Shubeita, G. T. Cargo transport: two motors are sometimes better than one. *Curr Biol* **17**, R478-486 (2007).
- 283 Bieling, P., Kronja, I. & Surrey, T. Microtubule motility on reconstituted meiotic chromatin. *Curr Biol* **20**, 763-769 (2010).
- 284 Arpag, G., Shastry, S., Hancock, W. O. & Tuzel, E. Transport by populations of fast and slow kinesins uncovers novel family-dependent motor characteristics important for in vivo function. *Biophys J* **107**, 1896-1904 (2014).
- 285 Larson, A. G., Landahl, E. C. & Rice, S. E. Mechanism of cooperative behaviour in systems of slow and fast molecular motors. *Phys Chem Chem Phys* **11**, 4890-4898 (2009).
- 286 Valentine, M. T. & Block, S. M. Force and premature binding of ADP can regulate the processivity of individual Eg5 dimers. *Biophys J* **97**, 1671-1677 (2009).
- 287 Valentine, M. T., Fordyce, P. M. & Block, S. M. Eg5 steps it up! *Cell Div* **1**, 31 (2006).
- 288 Valentine, M. T., Fordyce, P. M., Krzysiak, T. C., Gilbert, S. P. & Block, S. M. Individual dimers of the mitotic kinesin motor Eg5 step processively and support substantial loads in vitro. *Nat Cell Biol* **8**, 470-476 (2006).
- 289 Cyr, R. J. & Palevitz, B. A. Organization of cortical microtubules in plant cells. *Curr Opin Cell Biol* **7**, 65-71 (1995).
- 290 Pesquet, E. & Lloyd, C. in *The Plant Cytoskeleton* (ed Bo Liu) 277-306 (Springer New York, 2011).
- 291 Oda, Y. & Fukuda, H. Secondary cell wall patterning during xylem differentiation. *Curr Opin Plant Biol* **15**, 38-44 (2012).

-
- 292 Oda, Y. & Hasezawa, S. Cytoskeletal organization during xylem cell differentiation. *J Plant Res* **119**, 167-177 (2006).
- 293 Allard, J. F., Wasteneys, G. O. & Cytrynbaum, E. N. Mechanisms of self-organization of cortical microtubules in plants revealed by computational simulations. *Mol Biol Cell* **21**, 278-286 (2010).
- 294 Yu, W. & Baas, P. W. Changes in microtubule number and length during axon differentiation. *J Neurosci* **14**, 2818-2829 (1994).
- 295 Ma, Y., Shakiryanova, D., Vardya, I. & Popov, S. V. Quantitative analysis of microtubule transport in growing nerve processes. *Curr Biol* **14**, 725-730 (2004).
- 296 Wang, L. & Brown, A. Rapid movement of microtubules in axons. *Curr Biol* **12**, 1496-1501 (2002).
- 297 Dent, E. W., Callaway, J. L., Szebenyi, G., Baas, P. W. & Kalil, K. Reorganization and movement of microtubules in axonal growth cones and developing interstitial branches. *J Neurosci* **19**, 8894-8908 (1999).
- 298 Li, J. *et al.* Mutation of rice BC12/GDD1, which encodes a kinesin-like protein that binds to a GA biosynthesis gene promoter, leads to dwarfism with impaired cell elongation. *Plant Cell* **23**, 628-640 (2011).
- 299 Zhang, M. *et al.* Brittle Culm 12, a dual-targeting kinesin-4 protein, controls cell-cycle progression and wall properties in rice. *Plant J* **63**, 312-328 (2010).
- 300 Hanahan, D. Studies on transformation of *Escherichia coli* with plasmids. *J Mol Biol* **166**, 557-580 (1983).
- 301 Deblaere, R. *et al.* Efficient octopine Ti plasmid-derived vectors for *Agrobacterium*-mediated gene transfer to plants. *Nucleic Acids Res* **13**, 4777-4788 (1985).
- 302 Ashby, A. M., Watson, M. D., Loake, G. J. & Shaw, C. H. Ti plasmid-specified chemotaxis of *Agrobacterium tumefaciens* C58C1 toward vir-inducing phenolic compounds and soluble factors from monocotyledonous and dicotyledonous plants. *J Bacteriol* **170**, 4181-4187 (1988).
- 303 Cregg, J. M., Vedvick, T. S. & Raschke, W. C. Recent advances in the expression of foreign genes in *Pichia pastoris*. *Biotechnology (N Y)* **11**, 905-910 (1993).
- 304 Waterham, H. R., Digan, M. E., Koutz, P. J., Lair, S. V. & Cregg, J. M. Isolation of the *Pichia pastoris* glyceraldehyde-3-phosphate dehydrogenase gene and regulation and use of its promoter. *Gene* **186**, 37-44 (1997).
- 305 Hink, W. F. A serum-free medium for the culture of insect cells and production of recombinant proteins. *In Vitro Cell Dev Biol* **27A**, 397-401 (1991).
- 306 Meinke, D. & Scholl, R. The preservation of plant genetic resources. Experiences with *Arabidopsis*. *Plant Physiol* **133**, 1046-1050 (2003).

- 307 Kleinboelting, N., Huep, G., Kloetgen, A., Viehoveer, P. & Weisshaar, B. GABI-Kat SimpleSearch: new features of the Arabidopsis thaliana T-DNA mutant database. *Nucleic Acids Res* **40**, D1211-1215 (2012).
- 308 Alonso, J. M. *et al.* Genome-wide insertional mutagenesis of Arabidopsis thaliana. *Science* **301**, 653-657 (2003).
- 309 Prusicki, M. A. *et al.* Live cell imaging of meiosis in Arabidopsis thaliana. *Elife* **8** (2019).
- 310 Komaki, S. *et al.* Functional Analysis of the Plant Chromosomal Passenger Complex. *Plant Physiol* **183**, 1586-1599 (2020).
- 311 Karimi, M., Depicker, A. & Hilson, P. Recombinational cloning with plant gateway vectors. *Plant Physiol* **145**, 1144-1154 (2007).
- 312 Earley, K. W. *et al.* Gateway-compatible vectors for plant functional genomics and proteomics. *Plant J* **45**, 616-629 (2006).
- 313 Schiml, S., Fauser, F. & Puchta, H. CRISPR/Cas-Mediated Site-Specific Mutagenesis in Arabidopsis thaliana Using Cas9 Nucleases and Paired Nickases. *Methods Mol Biol* **1469**, 111-122 (2016).
- 314 Bryksin, A. V. & Matsumura, I. Overlap extension PCR cloning: a simple and reliable way to create recombinant plasmids. *BioTechniques* **48**, 463-465 (2010).
- 315 Hanahan, D., Jessee, J. & Bloom, F. R. Plasmid transformation of Escherichia coli and other bacteria. *Methods Enzymol* **204**, 63-113 (1991).
- 316 Green, R. & Rogers, E. J. Transformation of chemically competent E. coli. *Methods Enzymol* **529**, 329-336 (2013).
- 317 Mattanovich, D. *et al.* Efficient transformation of Agrobacterium spp. by electroporation. *Nucleic Acids Res* **17**, 6747 (1989).
- 318 Birnboim, H. C. & Doly, J. A rapid alkaline extraction procedure for screening recombinant plasmid DNA. *Nucleic Acids Res* **7**, 1513-1523 (1979).
- 319 Murashige, T. S., F. A Revised Medium for Rapid Growth and Bio Assays with Tobacco Tissue Cultures. *Physiologia Plantarum* **15**, 473-497 (1962).
- 320 Zhang, X., Henriques, R., Lin, S.-S., Niu, Q.-W. & Chua, N.-H. Agrobacterium-mediated transformation of Arabidopsis thaliana using the floral dip method. *Nature protocols* **1**, 641-646 (2006).
- 321 Wendler, C., Barniske, M. & Wild, A. Effect of phosphinothricin (glufosinate) on photosynthesis and photorespiration of C3 and C4 plants. *Photosynth Res* **24**, 55-61 (1990).
- 322 Block, M. D. *et al.* Engineering herbicide resistance in plants by expression of a detoxifying enzyme. *EMBO J* **6**, 2513-2518 (1987).

-
- 323 Waldron, C. *et al.* Resistance to hygromycin B : A new marker for plant transformation studies. *Plant Mol Biol* **5**, 103-108 (1985).
- 324 Harrison, S. J. *et al.* A rapid and robust method of identifying transformed *Arabidopsis thaliana* seedlings following floral dip transformation. *Plant methods* **2**, 19 (2006).
- 325 Jefferson, R. A., Kavanagh, T. A. & Bevan, M. W. GUS fusions: beta-glucuronidase as a sensitive and versatile gene fusion marker in higher plants. *EMBO J* **6**, 3901-3907 (1987).
- 326 Hoyer, H. Beiträge zur histologischen Technik. *Biologisches Zentralblatt* **2**, 17-24 (1882).
- 327 Kurihara, D., Mizuta, Y., Sato, Y. & Higashiyama, T. ClearSee: a rapid optical clearing reagent for whole-plant fluorescence imaging. *Development (Cambridge, England)* **142**, 4168–4179 (2015).
- 328 Stemmer, M., Thumberger, T., Del Sol Keyer, M., Wittbrodt, J. & Mateo, J. L. CCTop: An Intuitive, Flexible and Reliable CRISPR/Cas9 Target Prediction Tool. *PLoS One* **10**, e0124633 (2015).
- 329 Labuhn, M. *et al.* Refined sgRNA efficacy prediction improves large- and small-scale CRISPR-Cas9 applications. *Nucleic Acids Res* **46**, 1375-1385 (2018).
- 330 Ran, F. A. *et al.* Genome engineering using the CRISPR-Cas9 system. *Nat Protoc* **8**, 2281-2308 (2013).
- 331 Dyballa, N. & Metzger, S. Fast and sensitive colloidal coomassie G-250 staining for proteins in polyacrylamide gels. *J Vis Exp* (2009).
- 332 Higgins, D. a. C., J. *Pichia protocols*. 1 edn, (Humana Press, 1998).
- 333 Castoldi, M. & Popov, A. V. Purification of brain tubulin through two cycles of polymerization–depolymerization in a high-molarity buffer. *Protein Expression and Purification* **32**, 83–88 (2003).
- 334 Hyman, A. *et al.* Preparation of modified tubulins. *Methods Enzymol* **196**, 478-485 (1991).
- 335 Howard, J. & Hyman, A. A. Preparation of marked microtubules for the assay of the polarity of microtubule-based motors by fluorescence microscopy. *Methods Cell Biol* **39**, 105-113 (1993).
- 336 Blanchard, S. C., Kim, H. D., Gonzalez, R. L., Jr., Puglisi, J. D. & Chu, S. tRNA dynamics on the ribosome during translation. *Proc Natl Acad Sci U S A* **101**, 12893-12898 (2004).
- 337 Griffin, B. A., Adams, S. R. & Tsien, R. Y. Specific covalent labeling of recombinant protein molecules inside live cells. *Science (New York, N.Y.)* **281**, 269–272 (1998).

-
- 338 Widengren, J., Chmyrov, A., Eggeling, C., Lofdahl, P. A. & Seidel, C. A. Strategies to improve photostabilities in ultrasensitive fluorescence spectroscopy. *J Phys Chem A* **111**, 429-440 (2007).
- 339 Aitken, C. E., Marshall, R. A. & Puglisi, J. D. An oxygen scavenging system for improvement of dye stability in single-molecule fluorescence experiments. *Biophys J* **94**, 1826-1835 (2008).
- 340 Ruhnnow, F., Zwicker, D. & Diez, S. Tracking single particles and elongated filaments with nanometer precision. *Biophysical journal* **100**, 2820–2828 (2011).
- 341 Madeira, F. *et al.* The EMBL-EBI search and sequence analysis tools APIs in 2019. *Nucleic Acids Res* **47**, W636-W641 (2019).
- 342 Marchler-Bauer, A. *et al.* CDD/SPARCLE: functional classification of proteins via subfamily domain architectures. *Nucleic Acids Res* **45**, D200-D203 (2017).
- 343 Gasteiger, E. *et al.* ExPASy: The proteomics server for in-depth protein knowledge and analysis. *Nucleic Acids Res* **31**, 3784-3788 (2003).
- 344 Schindelin, J. *et al.* Fiji: an open-source platform for biological-image analysis. *Nat Methods* **9**, 676-682 (2012).
- 345 Letunic, I. & Bork, P. Interactive Tree Of Life (iTOL) v4: recent updates and new developments. *Nucleic Acids Res* **47**, W256-W259 (2019).
- 346 Lamesch, P. *et al.* The Arabidopsis Information Resource (TAIR): improved gene annotation and new tools. *Nucleic Acids Res* **40**, D1202-1210 (2012).
- 347 Simm, D., Hatje, K. & Kollmar, M. Waggawagga: comparative visualization of coiled-coil predictions and detection of stable single alpha-helices (SAH domains). *Bioinformatics* **31**, 767-769 (2015).

6 Supplement

Table S1: Amino acid sequences of recombinant proteins used in this thesis.

Protein	Amino acid sequence
AtKRP125b FL + 6 x His-tag From <i>E. coli</i> Size: 114 kDa	MSSRHDKEKGVNVQVLLRCRPFSDDELRSNAPQVLTCDLQREVAVSQNIAGK HIDRVFTFDKVFGPSAQKQDLYDQAVVPIVNEVLEGFNCTIFAYGQTGTGKTYT MEGECRRSKSAPCGGLPAEAGVIPRAVKQIFDTLEGQQA EYSVKVTFLELYNEEI TDLLAPEDLSRVAAEEKQKKPLPLMEDGKGGVLVRGLEEEIVTSANEIFTLLERGS SKRRTAETFLNKQSSRSHLSFSITIHKEATPEGEELIKCGKLNLDLAGSENISRSG ARDGRAREAGEINKSLLTLGRVISALVEHLGHVVPYRDSKLTRLLRDSLGGRTKTCII ATVSPA VHCLEETLSTLDYAHRAKNIRNKPEVNQKMMKSTLIKDLYGEIERLKA E VYASREKNGVYMPKERYYYQEESERKVM AEQIEQMGGQIENYQKQLEELQDKY VGQVRECSDLTTKLDITEKNLSQTCKVLASTNEELKKSQYAMKEKDFIIEQKKSE NVLVQQACILQSNLEKATKDSSLHQKIGREDKLSADNRKVV DNYQVELSEQIS NLFNRVASCLSQQNVHLQGVNKLQSRL EAHNKAILEM KKKVKASRDLYSSHLE AVQNVVRLH KANANACLEEV SALTSSACSID EFLASGDETTSSLFDELQSALSSH QGEMALFAREL RQRFHTTMEQTQEMSEY TSTFFQKLM EESKNAETRAAEAND SQINSIIDFQKTYEAQSKSDTDKLIADLTNLVSSHIR RQHELVD SRLHNFKDAVSS NKTFLDEHVS AVNNLTKDAKR KWETFSMQAENEAREGADFSAAKHCRMELL L QQSVGHAESA FKHCKITHESLKEMTSKQVTDVSSLVRSACDSNEQHDAEVD SA RTAAEKDVT KNSDDIIQQIERMSEDEKASVSKILENVR SHEKTLESFQQDQCCQA RCIEDKAQET FQQQYMEYEPTGATPTKNEPEIPTKATIESLRAMPIETLV EEFREN NSYESFATK ETKPQQLTRSPLSQVHHHHH
AtKRP125b FL + 6 x His-tag From <i>P. pastoris</i> Size: 124 kDa with α -factor; 114 kDa without α -factor	MRFPSIFTAVLFAASSALAAPVNTTTEDETAQIPAEAVIGYS DLEGDFDVA VLPFS NSTNNGLLFINTT IASIAAKEEGVSLEKREAEASSR HDKEKGVNVQVLLRCRPFSD DELRSNAPQVLTCDLQREVAVSQNIAGKHIDRVFTFDKVFGPSAQKQDLYDQ AVVPIVNEVLEGFNCTIFAYGQTGTGKTYTMEGECRRSKSAPCGGLPAEAGVIPR AVKQIFDTLEGQQA EYSVKVTFLELYNEEI TDLLAPEDLSRVAAEEKQKKPLPLME DGKGGVLVRGLEEEIVTSANEIFTLLERGS SKRRTAETFLNKQSSRSHLSFSITIHK EATPEGEELIKCGKLNLDLAGSENISRSGARDGRAREAGEINKSLLTLGRVISALV EHLGHVVPYRDSKLTRLLRDSLGGRTKTCIIATVSPA VHCLEETLSTLDYAHRAKNIR NKPEVNQKMMKSTLIKDLYGEIERLKA EVYASREKNGVYMPKERYYYQEESERKV MAEQIEQMGGQIENYQKQLEELQDKYVGQVRECSDLTTKLDITEKNLSQTCKVL ASTNEELKKSQYAMKEKDFIIEQKKSE NVLVQQACILQSNLEKATKDSSLHQKI GREDKLSADNRKVV DNYQVELSEQISNLFNRVASCLSQQNVHLQGVNKLQSRL LEAHNKAILEM KKKVKASRDLYSSHLEAVQNVVRLH KANANACLEEV SALTSS ACSID EFLASGDETTSSLFDELQSALSSHQGEMALFAREL RQRFHTTMEQTQEM SEY TSTFFQKLM EESKNAETRAAEANDSQINSIIDFQKTYEAQSKSDTDKLIADLT NLVSSHIR RQHELVD SRLHNFKDAVSSNKTFLDEHVS AVNNLTKDAKR KWETFS MQAENEAREGADFSAAKHCRMELL LQQSVGHAESA FKHCKITHESLKEMTSKQ VTDVSSLVRSACDSNEQHDAEVD SARTAAEKDVT KNSDDIIQQIERMSEDEKAS VSKILENVR SHEKTLESFQQDQCCQARCI EDKAQET FQQQYMEYEPTGATPTKN EPEIPTKATIESLRAMPIETLV EEFRENNSYESFATK ETKPQQLTRSPLSQVHHHH HH

AtKRP125b FL +
eGFP + 6 x His-
tag
From *P. pastoris*
Size: 150 kDa
with α -factor;
141 kDa without
 α -factor

MRFPSIFTAVLFAASSALAAPVNTTTEDETAQIPAEAVIGYSLEGDFDVAVLPFS
NSTNNGLLFINTTIIASIAAKEEGVSLKREAEASSRHDKEKGVNVQVLLRCRPFSD
DELRSNAPQVLTCLNDLQREVAVSQNIAGKHIDRVFTFDKVFGPSAQKDLQDQ
AVVPIVNEVLEGFNCTIFAYGQTGTGKTYTMEGECRRSKSAPCGGLPAEAGVIPR
AVKQIFDTLEGQQA EYSVKVTFLELYNEEITDLLAPEDLSRVAAEEKQKKPLPLME
DGKGGVLRGLEEEIVTSANEIFTLLERGSSKRRTAETFLNKQSSRSHLSFISITIIHK
EATPEGEELIKCGKLNLDLAGSENISRSGARDGRAREAGEINKSLLTLGRVISALV
EHLGHVVPYRDSKLT RLLRDSLGGRTKTCIIATVSPAVHCLEETLSTLDYAHRAKNIR
NKPEVNQKMMKSTLIKDLYGIEIRLKA EYASREKNGVYMPKERYYYQEESEKRV
MAEQIEQMGGQIENYQKQLEELQDKYVGQVRECSDLTTKLDITEKNLSQTCKVL
ASTNEELKKSQYAMKEKDFIISEQKSENVLVQQACILQSNLEKATKDNSSLHQKI
GREDKLSADNRKVVVDNYQVELSEQISNLFNRVASCLSQQNVHLQGVNKLSSQR
LEAHNKAILEM KKKVKASRDLYSSHLEAVQNVVRLH KANANACLEEV SALTSS
ACSIDFLASGDETTSSLFDELQ SALSSHQ GEMALFARELRQRFHTTMEQTQEM
SEYTSTFFQKLMEESKNAETRAAEANDSQINSIIDFQKTYEAQSKSDTDKLIADLT
NLVSSHIRRQHELVD SRLHNFKDAVSSNKTFLDEHVS AVNNTKDAKRKWETFS
MQAENEAREGADFSAAKHCRMELLLQQSVGHAESAFKHCKITHESLKEMTSKQ
VTDVSSLVRSACDSNEQHDAEVD SARTAAEKDVTKNSDDIIQQIERMSEDEKAS
VSKILENVR SHEKTLESFQQDQCCQARCIEDKAQETFQQQYMEYEPTGATPTKN
EPEIPTKATIESLRAMPIETLVEEFRENNSYEFATKETKPQQLTRSPLSQVSKGEE
LFTGVVPILVELDGDVNGHKFSVSGEGEGDATYGKLT LKFICTTGKLPVPWPTLV
TTLTYGVQCFSRYPDHMKRHDFFKSAMPEGYVQERTIFFKDDGNYKTRAEVKFE
GDTLVNRIELK GIDFKEDGNILGHKLEYNYNSHN VYIMADKQKNGIKVNFKIRHN
IEDGSVQLADHYQQNTPIGDGPVLLPDNHYLSTQSALS KDPNEKRDH MVLLEFV
TAAGITHGMDELYKHHHHHH

AtKRP125b FL +
tetracysteine-
tag + 6 x His-tag
From insect cells
Size: 115 kDa

MSSRHDKEKGVNVQVLLRCRPFSDDELRSNAPQVLTCLNDLQREVAVSQNIAGK
HIDRVFTFDKVFGPSAQKDLQDQAVVPIVNEVLEGFNCTIFAYGQTGTGKTYT
MEGECRRSKSAPCGGLPAEAGVIPRAVKQIFDTLEGQQA EYSVKVTFLELYNEEIT
DLLAPEDLSRVAAEEKQKKPLPLMEDGKGGVLRGLEEEIVTSANEIFTLLERGS
SKRRTAETFLNKQSSRSHLSFISITIIHKEATPEGEELIKCGKLNLDLAGSENISRSG
ARDGRAREAGEINKSLLTLGRVISALVEHLGHVVPYRDSKLT RLLRDSLGGRTKTCII
ATVSPAVHCLEETLSTLDYAHRAKNIRNKPEVNQKMMKSTLIKDLYGIEIRLKA E
VYASREKNGVYMPKERYYYQEESEKRVMAEQIEQMGGQIENYQKQLEELQDKY
VGQVRECSDLTTKLDITEKNLSQTCKVLASTNEELKKSQYAMKEKDFIISEQKSE
NVLVQQACILQSNLEKATKDNSSLHQKIGREDKLSADNRKVVVDNYQVELSEQIS
NLFNRVASCLSQQNVHLQGVNKLSSQRLEAHNKAILEM KKKVKASRDLYSSHLE
AVQNVVRLH KANANACLEEV SALTSSACSIDFLASGDETTSSLFDELQ SALSSH
QGEMALFARELRQRFHTTMEQTQEMSEYTSTFFQKLMEESKNAETRAAEAND
SQINSIIDFQKTYEAQSKSDTDKLIADLTNLVSSHIRRQHELVD SRLHNFKDAVSS
NKTFLDEHVS AVNNTKDAKRKWETFSMQAENEAREGADFSAAKHCRMELLL
QQSVGHAESAFKHCKITHESLKEMTSKQVTDVSSLVRSACDSNEQHDAEVD S
RTAAEKDVTKNSDDIIQQIERMSEDEKASVSKILENVR SHEKTLESFQQDQCCQ
RCIEDKAQETFQQQYMEYEPTGATPTKNEPEIPTKATIESLRAMPIETLVEEFREN
NSYEFATKETKPQQLTRSPLSQVFLNCCPGCCMEPHHHHHH

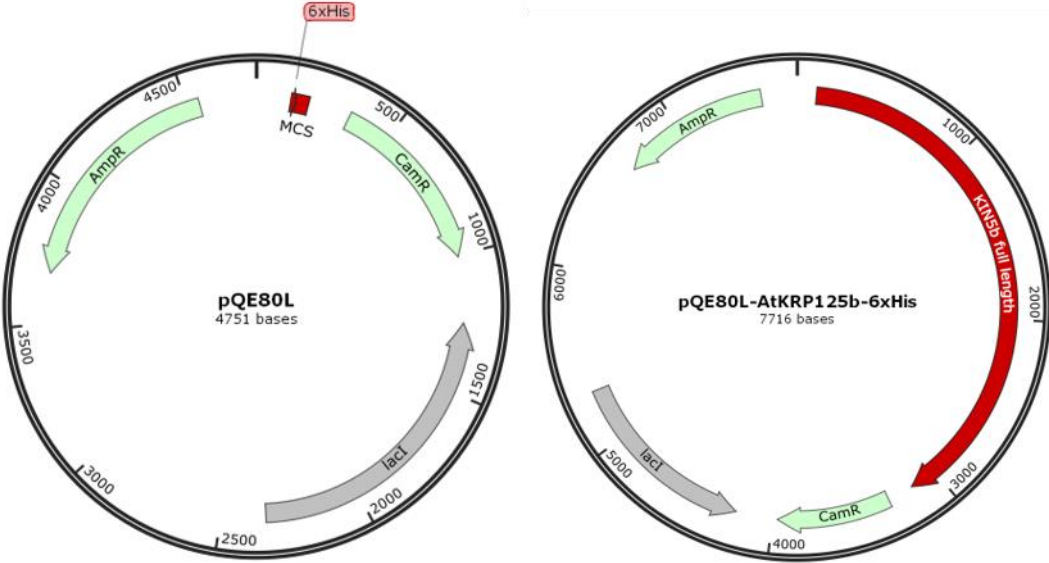


Figure S1: Schematic representation of expression vectors for *E. coli* generated in this thesis.

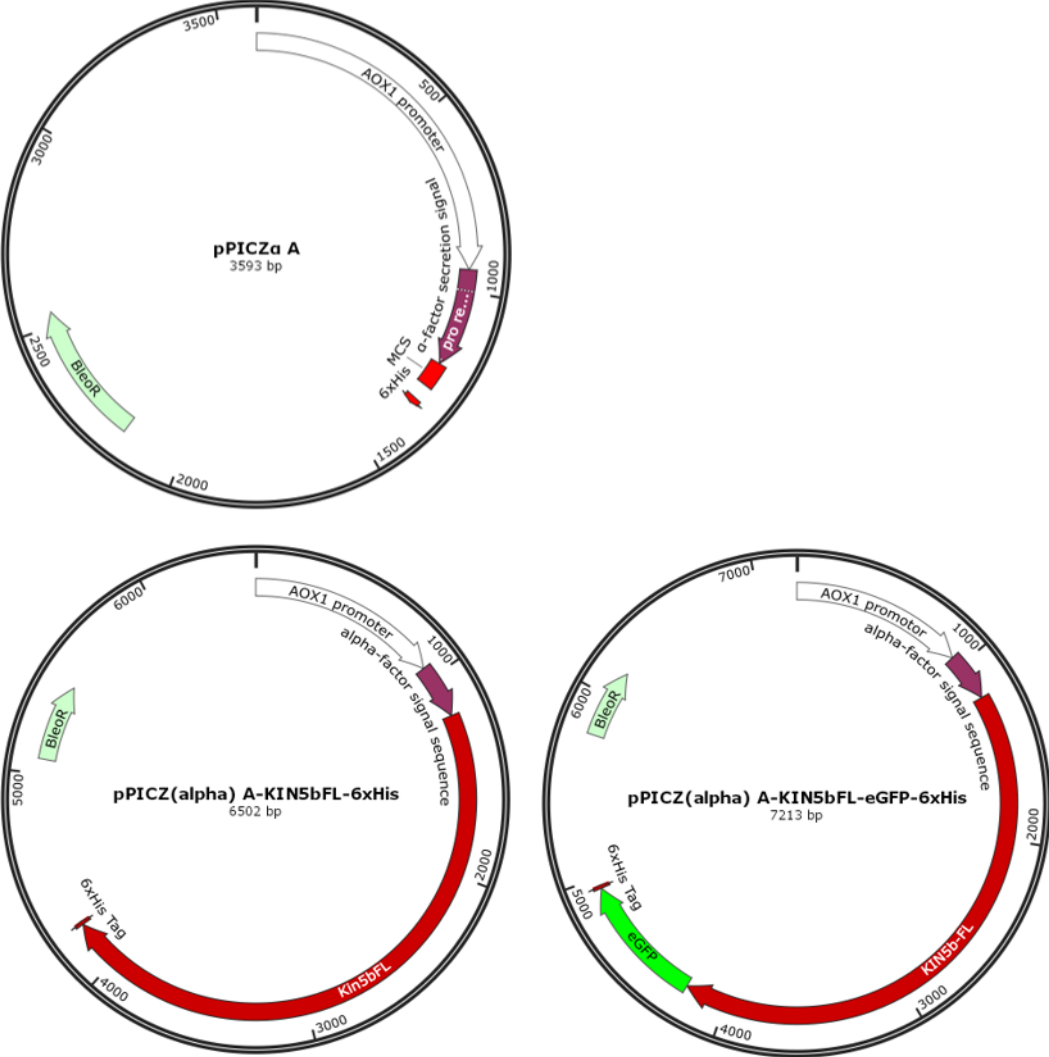


Figure S2: Schematic representation of expression vectors for *P. pastoris* generated in this thesis.

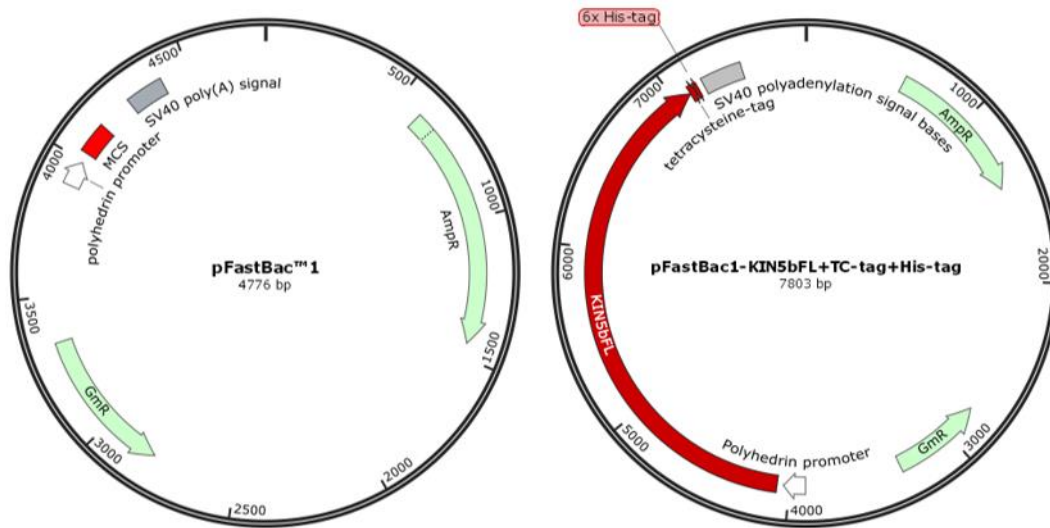


Figure S3: Schematic representation of expression vectors for insect cells generated in this thesis.

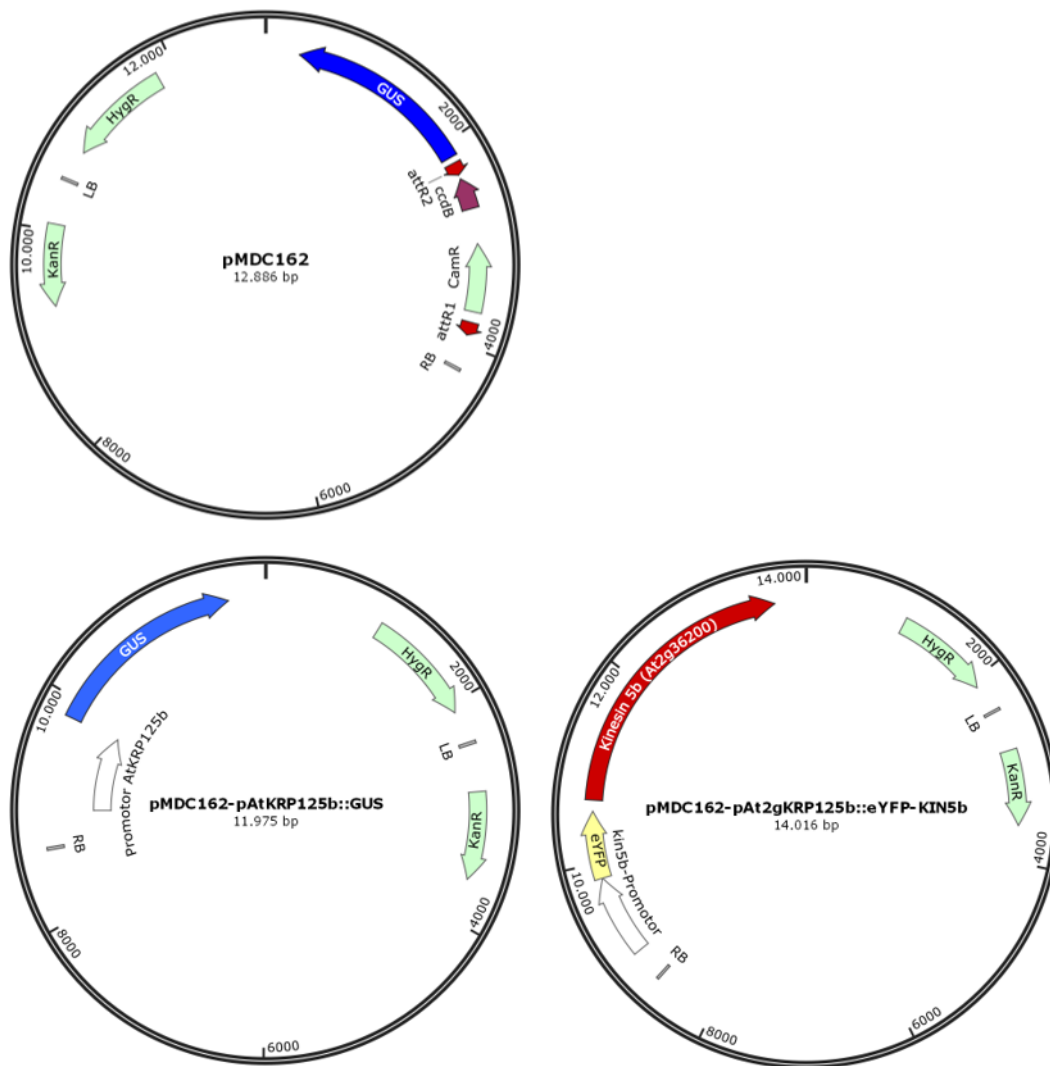


Figure S4: Schematic representation of vectors of reporter constructs based on pMDC162 generated in this thesis.

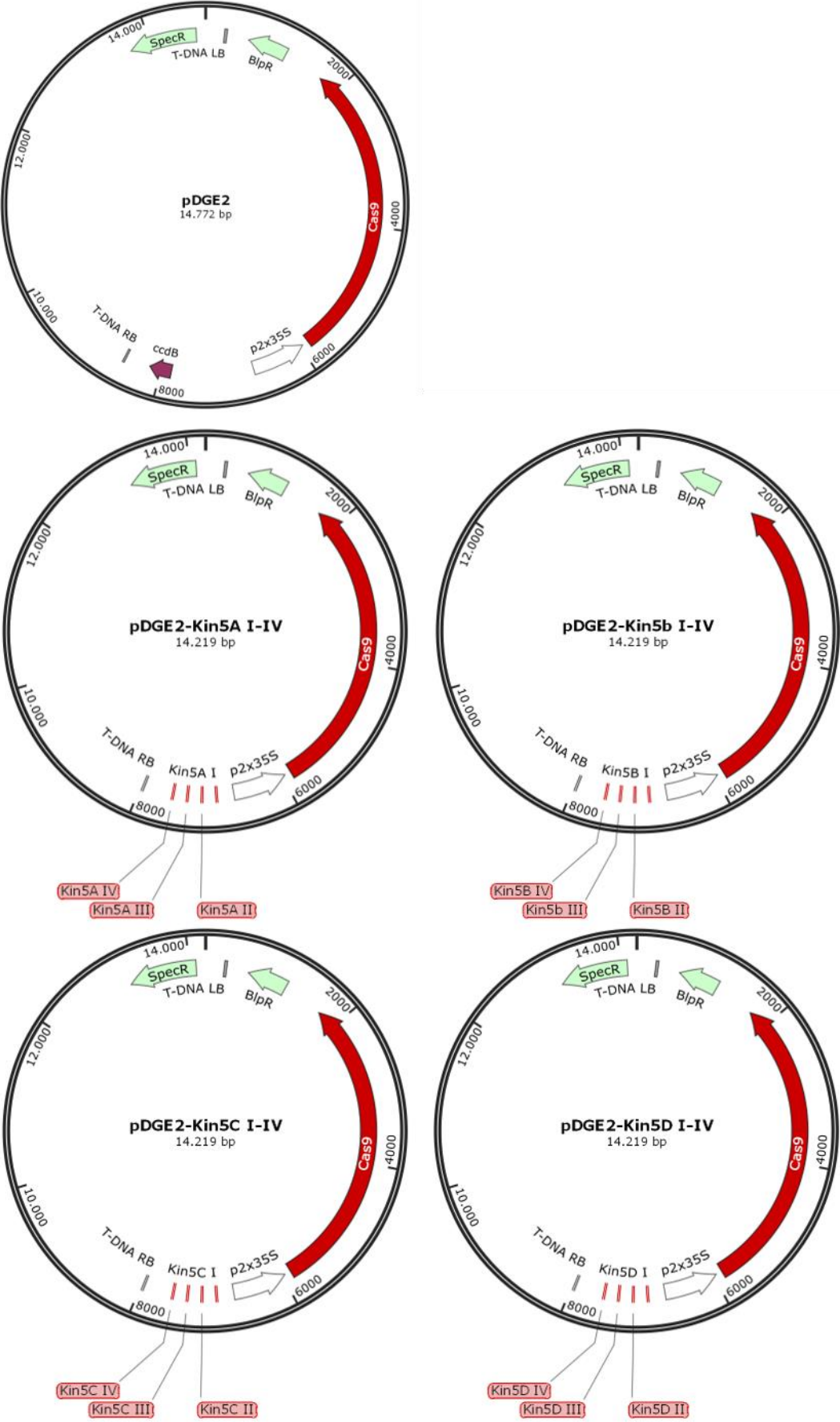


Figure S5: Schematic representation of genome editing vectors generated in this thesis following Stuttmann.

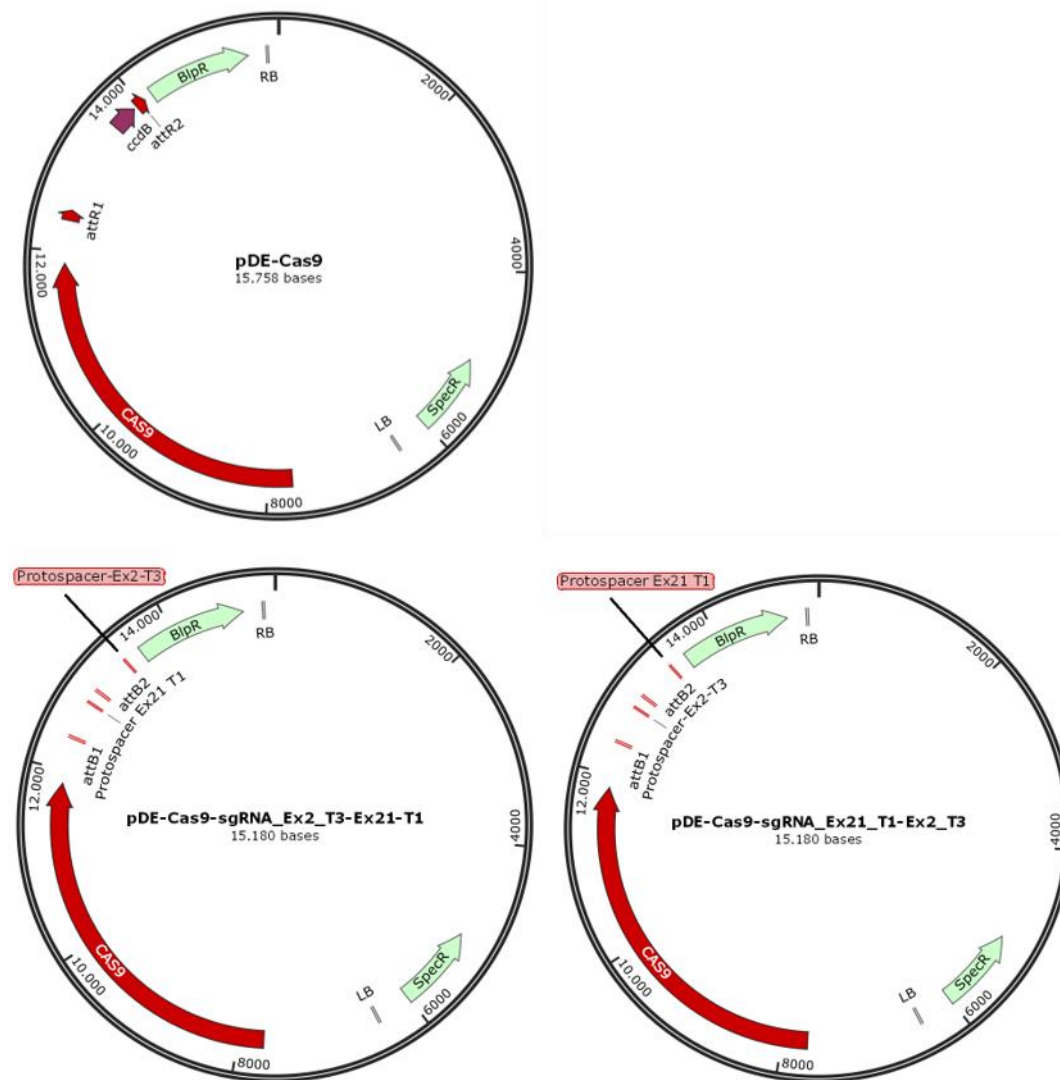


Figure S6: Schematic representation of genome-editing vectors generated in this thesis following Puchta.

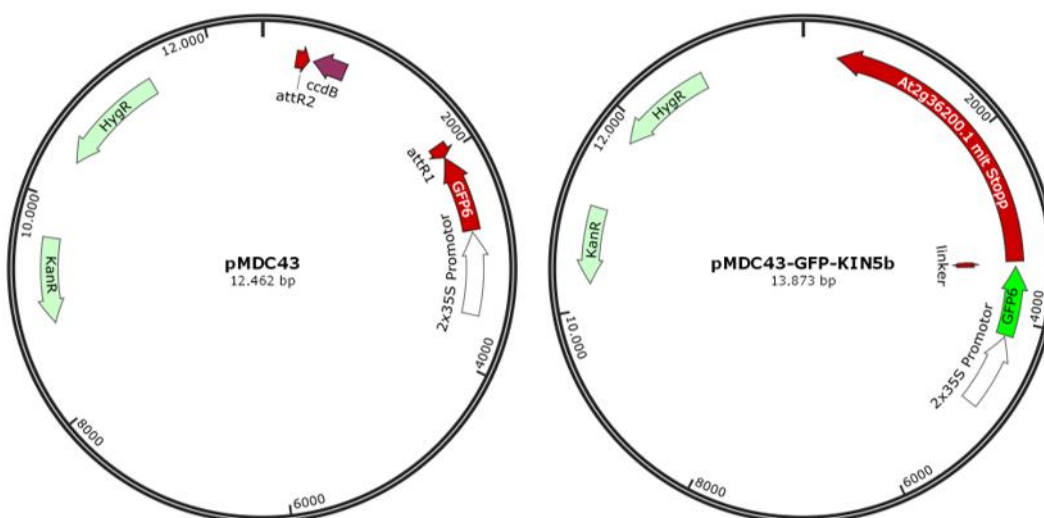


Figure S7: Schematic representation of vectors of reporter constructs based on pMDC43.

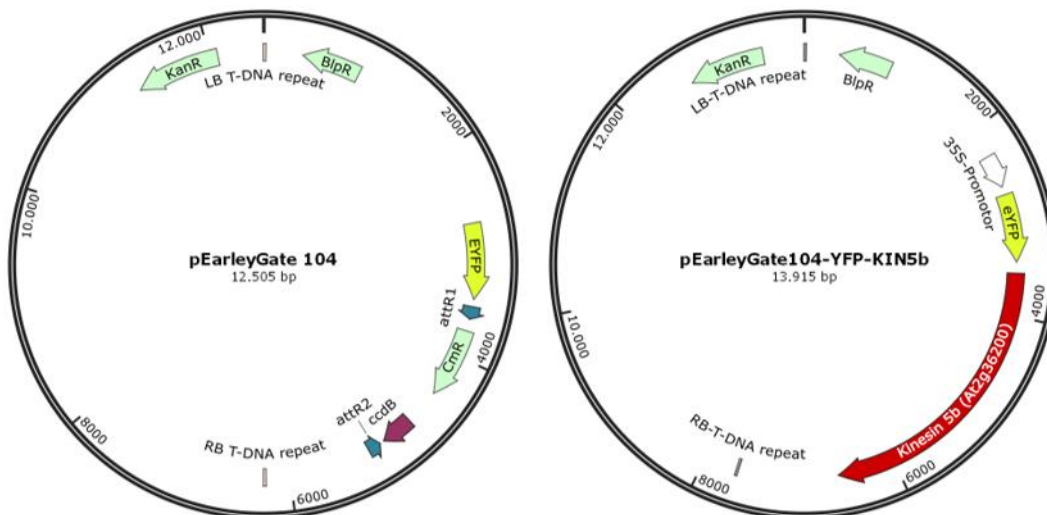


Figure S8: Schematic representation of vectors of reporter constructs based on pEarleyGate104.

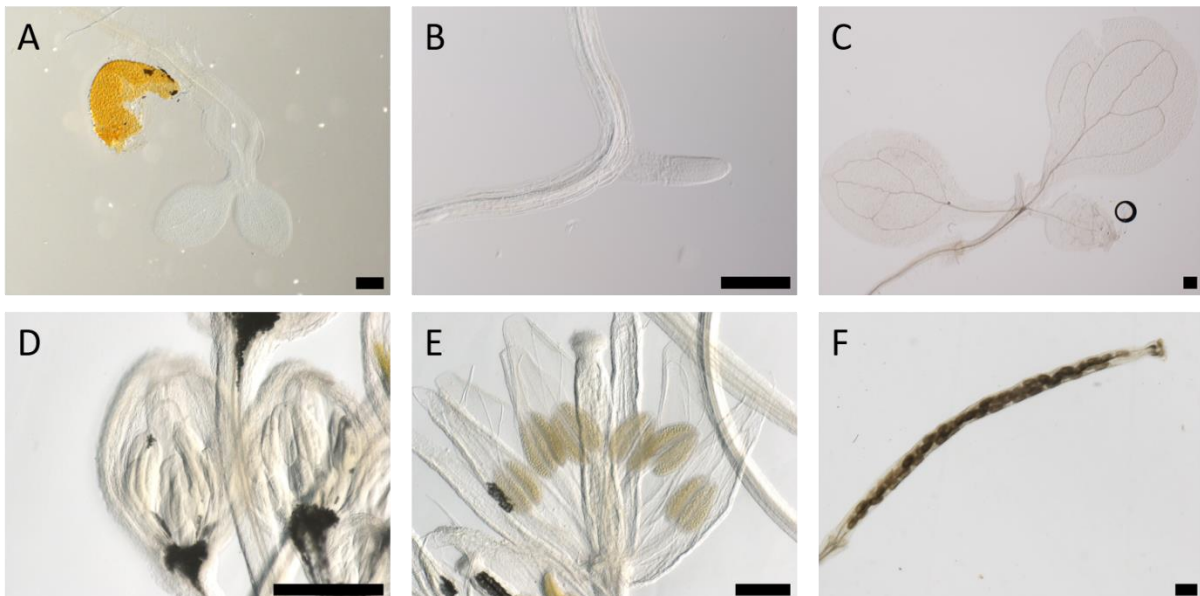


Figure S9: Macroscopic imaging of β -glucuronidase (GUS) activity in Col-0 WT at different time points. GUS staining of Col-0 plants, stained for 90 min at 37 °C with X-Gluc at different time points. The images show: (A) Young seedling, 2 dag; (B) emerging lateral root, 8 dag; (C) true leaves, cotyledons and hypocotyl, 8 dag; (D): young flower bud, 24 dag; (E) mature flower with stamen and pistil, 24 dag; (F) silique, 24 dag. Scale bar represents 200 μ m in all images.

Table S2: Transcriptome data of all four kinesin 5s. Sorted for the highest expression in At2g36200. Data obtained from "TRAVA".

Sample name	AT2G36200	AT2G37420	AT2G28620	AT3G45850
M8 - Inflorescence meristem at 14 days after germination	1.00	0.76	0.82	0.23
M4 - Meristem at 10 days after germination	0.95	0.84	0.94	0.26
M7 - Inflorescence meristem at 13 days after germination	0.92	0.84	0.87	0.30
AX - Axis of the inflorescence	0.86	1.00	0.95	0.64
M9 - Inflorescence meristem at 15 days after germination	0.85	0.84	0.79	0.31
M6 - Meristem at 12 days after germination	0.82	0.82	0.75	0.27
F.CA.y - Carpels of the young flower	0.82	0.80	0.78	0.38
F19+ - Flower 19+	0.81	0.79	0.78	0.41
M3 - SAM at 9 days after germination	0.78	0.57	0.60	0.17
L.PET.i1 - Petiole, intermediate 1	0.72	0.83	0.79	0.62
M2 - SAM at 8 days after germination	0.70	0.62	0.56	0.21
M5 - Meristem at 11 days after germination	0.70	0.45	0.54	0.13
M10 - Inflorescence meristem at 16 days after germination	0.70	0.70	0.63	0.34
L.PET.y - Petiole of the young leaf	0.66	0.64	0.74	0.34
OV.y6-7 - Ovules from 6th and 7th flowers	0.61	0.70	0.53	0.48
F.AN.ad - Anthers of the mature flower (before opening)	0.60	0.02	1.00	0.07
PED - Pedicel	0.58	0.63	0.53	0.70
SD.y3 - Young seeds 3	0.58	0.66	0.52	0.45
SD.y4 - Young seeds 4	0.56	0.52	0.46	0.33
F15-18 - Flower 15-18	0.55	0.53	0.52	0.39
SD1 - Seeds 1	0.54	0.42	0.57	0.20
M1 - SAM at 7 days after germination	0.53	0.84	0.65	0.33
SD.y5 - Young seeds 5	0.52	0.58	0.49	0.31
L.LAM.y - Leaf blade of the young leaf	0.49	0.55	0.67	0.49
POD.y6-7 - Carpel of 6th and 7th flowers	0.49	0.66	0.51	0.58
F.CA.ad - Carpels of the mature flower (before pollination)	0.47	0.53	0.44	0.46
F12-14 - Flower 12-14	0.46	0.47	0.38	0.42
L.LAM.i1 - Leaf blade, intermediate 1	0.44	0.36	0.39	0.76
SD.y2 - Young seeds 2	0.42	0.46	0.37	0.49
SD5 - Seeds 5	0.42	0.38	0.29	0.25
F6-8 - Flower 6-8	0.41	0.43	0.37	0.65
S.R - Seedling root	0.38	0.22	0.38	0.52
F5 - Flower 5	0.38	0.37	0.30	0.63
S.M - Seedling meristem	0.37	0.39	0.52	0.20

R.A - Root apex	0.36	0.26	0.40	0.53
SD.y1 - Young seeds 1	0.36	0.39	0.33	0.47
R - Root without apex	0.32	0.35	0.33	0.43
SD3 - Seeds 3	0.32	0.33	0.30	0.26
F9-11 - Flower 9-11	0.31	0.30	0.27	0.30
F2 - Flower 2	0.29	0.36	0.34	0.41
F3 - Flower 3	0.29	0.31	0.28	0.56
F4 - Flower 4	0.29	0.33	0.27	0.63
S.C - Seedling cotyledons	0.28	0.15	0.17	0.53
F.AN.y - Anthers of the young flower	0.28	0.12	0.12	0.20
IN - Internode	0.26	0.25	0.18	0.89
F1 - Flower 1	0.26	0.33	0.28	0.29
L.PET.i2 - Petiole, intermediate 2	0.23	0.21	0.17	0.85
SD.g3 - Germinating seeds 3 (third day after soaking)	0.22	0.19	0.21	0.46
SD.g2 - Germinating seeds 2 (second day after soaking)	0.22	0.10	0.11	0.42
SL2 - Silique 2	0.21	0.26	0.24	0.37
F.SP.y - Sepals of the young flower	0.19	0.19	0.20	0.80
L.VN.i2 - Leaf vein, intermediate 2	0.19	0.16	0.12	0.85
SL4 - Silique 4	0.18	0.21	0.17	0.47
SD7 - Seeds 7	0.17	0.16	0.09	0.34
SL8 - Silique 8	0.16	0.18	0.16	0.81
F.AN - Opened anthers	0.16	0.01	0.32	0.03
L.LAM.i2 - Leaf blade, intermediate 2	0.14	0.11	0.09	0.77
SL6 - Silique 6	0.14	0.16	0.10	0.63
S.H - Seedling hypocotyl	0.11	0.14	0.07	0.58
POD3 - Pod of the silique 3	0.10	0.16	0.12	0.55
POD1 - Pod of the silique 1	0.10	0.17	0.11	0.42
F.FM.ad - Stamen filaments of the mature flower	0.09	0.03	0.03	0.59
POD7 - Pod of the silique 7	0.08	0.08	0.08	1.00
L.PET.lg - Petiole of the mature leaf	0.07	0.14	0.05	0.25
POD5 - Pod of the silique 5	0.06	0.08	0.07	0.72
STI - Stigmatic tissue	0.05	0.03	0.03	0.66
SD.sn1 - Seeds of first yellowing silique.	0.05	0.13	0.00	0.01
SD.g1 - Germinating seeds 1 (first day after soaking)	0.04	0.03	0.01	0.22
F.PT.ad - Petals of the mature flower	0.03	0.03	0.06	0.79
F.SP.ad - Sepals of the mature flower	0.03	0.03	0.04	0.44
L.VN.lg - Vein of the mature leaf	0.03	0.09	0.03	0.26
SL.sn2 - Senescent silique 2	0.03	0.11	0.00	0.02
L.PET.sn - Petiole of the senescent leaf	0.02	0.17	0.01	0.07
L.lg - Whole mature leaf	0.02	0.07	0.02	0.18
L.VN.sn - Vein of the senescent leaf	0.01	0.10	0.01	0.09
IN.sn - Senescent internode.	0.01	0.44	0.00	0.12

POD.sn1 - Pod of the senescent silique 1.	0.01	0.14	0.00	0.05
SD.d - Dry seeds	0.01	0.05	0.01	0.00
L.LAM.lg - Leaf blade of the mature leaf	0.00	0.04	0.00	0.27

Table S3: Statistical analysis of root size measured by the amount of root pixel (px) from plants shifted to MS and MS with 150 mM NaCl after 7 dag. t-tests were used to determine a significant difference between certain groups. t-tests were chosen according the results of F-tests. Results, marked with a star (*) were tested with Students t-test, the other were tested with Welch test.

	12dag MS WT	12dag MS <i>kin5b-1</i>	12dag NaCl WT	12dag NaCl <i>kin5b-1</i>
Sum (px)	2051254	1301096	616270	354054
plants	86	78	86	81
Mean (\bar{X})	23851,7907	16680,71795	7165,930233	4371,037037
StD. (s)	7135,736836	4618,835027	2401,975534	1374,537072
StD. (σ)	7094,128686	4589,1316	2387,969726	1366,025924
	7dag MS WT	7dag MS <i>kin5b-1</i>	7dag NaCl WT	7dag NaCl <i>kin5b-1</i>
Sum (px)	331228	262813	277898	193969
Plates	86	82	86	80
Mean (\bar{X})	3851,488372	3205,036585	3231,372093	2424,6125
SD (s)	993,7618574	679,0323806	829,9775907	660,6371971
SD (σ)	987,9672782	674,8792384	825,13803	656,4952303
F-test	12dag MS WT	12dag NaCl WT	12dag MS WT	12dag MS <i>kin5b-1</i>
	12dag MS <i>kin5b-1</i>	12dag NaCl <i>kin5b-1</i>	12dag NaCl WT	12dag NaCl <i>kin5b-1</i>
F	2,39	3,05	8,83	11,29
FG1	85	85	85	77
FG2	77	80	85	80
p (0,05)	1	1	1	1
F-test	7dag MS WT	7dag NaCl WT	7dag MS WT	7dag MS <i>kin5b-1</i>
	7dag MS <i>kin5b-1</i>	7dag NaCl <i>kin5b-1</i>	7dag NaCl WT	7dag NaCl <i>kin5b-1</i>
F	2,14	1,58	1,43	1,06
FG1	85	85	85	81
FG2	81	79	85	79
p (0,05)	1	1	1	0
t-test	12dag MS WT	12dag NaCl WT	12dag MS WT	12dag MS <i>kin5b-1</i>
	12dag MS <i>kin5b-1</i>	12dag NaCl <i>kin5b-1</i>	12dag NaCl WT	12dag NaCl <i>kin5b-1</i>
t	7,71	9,30	20,55	22,59
FG	113	137	104	90
p (0,05)	1	1	1	1
p (0,01)	1	1	1	1
p (0.001)	1	1	1	1
t-test	7dag MS WT	7dag NaCl WT	7dag MS WT	7dag MS <i>kin5b-1</i>
	7dag MS <i>kin5b-1</i>	7dag NaCl <i>kin5b-1</i>	7dag NaCl WT	7dag NaCl <i>kin5b-1</i>

t	4,94	6,95	4,44	7,41*
FG	162	160	165	160*
p (0,05)	1	1	1	1
p (0,01)	1	1	1	1
p (0.001)	1	1	1	1

Table S4: Statistical analysis of root size measured by the amount of root pixel (px) from plants shifted to MS after 7 dag and cultivated either at 22 °C or at 17 °C. t-tests were used to determine a significant difference between certain groups. t-tests were chosen according the results of F-tests. Results, marked with a star (*) were tested with Students t-test, the other were tested with Welch test.

	12dag 22°C WT	12dag 22°C <i>kin5b-1</i>	12dag 17°C WT	12dag 17°C <i>kin5b-1</i>
Sum (px)	1155169	1120112	832501	748983
Plants	66	66	71	70
Mean (\bar{X})	17502,56	16971,39	11725,37	10699,76
SD (s)	5302,45	5709,53	3712,56	3067,79
SD (σ)	5262,12	5666,11	3686,32	3045,80
	7dag 22°C WT	7dag 22°C <i>kin5b-1</i>	7dag 17°C WT	7dag 17°C <i>kin5b-1</i>
Sum (px)	364174	287686	331994	285570
Plants	72	72	72	72
Mean (\bar{X})	5057,97	3995,64	4611,03	3966,25
SD (s)	1355,06	1198,84	1344,95	1169,98
SD (σ)	1345,62	1190,49	1335,57	1161,83
	12dag 22°C WT	12dag 17°C WT	12dag 22°C WT	12dag 22°C <i>kin5b-1</i>
F-test	12dag 22°C <i>kin5b-1</i>	12dag 17°C <i>kin5b-1</i>	12dag 17°C WT	12dag 17°C <i>kin5b-1</i>
F	1,16	1,46	2,04	3,46
FG1	65	70	65	65
FG2	65	69	70	69
p (0,05)	0	0	1	1
	7dag 22°C WT	7dag 17°C WT	7dag 22°C WT	7dag 22°C <i>kin5b-1</i>
F-test	7dag 22°C <i>kin5b-1</i>	7dag 17°C <i>kin5b-1</i>	7dag 17°C WT	7dag 17°C <i>kin5b-1</i>
F	1,28	1,32	0,99	1,05
FG1	71	71	71	71
FG2	71	71	71	71
p (0,05)	0	0	0	0
	12dag 22°C WT	12dag 17°C WT	12dag 22°C WT	12dag 22°C <i>kin5b-1</i>
t-test	12dag 22°C <i>kin5b-1</i>	12dag 17°C <i>kin5b-1</i>	12dag 17°C WT	12dag 17°C <i>kin5b-1</i>
t	0,55*	1,79*	7,43*	7,91
FG	130*	139*	135*	98
p (0,05)	0	0	1	1
p (0,01)	0	0	1	1
p (0.001)	0	0	1	1
	7dag 22°C WT	7dag 17°C WT	7dag 22°C WT	7dag 22°C <i>kin5b-1</i>
t-test	7dag 22°C <i>kin5b-1</i>	7dag 17°C <i>kin5b-1</i>	7dag 17°C WT	7dag 17°C <i>kin5b-1</i>

t	4,98*	3,07*	1,99*	0,15*
FG	142*	142*	142*	142*
p (0,05)	1	1	1	0
p (0,01)	1	1	0	0
p (0.001)	1	0	0	0

Acknowledgments

Das Ende dieser Dissertation ist erreicht und ich möchte die Gelegenheit nutzen, mich bei all den Menschen herzlich zu bedanken, die mich in den letzten Jahren und insbesondere in der finalen Phase intensiv unterstützt und begleitet haben.

Zunächst gilt mein Dank meinen beiden Betreuern, Stefan Hoth und Wim Walter, die mir die Möglichkeit gaben an diesem Thema in ihren Arbeitsgruppen weiterzuarbeiten. Lieber Wim, lieber Stefan, ich möchte mich für die zahlreichen guten Gespräche und Anregungen während der letzten Jahre bedanken. Vielen Dank für den Zuspruch, auch wenn es mal nicht so lief wie geplant und all die Ausflüge, Retreats und Konferenzen die den Forschungsalltag wunderbar aufgelockert haben. Insbesondere bedanke ich mich aber für euren begeisterten Zuspruch und die tolle Unterstützung bei dem Wunsch in dieser turbulenten Phase auch noch eine kleine Familie zu gründen.

Ich möchte mich auch ganz herzlich bei Nick Sinfield bedanken, der nicht gezögert hat seine Freizeit zu opfern um die Arbeit eines ihm unbekanntem Studenten zu kontrollieren. Danke auch an Alexander Staff, der mir kurzfristig weitere Tipps für die Arbeit gegeben hat. Vielen Dank dafür!

Ohne die tolle Kooperation mit Astrid Sydow und Gunnar Baermann vom UKE wäre ein wichtiger Teil dieser Arbeit undenkbar gewesen, vielen Dank für eure unschätzbare Unterstützung bei der Proteinexpression.

Unvergesslich bleiben natürlich die netten Kolleginnen, Kollegen und Studierenden aus der Molekularen Pflanzenphysiologie, die mich über die vielen Jahre in der Abteilung begleitet haben und so viele tolle Momente geteilt haben. Vielen Dank an euch alle! Besonderer Dank geht an Christiane mit ihrem großartigen Organisationstalent, an Julia, Wenke, Pierre, Judith, Isabel und Giuliana, die mich in zahlreichen Experimenten, unendlich vielen Genotypisierungen und im drum herum des Laboralltags hervorragend unterstützt haben und bei allen Doktoranden, mit denen ich zusammen in einem Boot saß und bei denen ich mich immer ausgiebig über Praktikumsprotokolle aufregen durfte. Danke an Saskia, Melanie, Lisa und Moni für das gründliche korrigieren dieser Arbeit und die gemeinsame Zeit in Labor und Büro, eure Tipps zu Methoden und eure Hilfe bei Auswertungen. Vielen Dank für stets offene Ohren, aufmunternde Worte und natürlich „Tons of fun“.

Der allergrößte Dank geht zum Abschluss noch an meine Familie und Freunde, die mir immer viel Verständnis entgegengebracht haben, auch wenn die Laune im Keller war, oder man vor

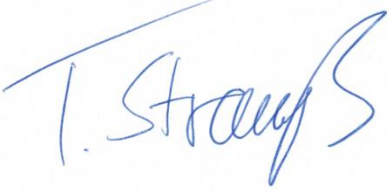
lauter Arbeit etwas zerstreut war und alles etwas länger gedauert hat als geplant. Vielen Dank für entspannende Spieleabende und zahlreiche Gelegenheiten um mal auf andere Gedanken zu kommen. Besonders aber mein Mann Thorben, hat immer wieder die nötige Motivation geschaffen um durchzuhalten und weiterzumachen, musste sich stundenlang Ausführungen über biologische Probleme anhören und kennt sich in manchen Belangen mittlerweile sicher besser aus als manch ein Biologie Student. Gerade in den letzten Monaten hast du mir toll den Rücken gestärkt und die nötigen Freiräume geschaffen, um die Arbeit zum Abschluss zu bringen! Ohne dich hätte ich das nie geschafft!

Vielen, vielen Dank!

Eidesstattliche Versicherung

Hiermit erkläre ich an Eides statt, dass ich die vorliegende Dissertationsschrift "Kinesin-5 in plants – Characterisation of AtKRP125b indicates new functions for motor proteins" selbst verfasst und keine anderen als die angegebenen Quellen und Hilfsmittel verwendet habe. Die Dissertationsschrift wurde in dieser oder ähnlicher Form noch keiner Prüfungskommission vorgelegt.

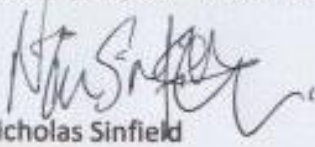
Hamburg, den 20.11.2020

A handwritten signature in blue ink, reading "T. Strauß". The signature is written in a cursive style with a large, sweeping initial 'T'.

Tobias Strauß

Confirmation of Linguistic Correctness: I hereby declare that I have read the thesis "Kinesin-5 in plants – Characterisation of AtKRP125b suggests a new function beyond cell division" by Tobias Strauss and can confirm, as a native English speaker, its linguistic correctness in English.

London, UK, 18th November 2019



Nicholas Sinfield